CONVECTIVE AND RADIATIVE HEAT TRANSFER IN A HIGH SWIRL DIRECT INJECTION DIESEL ENGINE

by

Saadoun Jallood Sulaiman

A Doctoral Thesis

Submitted in Partial Fulfilment of the Requirements

for the Award of

Doctor of Philosophy of Loughborough University of Technology

April 1976

Supervisor: J.C. Dent, Ph.D., C.Eng., M.I.Mech.E.

SUMMARY

The investigation described in this thesis is a study of instantaneous heat fluxes (total and radiative) and their variation with operating conditions in a high swirl direct injection diesel engine. The problem is approached experimentally and methods for prediction of convective and radiative components are suggested. Total heat fluxes were measured using a thin film type thermocouple developed in the course of the work, while the radiant flux was measured by a pyroelectric infrared detector.

The experimental observations demonstrate variations in local heat fluxes which are moderate under motored conditions but large in the fired engine. Some of the observed features of flux variation with time and with location have been shown to be qualitatively explicable in terms of probable local events during the cycle.

The prediction of instantaneous convective heat flux is attempted on the basis of existing data on heat transfer for flat plates and the observed solid swirl gas motion in the engine. A comparison of the experimental results with predictions by the new correlation and some previously proposed correlations are presented and discussed. Under fired operation, the bulk mean gas temperature was found inadequate for the prediction of local heat fluxes. A consideration of a simple two-zone temperature distribution (based on observed events) and of combustion induced swirl (based on conservation of momentum) improved the prediction of local heat fluxes. The prediction of surface mean heat fluxes on the basis of bulk mean temperature is shown to be valid.

The radiant flux measurements suggest that in high swirl engines the ratio of radiant to total heat transfer is much less than observed in quiescent chamber diesel engines. The analysis of present and published data on radiant emission from different diesel engines showed a large variation in flame absorption coefficients which seemed to be related mainly to the air-fuel mixing process. Therefore on the basis of similar flame temperatures observed in different diesel engines, and the evaluated flame absorption coefficients a method is outlined for reliable estimates of radiant flux in other diesel engines.

ACKNOWLEDGEMENTS

The author wishes to express his sincere thanks to:

Dr. J.C. Dent (Reader) for his helpful suggestions and supervision of this work.

All members of the technical staff of the Mechanical Engineering Department.

Mr. P.H. Clayton for his manufacture of the linkwork mechanism and help in the manufacture of other experimental equipment.

Mr. M.W. Quelch for his assistance with the infrared detector amplifier design.

Messrs. K. Topley and G. Hall for producing the photographic plates appearing in the thesis.

Mrs. J. Smith for typing the thesis.

Plessey Company Limited for providing the pyroelectric infrared detector.

The Iraqi Government for providing the scholarship support without which this work would not have been possible.

Finally the author is also indebted to his wife for her patient support during the period of study.

NOMENCLATURE

a - multiplying factor for convective transfer (e.g. in equation 1.2)

a' - coefficient of gas temperature change with time (equation 1.4)

A - area (m^2)

b - index of Reynolds number (m)

B - zone width (m)

c i) - multiplying factor for radiant heat transfer (-)

ii) - soot particle concentration, (number per unit volume) (equation 2.12)

iii) - specific heat of material (kJ/kg^oK)

c_1, c_2 - first and second Planck constants

c_p - specific heat of gas at constant pressure ($kJ/kg\ ^oK$)

CR - compression ratio

D - cylinder diameter, characteristic dimension (m)

E i) - hemispherical emissive power of a black or grey body (kW/m^2)

ii) - voltage output of transducer (V)

E_λ - monochromatic emissive power of a black or grey body (kW/m^2)

$E_{\lambda g}(E_s)$ - E_λ for a gas (surface)

f ( ) - denotes 'function of'

f_1 - frequency at which detector responsiveness = 0.707 its low frequency value (section 3.2) (Hz)

f_v - volume fraction occupied by particles (section 2.2.4(b))

F_{1R2} - angle factor between entrance and exit of opening (-)

F_{wd} - angle factor between viewing window and detector (-)

$\overline{gs}$ - direct-exchange area between gas and surface (m^2)

$\overline{gs}_e$ ($\overline{gs}_w$) - direct-exchange area in zoned right-circular cylinder, between gas zone and end (sidewall) zone. (m^2)

$\overline{g_i s_i}$ - direct-exchange area between gas zone i and surface zone j (m^2)

h - coefficient of heat transfer (local) ($kW/m^2\ ^oK$)

$\bar{h}$ - surface mean heat transfer coefficient ($kW/m^2\ ^oK$)

i - general zone number

I - intensity - radiant flux per unit solid angle of divergence (kW/m^2)

I_o - intensity on entry into system of interest (kW/m^2)

j - general zone number

K i) - equivalent grey-body absorption coefficient (1/m)

ii) - extinction coefficient in equation 2.10 (1/m)

k i) - absorption coefficient (1/m. (atm. or concentration)

ii) - thermal conductivity (kW/m^oK)

iii) - proportionality constant in equation (2.20)

k_c,(k_p)- absorption coefficient, concentration basis (pressure basis)

k_λ - monochromatic absorption coefficient

k' - absorption index

l - length; mean free path (m)

L - path length, distance, characterising dimension (m)

L_e - mean beam length (m)

L_m - average mean beam length (m)

m - mass (kg)

m' - mass flow rate ($kg.s^{-1}$)

n - polytropic index, refractive index

Nu - Nusselt number, dimensionless ratio (h.L/K)

p - partial pressure of gas (bar)

P - absolute pressure (bar)

p_s - polarisation coefficient of ferroelectric material coul. $cm^{-2}\ k^{-1}$

P_r - Prandtl number, dimensionless ratio ($\mu C_p/k$)

$\dot{q}$ - heat flux (kW/m^2)

q - heat flow (energy) per unit time (kW)

$q_R, (q_{g-s})$ - mean radiant flux (from gas to surface) (kW/m^2)

Q - heat transfer (kJ)

r - local coordinate of combustion chamber radius (m)

R i)- gas constant ($kJ/kg\ ^oK$)

ii)- electrical resistance (ohms)

R_e - Reynolds number dimensionless ratio $(\frac{\rho.U.L.}{\mu})$

S Entropy (units) ($kJ/^oK$)

SR - swirl ratio $(\frac{\text{gas swirl rpm}}{\text{crank rotation rpm}})$

t i)- time (s)

ii)- time constant (chapter 3) (s)

$T(T_g, T_s, T_f)$ temperature (of gas, surface, flame) (^oK)

$\dot{T}$ - temperature change with time ($^oK/s$)

u - internal energy $\frac{1}{2}$ (kJ/kg)

$U(U_b, U_u)$ - velocity (of burned, unburned mixture) (m/s)

v or V- volume (m^3)

V_p - piston speed (m/s)

V_s - signal voltage of transducer (V)

x - general length coordinate (m)

α - i) thermal diffusivity, dimensionless $(\frac{k}{\rho C})$

ii) absorptivity, absorptance

iii) excess air factor $(\frac{\text{actual (air/fuel) ratio}}{\text{stoichiometric (air/fuel) ratio}})$

α_{gs} - absorptivity of a gas for radiation from a surface

γ - adiabatic index (C_p/C_v)

δ - boundary layer thickness (m)

δ_i - boundary layer momentum thickness (m)

$\epsilon, (\epsilon_g, \epsilon_s)$ emissivity (of a gas, of a surface)

$\epsilon_a (\epsilon_\lambda)$- apparent emissivity of grey body (monochromatic emissivity)

λ - wavelength μ (micron)

μ - dynamic viscosity (kg/m.s)

ρ - density (kg/m^3)

σ - Stefan-Boltzman constant 56.7×10^{-12} $(kW/m^2.k^4)$

σ_o - " " " 56.7×10^{-4} $(kW/m^2.k^4)$

ϕ - equivalence ratio $(\frac{\text{actual (fuel/air) ratio}}{\text{stoichiometric (fuel/air) ratio}})$

ω - angular velocity (rev/min) or (rad/sec)

θ - crank angle displacement (degrees)

Subscripts

a - air, apparent

b - burned product, black body

f - flame

g,s - gas, surface

i,j - identification numbers of zones

m - chemically correct mixture of air and fuel

R.T - denotes radiant or total heat flux

Abbreviations

ATDC	after top dead centre
BTDC	before top dead centre
CI	compression ignition
DC	direct current
DI	direct injection
EVO	exhaust valve open
FNL	fired no load (engine operating condition)
F40%L	fired 40% load
F80%L	fired 80% load
IMEP	indicated mean effective pressure
IVC	inlet valve closed
IDI	indirect injection
MOT	motored (engine operating condition)
RPM	revolutions per minute
SI	spark ignition

University of Technology

LOUGHBOROUGH LEICESTERSHIRE LE11 3TU Telephone: 050-93 63171 Telex: 34319

Extn 205

Higher Awards Section

CERTIFICATE OF ORIGINALITY

This is to certify that I am responsible for the work submitted in this thesis, that the original work is my own except as specified in acknowledgements or in footnotes, and that neither the thesis nor the original work contained therein has been submitted to this or any other institution for a higher degree.

S. J. Sulaiman
.....

Signed

25.5.76
.....

Date

INDEX OF CONTENTS

CHAPTER 1

INTRODUCTION AND LITERATURE SURVEY

1.1 Introduction

Heat transfer in internal combustion engines is a complex process involving both convective and radiative modes, which are not yet clearly understood. The convective component of heat transfer is controlled mainly by gas motion, temperature difference between the working fluid and walls and fluid properties adjacent to the walls. The rapidly varying conditions under which convection heat transfer takes place in reciprocating engines makes evaluation of the parameters influencing it difficult.

Heat transfer by radiation may be divided into two types: non-luminous (banded emission spectra) gas radiation, due to changes of vibrational and rotational energy of the molecules, and luminous (continuous emission spectra) flame radiation due to solid carbon particles. At gas temperature levels reached in I.C. engines, the major contribution to gas radiation is from gases H_2O and CO_2 (2.7, 2.8, 4.4 & 6.3μ). If the instantaneous concentration of the combustion products is known then gas radiation can be calculated in a relatively accurate manner. Luminous flame radiation is produced and controlled by carbon particle concentration (formed by thermal decomposition of the hydrocarbons), the flame size and temperature distribution within. These factors are complex under the rapid combustion conditions in the diesel engine which makes a prediction of diesel radiant emission from basic principles almost impossible.

Under the condition of homogeneous combustion existing in the spark-ignition engine, no solid intermediate (carbon) products are formed, and only emission from H_2O and CO_2 may be considered. On the other hand in compression ignition engines, solid carbon particles are formed in the diffusive flame of localised fuel droplets apparently by polymerisation and then condensation followed by graphitisation.

The incandescent carbon particles produce radiant emission which is approximately an order of magnitude greater than radiation from the non luminous gas radiation at the same temperature.

Estimation of instantaneous heat transfer rates at the interface of the working gas and the containing walls in internal combustion engines is of importance to the designer in order to:

1) Improve engine cycle simulation on computers for investigation of performance and efficiency, and to assess the probable bulk and cost associated with disposal of heat rejected to the coolant.

2) To solve the problem of cyclic thermal loading which impose a limit on the maximum power obtainable.

Many attempts have been made to calculate instantaneous heat fluxes, but because of lack of data and knowledge on gas motion, the resulting empirical relations are unable to accurately predict the convective and radiative energy transfer from the working gas to the cylinder walls. In general, investigators have treated the transient heat transfer in engines as quasi-steady, and correlations of heat transfer coefficient h in terms of Nusselt and Reynolds numbers have been used. Furthermore a homogeneous mixture is usually assumed and the driving temperature for heat transfer is taken as the difference between the bulk mean gas temperature and the wall surface temperature. Therefore the instantaneous heat flux is expressed by:

$$\dot{q} = h\,(T_g - T_w) \qquad (1.1)$$

The relative importance of the radiant contribution to total heat transfer in compression-ignition engines has been the subject of debate for many years. Recently published work shows measured radiant heat transfer amounting to between 20% and 40% of the total heat transfer averaged over the complete engine cycle. The fact that radiant heat transfer depends on the fourth power of radiation source temperature compared to the linear dependance of convection transfer on the gas-wall temperature difference, makes the radiant component important.

Therefore there is a need for further experimental data and alternative methods of approach in predicting the heat transfer in internal combustion engines. Hence, this project was undertaken to investigate convective heat transfer in the engine under both motored and fired operation and to study the relative importance of radiative heat transfer in a direct injection, high swirl diesel engine.

1.2 Review of Previous Investigation

The review of the previous work on heat transfer correlations is divided into two major sections. The first section will deal with a review of literature on total heat transfer measurements and correlations. The second section deals with that work which is more specifically related to the radiation heat transfer in engines and will comprise a review of current work in this field. To complete the survey, a brief outline of the theoretical investigations and its limitation is also given.

In presenting the correlations of the various researchers, no attempt is made to rearrange the equations to any standard set of units, as the interest in this presentation is mostly in the form

of the correlation and the variables involved. In several cases, ranges of values for certain constants are noted so that a more complete picture of the importance and effect of the various parameters in the correlation may be obtained.

1.2.1 Total heat transfer correlations and measurements

Before presenting the review, a classification of the available literature on the basis of the method used for evaluation of surface heat transfer, and methods of correlation with other engine parameters is considered. The methods for evaluation of surface heat transfer due to convection are:

a) Measured instantaneous heat transfer using surface temperature measuring devices.

b) Measured time-averaged heat transfer obtained from heat balance.

1.2.1a Correlations and measurements based on instantaneous heat transfer

The relevant literature on heat transfer in reciprocating engines has been reviewed by many researchers, but an outstanding discussion and analysis of the accepted heat transfer correlations for diesel and spark ignition engines has been presented by Annand (6). It is not necessary for the same ground to be covered here, instead most of the early correlations are listed in Table (1.1) with a brief discussion and critique of each.

Annand analysed each correlation for dimensional homogeneity and form. He reasoned that if a correlation were to be used for extrapolation of a previously observed trend, it should be based on a dimensionless group of significant parameters within the engine, and

TABLE (1.1)

Total instantaneous (space mean) heat transfer correlations

Researcher	Correlation form	Basis of correlation or supporting observation	Remarks
Nusselt (1) (1923)	$\dot{q}_T = a(1 + b\,V_p)(P^2 T_g)^{1/3}[T_g - T_w] + c(T_g^4 - T_w^4)$	Measurement of heat transfer from homogeneous mixture explosions in bombs and forced convection heat transfer from plane surface	Simple and separate terms for convection and radiation, but dimensionally incorrect
Brilling (6) (1931)	Modified $f(V_p)$ in Nusselts correlation $(1 + 1.24\,V_p)$ to $(2.45 + .185\,V_p)$	Measurement of time-averaged data on diesel engines	Attempt to represent actual engine conditions, but still dimensionally incorrect.
Tijen (3) (1959)	Modified $(1 + 1.24\,V_p)$ to $(3.19 + 0.885\,V_p)$	Survey of published tests on seven different oil engines	Same as above
Eichelberg (5) (1939)	$\dot{q}_T = a(V_p)\,(PT_g)^{\frac{1}{2}}[T_g - T_w]$	Measurement of instantaneous heat transfer in large-slow diesel engines using sub-surface thermocouples	Simple, but radiation and convection lumped in one term. Not dimensionless.
Eichelberg & Pflaum (7) (1951)	$\dot{q}_T = a.b.f(V_p)(PT_g)^{\frac{1}{2}}[T_g - T_w]$ where $f(V_p) = 3 \pm 2.57[1 - e^{\pm(1.5 - 0.127\,V_p)}]$ +ve if $V_p > 11.8$ and -ve if $V_p < 11.8$ ft/s	Measurement of time-mean heat transfer rate, high speed diesel engine at various manifold pressure	Same as before but has factors a and b for effect of manifold pressure and location in cylinder

Pflaum (8) (1962)	$\dot{q}_T = a(PT_g)^{\frac{1}{2}} P_i^{\,b}[6.2 - 5.2(5.7)^{-(.1\,V_p)^2} + .025\,V_p] \times [T_g - T_w]$	Measured local time-average heat flux using many thermocouples	Account for local variation and manifold pressure but still dimensionally incorrect
Elser (12) (1954)	$\dot{q}_T = \frac{ak}{D}(1 + b\frac{\Delta S}{C_p})(Re.Pr)^{\frac{1}{2}}(T_g - T_w)$	Theoretical analysis and measurements on 2-stroke and 4-stroke diesel engines using subsurface thermocouples. Applied dimensional analysis and resolved gas properties at $(T_g + T_w)/2$	No separate term for radiation but considered effect of rate of heat release by entropy change (S) per unit mass
Oguri (13) (1960)	$\dot{q}_T = \frac{ak}{D}(1 + \frac{\Delta S}{C_p})\,Re.Pr^{\frac{1}{2}}(2 + \cos(\theta - 20) \times [T_g - T_w]$	Accepted above correlation and modified by experiments on 4-stroke spark ignition engine using a true surface thermocouple	As above and introduced a term $\cos(\theta - 20)$ to account for gas motion. θ = CA degree ATDC
Overbye (14) (1960)	$\dot{q}_T = 3600\,\frac{k_i\,T_i}{L}\,(\frac{L.V_p\;_i\,Cp_i}{ki})(\frac{.26P}{r\,P_i} - 0.035) \times 10^{-4} + 0.1\,\frac{p}{r.P_i} - 0.02$	Measured instantaneous heat flux in spark ignition engines using a surface thermocouple	The driving temperature $T_g - T_w$ do not appear in the expression, i.e. an important factor ignored.
Taylor (11) (1957)	$\bar{q}_T = a.\,\frac{k}{D}(Re)^{.75}[T_g - T_w]$	Time-averaged data on large number of commercial engines (diesel and S.I. engines)	Valid only for time-mean heat transfer calculation. Account for radiation lumped form.

Alcock (19) (1961)	$\bar{q}_T = a \left(\frac{\text{Fuel flow rate}}{\text{Piston area}} \right)^{0.75}$	Time averaged data obtained by traversing thermocouples, in swirl, no-swirl and divided chamber diesel engines	Application limited to types of engines tested because poor injection inadequate airflow and fuel calorific value could significantly affect fuel flow and heat transfer
Brock and Glasspool (28) (1964)	In Alcock's equation, suggested index = 0.6	Same as above	Different index to account for different locations
French (29) (1964)	Suggested index = 0.7 - 1.2	Same as above	

that it must have two terms, to account for radiation and convection separately. He reasoned that because of the great difference in form of the radiant and convective heat transfer mechanisms, no relationship which lumped the two effects into a single term (e.g. Eichelberg's relationship) could prove adequate in describing heat transfer over any considerable range in operating variables. He also reasoned that in view of the difference in luminosity of spark ignition flames and diesel flames, some accommodation for these differences in the nature of combustion must be included, when considering the radiant heat transfer.

Annand expressed some concern over the question of whether or not the concept of an instantaneous heat transfer coefficient was rigorously correct. He discussed the work of Overbye (14) which showed a phase difference between the instantaneous heat transfer and mean gas-wall temperature difference. Fortunately the situation where heat transfer at the gas-wall interface occurs with driving temperature difference of zero (hence $\pm\infty$ heat transfer coefficient) is at positions in the engine cycle where low heat flow occurs and is relatively unimportant from a practical point of view.

After his review and critique of the previous correlations, Annand presented a new correlation based on dimensionless groups with terms to account separately for both the convective and radiative transfer. His expression had the form:

$$\dot{q}_T = \frac{a.k}{D} (Re)^b (T_g - T_w) + c (T_g^4 - T_w^4) \qquad (1.2)$$

Reynolds number was based on mean piston speed and cylinder bore, although the use of actual gas motion if available, was preferable for a more precise expression. The values of the empirical constant a, b, and c were obtained from analysis of experimental data

on instantaneous heat transfer for 2-stroke and 4-stroke diesel engines by Elser (12). Annand suggested on the basis of correlation a value for (b) of 0.7 while the values of (a) and (c) depend on the engine type and position in the cycle. Higher values of (a) were obtained for the 2-stroke engine, which most probably reflects the effect of higher gas motion and different flow patterns in this type of engine. Values of 0.35 to 0.8 were proposed for (a), the value of (a) increasing as air charge motion increases. For the constant (c), Annand suggested a value of $c = 0.0$ during the compression stroke.

For the combustion period and the expansion stroke with $c = 1.6 * 10^{-12}$ for diesel engine, and $c = 2.1 * 10^{-13}$ $Chu/ft^2 . k^4$ for spark ignition engines, Annand based his correlations on data from the compression and expansion strokes only and considers the correlation inapplicable for intake and exhaust processes.

In conclusion, Annand stated that although formula (1.2) is strictly inapplicable because of the phase lag between gas temperature change and heat flux variation which occurs because it is dimensionally consistent, and is compatible with a wide range of experimental data.

In a discussion of Annand's paper, Knight criticised the use of piston mean speed in Reynolds number. He concluded that in engine heat transfer calculations, some form of calculation must be made (on the basis of kinetic energy or momentum conservation) of the charge velocity variation with time. Hence the instantaneous heat flux is calculated and the mean (cycle averaged) heat flux can be readily computed.

Knight (16) put forward the concept of a "space mean velocity" defined as that corresponding to the total instantaneous kinetic energy of the gas charge in the cylinder. Based on the fact that gas boundary layer at the wall depends upon the instantaneous main stream gas velocity and the properties in the boundary layer, Knight computed the instantaneous heat transfer coefficient from the McAdams pipe flow correlations:

$$Nu = 0.023\ Re^{0.8}\ Pr^{0.4} \tag{1.3}$$

These results when compared with measurements using a sub-surface thermocouple were poor, the reason extended for this was wall roughness. Agreement between computed and experimental results was achieved when applying corrections which involved unacceptably large (0.3 - 0.5 mm p/p) roughness elements. Therefore it seems that the complete difference between the actual and calculated gas flow patterns in the engine is at the root of the matter.

Knight assumed radiation to be negligible compared to convection heat transfer, particularly at high engine speeds. Discussing this work, Annand suggested that influence of radiation was clearly described by the trend with which the multiplying factor (used in order to obtain agreement between the measured and calculated values) varied. The multiplying factor increased with increasing load and decreasing speed of the engine, which is the trend the radiant heat transfer is expected to take.

Annand and Ma (15), investigated the instantaneous heat transfer, using a new form of thin film thermocouple constructed on the cylinder head surface of a small 4-stroke diesel engine. Heat fluxes were measured at five locations for several engine speeds and fuel-air

ratios. In this investigation, the relationship:

$$\dot{q}_T = a \frac{k}{D} (Re)^{0.7} (T_g - T_w) + c (T_g^4 - T_w^4) \qquad (1.2)$$

from Annand (6) was examined. However, here the Reynolds number was based on bore diameter (D) and the energy mean velocity of Knight (16). The other significant consideration in this study was some compensation for the non-steady nature of heat transfer by adding to the above quasi-steady relation, a term involving the time derivative of the bulk mean temperature. The modified equation was:

$$\dot{q}_T = \frac{k}{D} (Re)^{0.7} \quad a (T_g - T_w) + \frac{a'}{w} \frac{d T_g}{dt} + c\sigma(T_g^4 - T_w^4) \quad (1.4)$$

Analysis of the experimental results, based on space averaged heat fluxes in terms of bulk mean properties yielded the following values for the coefficients: a = 0.12, a' =-0.2 and c = 1.5

It can be shown that the value assigned to (a) in Equation (1.4) is the same as the corresponding value in Equation (1.2). Taking the mean calculated value of gas velocity by conservation of kinetic energy (15) which is approximately equal to 4.2 times piston mean speed. Then $(4.2)^{0.7}$ x (a = 0.12) = 0.33, which compares with a = 0.38 proposed originally in Equation (1. 2) for low swirl engines.

Therefore, the significant difference between Equations (1. 2) and (1.4) are in the values of c and the introduction of $\frac{a' d T_g}{\omega dt}$ term.

The radiation term constant c = 1.5, is now 2.5 times larger than the value previously suggested. This reflects the fact that the actual radiation source temperature is much higher than the bulk mean

gas temperature T_g. It is felt, however, that this value of the constant c, would not compensate for the effects of the higher actual radiant temperatures raised to fourth power, e.g. in a diesel engine $T_g \simeq 1500^{o}K$ near TDC. Flame temperature $T_F \simeq 2000^{o}K$. Therefore $c\,T_g^4 = 1.5 \times (1500^{o}K)^4 = 7.5 \times 10^{12}$

while $T_F^4 = (2000)^4 = 1.6 \times 10^{13}$

The prediction of measured heat fluxes without and with the term $\frac{a'}{\omega}\frac{d\,T_g}{dt}$ is shown in Figs. (1.1) and (1.2) respectively. The improvement effected by the introduction of this term seems to compensate reasonably for the phase shift between the driving temperature and heat flux, particularly at the steep rise during early combustion and after combustion is complete.

Henein (18) studied instantaneous heat fluxes at the surface of the main chamber wall in a Lanova type divided chamber diesel engine. Local instantaneous heat fluxes evaluated from measured surface temperatures, were compared with predicted heat fluxes using Eichelberg's (5) equation (see Table 1.1). Good agreement for the compression stroke (Fig. 1.3) was obtained when instantaneous gas velocity rather than mean piston speed was used in the computation. The computed gas velocity was carried out using Alcock's method (19) based on momentum conservation from inlet valve closure. Fig. (1.4) shows the calculated gas velocity. It was noted that heat transfer coefficients calculated for the combustion and expansion period were much in excess of those predicted by Eichelberg's relationship using the instantaneous gas velocity. The author suggested that this effect was due to combustion induced gas motion leaving the energy cell, which was estimated to be about 500 m/s. An alternative reason, could be the possibility of flame front impingement on the surface thermocouple, and the contribution of radiation flux which is not accounted

for in the analysis presented. Support for this argument is given by the following tests, (Chapter 6).

Work of Le Feuvre et al (20). Le Feuvre, et al, measured the local instantaneous heat fluxes at up to eight locations within the cylinder volume of a 4-stroke, direct injection diesel engine. The tests covered a range of

Equivalent ratio $0 \leqslant \phi \leqslant 0.72$

Manifold pressures 30" Hg $\leqslant$ Pi vacuum $\leqslant$ 75" Vac.

Engine speed $1000 \leqslant$ RPM $\leqslant 2500$

Eight Bendersky (72) type surface thermocouples were installed where the heat flow paths were approximately one-dimensional and normal to the chamber surfaces. Output signals from the thermocouples were recorded on analog magnetic tape, and later an average cycle (over 50 cycles) digitised at every crank angle position. Data presented on local heat transfer rates shows large spatial and temporal variations throughout the cylinder. Values of the integrated time average heat fluxes were normally four times greater in the cylinder head area than in the cylinder sleeve. Peak rates of instantaneous heat transfer in the cylinder head deck area reached values as high as 5047 kW/m^2.

The average heat transfer rates in the cylinder head were shown to vary from 108 kW/m^2 under motoring conditions to 529 kW/m^2 at an equivalence ratio of 0.72. Supercharging (75" Hg inlet pressure) was shown to increase the average heat transfer in the cylinder head from 300 kW/m^2 (at 30" Hg) to 435 kW/m^2. The average rate of heat transfer in the head rose from 261 kW/m^2 to 423 kW/m^2 as the speed was increased from 1000 to 2500 rpm, while the average rates of heat transfer stayed relatively constant with a $\pm$ 10 degree variation in

fuel injection timing.

A point of interest worth noting is that the heat flux data of Le Feuvre, et al, showed strong local variation in magnitude, the position of the maxima depending on the conditions of operation (motored or fired) of the engine.

Le Feuvre presented predictions for instantaneous heat transfer rates obtained from the available heat transfer correlation in the literature, and compared these results with experimental data as shown in Figs. (1.5) to (1.8). Since all previously proposed models are for spatially averaged conditions, the correlation cannot produce a variation in heat transfer with location as was observed experimentally.

Except for the case of motored data, the correlations failed to predict the temporal variations which were obtained experimentally. The reason for the discrepancy observed in the fired engine is obviously due to the use of bulk mean gas temperature which is not adequate for prediction of local heat fluxes.

Le Feuvre also made attempts to fit two new heat transfer models to his experimental data. His first attempt was an unsteady compression-conduction model as had been used by Wendland (22). This model treated the cylinder volume as a group of separate masses which could transfer energy to one another through conduction heat transfer or work transfer. The model then could be solved iteratively with time as the independent variable and be used to predict the conduction heat transfer to the wall from the gas layer adjacent to the wall. This model predicted lower values than measured for the heat transfer under motored conditions, because application of the model to engine conditions ignored gas velocities parallel to cylinder head and piston surfaces.

The second type of model presented by Le Feuvre was a convective heat transfer model using the swirl as the dominant velocity, and radius from the axis of cylinder as the characteristic distance. Solid body rotation of the gas was assumed. The form of the correlation was:

$$\dot{q}_r = a \frac{k}{r} (Re)^{0.8} (Pr)^{0.33} [T_g - T_w] \qquad (1.5)$$

where $Re = \frac{r^2 \omega}{\upsilon}$

r = radius from bore axis

ω = swirl angular velocity

υ = kinematic viscosity

Since this form incorporates the radius to the location under consideration, it does predict spatial variations in heat flux. However, Le Feuvre, has assumed a constant swirl velocity throughout the engine cycle, although he pointed out that both squish and swirl velocities would be expected to vary with position. Therefore, an important factor in time variation of gas motion has again been ignored.

The value of 0.047 was suggested for the constant (a). Le-Feuvre found that this model would predict both the spatial and temporal trends observed in his motored engine runs over the range of engine operating conditions studied. Attempts to extend the correlation to fired runs were not as successful. The changes in the relative magnitude of local heat transfer rates could not be predicted by the model. Le Feuvre concluded that additional measurements would be required before a reliable model for diesel engine heat transfer could be developed. He suggested a need for information

concerning the spatial and temporal variation of local gas velocities in an operating engine and a need for reliable measurement of the radiant portion of the instantaneous heat transfer.

In the review so far covered, the inadequate representation of gas motion in the engine cylinder by mean piston speed or its functions, is an obvious weakness which appeared in most of the correlations discussed. In an attempt to obtain useful experimental data and to avoid the above weakness, Hassan, 1967 (37) studied the unsteady forced convective heat transfer under motored conditions, inside a specially designed pre-combustion chamber. Measurements were made of instantaneous gas velocity (using a constant-temperature hot wire anemometer) and the gas temperature (with the anemometer used as a resistance thermometer). Heat fluxes were computed from analysis of surface temperature records obtained with a thin film thermocouple. The tests covered a range of compression ratios (8.5, 9.8 and 11.5) at several engine speeds (600, 900 and 1100 rpm). It was shown that the experimental data could be represented by the relationship for forced convection from a flat surface:

$$Nu = C\, Re^{0.8} \qquad (1.6)$$

where values of theconstant C varied between 0.0276 to 0.0184, in order to account for the difference observed between the compression and expansion stroke. Hassan reasoned this difference was due to slight underestimation of gas temperature (because of finite thermal inertia of the sensor) on the compression stroke and vice versa on the expansion stroke.

Kim Dao, et.al (40), studied the instantaneous heat transfer on a motored engine cylinder head, under a range of operating conditions:

1. Engine speed (600 - 1200 rpm).
2. Compression ratio (8-14).
3. Intake pressure (14.5 - 30 psi).
4. Swirl ratio (0.0 - 7.5).
5. Shape of the piston top, that is, flat or with a cylindrical cavity.

An interesting approach in the correlation of the data was also attempted.

A heat flux meter consisting of a thin pyrex substrate (0.005 inch thick) having a thermistor ($3 * 10^{-6}$ inch thick) deposited on both faces was used. The similarity between a heat flow-temperature field and electrical flow-voltage field was applied to obtain the surface heat flux. Most of the data presented was said to have been obtained with a thin oil layer on the sensor resulting from the movement of the piston. Its effect was estimated to result in an amplitude reduction of the heat fluxes of up to 26% and a phase shift of about 7^{o}CA.

The importance of induction-induced charge motion as compared to piston generated gas motion effects (flat piston) on instantaneous heat flux was demonstrated. Fig. (1.9) is the heat flux trace for two successive cycles without induction process between. Although the smooth recompression trace indicates clearly the absence of intake induced fluctuations, the reduction in peak heat flux must be partially attributed to lower gas temperature and pressure in the recompression cycle because of loss through blow by and heat transfer. It can be shown that by accounting for the cylinder pressure change as shown in Fig. (1.9) with a drop of 6% in peak value, and using the gas temperature at the beginning of the recompression cycle (heat

loss calculated by a typical correlation, e.g. Annand's), the peak gas temperature in the recompression cycle is about 10% less than in the first cycle. Thus a drop of at least 10% in heat flux which is attributed to losses in the recompression cycle.

Data presented on swirl effects showed that, under high swirl conditions (described as being orderly flow with few eddies) heat fluxes were reproducible within 5% of peak value. On the other hand at low swirl conditions heat flux at TDC caried by as much as 50% from cycle to cycle and was characterised by spiky fluctuations which was explained by irregular flow with large eddies. Generally the peak heat flux increased with increase of swirl ratio as shown in Fig. (1.10).

Interesting data were reported on local heat transfer variation when a flat piston crown and a piston with concentric cylindrical cavity was used. In the case of a flat piston it was shown that with high swirl ratio, there was a large decrease in peak heat flux from $r = 0.3$ (cylinder bore = 3.125 inch) to $r = 0.8$ inch (Fig. 1.11), followed by an increase from $r = 0.8$ to $r = 1.46$ inch. The initial decrease was reasoned as due to eddies, while the increase in the outer region was explained by the increased linear velocity. The trend perhaps reflects the fact that a uniform solid body type of rotational motion does not exist with flat pistons. Fig. (1.12) compares heat fluxes obtained with and without cavity in the piston. Note that except in the central part of the cylinder head surface, where the heat fluxes at the last measured point ($r = 0.3$ inch) are about the same, the presence of a bowl enhances the peak heat flux in the annular space by about 25% and by about 100% near the outer radius of the cavity. The increase of heat fluxes in the annular region was explained by the additional turbulence created by the squish. The sharp increase in peak heat flux near the outer radius

of the cavity was reasoned by the eddies created at the edge of the bowl by the squish and by the increase in swirl velocity in the cavity. It was argued that 'if angular momentum is considered to be conserved, the angular velocity in the cavity must be about three times higher than the angular velocity in the annular space at near TDC.' This, however, is different to findings of Dent and Derham (62), Horvatin (67) and other workers in detecting approximately a solid body type of rotational motion.

The effect of engine speed, intake pressure and compression ratio on peak heat flux were as shown in Figs. (1.13) to (1.15) respectively, which reflects the direct effect of these parameters on the gas motion, gas temperature and pressure, hence directly upon heat flux.

The observed strong influence of compression ratio and engine speed on peak heat fluxes, suggested that the rate of compression work plays an important role in the energy transfer process. Therefore Kim Dao, et al, concluded that any method of calculation of the convective heat transfer rates in engines must as a minimum take into account at least two things:

1. The pressure variation with time.
2. The gas motion.

The generation of energy by combustion is a third important factor which was not considered in their investigation. Kim Dao presented a one-dimensional model described by a system of non linear partial differential equations (the continuity and energy equations). The model was based upon the concept of a large reservoir of gas having uniform, but time-dependant properties and exchanging energy with local elements of the wall surfaces through thin layers of gas by compression, expansion, condution and convection.

This model was approximated by a linear partial differential equation that could be solved analytically. The solution of the linearised equations yielded the following formula for the calculation of the heat fluxes:

$$\dot{q} = T_i \; K_w \sqrt{\frac{P_i \, \omega}{P_a \, \alpha_w}} \; (1 + K_T^*)(P^*)^{(2\gamma-1)} \; x \left[\frac{\bar{T}^* + K_T^*}{\bar{T}^* \; (1 + K_T^*)} \right]^{\frac{1}{2}} H(\tau) \qquad (1.7)$$

where:
$$H(\tau) = \frac{F(\tau)}{\sqrt{\pi}} \left[\frac{1}{\sqrt{\tau}} \; (1 - \frac{T_w}{T_i}) - \int_0^{\tau} \frac{dG}{d\eta} \; \frac{d\eta}{\sqrt{\tau - \eta}} \right]$$

$$F(\tau) = \text{Exp.} \left[- \int \frac{L}{P^* \; (1 + K_T^*)} \, d \right]$$

$$G(\tau) = \left[\frac{P^* \; (1 - \gamma)/\gamma}{T_i / T_w} - 1 \right] \frac{1}{F(\tau)}$$

$$\tau = \int_0^{t^*} P^* \; (1 + K_T^*) \, dt^* \quad \text{or} \quad t^* = \int_0^{\tau} \frac{1}{P^* \; (1 + K_T^*)} \, d\tau$$

A best fit of the data was used to calculate the parameters L and K_T^* which gave (L = 0.85) and:

$$K_T^* = 0.00156 \left[\frac{P_i}{P_a} \; \frac{C^2 \omega}{\upsilon_w} \; \frac{T_w}{T_i} \; \frac{r}{C} \; SR.CR \right]^{0.75}$$

$$x \; (\frac{S}{C})^{1/7} \; (\frac{T_w}{T_g})^{0.58} \qquad (1.8)$$

where: T_i, P_i = gas temperature and pressure at inlet

K_w, α_w, υ_w = gas conductivity, thermal diffusivity and kinematic viscosity at wall temperature T_w

K_T^* = dimensionless eddy-thermal conductivity,

P^* = gas pressure/ambient pressure (P_a),

$\overline{T}^*$ = dimensionless temp. $(\frac{T_w}{4} + \frac{3}{4}$ gas mean temperature $(T_g))$.

L = dimensionless constant, ω = flywheel angular velocity,

t^* = x time, S = distance between cylinder head and piston top,

C = S at TDC, r = radius from cylinder axis, η = dummy variable for τ.

The well known concept of Prandtl mixing length and eddy-thermal conductivity K_T' in pipe flows was used as a model for the interaction of the swirls with the walls. Thus the convective term for the effect of the swirl could be written as a conduction term in the energy equation as $-K_T' \frac{\delta T}{S \delta Y}$. This approach is promising, because it avoids the uncertainty caused by the application of heat transfer coefficient concept to the unsteady state heat transfer encountered in internal combustion engines, but others are introduced such as the variation of the mixing length with distance from the cylinder surface. However, due to the nature of the assumptions as related to the model used, the proposed formula is applicable only to flat combustion chambers with no combustion process. This renders it useless to the usually complex combustion chamber geometries and under normal operating conditions where combustion is present.

1.2.1(b) Correlations and measurements based on time-averaged heat transfer

To avoid confusion, the correlations reviewed in this section, are of two types. Those proposed by Woschni (2) and Sitkei (24) are for the prediction of instantaneous heat transfer in internal combustion engines, while those of C.F. Taylor (11), Alcock (19) etc. are to predict mean heat transfer rates. These investigators share in common the fact that the resulting correlations are verified by the measured time-mean heat transfer obtained either from energy balance, or by use of traversing thermocouples through the combustion chamber walls.

To calculate the instantaneous mean heat transfer coefficient in piston engines, Woschni (2) suggested the use of the correlation for forced convective heat transfer in pipe flow for gases:

$$Nu = 0.035\ Re^{0.8} \qquad (1.9)$$

Considering the changes in the properties of the gas with pressure and temperature, the following relationship was derived:

$$h = C\, d^{-0.2}\, p_g^{0.8}\, V^{0.8}\, T_g^{-0.53} \qquad (1.10)$$

Woschni indicated that, although the gas velocity is a function of piston mean speed, the exact functional relationship need not be the same throughout the engine cycle, and suggested the relation $V = a \cdot V_p$ where a is constant and varies for different parts of the cycle.

A series of experiments were done in which a 4-stroke engine was first run with every stroke a scavenging stroke (through use of a double lobed cam shaft) but supplied with hot air to simulate actual running conditions. The overall heat transfer rate measured provided Woschni with a scavenging heat transfer correlation:

$$\dot{q} = 110 \left[d^{-0.2}\, p^{0.8}\, (a.V_p)^{0.8}\, T_g^{-0.53} \right] (T_g - T_w) \qquad (1.11)$$

This scavenging correlation was then modified by adding the effect of compression-expansion processes in the motored engine. The difference between the scavenging process and the compression-expansion process obtained was in the intensity of corresponding gas motion.

Woschni suggests values of:

$a = 6.18$ for scavenging period

$a = 2.28$ for compression-expansion strokes.

Tests on the fired engine, resulted in larger measured heat transfer rates than those calculated from equation (1.11). Woschni argued that, due to the similarity of the scavenging and compression

process in both fired and motored engine (from the types of tests run), the excess heat transfer during the firing tests must be transferred during the combustion and expansion phase only. Woschni considered an additional combustion generated gas motion superimposed on the velocity caused by piston motion, to promote convective heat transfer during the combustion expansion phase. As a result of these tests, Woschni presented a correlation of the form:

$$\dot{q} = 110\, d^{-0.2}\, P^{0.8}\, T_g^{-0.53} \left[a\, V_p + b\, \frac{V\, T_g}{P_1\, V_1} (P - P_o) \right]^{.8} (T_g - T_w) \tag{1.12}$$

A value of 3.24×10^{-3} was recommended for (b).

Woschni suggested that radiant heat transfer would obey the law:

$$\dot{q}_R = \epsilon\, \sigma_o \left[\left(\frac{T_f}{100}\right)^4 - \left(\frac{T_w}{100}\right)^4 \right] \tag{1.13}$$

where ϵ is the emissivity of the radiating agent and σ_o is the Stefan-Boltzman constant. The radiation from the working gas (H_2O and CO_2) was considered negligible. Greater importance was attached to flame radiation and an emissivity of 0.6 for ϵ (determined on steady diesel fuel flames) was suggested to be used in Equation 1.13 along with the mean gas temperature instead of unknown flame temperature.

Woschni concluded that the importance of radiant transfer in diesel combustion chambers had been over-rated.

Sitkei (24) presented an anlysis of diesel engine heat transfer in which he divided the correlation of data into three parts:

1. Convection.
2. Gas radiation.
3. Flame radiation.

Sitkei started with the basic relationship for convective heat transfer for pipe flow.

$$Nu = \text{Const.} \times Re^{n} \tag{1.14}$$

and suggested a value of $n = 0.7$ on the basis of his experimental data. Furthermore, by taking the variation in k and μ as proportional to T_g and $T_g^{0.7}$ respectively, the following correlation for convection heat transfer was obtained:

$$\dot{q}_c = a\,(1 + b)\,\frac{p^{0.7}\,V_p^{0.7}}{T_g^{0.2}\,d_e^{0.3}}\,(T_g - T_w) \tag{1.15}$$

$d_e = \dfrac{4 \cdot V}{A}$ is the "equivalent cylinder diameter"

The factors $a = 0.033$ (based on motored engine results), and b ranged from 0.0 to 0.4 as engine air turbulence increased as a function of combustion chamber configuration. In a later publication Sitkei and Ramanaiah (23) suggested the following new values for these factors:

$$a = 0.04$$

and b varied for different types of combustion chambers as follows:

Direct combustion chamber (Hesselman type)	0 - 0.03
Piston chamber	0.05 - 0.1
Swirl chamber (toroidal bowl)	0.15 - 0.25
Precombustion chamber	0.25 - 0.35

Sitkei (36) in his analysis, claimed up to 80% of heat transferred to the walls of the diesel engine he studied, was accounted for by convection.

For gas radiation Sitkei considered the equation:

$$\dot{q}_{R.g} = \epsilon_g \, C \left[\left(\frac{T_g}{100}\right)^4 - \left(\frac{T_w}{100}\right)^4 \right] \qquad (1.16)$$

The value of ϵ_g, the non luminous gas emissivity, comes from an analysis of the instantaneous concentration of CO_2 and H_2O in the combustion products and emissivity charts, as presented by Hottel (51). His analysis of the potential for heat transfer from gas radiation yielded a value of 3.8% of the total.

For flame radiation Sitkei used:

$$\dot{q}_{R.f} = \epsilon_f \, C \left[\left(\frac{T_f}{100}\right)^4 - \left(\frac{T_w}{100}\right)^4 \right] \qquad (1.17)$$

Values for flame emissivity ϵ_f, were obtained from analysis of the emissivities of oil burner furnace flames. His analysis showed flame radiation responsible for 15.3% of the total engine heat transfer. However, in a recent study, Sitkei and Ramanaiah (23) modified the method of predicting radiation heat transfer in diesel engines, making use of measured radiation from precombustion chamber of a Steyr diesel engine. This will be covered in the following section.

In the above correlations, the constants in the expressions were determined by fitting the time-averaged properties in the correlation to steady heat balance data for the engine. In such an approach one must realise that, although the predicted heat flux integrated over the whole cycle may give the same result as measured time average transfer the temporal distribution of the instantaneous heat flux could be of any form. This fact could be noticed to some extent in Figs. (16a) and (16b), where the correlation of Woschni is compared with measured instantaneous local heat transfer coefficient of Elser and Kind (2).
While reasonable agreement is achieved for peak heat flux, the difference is significant at other parts of the cycle. Therefore, unless such correlations are verified by measured instantaneous mean heat fluxes, they should be used with certain reservation.

An interesting approach, though not relevant to unsteady heat transfer, was proposed by Alcock (21). The time average heat transfer rate was related to the fuel flow rate by a power law. The data were obtained with a special thermocouple probe which could be positioned at various depths in a blind hole from the outside of the combustion chamber wall and thus obtained temperature gradients and heat fluxes. Alcock presented extensive data of the variation of time averaged heat transfer rate as a function of location in the combustion chamber of spark ignition and diesel engines. He also varied engine load conditions and arrived at a correlation stating that the total heat loss (time averaged) was proportional to the 0.64 power of the fuel-input rate.

Alcock (26) 1961, in another investigation on non-swirl and swirl-type direct injection diesel engines, suggested the following relationship:

$$(\text{Local flux Chu/in}^2\ \text{hr}) = FF \times \left[\frac{\text{Fuel rate lb/in}^2\ \text{piston area hr}}{}\right]^{0.75} \qquad (1.18)$$

FF defined as heat flux factor which is different for various parts of the combustion chamber.

Similar relationships were reported by Brock and Glasspool (28) with index = 0.6, French (27) and French and Hartles (28) in which the power index suggested between 0.5-1.2 for various locations. It is obvious that application of such formulae is limited to the type of engine and the conditions under which the experiments are carried out, because poor fuel injection (inefficient combustion), inadequate air flow and the calorific value of the fuel are some of the variables which could alter the fuel flow considerably and the effect of these on heat transfer could be substantial. Also the index variations reported, are too wide for design purposes.

1.2.2 Radiation Related Measurements and Correlations

The study of this mode of heat transfer in internal combustion engines has taken a smaller share of the total amount of work carried out on study of heat transfer in these machines. This perhaps reflects the difficulties involved in measuring or estimating this quantity.

Nusselt (1), with his work on heat transfer in spherical combustion bombs, provided a starting point for much of the engine heat transfer analysis that was to follow. He studied the influence of radiation by using gold-plated or blackened iside-surface coating on the combustion chamber to explore possible differences with and without radiant heat losses and suggested the following expression for radiant heat transfer:

$$\dot{q}_R = C\ (T_g^4 - T_w^4) \qquad (1.19)$$

Use of the constant given with this expression will give radiant heat transfer, that is, the order of magnitude of 5% of the total heat transfer predicted by the complete Nusselt formula quoted in Table (1.1). In view of recent studies (to be discussed below), the figure may well be correct for S.I. engines, for which it was basically developed, but it is unlikely to be so for C.I. engines.

As part of a general investigation of combustion in spark ignition engines, Steel et al (30) investigated the radiant intensity from a region close to the spark plug and from the so called "detonation zone" using a sensitive antimony-bismuth vacuum thermocouple. The measured results of thermal radiation had no absolute significance. However, it was possible to make quantitative comparison of data. All observations on the engine indicated that infrared radiation from the gas explosion appeared very largely in the spectral regions characteristic of radiation from water vapour and carbon dioxide. It was stated that no appreciable energy relative to the total amount measured, was radiated by incandescent carbon particles, even with excessively rich mixtures giving bright red-yellow flames. This point proved the fact that carbon particle radiation is not significant in S.I. engines.

Myers and Uyehara (42) used a two colour pyrometer technique for the measurement of flame temperatures in a pre-combustion chamber diesel engine. To obtain temperature Myers and Uyehara compared the relative intensities of two wavelengths in the visible and near infrared. This relative intensity ratio combined with Hottels (43) data on the emissivity of carbon particles as a function of wavelength, allowed the calculation of apparent radiation

temperature. The temperatures reported by Myers and Uyehara were in the range 2111°K to 2250°K, and were relatively constant for a time period of 50 or 60 degrees of engine crank rotation after TDC. Most sources agree that the luminosity of diesel flame was caused by the radiation from carbon particles formed in the flame.

In a study designed to explore the infrared emission spectra for diesel and spark ignition engine combustion reactions, Lyn (31) found that during the combustion and the early part of the expansion period in a diesel engine, emission from the carbon particles in the flame was very high. The relative emission from the combustion chamber was presented as a function of wavelength and time during the engine cycle. Only relative values could be presented because of the uncertainties in transmissivity of the combustion chamber window deposits. Lyn's data demonstrated that the radiation emitted by the carbon particles in the engine formed a continuous spectral distribution of an intensity between wavelengths of 1–5μ, such that the non luminous gas radiation due to CO_2 and H_2O was obscured. Fig. (1.17) shows the spectra obtained with 80 psi BMEP and 1100 rpm using gas oil. Lyn compared the relative intensity versus wavelength dispersion from the diesel combustion with the data generated by use of Hottel's correlation describing the wavelength dependance of carbon particle emissivity, and a common radiation temperature for all wavelengths substituted into Wein's Law. The comparison of the data revealed that, with the values of optical thickness that Lyn assumed, Hottel's model for hot carbon particle emission would not explain the measured intensity variation as a function of wavelength. After making this comparison, Lyn resorted to the evaluation of what he called "distribution temperature". He noted that if his data were plotted showing $\text{Ln}\ (I_\lambda \cdot \lambda^5)$ versus $1/\lambda$, a straight line was obtained (Fig. 1.18) over the region between 1 μ and 2.4 μ.

This fact, along with analysis of the equation for emission from a grey body using Wein's Law yielded the following relationship:

$$L_h\ (I_\lambda \cdot \lambda^5) = -\frac{C_2}{T_R}\left(\frac{1}{\lambda}\right) + \text{Const.} \qquad (1.20)$$

The slope of the curve in the logarithmic plot could be used to evaluate apparent temperature. Analysis of the slopes of these plots yielded temperatures as high as 1960^{o}K during combustion. These results are somewhat lower than those reported by Myers and Uyehara (42).

In contrast, Lyn's measurements on the flame of spark ignition engines showed almost no continuous spectra. The radiation detected was related to specific spectral lines of such components as water vapour, carbon dioxide, and hydrocarbon combustion intermediaries, as reported by Steel (30).

Although Lyn's data could not be used for the calculation of potential radiant heat transfer, they did point to the fact that the continuous emission of the carbon particles was more likely to be of importance to radiant heat transfer than the banded gaseous emission.

Ebersole et al (32) made measurements of the value of the steady state ratio of radiant heat transfer to total heat transfer rates in an open chamber two stroke diesel engine. To accomplish this, a plug containing a surface thermocouple was placed in the cylinder head deck of the engine. The steady state rates of total heat transfer to the head were determined by measuring the temperature difference across the plug. Data were taken at various fuel air ratios and a constant speed with the engine inlet manifold pressure at 39 inch Hg.abs. The plug was then replaced by a similar surface thermocouple but with the couple junction shielded from conductive

and convective heat transfer by a sapphire window, so that only the radiative component of heat transfer could be detected.

Ebersole's data for the radiant to total heat transfer ratio, when plotted against engine power output is shown in Fig. (1.19). The ratio rises to 40% at about 85% of the engine's rated output for the 1200 rpm operating speed. Tests were run with both a n-heptane oil mixture and a No. 2 diesel fuel. Also included were tests using thermocouples with clean metal surfaces and soot covered surfaces. The results of the tests revealed that the radiant to total heat transfer ratio was higher when the soot covered thermocouples were used, and that the ratio was also higher for No. 2 diesel fuel than for the heptane oil mixtures.

The results of Ebersole's tests indicate that radiation should be considered a significant contributor to total engine heat transfer. Also of note was the fact that the results obtained with the clean and soot covered thermocouples agreed with what one might expect and theoretically predict assuming that the soot covered surface exhibits a higher emissivity than the clean metal surface and therefore, absorbed a greater amount of the incident radiant energy. The results of the tests with different fuels also tend to agreed with the well established fact that the normal paraffins are lowest of all hydrocarbons in their affinity for smoke or carbon particle formation, of course accepting that most of the radiant emission in the engine arises from carbon particle radiation.

Oguri and Inaba (33) used a technique similar to Ebersole's (32), but, measured the instantaneous rate of radiant heat transfer and simultaneously measured the total rate of heat transfer by similar unshielded thermocouples. In order to avoid errors due to

soot accumulation on the viewing window, Oguri resorted to sudden firing and loading of the previously motored test cylinder and applied a correction to the transient signal which was superimposed on the steadily rising mean surface temperature signal. The data obtained for three direct injection, medium and high speed diesel engines of differing sizes confirmed, once again, the importance of the radiant heat transfer in the diesel engine. Comparison of the measured radiation heat fluxes with calculated values using the radiant term in the original formula recommended by Annand (6) showed good agreement (Fig. 1.20) except in the case of the supercharged engine, where the low mass averaged gas temperature resulted in low calculated values. The ratio $\dot{q}_R/\dot{q}_T$ increased continuously with IMEP for the sooty thermocouples. For the clean thermocouples this ratio increased initially with IMEP but levelled off at higher load conditions. This was probably due to the fact that the change of the detected radiant heat flux with increasing load did not exceed the one for total heat flux. Fig. (1.21) shows the ratio $\dot{q}_R/\dot{q}_T$ plotted as a percentage of the engine maximum IMEP. It indicated that larger and higher output engine curves lie above the ones for smaller and lower output engines. The result suggests radiation heat loss could be very significant in large, slow speed engines where convective transfer is expected to be low because of low air motion.

Sitkei and Ramanaiah (23) made an attempt to improve the prediction of instantaneous heat transfer and in particular, the radiant heat transfer in diesel engines. Through detailed calculations, they suggested that gas radiation is a negligible part of the total heat transfer, but considered flame radiation to be relatively significant and therefore cannot be ignored as suggested by some researchers, Knight (16) and Woschni (2).

Sitkei's approach was based on estimating the radiating flame emissivity and its variation with time. Assuming the flame a grey body, he measured the black body temperature in the pre-combustion chamber of the diesel engine using a quick response photo-electric pyrometer. The actual flame temperature was not measured, but after a survey of the relevant literature which, according to Sitkei, revealed that flame temperatures in different engines are nearly of the same magnitude and vary little with load, he accepted flame temperatures measured by Belinskiy (25) in a small (140 mm bore) open chamber diesel engine with minor modification near TDC, (using two colour method and assuming grey body radiation). Hence, flame emissivity as a function of both time (CA degree) and load (excess air ratio) was calculated by:

$$\epsilon = \frac{T_b^4}{T_f^4} \qquad (1.21)$$

The results thus obtained for the precombustion chamber were generalised by expressing emissivity as follows:

$$\epsilon = 0.8 \ (1 - e^{-kPL}) \qquad (1.22)$$

and a factor k known as "absorption factor" was calculated as a function of time and load, Fig. (1.22). These values of k, which correspond to measurements from the precombustion chamber, were said to be universally applicable for all designs of engines operating with various load conditions. Calculated flame emissivities in the main chamber of a Styer engine and the corresponding flame radiation heat transfer are shown in Figs. (1.23) and (1.24).

Sitkei concluded that radiant heat transfer in diesel engines is mainly due to carbon particles and amounts to 20-30% of the total heat transfer at full load. Flame emissivity, in the main combustion chamber increased with load, whereas in pre-or swirl-combustion chambers, flame emissivities increased up to a certain load and then decreased. This decrease of radiation was believed to result from excessive radiation absorption by increased concentration of decomposed hydrocarbon at heavy load.

Work of Flynn et al (34). A most significant and up to date experimental work on investigation of the radiant heat transfer in diesel engines was carried out at the University of Wisconsin by Flynn et al (34). An instrument and data reduction system were developed to obtain instantaneous rates of radiant heat transfer within an operating direct injection diesel engine. Data were obtained over a speed range (1000 - 2500 rpm), load (equivalent ratio 0.23 - 0.749), inlet manifold pressure (30.1 - 75.4 inch Hg.abs) and fuel injection timing (10 - 30^{o} CA BTDC). Data were also obtained with different fuels and fuel additives.

A photo-conductor sensor and infrared monochromator were chosen for intensity measurement and wavelength identification. The value of the absolute monochromatic emission intensity at any instant was measured with reference to a tungsten filament radiation source, so that obscuration of windows by soot were accounted for in the calibration.

The data, as extracted by the acquisition system, took the form of seven distinct emission measurements at seven different wavelengths (1, 1.5, 2, 2.5, 3, 3.5 and 4μm), averaged over 50 cycles, for each crank angle of engine rotation. These seven emission

values represented points on a curve describing emission as a function of wavelength. In order to obtain the Emissive Power (radiant heat transfer) from the combustion products, Flynn abandoned the idea of evaluating the area under the spectral emission curve by numerical integration technique for the following reasons:

1. Limited accuracy when obtaining the integral with only seven points representing the emission-wavelength relationship.

2. No information could be gained concerning the apparent radiant emission temperature or emissivities which are concealed in the emission intensity-wavelength distribution of the radiating agent.

Instead he attempted to fit various forms of radiant emission models to the available data in order to extract further information. The attempt to fit a grey body emission model was not satisfactory, but a very good fit of the data was obtained with an emission model proposed by Hottel (43) for a system of very small particles in thermal equilibrium described by:

$$\epsilon_\lambda = 1 - e^{(-kL/\lambda^{0.95})} \tag{1.23}$$

This formula was combined with Planck's radiation distribution function to obtain a relationship for energy emission as a function of wavelength:

$$E_\lambda = (1 - e^{-kL/\lambda^{0.95}}) \left[\frac{C_1}{5 \left(e^{C_2/\lambda T_R} - 1\right)} \right] \tag{1.24}$$

This relationship was then used to obtain the radiating temperature and values of the apparent optical thickness (kL) which yielded a fit to the seven observations for each crank angle position. Once fitting the model to the experimental data was established, a closed form solution of the integral of the model over all wavelengths (0 - ∞) proved unsuccessful. Therefore Flynn resorted to a numerical technique to determine the model integral over the wavelength range between 0.5 μ to 10 μ which contained nearly 95% of the energy emitted by the particles. The numerical integral was combined with the numerical integral of Planck's radiation distribution function over the same wavelength interval to extract an apparent emissivity as shown below:

$$\epsilon_a = \frac{\int_{0.5}^{10} (1 - e^{-kL/\lambda^{0.95}}) \left(\frac{C_1}{5\,(e^{C_2/\lambda T_R} - 1)} \right) d\lambda}{\int_{0.5}^{10} \frac{C_1}{\lambda^5\,(e^{C_2/\lambda T_R} - 1)}\, d\lambda} \qquad (1.25)$$

This apparent emissivity was then combined with the apparent temperature to calculate the emissive power (radiant heat transfer rates) by:

$$\dot{q}_R = \epsilon_a \sigma T_R^4 \qquad (1.26)$$

A further attempt was made by Flynn to overcome the difficulty faced in obtaining a closed form solution for the emission model integral. His analysis of the pseudo-grey emissivity integral suggested, to a good approximation, that emissivity (ϵ_a) is a unique function of the product of T_R kL. The function, thus obtained, took the following form:

$$\epsilon_a = -10.04 + 6.092\ \mathrm{Ln}(T_R\ kL) - 1.36\ (\mathrm{Ln}(T_R\ kL))^2 + \\ + 0.1315\ (\mathrm{Ln}(T_R\ kL))^3 - 0.004546\ (\mathrm{Ln}(T_R\ kL))^4 \qquad (1.27)$$

Therefore, the combination of the expressions for ϵ_a and $\dot{q}_R$ allowed the direct evaluation of emission power once values for T_R and kL were known.

The engine observations showed radiant emission from the combustion process within a diesel engine to be significant. Figs. (1.25) to (1.29) show the experimental results of instantaneous radiation emission, extracted kL, T_R, emissivity and heat release as affected by operating conditions. Radiant temperatures as high as 2395^{o}K and peak emission rates (1640 kW/m^2) (nearly equivalent to that of a black body at this radiant temperature) were observed. The apparent time averaged radiant heat transfer rate increased with increased inlet manifold pressure at fixed F/A, nearly proportionately. Injection timing advance showed large increase in emission rates which appeared to be associated with corresponding changes in the engine cycle temperature history.

Data from runs in which engine speed was varied yielded increasing apparent time averaged rates of radiant heat transfer as engine speed was increased up to 2000 rpm. Above this speed the emission rate ceased to increase. The increased time-averaged heat transfer with speed is not surprising as the duration (in terms of CA degrees) of high radiation increase correspondingly, if one associated a more or less fixed time interval for combustion. The radiant transfer may cease to increase at higher speeds by less efficient combustion of soot formed because of the short time available. Tests varying the F/A while holding other variables constant, indicated a sharp rise in emission as F/A was increased

to an equivalent ratio of 0.514. At an equivalent ratio above 0.514 the emission rate was observed to drop sharply. The observed trend may be explained by the fact that the spray orientation used, would result in air-fuel mixture zones in the viewing field, much richer than the overall mixture. Hence increased soot concentration under the high cylinder pressures, according to Macfarlane and Holederness (45) and Kunitomo (46), which prevent transmission of the radiant emission from the hotter particles in the reaction zone to the detector.

The foregoing discussion suggests that, in addition to the problem of the formation of carbon particles under the transient conditions in the engine, we must also consider that of combustion of the particles.

Tests with No. 2 diesel fuel and 50/50 blend of secondary diesel fuels yielded nearly equivalent emission rates, while a test run with normal heptane produced lower emission rates, as had been previously shown by Ebersole (32). Rotation of the nozzle hole pattern relative to the viewing access port indicated increased emission rates when no fuel was deliberately injected into the viewing hole.

Under all operating conditions, the peak values of radiant heat transfer were significant (20% - 50%) compared to peak values of total heat transfer measured in the same engine with slightly different combustion chamber by Le Feuvre (20). The time average values of radiant heat transfer amounted to approximately 20% of the time average total heat transfer reported by Le Feuvre. This ratio is low compared to Ebersole's findings of up to 40% and it was reasoned to be the difference in combustion chambers employed by Le Feuvre and Ebersole as well as their specific observation locations

in the combustion chamber in relation to viewing field and local gas motion.

Flynn et al indicated that extensive analysis of the data uncovered no basic method for predicting values of apparent radiant temperature and optical path length as a function of time during the engine cycle. Therefore an empirical function for the instantaneous radiant emission was fitted to the engine observations using a form similar to the Wiebe function used for heat release rate correlation. The correlation function was as follows:

$$\dot{q}_R = (2\,\bar{q}_R)\,(b)\,(a+1)\left[\frac{t - t_1}{360}\right]^a \exp\left[-b\left(\frac{t - t_1}{360}\right)^{\alpha+1}\right] \qquad (1.28)$$

The values for the $\bar{q}_R$, a, b and t_1 parameters were fitted with interpolation formulae including first and second order terms in each of the independent variables used in the test runs (e.g. engine speed, inlet manifold pressure, etc).

The above function was used by Flynn et al to serve as a distribution function with the shape desired for correlation. Thus the interpolation formulae which are fitted to the results obtained by Flynn, are applicable only to the engine used, and will have to be modified for any other application.

Finally a comparison of the results obtained by Flynn with the results of Oguri and Sitkei, showed that under normal operating conditions, the radiant emission starts rising between 10-5° CA BTDC with peak values attained between TDC to 10° CA ATDC in the case of Flynn's tests, compared to emission increase at 5 to 10° CA ATDC with peaks between 20 to 40° CA ATDC in the case of Oguri and Sitkei's observations. This fact raises some doubts about the sensitivity of the detection devices used by Oguri and Sitkei. The other possibility

is that radiant emission from precombustion chambers, as observed by Sitkei, may behave differently from the main chamber because of the rich mixtures involved which affect ignition delay.

1.2.3 Theoretical investigations

Many theoretical researches are reported on periodic heat transmission in reciprocating engines. The majority have considered the problem as one of heat conduction through the engine cylinder head and liner walls. A few have considered the convective and radiative aspects of the problem.

1.2.3(a) Heat transfer considering conduction in the solid wall

The familiar one-dimensional Fourier equation for unsteady heat transfer is:

$$\frac{\delta T}{\delta t} = \alpha \frac{\delta^2 T}{\delta x^2} \qquad (1.29)$$

where: $\alpha = \frac{k}{\rho c}$ is the thermal diffusivity of the solid material.

Now, if the time variation of the wall surface temperature is known, then a solution of Equation 1.29 is possible, from which the calculation of periodic surface heat flux follows. Equation 1.29 is a second order partial differential equation which requires two boundary conditions for its solution. In engine work, because the transient heat transfer is required, the inner surface temperature with time is used and the outer wall temperature in addition to the assumption of one-dimensional heat flow. However, the surface temperature variation due to cyclic changes in the gas is not readily predictable (see below), but reliance has been on experimentally recorded surface temperature to obtain actual heat flux at the surface.

This approach is made to evaluate the experimental heat fluxes (Appendix A).

1.2.3(b) Heat transfer considering the gas region

The theory of heat transfer in the cylinder gases has been tackled by few researchers. Pfriem (10) investigated widely the problem of non-steady heat transfer from the working gases and laid the foundation to this theme. Elser (12), improved Pfriem's results and was able to compare the results of theoretical calculations with his own experiments. Both Elser and Pfriem calculated the heat flow to the metallic wall from the gas zone assuming adiabatic compression and expansion. Recently Oguri (13) extended the investigation to include heat generation in the gas at constant volume as the case in spark ignition engines. The calculated results showed fair agreement with the experimental results. Jacob (53) has treated the case of periodic change in the temperature of a medium in contact with the plane surface of an infinitely thick plate. As the simplifying assumptions made by Jacob, were all those used in deriving equation 1.29, from the general equation for energy within a control volume, the results of the analysis were purely of theoretical interest. Elser's analysis makes the same simplifying assumptions except that the pressure work and internal energy conversion are not taken as zero, but assumed to vary periodically with time. Thus the energy equation for a small control volume becomes:

$$\frac{\delta T_g}{\delta t} = \alpha_g \frac{\delta^2 T_g}{\delta x^2} + \frac{1}{(\rho c)_g} \frac{\delta P}{\delta t} + \frac{\dot{q}_i}{(\rho c)_g} \qquad (1.30)$$

At a great distance from the wall, conduction is zero. If the gas temperature $T_{g\infty}$ in this region is:

$$T_{g\infty} = T_{\infty} \sin \omega t$$

it is possible to continue and obtain a solution to equation using continuity at the wall ($T_g = T_w$ and $k_w \frac{\delta T_w}{\delta x} = k_g \frac{\delta T_g}{\delta x}$ at $x = 0$) as a boundary condition. The procedure is summarised by Overby et al (14). The result of the analysis showed that:

1. The wall surface temperature is in phase with gas temperature at a great distance from the wall and is a miniature replica of it.

2. The heat flux through surface leads both gas temperature and surface temperature by exactly $\frac{\pi}{4}$.

However, the later derivation will lead to positively and negatively infinite values of h if the steady state definition of heat transfer coefficient is used.

$$\dot{q} = h \, (T_{g\infty} - T_w) \; x = 0 \qquad (1.31)$$

It must be pointed out that the assumptions made in the above analysis are very unrealistic, in that they consider the gas density to be constant. However, development of the basic theory has helped to some extent in understanding the mechanism of unsteady heat transfer in IC engines in respect of the effect of different parameters on heat transfer and in showing the presence of a phase lag between heat flux and the driving temperature.

Due to the difficulties involved in the exact solution of unsteady heat transfer problems, which require many unrealistic simplifying assumptions, Elser (12) concluded that valid quantitative data on the non steady heat transfer in IC engines can only be obtained

experimentally. Therefore, Elser and other workers have resorted to dimensional analysis to define relationships between the engine heat transfer and certain selected variables. The most recent empirical equations obtained on the basis of dimensional analysis and experimental results are those proposed by Annand (6 and 15) and Le Feuvre et al (20).

1.3 Summary of Discussion and Conclusions

The majority of the formulae discussed so far with the exception of Le Feuvre's (20), are for prediction of mean instantaneous heat transfer rates for the whole combustion chamber surface. Therefore it is expected that measured local heat transfer rates will not be predictable by most of the correlations, even if used for some engines on which the correlations were originally established. This was clearly demonstrated by Le Feuvre as in Figs. (1.5) to (1.8). Comparison of the predicted heat fluxes in engines by various correlations, were also presented by Woschni (2) as in Fig.(1.30), by Walker (36), as in Fig.(1.31) and by Hassan (37) as in Fig.(1.32). The wide variation observed of predicted heat flux is not surprising if one considers the following facts:

a) Dimensionally incorrect correlations (e.g. Nusselt's and Eichelberg's) applied to engines operating under conditions far removed from those under which the correlations were obtained.

b) Correlations based on dimensional analysis, such as Annand's and those based on pipe flow heat transfer such as Woschni's, appear more hopeful, but in the use of piston mean speed in evaluating Re, they do not account accurately for spatial or temporal variation of gas velocity during the cycle.

c) The relative importance attached to radiation heat transfer varies in each correlation, e.g. Woschni and Knight did not consider radiation to be significant, while Eichelberg accounted for radiation in lumped form with convection. Others (1, 6, 23) considered radiant heat transfer relatively important in diesel engines and expressed it by a separate term.

The prediction of the radiant heat transfer component also involves difficulties. The factors that control the radiant heat transfer (e.g. flame shape and its absorption coefficient and the effective radiant temperature) are not readily predictable and their variation with time in the diesel engine is not yet accurately known. It is worth remarking here that conditions (pressure and rate of heat release) in small high speed engines are very different from those found in boiler furnaces, so that direct application of furnace flame data is not possible. Nevertheless, the results obtained by Macfarlane and Holderness (45) and by Kunimoto and Kodama (46) on luminous flames of liquid fuels under steady conditions, represents a practical demonstration of the effects of pressure and excess air on carbon formation and radiation. The combined effects of pressure and excess air (α) on soot formation may give an insight into the mechanism of diesel engine combustion so far as radiation is concerned. Fig.(1.33) illustrates the variation of flame radiation with the equivalent ratio, at four operational pressures, obtained by Macfarlane and Holderness (45) for atomized kerosene flames. It is interesting to note that the intensity of flame radiation decreases with very rich mixtures, due to the absorption effect of the carbon particles and decomposed hydrocarbon molecules. This trend was observed by

Flynn et al (34) at high equivalence ratio.

Kunitomo and Kodama (46), computed average flame absorption coefficients and the average non-luminous absorption coefficients as a function of excess air ratio and pressure which are shown in Fig.(1.34). The workers claimed close agreement with experimental measurements and had no doubt about the applicability of the calculation procedure to pressures larger than 20 atmospheres. Application of their method and correlations require knowledge of excess air factor, which is expected to vary locally in diesel engines. However, calculations on the assumption of homogeneous mixtures of excess air factors 0.8, 0.9, 1.0 and 1.15 produced the following results.

Excess Air Factor	Absorption Coefficients m^{-1}		Overall Emissivity
	Gas	Flame	
0.8	0.45	328	1
0.9	0.5	50	0.966
1.0	0.51	15.5	0.622
1.15	0.46	1	0.06

It is interesting to note the high emissivities for rich mixtures and the sharp drop when excess air (weaker than stoichiometric) is available for reaction, thus minimising soot formation. The observation of high emissivities in diesel engines (23 and 34) normally running with excess air factor $\gg$ 1.15, suggest presence of rich (ϕ>1) mixture zones during combustion.

In the foregoing review and discussion of the previous work on unsteady heat transfer, the following conclusions may be drawn:

1. A correlation to predict accurately the spatial and temporal variation of instantaneous convection heat transfer in various

reciprocating engines does not exist. In order to arrive at such correlation, experimental and theoretical information concerning spatial and temporal gas velocities and effective temperatures within the engine is needed.

2. Although there have been differences in opinion concerning the relative importance of various modes of heat transfer in the diesel engine, recent investigations show that radiant heat transfer may be significant. The effect of gas motion on radiant heat transfer through lower soot formation and its effect on enhancing convection require further investigation, in order to verify the expected effect on reducing the (radiant/total) heat transfer as gas motion increases.

3. Need for a satisfactory model of the combustion process, that would enable both the rate of burning and the development of the flame shape to be predicted. Also more information on soot formation-combustion processes which affect flame emissivity under engine conditions is needed.

1.4 Objectives

The overall objective of this study is to contribute in better understanding of instantaneous heat transfer in diesel engines and to suggest a method for accurate prediction of spatial and temporal heat transfer utilising measured local instantaneous gas velocities. Also, to determine the relative importance of radiation heat transfer. In order to accomplish this, the following tasks were undertaken.

1. Design and develop a device for the determination of total local instantaneous heat transfer at various points in the combustion chamber.

2. Devise a system for the determination of instantaneous radiation heat transfer based on current advances in infrared technology.

3. Obtain experimental data on instantaneous heat transfer at various locations on cylinder head and piston crown, over a wide range of engine loads, speed.

   Obtain data on instantaneous radiation heat transfer taken in the same engine and under the same conditions above.

4. To establish methods of predicting instantaneous convective and radiative heat transfer.

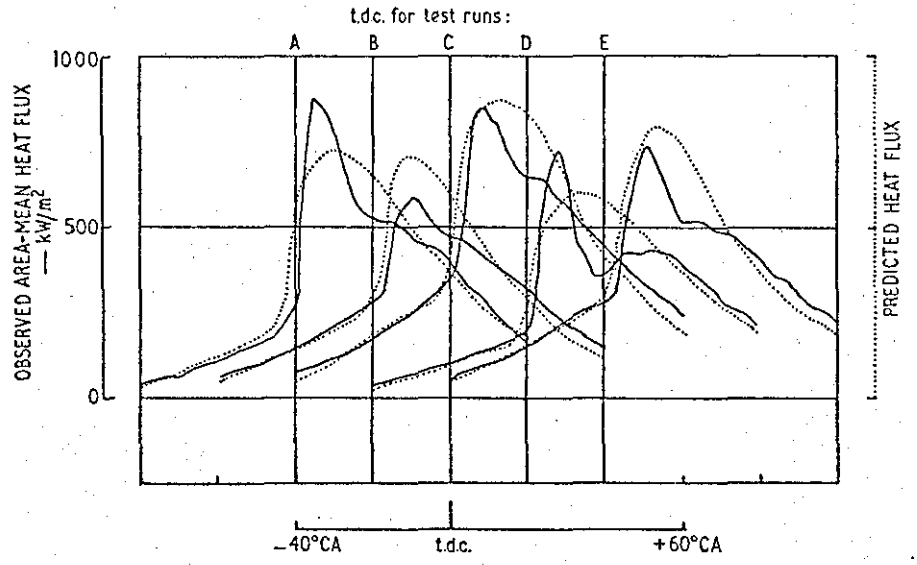

Fig.1.1 Observed heat fluxes compared with prediction by Annand's equation (1.2) (without term $\frac{a'}{w}\frac{d\,T_g}{dt}$) Annand and Ma (15)

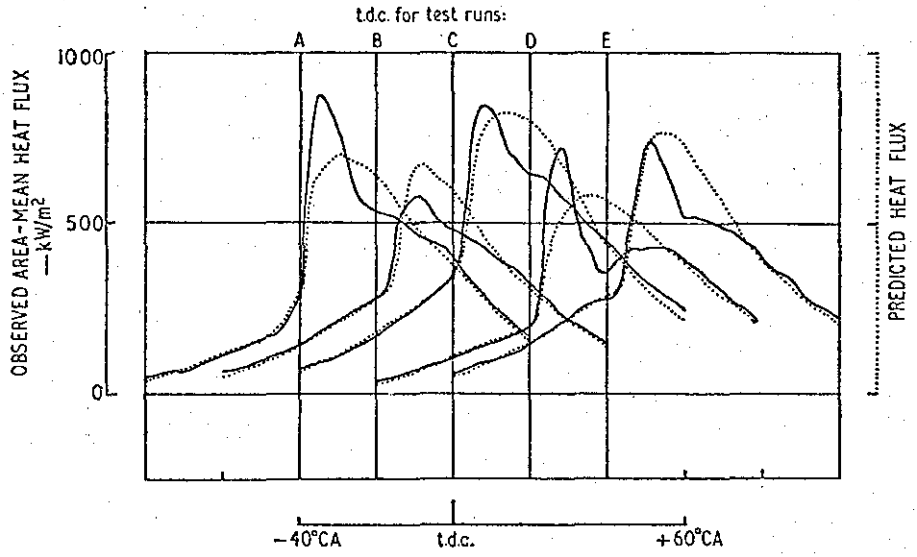

Fig. 1.2 Observed heat fluxes compared with prediction by Annand's equation (1.4) (with term $\frac{a'}{w}\frac{d\,T_g}{dt}$) Annand and Ma (15)

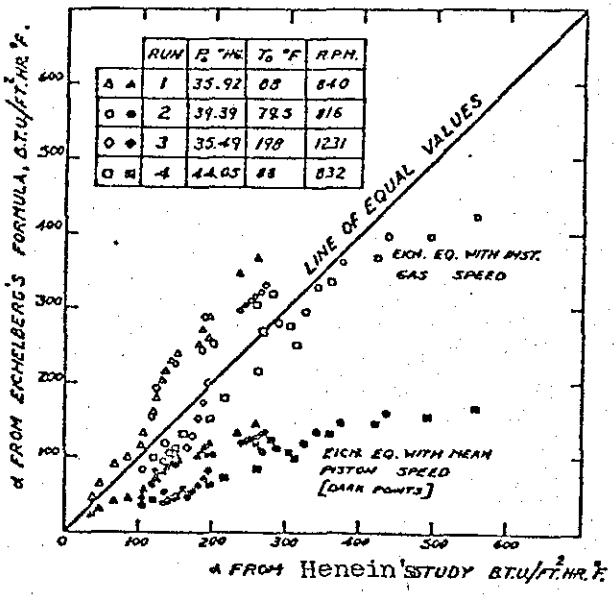

Fig. (1.3) Experimental heat transfer coefficient versus prediction by Eichelberg's equation using calculated instantaneous gas velocity or piston mean speed. Henein (18).

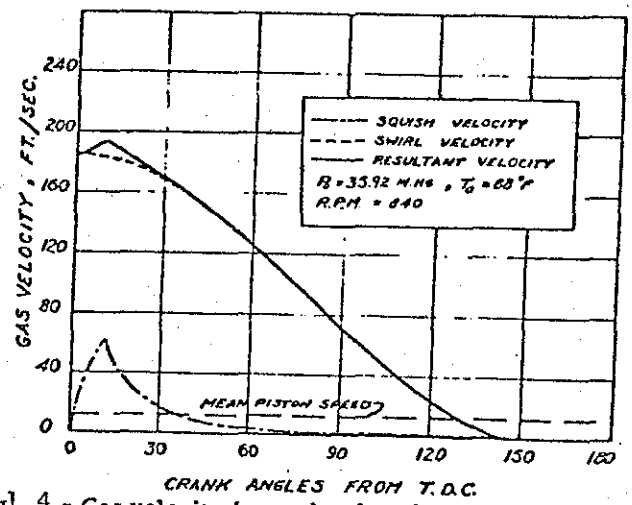

Fig. 4 - Gas velocity in combustion chamber due to primary turbulence Henein (18)

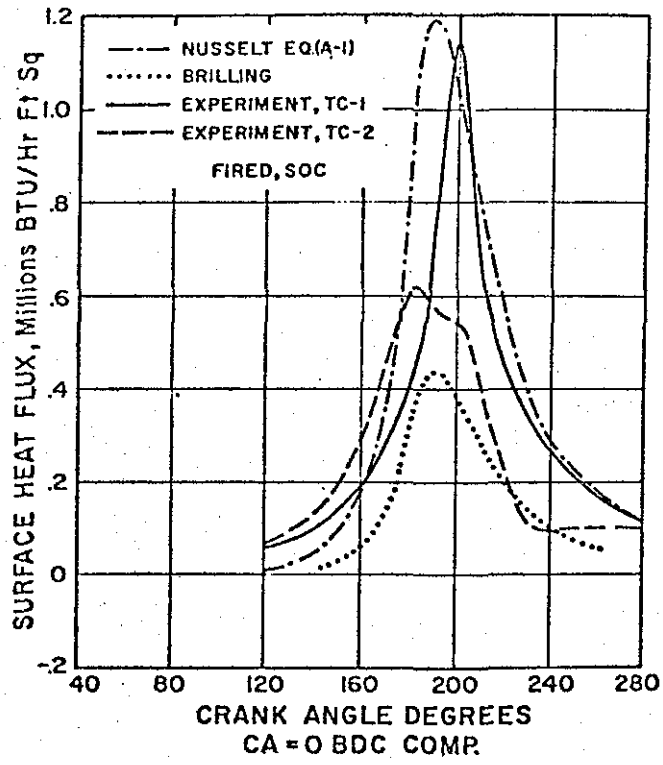

Fig.1.5 - Comparisons of predictions of Nusselt and Brilling with experimental data from cylinder head for fired operation

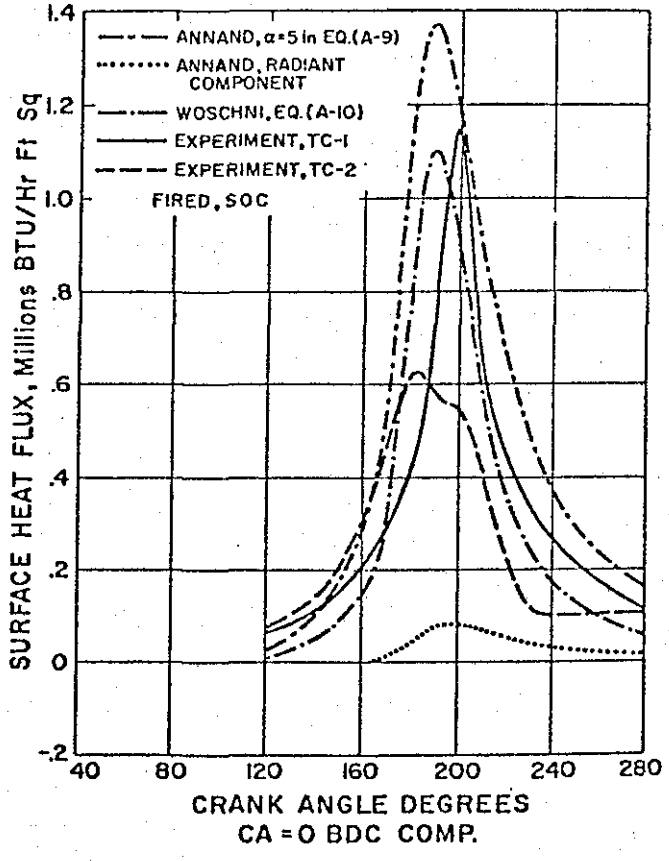

Fig.1.6 - Comparisons of predictions of Annand and Woschni with experimental data from cylinder head for fired operation

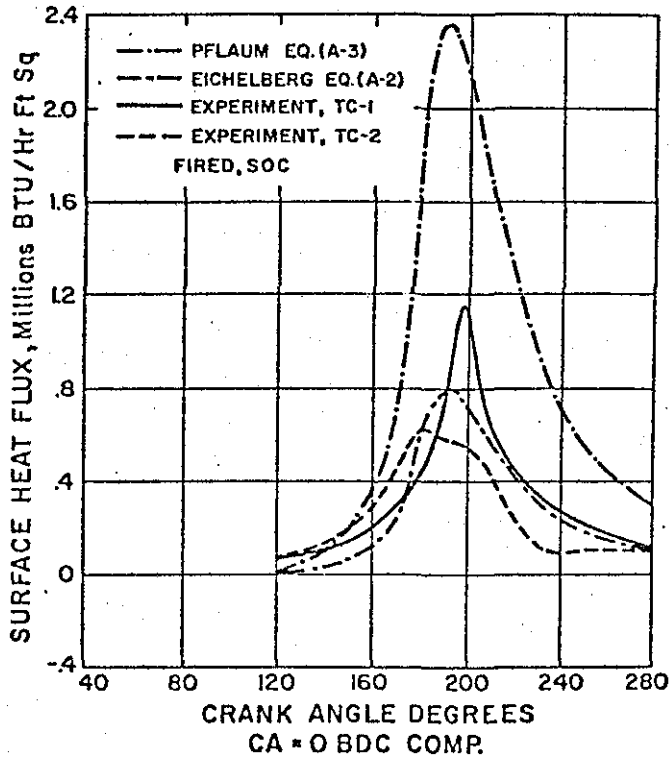

Fig.1.7 - Comparisons of predictions of Eichelberg and Pflaum with the experimental data from cylinder head for fired operation

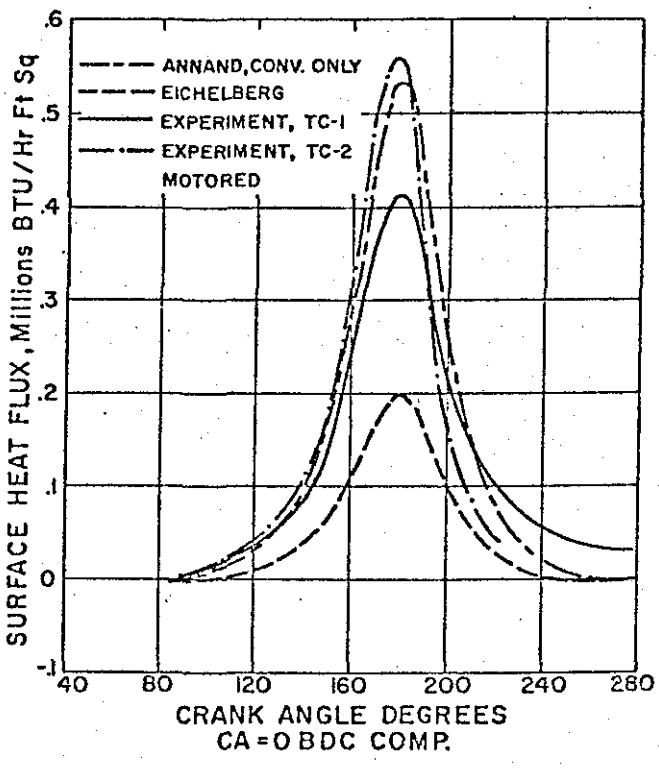

Fig.1.8 - Comparisons of predictions of Annand and Eichelberg with experimental data from cylinder head for motored operation

Engine: 4 stroke D.I. diesel
4.5" bore, 4.5 stroke. CR = 15.4 Le Feuvre et al (20)

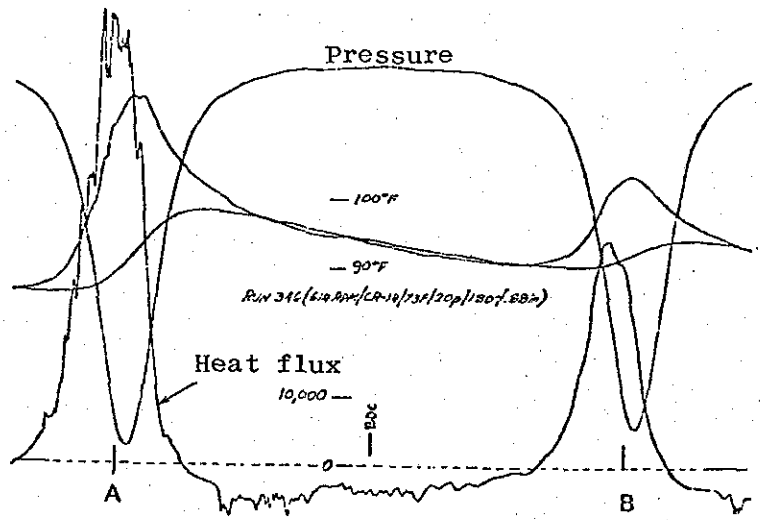

Fig 1.9- Oscillogram showing two successive compression cycles without intake between

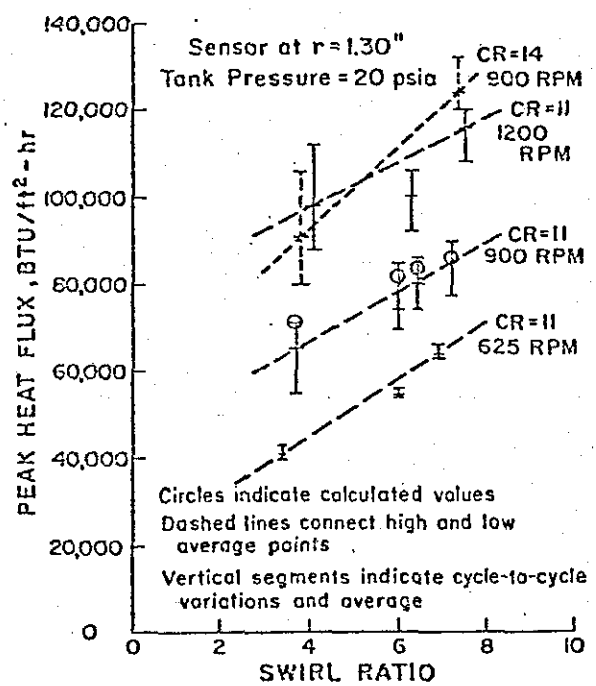

Fig 1.10 Plot of peak heat flux versus swirl ratio for different compression ratios

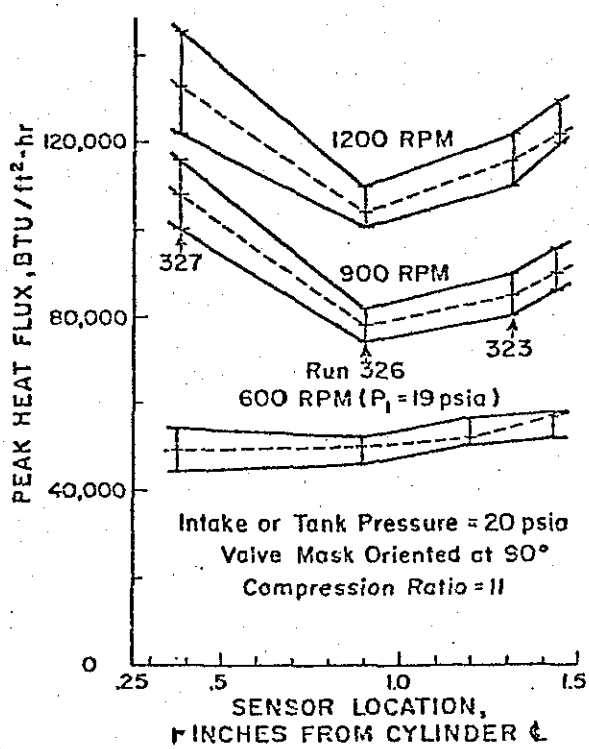

Fig 1.11- Plot of peak heat flux versus distance from cylinder centerline

Engine: 4 stroke, flat piston, 3.125" bore x 4.0 stroke, variable CR.
Kim Dao et al (40)

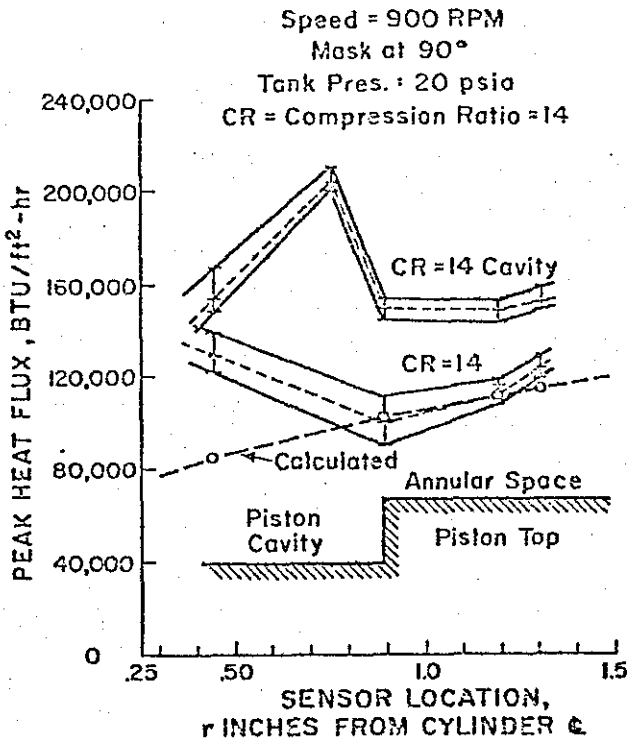

Fig. 12 Peak heat fluxes at different sensor locations with squish and without squish

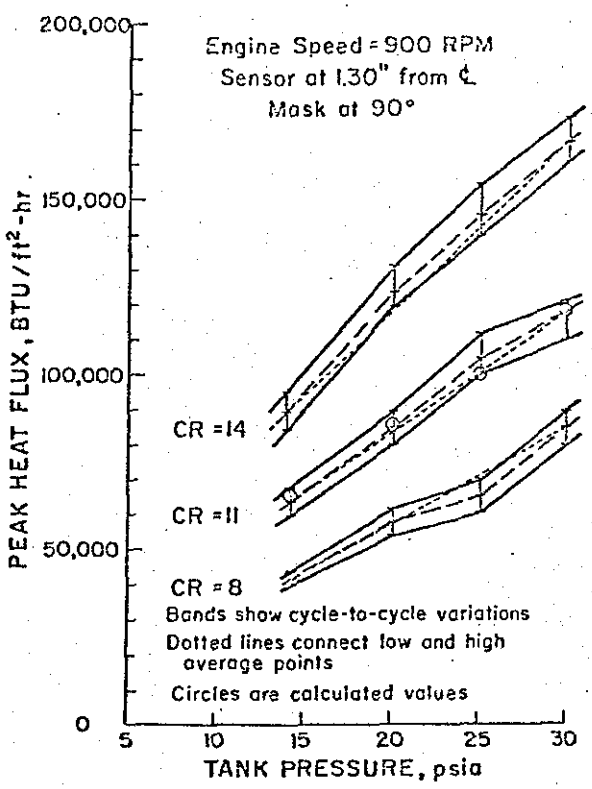

Fig. 14 Plot of peak heat flux versus inlet air pressure

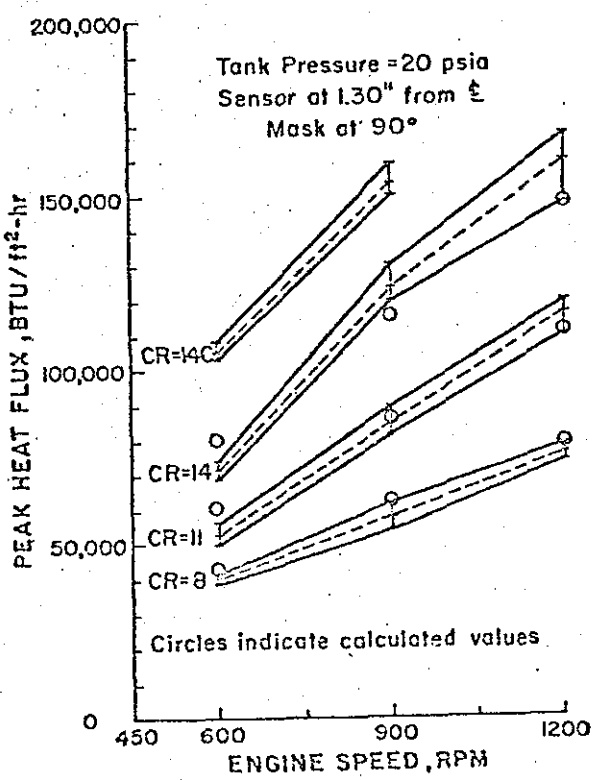

Fig. 13 Plot of peak heat flux versus engine speed

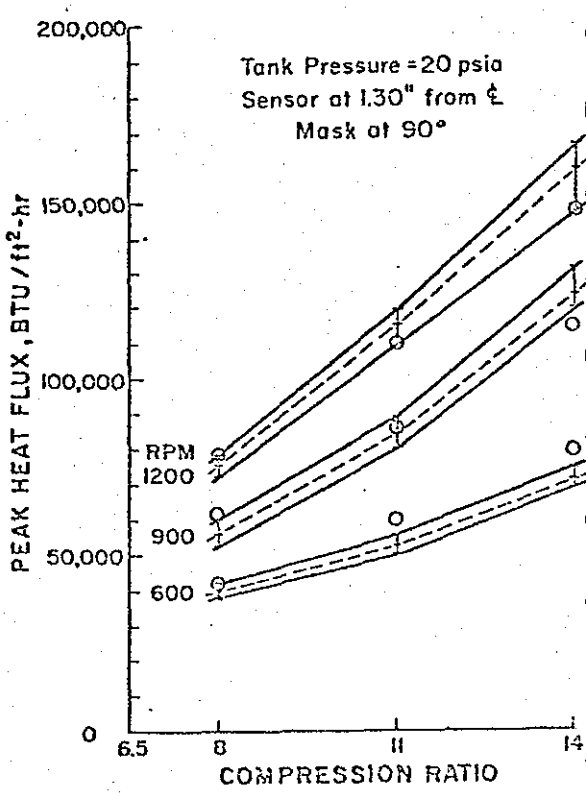

Fig. 15 Plot of peak heat flux versus compression ratio

Engine: 4 stroke, flat piston, 3.125" bore x 4.0" stroke.
Kim Dao et al (40)

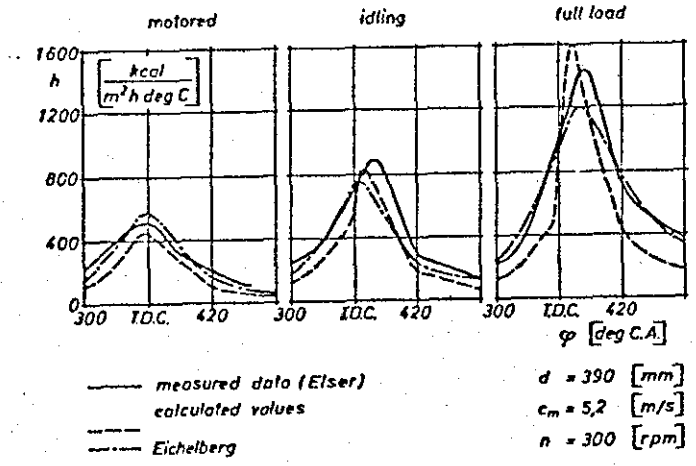

Fig.a) - Comparison of measured and calculated heat transfer coefficients

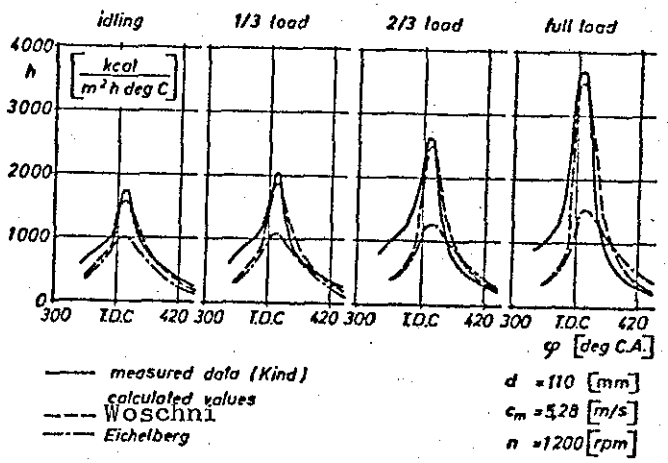

Fig. b) Comparison of measured and calculated heat transfer coefficients

Fig. (1,16a and b) Woschni (2)

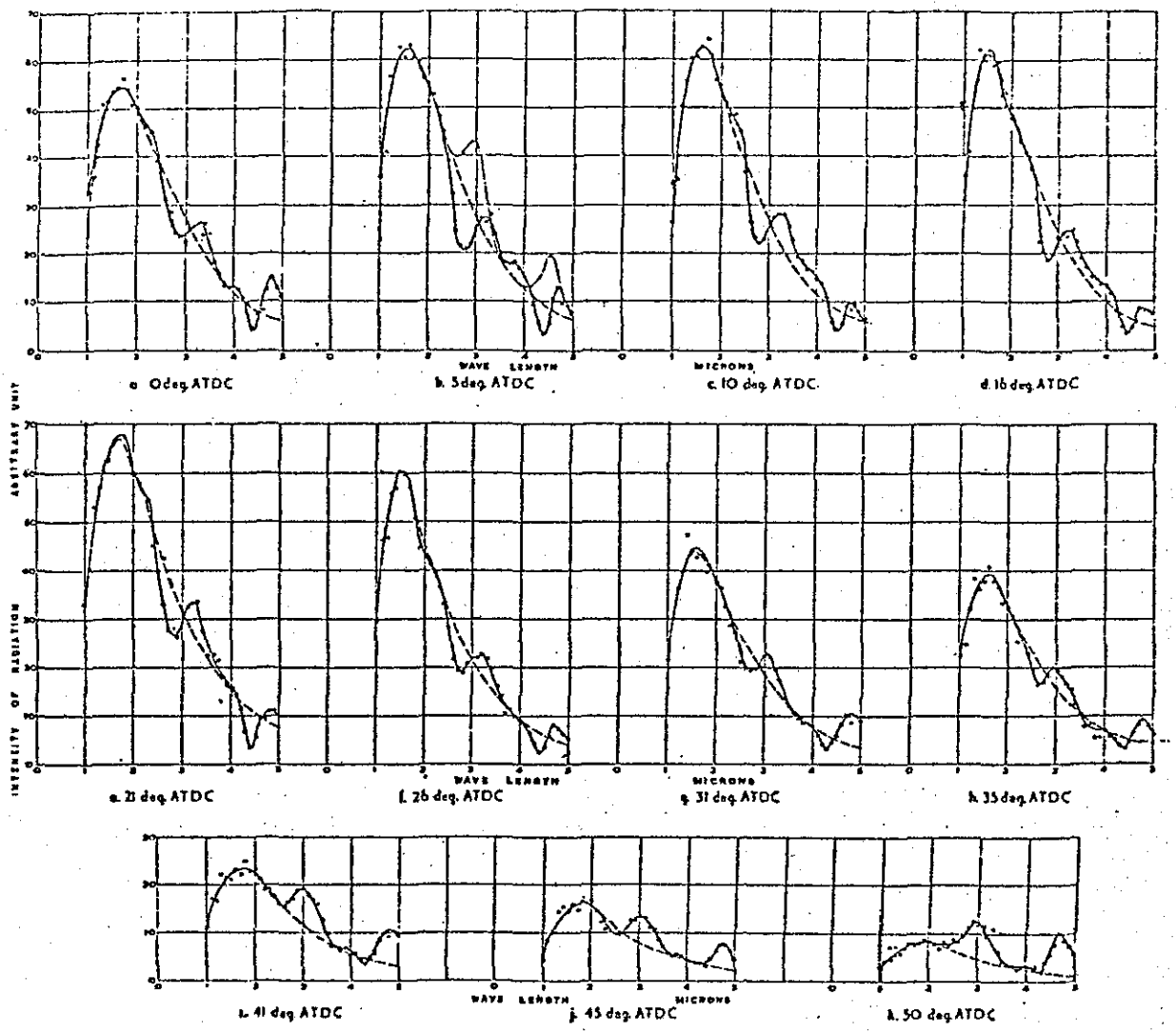

FIG (1.17)

SPECTRA AT 80 P.S.I. B.M.E.P., 1100 REV/MIN USING GAS OIL.

Measurements from spherical combustion chamber of a Ricardo Mk. II Comet 2.2" Ø Lyn (31).

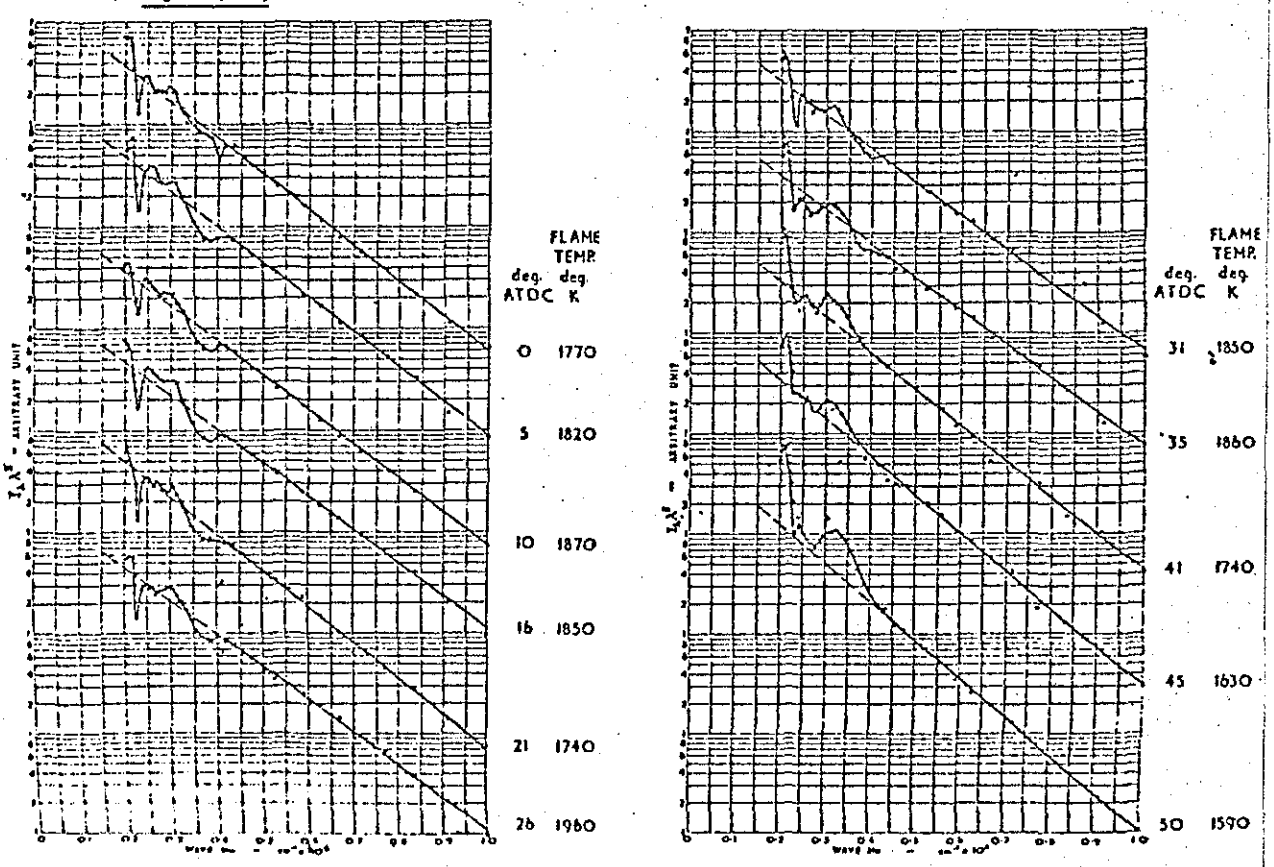

FIG (1.18)

LOG $I_\lambda\lambda^5$ v. $1/\lambda$ PLOT FOR FIG (1.17)

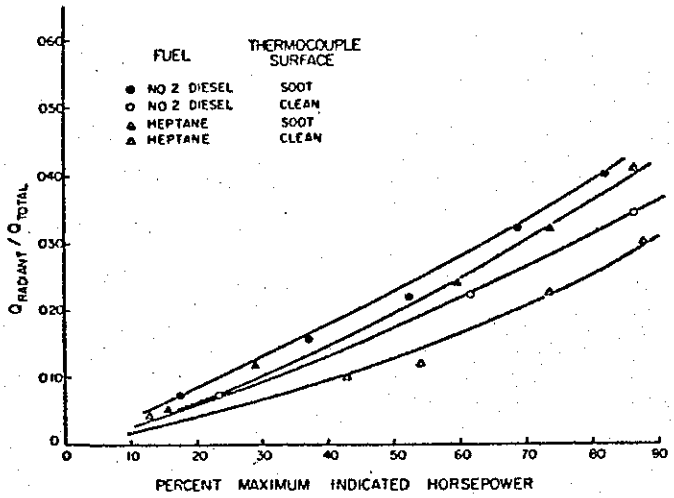

Fig. 119 - Heat flow ratios for diesel fuel and heptane with clean and sooty thermocouple surfaces

Ebersole et al (32)

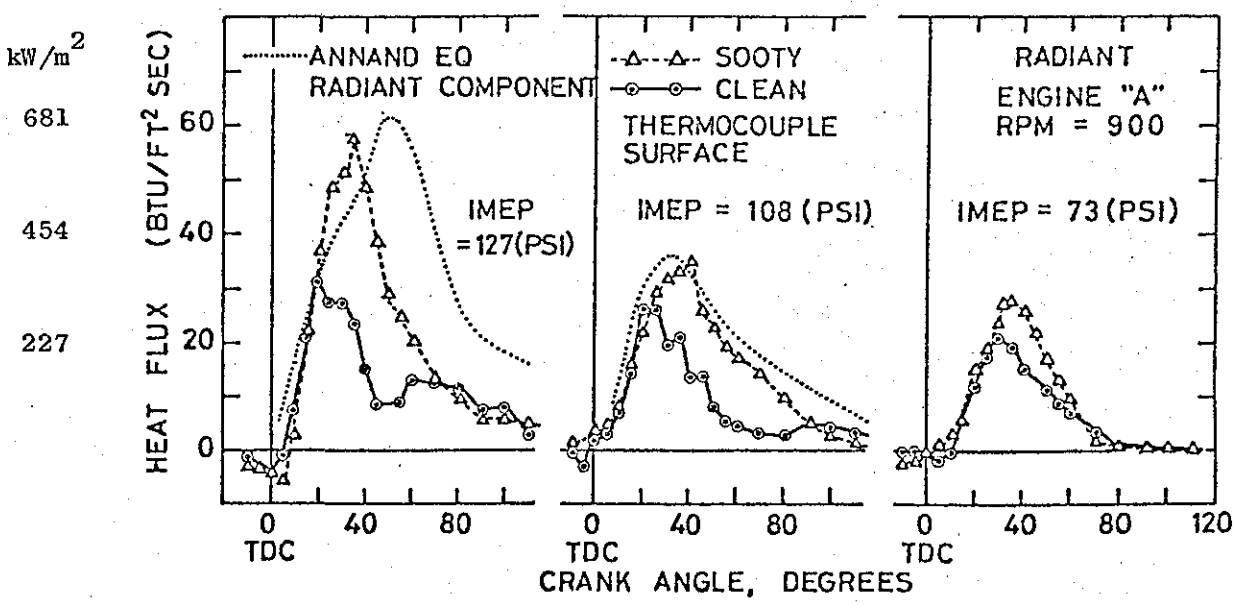

Fig. (1.20) Comparison of $\dot{q}_R$ with thermocouple surface sooty and clean, Oguri and Inaba (33).

Engine (A) D.I. 5.9" bore x 8.6" stroke

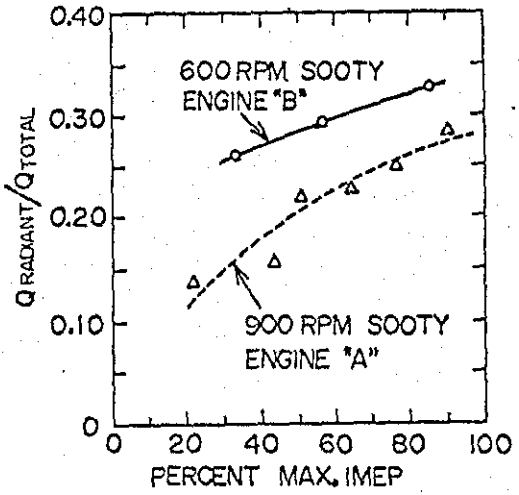

Fig.1.21 Ratio Q_r/Q_t versus percentage of maximum imep for each engine

Oguri and Inaba (33)

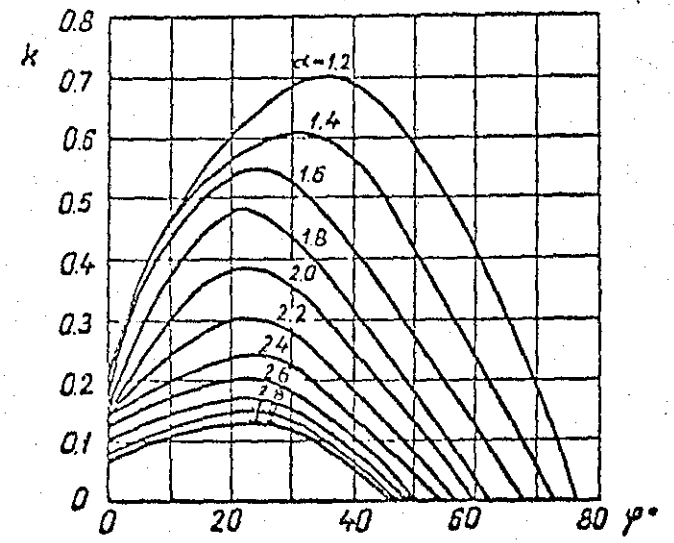

Fig.1.22 Absorption factor versus crank angle at different excess air factors in precombustion chamber (2,6 cm thick) CR = 18 Sitkei and Ramanaiah (23)

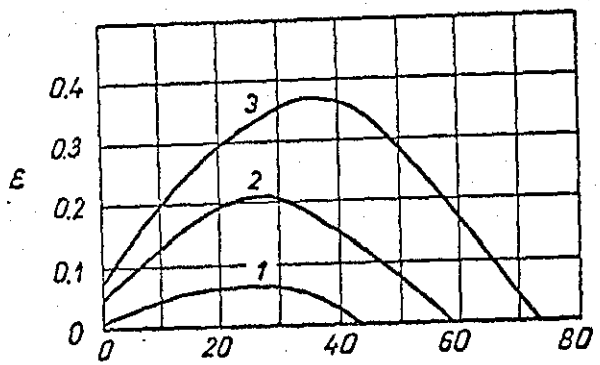

Fig.1.23 Flame emissivities for main chamber. 1 - no load, 2 - half load, 3 - full load

Sitkei and Ramanaian (23)

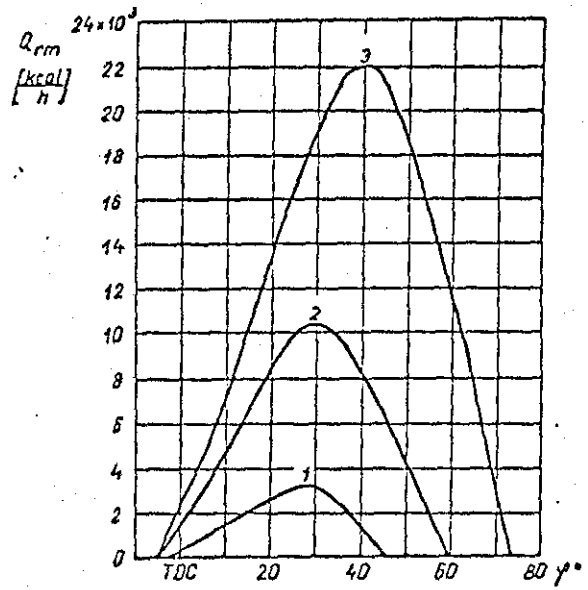

Fig.1.24 Heat transferred to cylinder walls due to flame radiation. 1 - no load, 2 - half load, 3 - full load

Sitkei and Ramanaiah (23)

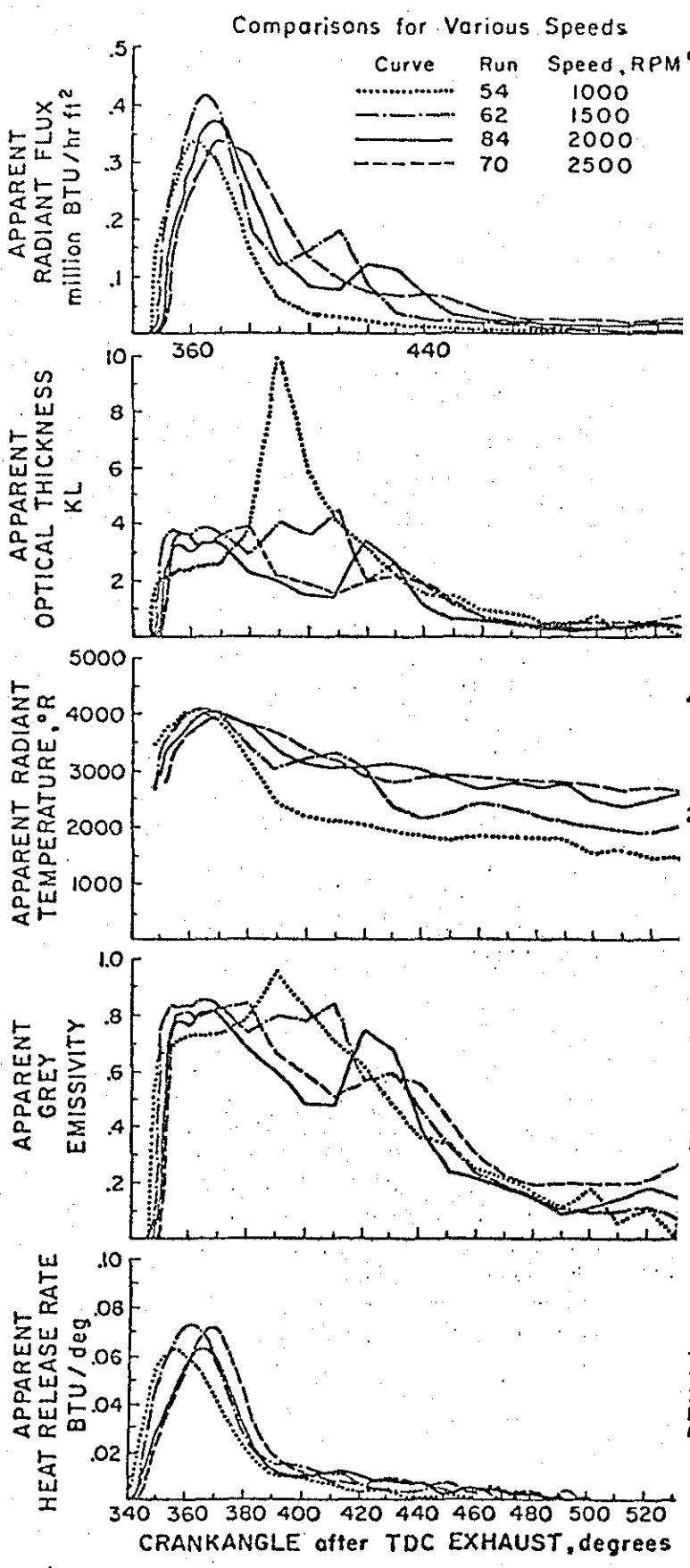

Fig. (1.25) Radiant emissions and heat release rates when engine speed is varied

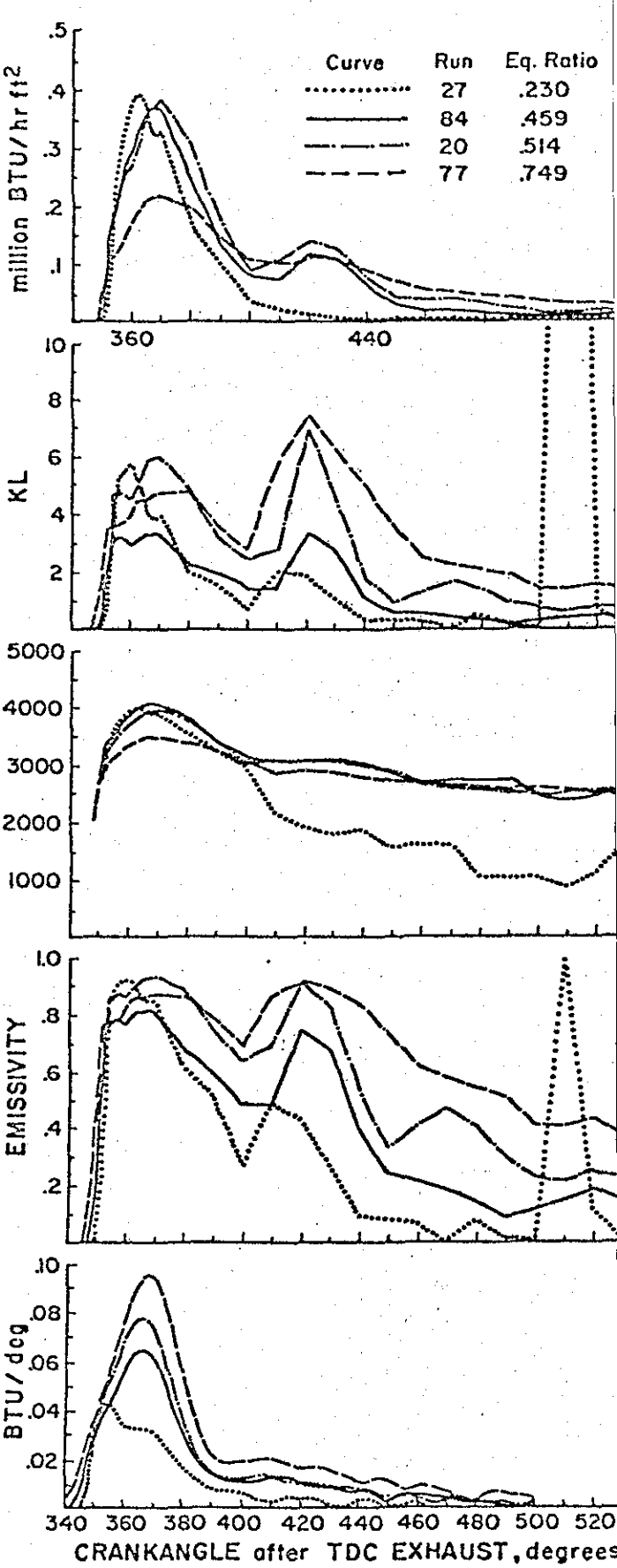

Fig. (1.26) Radiant Emissions and heat release rates when equivalence ratio is varied

Engine D.I. 4.5" bore x 4.5" stroke CR = 16.7
Flynn et al (34)

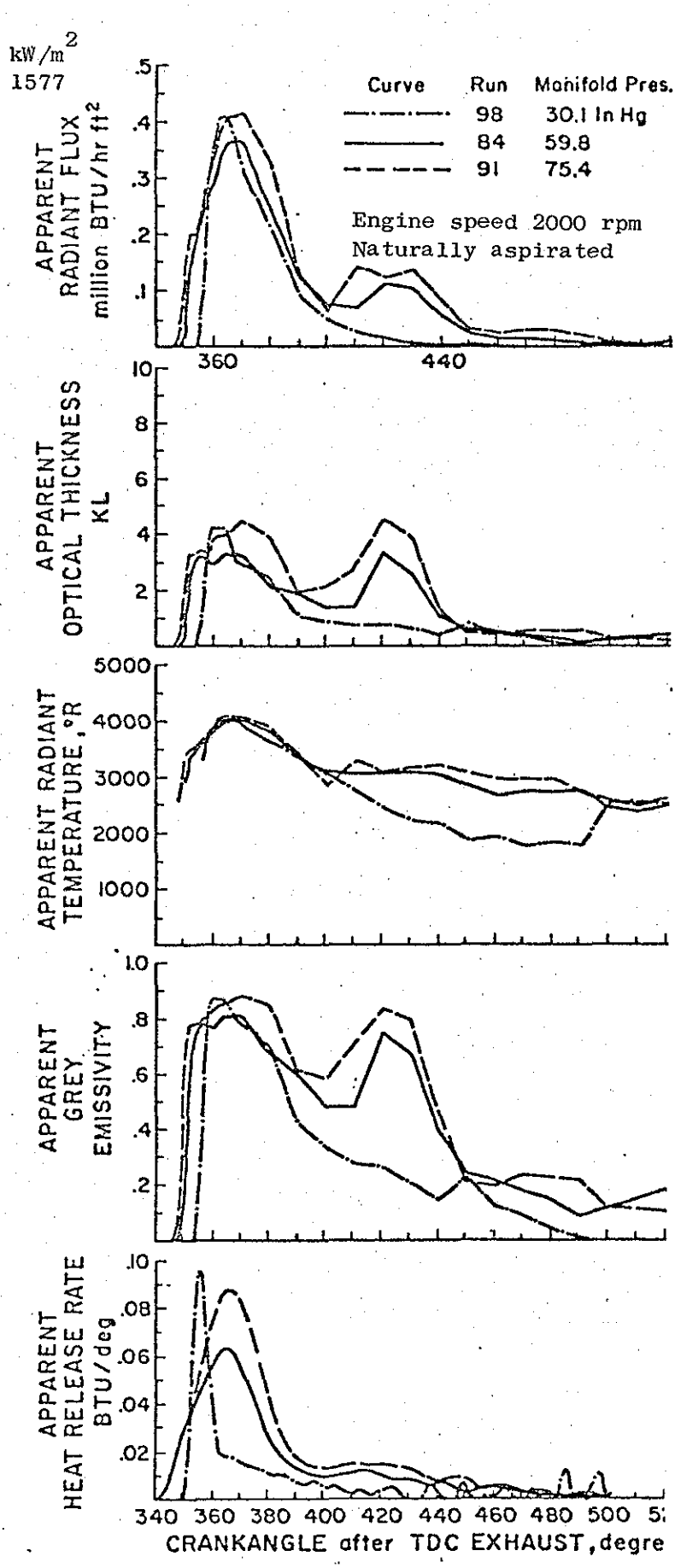

Fig. (1.27) Radiant emissions and heat release rates when inlet manifold pressure is varied

Flynn et al (34)

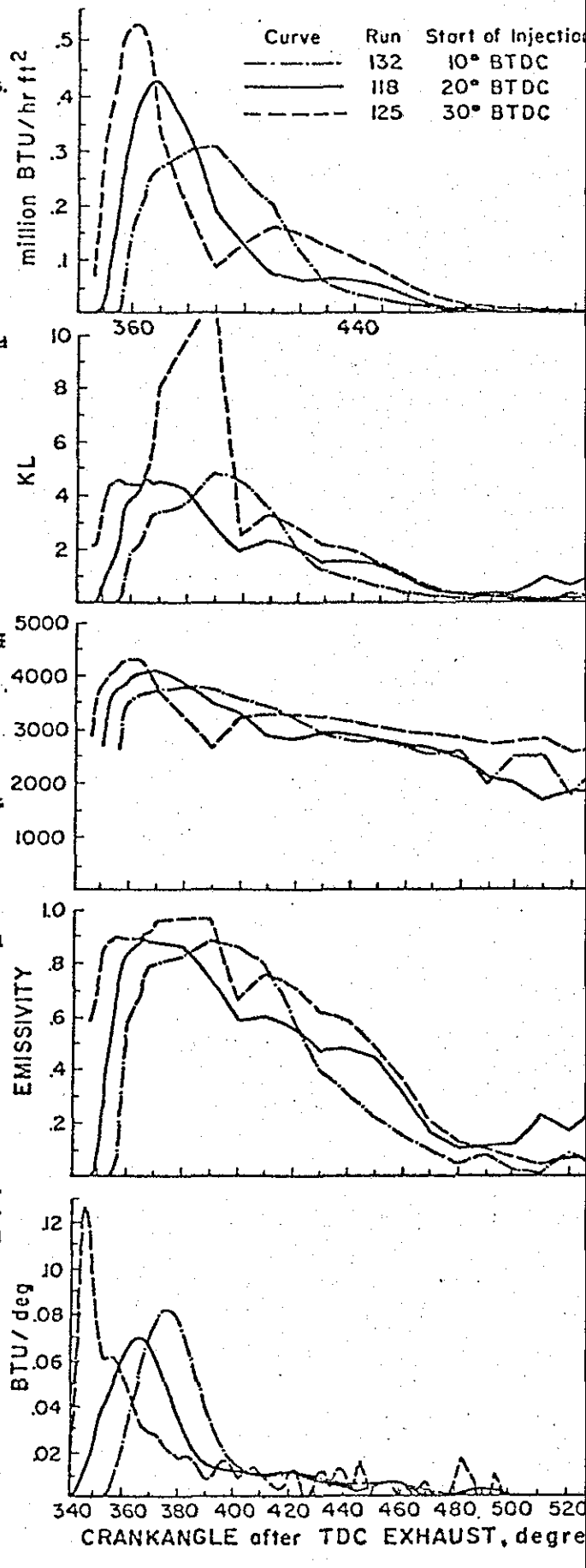

Fig. (1.28) Radiant emissions and heat release rates when injecti timing is varied

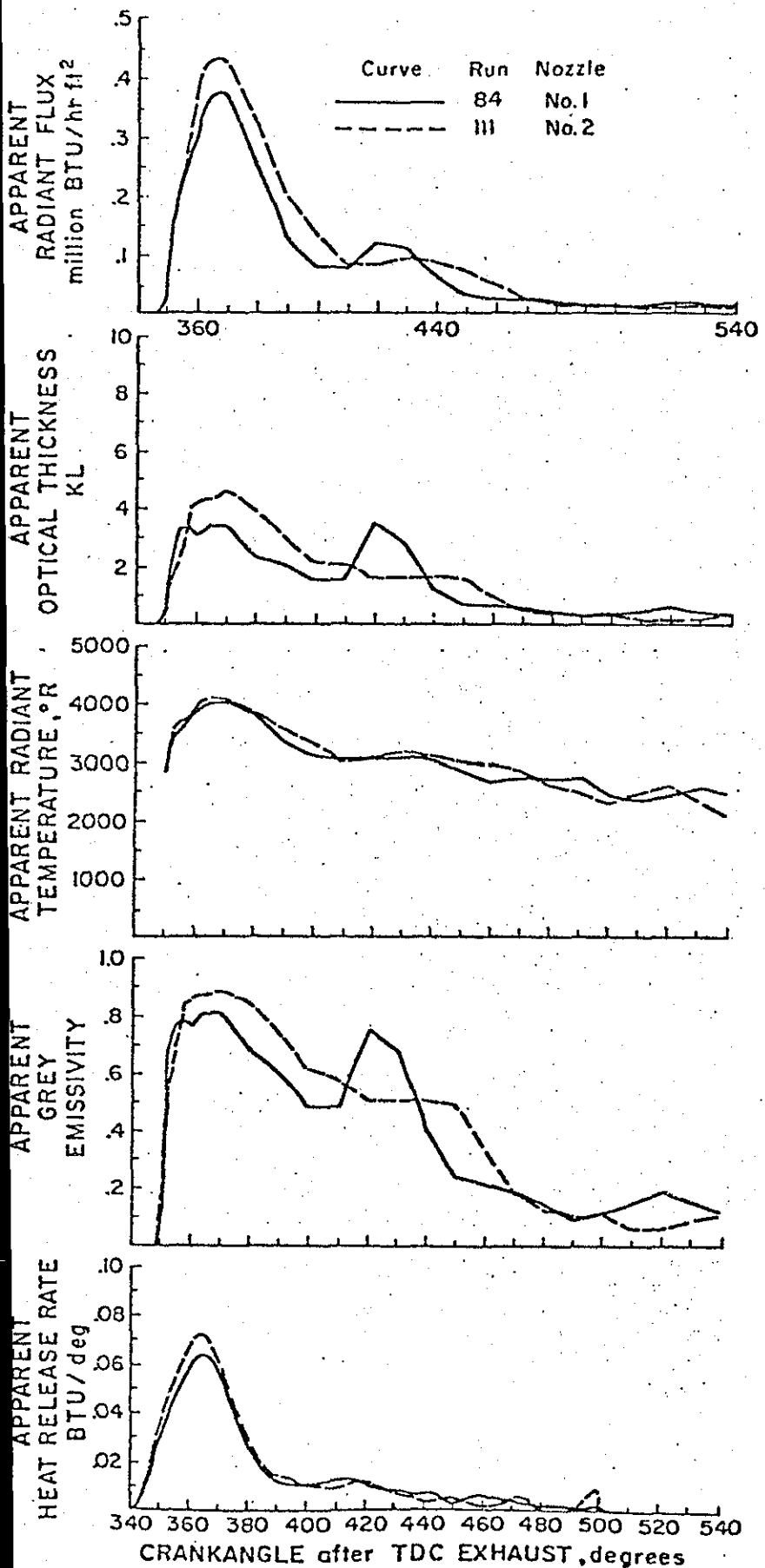

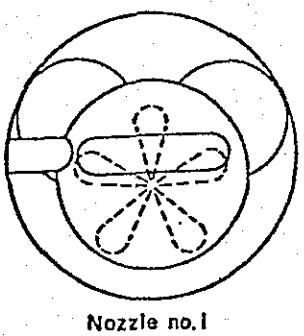

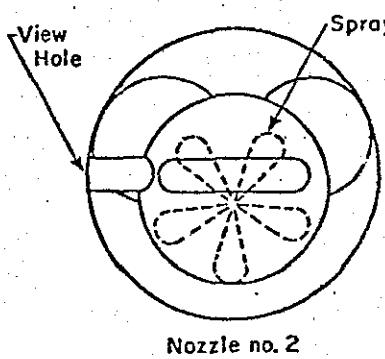

Plan view of spray patterns of nozzles 1 and

Nozzle tip 5 * .25 mm hole
150° cone.

Flynn et al (34)

Fig. (1.29) Radiant emissions and heat release rates when nozzles 1 and 2 were used

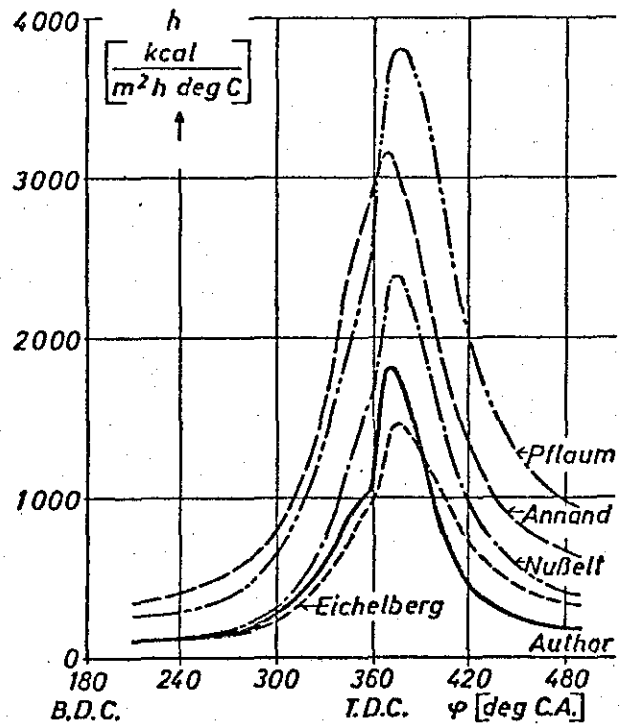

Fig.1.30 Comparison of heat transfer coefficients calculated from different formulas

Woschni (2)

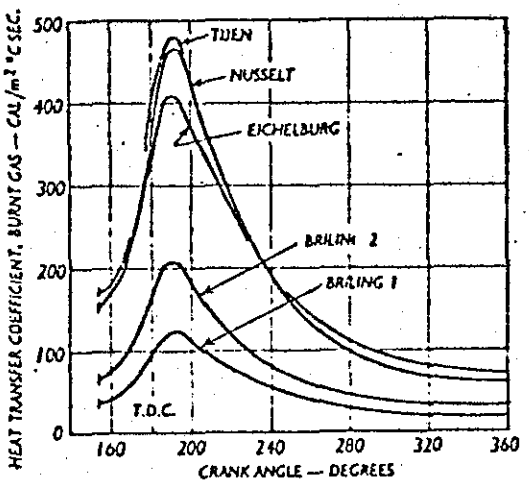

Fig. (1.31) Heat transfer coefficient for burnt gas v, crank angle at 1500 rev/min

Engine: CFR S.I. 4-stroke, 3.25" bore x 4.5" stroke
CR = 8:1. Walker (36)

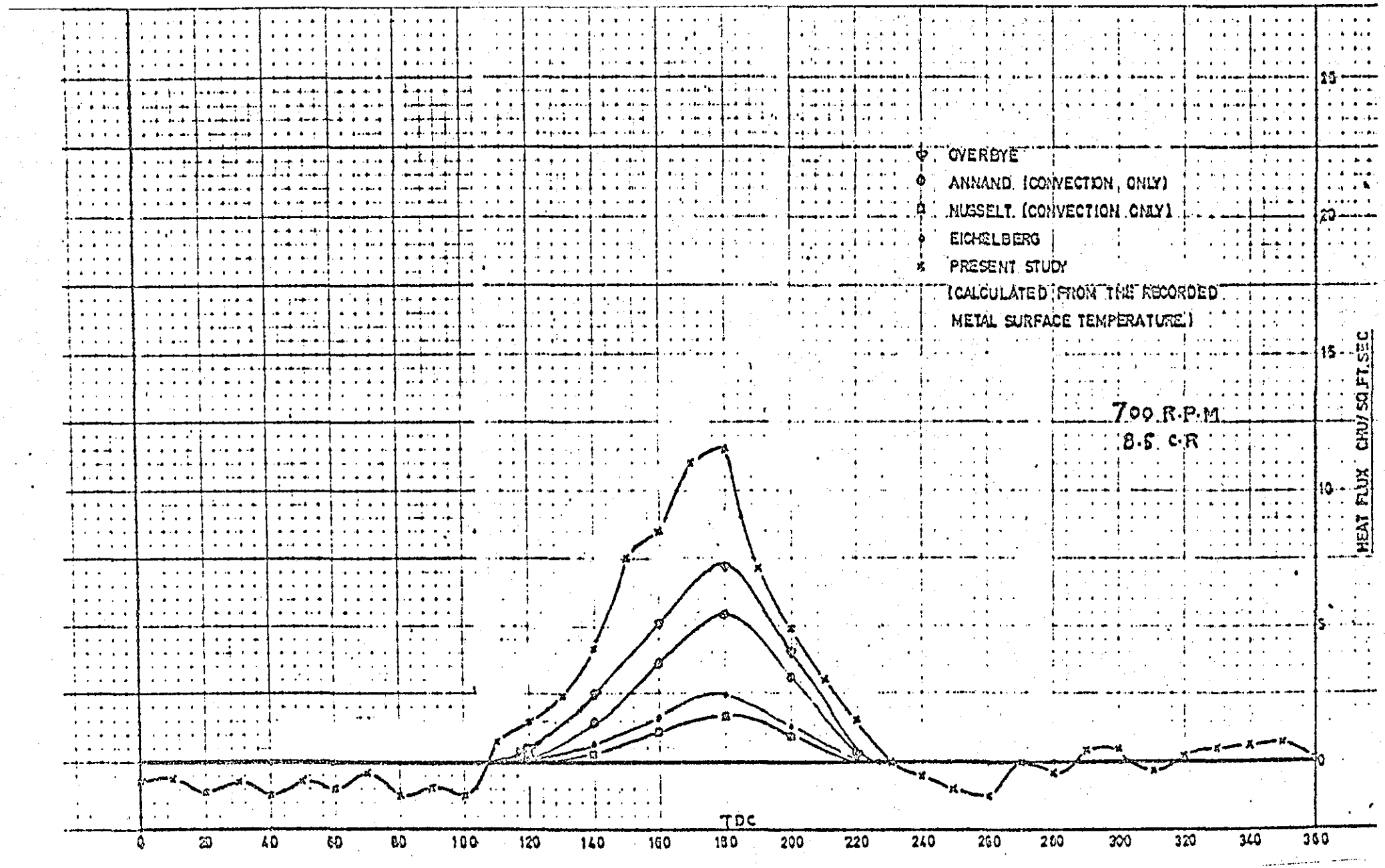

Fig. (1.32) Measured and calculated heat flux in precombustion chamber under motored conditions Hassan (37)

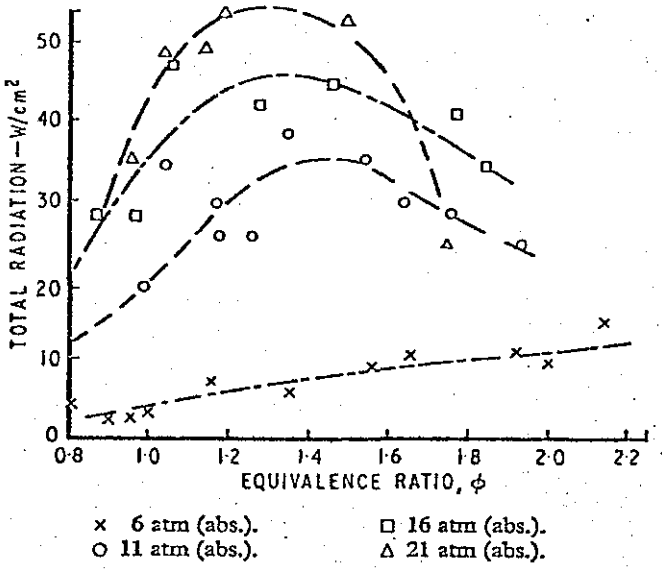

Fig.1.33 Variation of flame radiation with equivalence ratio at four operating pressures for atomized kerosine flames

Macfarlane and Holderness (45)

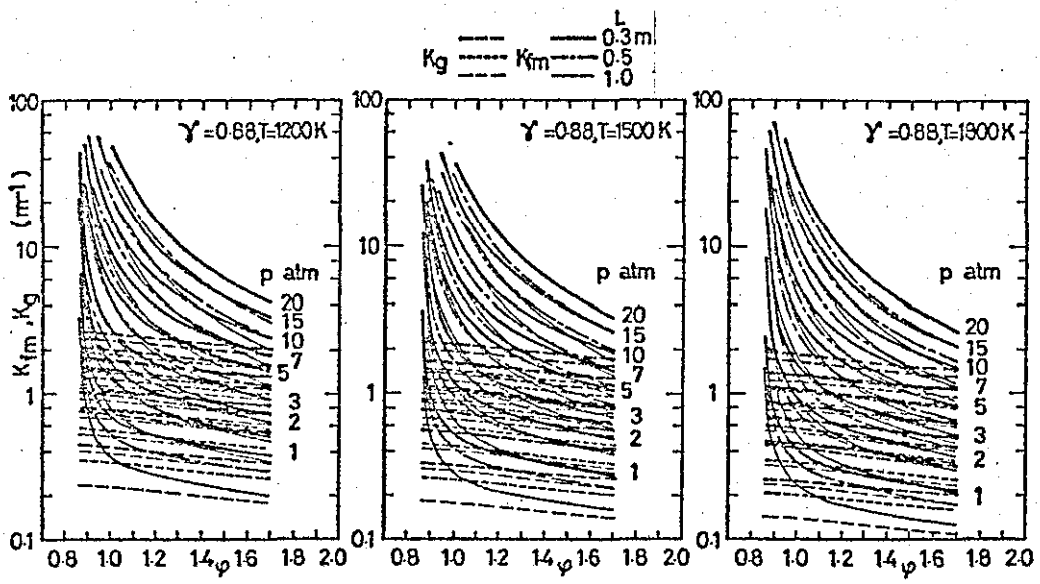

Fig. (1.34) Calculated flame mean absorption coefficients (kfm) and non-luminous gas absorption coefficients (kg) as a function of excess air ratio, for liquid fuel (specific gravity = 0.88)

Kunitomo and Kodama (46)

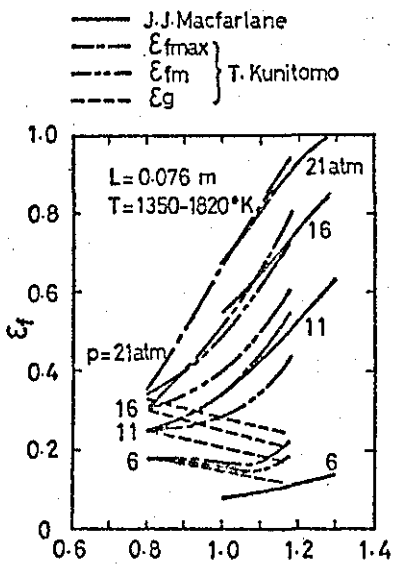

Fig. (1.35) Emissivity of luminous flame (comparison of Kunitomo's calculation with experimental results by Macfarlane & Holderness) Kunitomo and Kodama (46)

CHAPTER 2

GENERAL CONSIDERATIONS RELATING TO INSTANTANEOUS HEAT TRANSFER IN ENGINES

2.1 Convection Heat Transfer

2.1.1 General considerations

It has been generally accepted that due to the intense movement of the gas in the combustion chamber, the dominant component of heat transfer in reciprocating engines is by forced convection. The gas movement primarily caused by piston motion and manifold configuration, usually induces a flow pattern in the form of swirl and squish. In most cases, small scale eddies created by viscous dissipation are also superimposed upon the primary motion. In compression-ignition engines, where combustion often starts at several individual zones, rapid movement of the charge is expected. This combustion-induced turbulence would be additional to the existing movement before combustion.

It is the difficulty in describing phenomena, such as charge motion and temperature distribution involved that makes analytical solution impossible (Chapter 1). The usual approach has, therefore, been to obtain empirical relations, where the gas motion is represented by the mean piston speed and the gas bulk mean temperature as the driving temperature for heat transfer.

In Chapter 1 it was concluded that all the empirical relations proposed to date, have a limited range of application. This is not surprising because:

a) No precise description of charge motion and driving temperature has been possible or available.

b) Experimental observations indicate large variation in the magnitude of convective heat transfer from engine to engine or even from point to point in the same engine.

Fortunately, in the present engine, the instantaneous charge motion under motored conditions is known, Derham (44). Thus it was hoped that this information will lead to a relationship for periodic heat transfer of wider application than previous attempts, and also to recognise any effect of combustion-induced turbulence.

2.1.2 Validity of quasi-steady model

As mentioned before, the concept of heat transfer coefficient as applied to steady conditions has been used in the study of periodic heat transfer in engines. This assumes that heat flux is proportional to the driving temperature difference between the fluid and the surface and in phase with it:

$$\dot{q} = h\,(T_g - T_w) \qquad (2.1)$$

Theoretical analysis of heat transfer (Chapter 1) suggests the possibility of a phase difference between the driving temperature and the resulting surface heat flux. This arises because of the finite thermal capacity of the boundary layer and by effect of rate of change of pressure work (6 and 14). The seriousness of this problem is reduced by the fact that in real engine cycles, the phase differences are not as great as predicted by theoretical analysis. Also the periods during which the heat transfer coefficient (h) becomes infinite occurs in those parts of the cycle where heat transfer is not significant.

Le Feuvre et al (20) pointed out that if the diffusion time (defined as the time for a charge in the free stream condition to diffuse through a laminar boundary layer approximately equals $\frac{\delta^2}{\nu}$, where δ = boundary layer thickness, and ν the momentum diffusivity

in the boundary layer) is small, relative to other significant times in the problem, the boundary layer may be considered quasi-steady. For turbulent engine conditions, a diffusion time of 0.5^{o} CA was estimated, on the basis of which a quasi-steady model was said to be justified.;

In calculating the diffusion time (0.5^{o} CA), Le Feuvre et al (20) assumed the boundary layer thickness which presents the greatest resistance to diffusion, to be where velocity achieves 50% of its maximum value in the region of the boundary layer. Instead of this arbitrary assumption, the momentum thickness δ_i (related to loss of momentum in the boundary layer as compared with potential flow) across which the velocity gradient is large, can be assumed to present the greatest resistance to diffusion. The relationship for the momentum thickness for turbulent flow over flat plates, derived (Schlichting 99) on the basis of 1/7th power law velocity distribution is:

$$\delta_{i_x} = 0.036x \ (Re_x)^{-1/5} \qquad (2.1a)$$

where the subscript x denotes location x on the flat plate.

Therefore, substituting the conditions near TDC in the fired engine at 1050 rpm (solid swirl = 21 000 rpm) and for mean radius location $r = 0.025m$, the bulk mean temperature may be taken as $1500^{o}K$ at which air viscosity is found to be approximately 5.4×10^{-5} kg/m.s, and knowing the density $\rho = 13$ kg/m^3 a value of $\delta_i = 4.9 \times 10^{-5}m$ is obtained.

Hence the defined diffusion time $\frac{\delta_i^2}{\nu} = 5.75 \times 10^{-4}$ sec. which is equivalent to 3.6° CA at an engine speed of 1050 rpm. The diffusion time calculated for the conditions at the end of induction correspond to only 1.4° CA. These diffusion times are small compared to other times of major changes, e.g. of gas temperature and pressure which are significant between 90° CA BTDC to 90° CA ATDC. Therefore the assumption of quasi-steady model for heat transfer in internal combustion engines is reasonable.

2.1.3 Present convection heat transfer model

Theoretical analysis (modifications of the Reynolds analogy) of heat transfer in the turbulent boundary layer on a flat plate, combined with empirical relations describing skin friction, have been used to obtain the following relationship:

$$Nu_x = 0.0292 \, (Re_x)^{0.8} \, (P_r)^{1/3} \tag{2.2}$$

where Nu_x = local Nusselt number

Re_x = local Reynolds number

P_r = Prandtl number.

For a plate length L, an average Nusselt number may be evaluated by integration:

$$Nu = 0.037 \, (R_e)^{0.8} \, (P_r)^{1/3} \tag{2.3}$$

This relation assumes that the boundary layer is fully turbulent from the leading edge of the plate. In spite of the many simplifications,

relation (2.3) is found to give adequate results if the fluid properties are evaluated at the mean film temperature (Eckert and Drake 98) and as long as $P_r \simeq 1$.

From equation (2.3) it is seen that if a correlation containing some spatial variation is to be developed, the significant velocities and/or significant distances must be spatially dependent. The other significant quantities involved are essentially all functions of the gas temperature which must be determined from the cylinder pressure and density which are assumed to be spatially independent.

Equation (2.3) was chosen for predicting heat transfer to the combustion chamber walls for the following reasons:

1) Gas velocity measurements by Derham (44) showed that after approximately 90° CA during the induction period, an orderly swirl is developed which continues to exist throughout the compression period. The bulk of the gas was found to exhibit a forced vortex velocity profile. Thus the gas velocity variation with radius will allow for spatial variation of predicted heat flux in equation (2.3).

2) The forced vortex velocity profile implies that instantaneous gas velocity is constant at radius r and parallel to the surface. Therefore equation (2.3) is applicable to the flat cylinder head and the flat portion of the piston crown. Even in the piston bowl, the surface can be considered flat in the direction of the gas motion.

3) Equation (2.3) gives the mean heat transfer coefficient over a flat plate length L under fully developed turbulent conditions. Taking the characteristic length in the combustion chamber as $2\pi r$ (constant velocity path length) the spatial mean heat transfer coefficient at any radius can be represented.

The above discussion indicates that a relation would follow from equation (2.4) such that the average Nusselt number at radius r is given by:

$$Nu_r = \frac{h_r \cdot (2\pi r)}{k} = 0.037 \left[\frac{\rho \cdot (2\pi r\omega) \cdot 2\pi r}{\mu}\right]^{0.8} P_r^{1/3} \qquad (2.4)$$

where h_r = mean heat transfer coefficient at radius r

$(2\pi r)$ = characteristic length.

$(2\pi r\omega)$ = gas velocity (V_r) at radius r.

ω = swirl in rpm.

Integration of equation (2.4) over the cylinder head surface or piston area $(r = 0 - \frac{D}{2})$ will give a surface mean heat transfer coefficient:-

$$\bar{h} = \frac{1}{\pi D}\left[0.037\ (P_r)^{1/3}\ (\frac{\rho \cdot 4\pi^2\omega}{\mu})^{0.8}\ k \int_0^{D/2} r^{0.6}\, dr\right]$$

from which it follows that:

$$\frac{\bar{h} \cdot (\pi D)}{k} = 0.0225 \left[\frac{\rho \cdot (\omega \pi D) \cdot \pi D}{\mu}\right]^{0.8} P_r^{1/3} \qquad (2.5)$$

The instantaneous heat flux at radius r is calculated by substituting h_r obtained from equation (2.4) into equation (2.1):

$$\dot{q}_r = h_r (T_g - T_w) \tag{2.6}$$

In the motored engine, the driving temperature is taken as the difference between the bulk mean gas temperature (T_g) and wall surface temperature. In the fired engine, however, the temperature distribution is very complex and a representation by the bulk mean temperature will be unrealistic. This fact was clearly indicated by the large differences in the local heat fluxes observed experimentally (section 6.5). In an attempt to approximate to actual conditions, a two zone temperature field is necessary to be considered. In the region where most of the combustion takes place (e.g. piston bowl), the temperature may be represented by that of a chemically correct mixture. On the other hand, other regions may be considered to consist of air, at least early during combustion (section 6.8).

2.2 Radiation Heat Transfer

2.2.1 General considerations

The problem of evaluating the expected radiant heat transmission from flames received early attention (Hottel and Schack) because of its practical importance in the design of industrial furnaces and the evaluation of heat transmission in internal combustion engines. In the latter case, the contribution of radiative heat transfer, though small compared with the convective component, varies

considerably with the type of combustion process and increases rapidly with increase in temperature levels.

Radiation from gaseous media is dependent on the path length, or dimensions of the space containing the gas. If it is assumed that no solid carbon particles are formed during combustion and expansion periods, as is commonly taken to be the case in spark ignition combustion, then radiation may be justifiably ignored on the grounds that path lengths are small and the gas mass non luminous. In the diesel engine, combustion proceeds by means of a diffusion flame between unmixed fuel and air. There are many sources of ignition and the production of highly luminous flame involves the formation of solid carbon particles as an intermediate step. It is a difficult task to calculate the spatial distribution of the unburned gas and combustion products. The usual application of shape factors to account for the variation in the incidence angle of the radiation over any given surface, becomes a difficult procedure in the case of the often complex geometry of the engine combustion space.

A survey of the literature (23, 31, 42, 39 and 49) indicated that in different engines, the measured flame temperatures are not very different. Thus an attempt is made to combine this knowledge with observed data in order to predict radiant heat flux in diesel engines.

2.2.2 Thermal radiation laws and the concept of a black body

The term thermal radiation is used broadly to describe radiant energy emitted as a consequence of the temperature of a body. Like the ideal gas, the black body is a theoretical concept which can only be approximated in practice. The laws related to this ideal body

are presented below.

Kirchoff's Law; states that at thermal equilibrium the ratio of the emissive power of a surface to its absorptivity is the same for all bodies. Kirchoff's laws place an upper limit on the emissive power of a body, which occurs when absorptivity has its maximum value of unity, a condition which applied precisely to a black body. The emissive power of a black body depends on its temperature only, and is given by:

$$E_b = \sigma T^4 \tag{2.7}$$

which is known as the Stefan-Boltzman law (Wiebelt 96) and the proportionality constant σ is known as the Stefan-Boltzman constant (56.7×10^{-12} kW/m^2).

Other properties of blackbody radiation of interest in heat transfer is the spectral distribution of the emissive power and the shift of that distribution with temperature. If $E_{b\lambda}$ is the monochromatic emission power at wavelength λ such that $E_{b\lambda} .d\lambda$ is the energy emitted from a surface throughout a hemispherical angle per unit area per unit time in the wavelength interval λ to $\lambda + d\lambda$, the relation among $E_{b\lambda}$, λ and T is given by Plancks Law (56)

$$E_{b\lambda} = \frac{C_1 \lambda^{-5}}{e^{C_2/\lambda T} - 1} \tag{2.8}$$

where λ = wavelength in

T = temperature of the body ^oK

C_1 = 3.7415×10^4 W cm^{-2} micron^4

C_2 = 1.43879×10^4 micron ^oK

At temperatures of engineering interest, the emissive power is appreciable over wavelengths from 0.3 to at least 50 μ.

The wavelength of maximum intensity is seen to be inversely proportional to the absolute temperature (Wein's displacement Law). The relation (Wiebelt 96) is:

$$\lambda_{max.}\ T = 0.2898\ cm\ ^{o}K$$

Radiation from real surfaces or bodies including gas, differs in several aspects from black body radiation. According to Kirchoff's Law, a real surface or body always radiates less than a blackbody at the same temperature. For the purpose of heat-transfer calculations, real sources are usually regarded as grey, and its emissive power E is given by:

$$E = \epsilon_a\ \sigma\ T^4 \qquad (2.9)$$

where ϵ_a = apparent grey body emissivity

$$= \frac{E}{E_b} = \frac{E_\lambda}{E_{\lambda b}}$$

In order to add more light to the problem of gas radiation, the basic attenuation laws and definitions of gas emissivity are first briefly discussed.

2.2.3 Attenuation laws and gas emissivity

The attenuation $-dI$ due to absorption of a beam of collimated monochromatic radiation of intensity (I) on passage through a differential slab (dl) is proportional to the intensity and the path length traversed.

$$-dI = K\, I\, dl \tag{2.10}$$

and the proportionality constant K (related to a narrow bandwidth) is variously known as the attenuation or total extinction coefficient.

If the beam is incident on a slab of thickness L with intensity (I_o) and if (K) is independent of position, integration of equation (2.10) for monochromatic radiation or for total radiation in a grey medium gives the relation:

$$I = I_o\, e^{-KL} \tag{2.11}$$

If one considers the interceptions of a collimated beam of radiation by large black particles, then in Equation (2.10):

K = (number of particles per unit volume (C)) * (projected area per particle (A))

$= CA.$

For a gas it is customary to define an absorption coefficient k_c for use in combination with molecular concentration, or k_p with partial pressure of the gas, again considering a narrow bandwidth:

$$K = k_c\, C = k_p\, P \tag{2.13}$$

k_c has the dimension of area and is sometimes called the capture cross section of a molecule. The extinction law written in terms of the absorption coefficient:

$$I = I_o e^{-k_c CL} \tag{2.14}$$

is the familiar Beer's Law.

A complete measure of the gas properties necessary for the calculation of the radiative exchange between an isothermal gas mass and its surroundings is given by monochromatic absorption coefficient (k_λ) as a function of wavelength, temperature and the pressures of all the gases in the radiation mixture. Experimental measurements of k_λ are complicated by the limit of resolution of spectrometers, and have been made for only a very narrow range of conditions. Emissivities and absorptivities over wavelength regions including many lines or over the entire spectrum are more frequently measured.

The term gas emissivity has meaning only in reference to emission from an isothermal gas shape to a specified portion of its bounding surface. The standard emissivity of a gas is the radiation from an isothermal gas hemisphere to a spot on the centre of its base, expressed as a ratio to hemispherical black body radiation.

Kirchoff's law applied to toal radiation, is equally valid for monochromatic radiation, that is, at thermal equilibrium the monochromatic absorptivity α_λ of any surface is equal to its monochromatic emissivity ϵ_λ. Therefore from Beer's Law:

$$\epsilon_\lambda = \alpha_\lambda = 1 - e^{-k_\lambda pL} \tag{2.15}$$

The total emissivity or absorptivity may be obtained by integration over all wavelengths:

$$\epsilon_g = \frac{\int_0^\infty \epsilon_\lambda E_{\lambda g}\, d\lambda}{\int_0^\infty E_{\lambda g}\, d\lambda} = \frac{1}{\sigma T_g^4} \int_0^\infty \epsilon_\lambda E_{\lambda g}\, d\lambda \qquad (2.16)$$

$$\text{and} \quad \alpha_{gs} = \frac{\int_0^\infty \alpha_\lambda E_{\lambda s}\, d\lambda}{\int_0^\infty E_{\lambda s}\, d\lambda} = \frac{1}{\sigma T_s^4} \int_0^\infty \alpha_\lambda E_{\lambda s}\, d\lambda$$

$$= \frac{1}{\sigma T_s^4} \int_0^\infty \epsilon_\lambda E_{\lambda s}\, d\lambda \qquad (2.17)$$

where $E_{\lambda g}$ and $E_{\lambda s}$ are Planck's functions - the hemispherical monochromatic black emissive power evaluated at the gas and wall surface temperatures respectively, in order to evaluate ϵ_g and α_{gs}.

2.2.4 Thermal radiation in diesel engines

The major contribution from flames and gases of conventional fuels is thermal radiation from water vapour, carbon dioxide, soot and carbon monoxide. Carbon monoxide is generally present to such small extent that its contribution can be neglected; and if attention is momentarily restricted to non-luminous flames, CO_2 and H_2O are left as the major sources of flame radiation.

2.2.4(a) Radiation from non-luminous gases

Radiation from gases at temperature levels reached in I.C. engines and furnaces is of importance only in the case of heteropolar gases, of which CO_2 and H_2O are the major contributors. If the radiating gas is assumed to be isothermal, then the variables required to define total gas emissivity and absorptivity are given by:

$$\epsilon_g = f_1 (L, p, P, T_g) \tag{2.18}$$

$$\alpha_{gs} = f_2 (L, p, P, T_g, T_s) \tag{2.19}$$

Experimentally determined total emissivities of CO_2, H_2O and CO in the form of charts have been available since the 1930's. The emissivity is expressed as a function of T_g and PL. Hottel (51) introduced a correction factor to allow for pressure broadening effects (i.e. greater emission or absorption at wings of a line) dependent on p and P, and another correction factor to account for the overlap among the emission bands of the different molecules, because each gas is somewhat opaque to the other. Therefore knowing the products of the combustion, the partial pressures of H_2O and CO_2 can be calculated. To account for the shape of the radiating gas, the mean beam length L has to be evaluated, hence the gas emissivity from the charts can be read.

2.2.4(b) Radiation from clouds of luminous particles

The treatment of radiation from powdered coal or atomised oil flames, and from flames made luminous by the thermal decomposition of hydrocarbons to soot involves the evaluation of radiation from clouds

of particles. Evidence of the dominant rate of luminosity in radiation from many industrial-furnace flames is long-standing. In diesel engines, Lyn (31) found that radiation emitted by the carbon particles in the luminous diesel flame formed a continuous spectral distribution of an intensity so high that it obscured the emission from gas radiation. Flynn et al (34) measured total flame emissivities up to 0.9, attributed mainly to soot particles.

Considering flames, the luminosity of which are due primarily to soot rather than to suspended macroscopic particles, the monochromatic absorption coefficient of the cloud is proportional to the volume fraction f_v of space occupied by particles, and to reciprocal wavelength $1/\lambda$. The proportionality constant k depends on the refractive index n and absorption index k' (Hottel and Sarrafim (52), Chapter 12). The emissivity is then given by:

$$\epsilon_\lambda = 1 - e^{-[\, k(n,k')\, f_v\, L/\lambda \,]} \qquad (2.20)$$

If the soot composition, mass concentration and the optical properties (which are a function of wavelength and C/H ratio) of soot are known, it is then possible to estimate the flame emissivity. If for simplicity, it is assumed that n and k' are independent of wavelength and temperature, i.e. $k(n,k')$ = constant in equation (2.20) the total emissivity may be calculated, with spectral distribution of black body radiation expressed by Wein's equation rather than Planck's because of low λT range of main interest.

$$\epsilon_g = \frac{\int_0^\infty \lambda E_\lambda \, d\lambda}{\int_0^\infty E_\lambda \, d\lambda} \qquad \frac{\int_0^\infty (1 - e^{-k f_v L/\lambda}) \, c_1 \lambda^{-5} e^{-c_3/\lambda T} \, d\lambda}{\int_0^\infty c_1 \lambda^{-5} e^{-c_2/\lambda T} \, d\lambda}$$

$$= 1 - \left[\frac{1}{1 + k f_v LT/c_2} \right]^4 \qquad (2.21)$$

Based on various experimental work, Hottel recommended a value of $k/c_2 = 5 \text{ cm}^{-10} \text{ K}^{-1}$.

Hottel and Broughton (43) made an analysis of the variation in emissivity of carbon particles as a function of wavelength, which leads to a formula for the wavelength variation of emissivity as follows:

$$\epsilon_\lambda = 1 - e^{-kL/\lambda^\alpha} \qquad (2.22)$$

In this empirical expression, k and L combine to determine the optical thickness of the radiating carbon particle layer, and the power to which was raised was obtained to give agreement with the experimentally observed variation in emissivity with wavelength. Hottel suggested a value of:

$\alpha = 0.95$ for range $\lambda = 0.8 - 10$

$\alpha = 1.39$ for range up to $\lambda = 0.8$

Libert (34) in a recent study of soot emissivities also suggested the above correlation for soot emissivity versus wavelength. Further justification for a model using an emissivity variation with wavelength was obtained by examining the suggested relationship for emission from very small particles ($<$ 0.6 times the wavelength of radiation under consideration). Hottel (52) presented a theoretically derived relationship of the form:

$$\epsilon_\lambda = 1 - e^{-kL/\lambda} \qquad (2.23)$$

Flynn et al (34) used the relation $\epsilon_\lambda = 1 - e^{\frac{-kL}{\lambda^\alpha}}$ in combination with Wein's Law and experimental measurement of radiation at two wavelengths, to evaluate the emissivity of the radiating flame.

Despite this background of understanding of the mechanism of radiation from particulate matter, the mechanism of formation of soot in flames is not quantitatively understood. There is no present possibility in the rigorous approach to flame radiation in diesel engines, of finding from first principles how much soot will be generated at particular locations in the flame. Reliance must instead be put on empirical extrapolation of experimental data on existing furnaces and diesel engines, to provide an engineering approximation as to how much luminosity may be expected, and how it is distributed in space in a combustion chamber when a given fuel is burned in a given way.

2.2.5 Prediction of radiant heat transfer from flames using Hottel's approach

2.2.5(a) Mean beam length and exchange area-factors

Allowance for the shape of an enclosure is usually presented

in one of the two forms, as an exchange area or as a mean beam length (Hottel 52), starting from the exchange between a hemispherical gas body of radius L and a spot in the centre of its base where the total length of each radiating beam equals L. Any other gas body may be replaced by an equivalent hemispherical body of radius L_e known as the mean beam length of the shape.

Hottel defined the direct-exchange area for the gas (grey isothermal) - surface (black) total radiative exchange by:

$$q_{g-s} = E_g \frac{\overline{g_s}\,(KL)}{A} \qquad (2.24)$$

where E_g = emissive power of a black body at the temperature of the gas,

q_{g-s} = mean flux density at surface element

$\overline{g_s}\,(KL)$ is the exchange area which is a function of equivalent grey body absorption coefficient K of the medium, some characteristic length L, the shape of the gas and surface and their relative orientation.

The relationship between direct-exchange area $\overline{g_s}$ and standard gas emissivity corresponding to a fixed path length of gas as found in a hemisphere (radius L_e) radiating to a spot on the centre of its base is given by:

$$1 - e^{-KL_e} = \left[\ \overline{g_s}\,(KL)\ \right]/A \qquad (2.25)$$

Instead of L_e (equal to $\frac{4V}{A}$ when $K = 0$) which is dependent on K, a constant L_m known as "average mean beam length" is chosen such that minimum error is introduced in the range of K values of practical interest.

Hottel and Egbert (57) have calculated average mean beam length of various geometrical bodies radiating to a particular point or to the whole surface. It was pointed out that for a gas mass of arbitrary shape,

$$L_m \simeq 3.6\ V/A \quad \text{and} \quad L_e = (4V/A)_{K=0}$$

More accurate determination of radiation interchange necessitates evaluation of gas-surface interchange factors $(\overline{g_s})$ for the shape in question. This approach is particularly useful when account of non-uniform distribution of temperature is considered. The direct-exchange areas are evaluated in the following manner:

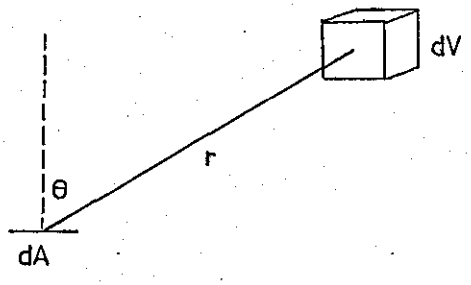

For a grey gas the radiation flux at the surface element dA from a differential volume dV equals:

$$\underbrace{[\ 4\ k\ dV\ E\ ]}_{\substack{\text{emission by dV} \\ \text{in } 4\pi \text{ steradians}}} \times \underbrace{\left[\ \frac{dA\ \text{Cos}\ \theta}{4\pi\ r^2}\ \right]}_{\substack{\text{fraction directed} \\ \text{toward dA}}} \times \underbrace{[\ \tau(r)\ ]}_{\substack{\text{fraction} \\ \text{transmitted}}} \qquad (2.25)$$

Integration of this equation over the appropriate surfaces or volumes yields $\overline{g_s}$.

$$\overline{g_i \; s_j} = \int_{V_i} \int_{A_j} \frac{K_i \; dV_i \; dA_j \; \text{Cos} \; \theta_i \; (r)}{\pi \; r^2} \qquad (2.27)$$

Hottel and Sarrafim (52) numerically evaluated the direct-exchange factors for gas-gas, gas-surface and surface-surface zone interchange for rectangular parallel pipeds and cylinders. Rectangles are divided into small cubes and square zones, while cylinders are subdivided into right circular coaxial gas cylinders and coaxial cylinder wall and end ring zones. The factors are determined for all possible combination of interchange and are plotted or tabulated for range KB = 0 - 1.25 for cylinder and KB = 0 - 14 for rectangles, where B is the characteristic length of the zones.

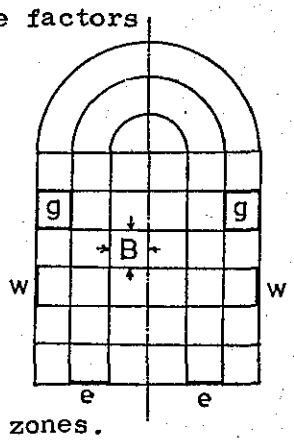

From these factors one can determine the net exchange factor for any zone pair, making due allowance for interaction with all other zones.

2.2.5(b) Prediction of radiant flux from a medium of known absorption coefficient

Knowing the absorption coefficient K, the exchange factor $\overline{g_s}$ for the combustion chamber under study can be determined. The combustion chamber may first be approximated by a cylinder which is divided into a number of coaxial cylinders, each characterised by

thickness B. The $\overline{g_s}$ of each gas element to the surface element considered is summed to obtain the resultant factor:

$$\sum \overline{g_s}\ e\ /\ (KB)\ B^2$$

$$\sum \overline{g_s}\ w\ /\ (KB)\ B^2$$

Net exchange factors from cylindrical gas volume to a particular cylinder end surface element or the cylinder wall surface element as a function of gas absorption coefficients, are shown in Fig. (2.1). The curves would correspond to any cylindrical combustion chambers of diesel engines which can be divided to equal number of zones as shown (Fig. 2.1) as long as the range of KB are not exceeded.

Hence the radiant flux at the required surface may be calculated if the radiant temperature is known:

$$\dot{q}_R = \sigma\ T_f^4 \quad \frac{\left[\ \overline{g_{s_e}}\ /\ (KB)\ B^2\right]}{A} \times (KB)\ B^2 \qquad (2.28)$$

where A is the area of the zone considered

T_f is the flame temperature.

2.2.6 Calculation of radiant heat flux in the diesel engine

Experimental work on radiation heat transfer from diesel engines (Lynn, Flynn and Sitkei) have shown negligible CO_2 and H_2O radiation compared to the continuous radiation from the luminous soot particles in the combustion process. It is obvious from previous discussions that detailed theoretical calculation of gas emissivity is very complicated, and usually involves simplifying assumptions. Therefore reliance must instead be put on experimental

data obtained on diesel engines to provide reliable estimates of radiation heat transfer. The available data (present and past) on diesel engines could be generalised in the following manner:

1) The literature reveals that flame temperature in diesel engines may be assumed the same in magnitude and rate of change near TDC. The measured flame temperature in several diesel engines plotted in Fig. (6.49), shows close agreement considering the difficulty and errors involved in measuring it.

2) An approximate average mean beam length for the particular combustion chamber at a particular time can be calculated ($L_m = \frac{3.6V}{A}$). Accurate allowance for the effect of shape can also be calculated following the method presented by Hottel (52) (Section 2.2.5).

3) Instantaneous apparent flame emissivity can be estimated from measured instantaneous radiant flux and the assumed flame temperature (measured in a similar engine):

$$\epsilon_a = \frac{\dot{q}_R}{\sigma T_f^4} \qquad (2.29)$$

4) A corresponding absorption coefficient (K) for the flame can be calculated using the definition:

$$\epsilon_a = (1 - e^{-KL}) = (1 - e^{-K_p P_L}) \qquad (2.30)$$

5) In the present investigation, the absorption coefficient was obtained without using the relationship: $\epsilon = 1 - e^{-KL}$ Instead, the combustion chamber was simulated by a cylinder, subdivided into a number of zones (section 2.2.5). The overall shape factor of all gas zones in relation to the measurement location (surface zone) was obtained as a function of absorption coefficient as shown in Fig. (2.1). Thus, the value of $\left[\sum \overline{gs} \; / \; (KB) \; B^2 \right] * (KB)$ obtained from equation (2.28) was used to obtain K from Fig. (2.1).

6) The estimated absorption coefficient could then be used in combination with an approximation of the flame shape to predict heat flux in other diesel engines. The shape of the combustion chamber may be represented by a mean path length, or more accurately by exchange area factors as outlined in previous section.

An example of the foregoing procedure can be shown as follows: Consider a diesel engine combustion chamber of dimensions 6.4 cm diameter and 1.28 cm deep near TDC position. The approximate average mean beam length would be:

$$L = \frac{3.6V}{A} = 0.018m$$

Assuming a flame temperature of 2000°K, and measured radiant flux of 500 kW/m^2 at the cylinder end, following steps (3) and (4), equation (2.29) give an apparent grey body emissivity:

$$\epsilon_a = \frac{\dot{q}_R}{\sigma T_f^4} = \frac{500}{56.7 * 10^{-12} * (2000)^4} = 0.55$$

Then from equation (2.30):

$$0.55 = 1 - e^{-KL}$$

$$KL = 0.8 \text{ and hence } K = 44 \text{ m}^{-1}.$$

On the other hand, following step (5) above, the cylinder is divided to 10 co-axial cylindrical zones, each characterised by thickness B = 0.64 cm. Then substitution of measured $\dot{q}_R$ assumed T_f, B and surface area (A) of zone considered (corresponding to measured flux location) in equation (2.28). It is found that

$$\left[\sum \overline{g_s}\right] * KB = 5.19.$$

Now this value represents a point on the relevant curve in Fig. (2.1) corresponding to KB = 0.26 and $\sum \overline{gs} = 20$. Hence a value of $K = \frac{.26}{B} = 41 \text{ m}^{-1}$ which is approximately the same as the above estimated value of 44 m^{-1}.

It is obvious, therefore, that a knowledge of absorption coefficient and flame temperature would enable the estimate of radiant flux by calculation in reverse of the above procedure.

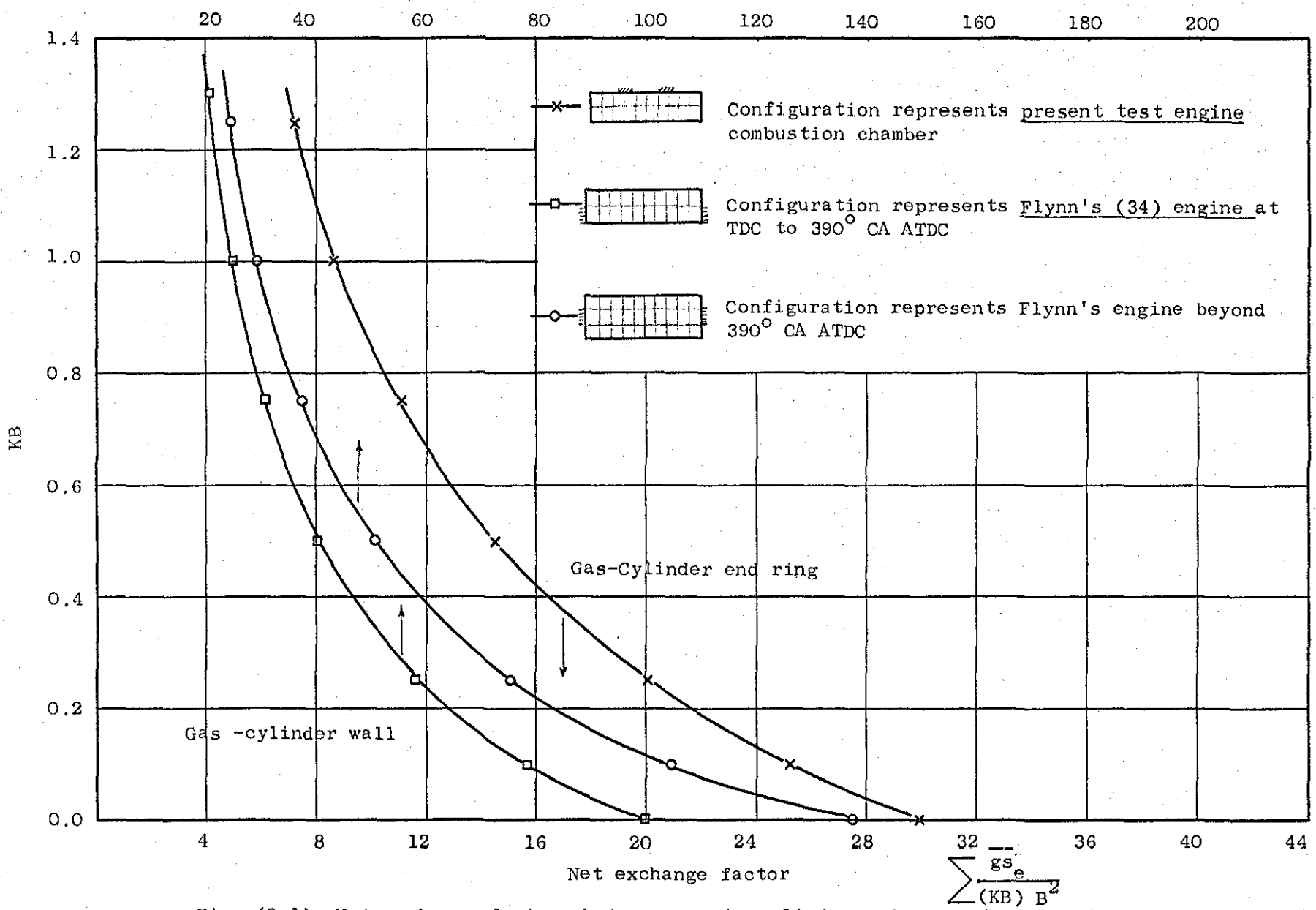

Fig. (2.1) Net exchange factors between gas in cylinder and a particular cylinder end ring or cylinder wall element, as a function of medium absorption coefficient.

CHAPTER 3

DEVICES FOR MEASUREMENT OF TRANSIENT HEAT FLUXES

3.1 Design and Development of the Surface Thermocouple

3.1.1 Introduction

In internal combustion engines, the analysis of instantaneous heat transfer and estimates of thermal stresses in the combustion chamber require the temperature history of metal surface. This has previously been achieved (Overbye et al (14), Le Feuvre et al (20), Law (39), Hassan (37) etc) using Hackmann (71) or Bendersky (72) type surface thermocouples, the construction of which is shown in Fig. (3.1). This type of thermocouple is simple in construction and cheap, but suffers from the following disadvantages:

i) Deterioration with use as result of damage to oxide coating which perhaps is weakened in the manufacturing (crimping) process.

ii) Excessive electrical noise interference caused by central wire vibration.

iii) Its use for heat transfer studies limited to iron or steel walls.

Thin film elements (resistance or thermocouples) with time constant in the micro-second range have been developed (72, 73, 84 and 85) which will be adequate for present investigation where 1^{o} CA corresponds to about 100 μs at maximum engine speed. These devices possess negligible thermal capacity and are in intimate contact with the surface examined. Ma (17) prepared a composite film surface thermocouple deposited directly on the combustion chamber of a diesel engine. The major set back in the design was the use of pressure contacts between the thin films and wire leads which produced electrical noise interference, and that a new set of thermo-

couple junctions had to be deposited when carbon deposit became excessive, because of difficulty in cleaning without damaging the unprotected metal films.

3.1.2 Design and development of the surface thermocouple

A surface thermocouple, essentially a development of Ma's (17) composite-film thermocouple, was designed for the present investigation. The construction of the thermocouple is shown in Fig. (3.2). The essential features of the thermocouple are:

i) Body.
ii) Thermocouple wires.
iii) Electrical insulation.
iv) Thin films (vacuum deposited).

i) Thermocouple Body

The test engine cylinder head and piston material were not suitable for vacuum deposition processes due to their porous structure. A material (HE28 W.P. BS) in the form of a drawn bar (non-porous) which has similar thermal conductivity to cylinder head (LM14 BS) and piston (LM13 BS) materials (0.33 cal/cm.s.^{o}C compared to 0.35-0.4 and 0.34 cal/cm.s.^{o}C respectively). The thermal conductivities were also checked by measuring the electrical conductivities of the metal and using Lorenz' constant (89). Thermal conductivities within 15% of the specified values were obtained.

ii) Thermocouple wires

The combustion chamber wall temperature in internal combustion engines (less than 400^{o}C) is not a limiting factor in the choice of

thermocouple wire materials which was based on the following factors:

a) Materials most suitable for vacuum evaporation and which form thin films adherent to the thermocouple body material or to dielectric materials.

b) Pairs of materials with largest emf per degree in temperature.

In the light of these factors, iron, constantan, nickel and copper were tested. Iron and constantan proved most successful.

iii) Electrical insulation

From the sketch shown in Fig. 3.2, it is evident that the electrical insulation between the thermocouple wires, thin metal film and the substrate must be maintained. The insulation between the wires and the body was achieved by using Pyrex tubes. The difficult problem encountered in the preparation of the thermocouple and indeed the most critical process, was the filling of the cavity between the end of the wires and the body (point X in Fig. 3.2) with a non-conducting material. The material must adhere to both metals and provide a surface between the end of the wires and the thermocouple body, suitable for deposition of films by the vacuum technique. Araldite epoxy resin could not be used because it burns at about 180^{o}C. On the other hand, ceramic materials or ordinary glass could not be used because of their higher melting temperatures than that of aluminium alloy used for thermocouple body.

A glazing flux, used by Pyrotenax Limited, for sealing the end of sheathed cables was utilised for the present surface thermocouple. This glazing flux is of glass base, suitable for application in the temperature range 180^{o}C to 350^{o}C. The maximum temperature being limited by the melting point of the flux. The glazing flux, initially

of fine powder, is run into the cavity by using a drip wire. The wire is coated with a thick layer of glazing flux by heating to red, then dipping it in the powdered flux and puddling the molten flux into the cavity. The procedure is repeated until the seal cavity is full. The quality of the filling was affected by several factors, such as flame intensity, substrate temperature, etc. Therefore the process of cavity filling may be repeated several times before a satisfactory filling is obtained.

iv) Vacuum deposited thin films

The leads for the thermo-junction of the thermocouple are deposited in thin film form on top of electrically non-conducting layer, previously deposited on the metal substrate. The vacuum deposition was carried out using an Edward Vacuum Ltd. unit type E500.

A popular material for dielectric films for electrical purposes is SiO. However, AL_2O_3, MgF_2, M_gO and SiO_2 are all well known as dielectric materials and a layer of less than 1000 $\mathring{A}$ of one of these materials would be suitable. MgF_2 is preferred to SiO_2 and Al_2O_3 for two reasons:

a) Ease of evaporation.

b) It provided the most adherent film with thermocouple plug material.

The shape of the junction leads, dielectric layers and contact areas were formed by evaporating the film material through alternative masks of thin aluminium foil strips held in position by holders. The metals were evaporated using the standard techniques described by Holland (80).

The vacuum evaporation process, the problems involved in the development of the surface thermocouples and step-by-step procedure of the manufacturing has been described in detail in a departmental report (70). Fig. (3.4) shows one of the manufactured surface thermocouples used in the present investigation for measurements on the cylinder head.

3.1.3 Calibration of surface film thermocouple

3.1.3.1 Static calibration of surface thermocouples

According to Marshall et al (76), the thermal emf characteristics of thin film thermocouples is affected by film thickness and deposition conditions. Therefore the calibration of individual thermocouples produced was necessary. Several thermocouples could be calibrated at the same time, in the termpature range 20-200^{o}C using a silicon oil bath. The bath was enclosed in a suitable container and brought up to temperature by means of a controlled heater. The bath temperature was measured using a standard iron-constantan thermocouple. The oil bath was later replaced by a furnace which had an exceptionally uniform temperature zone, with control to within $\pm$ 1^{o}C at 200^{o}C. The result of the calibration showed good agreement between the surface thermocouples and the standard iron-constantan thermocouple. The thermal emf characteristic of one batch of thermocouples produced together were exceptionally similar. Typical curves for iron-constantan thermocouples are given in Fig.(3.5).

3.1.3.2 Dynamic response of the surface thermocouple

The aim of this test was to present an observation on the dynamic behaviour of the surface thermocouple, or rather the behaviour of the surface thermocouple followed by an amplifier and then a magnetic tape recorder or oscilloscope which were used together for recording surface temperature changes in the engine combustion

chamber. The intention here was to compare the dynamic characteristic of the surface thermocouple with the known characteristics of Kistler pressure transducer type 601H (resonant frequency = 130 kHz, rise time 3 microseconds).

The two transducers were mounted at the end of a shock tube, with the sensing elements in the same plane. This was to ensure simultaneous response of the two devices by the shock impact.

Fig. (3.6a) shows the signal obtained from a pressure transducer used to determine the velocity of the shock wave. This transducer was located 31.8 cm ahead of the test pressure transducer fixed adjacent to the surface thermocouple. The speed of the shock was estimated to be 482 m/s.

Fig. (3.6b) shows the signal obtained for the pressure and surface temperature changes caused by the shock impact. It is obvious from these traces that the initial surface temperature rise a-b is caused by the shock impact, while the later slow rise b-c is mainly by conduction heat transfer from the compressed gas. The time taken for the pressure and surface temperature signals to reach maximum value induced by shock were 50 μs and 200 μs respectively. Therefore if the time constant is defined as the time taken for the signal to reach 63.3% of its maximum value, the time constant for the surface thermocouple is 125 μs.

At the maximum engine speed (1750 rpm) investigated, the time corresponding to 1 deg. CA is 96 μs. Under such conditions, the thermocouple is capable of detecting any significant heat release in 125 μs, i.e. over 1.25 deg CA. This time is relatively short when compared to the usual combustion time of 30-40 deg CA. Hence the thermocouple is considered adequate for the measurement of heat flux in IC engines, particularly at engine speeds $<$2000 rpm.

3.2 Infrared Radiation Detection System

3.2.1 Introduction

Infrared radiation is a form of electromagnetic energy. It is therefore possible to detect by absorbing it and hence converting the energy to heat. This was the basis of early experiments using a blackened thermometer bulb. However this is slow, insensitive and inconvenient. A device that gives an electrical output is more desirable.

3.2.2 Infrared detector types

Radiation detectors fall into two basic categories, heat sensors and photon counters. The first of these categories contain all devices in which the energy of the absorbed photons is re-distributed as a thermal excitation. This change in thermal excitation is then measured by observation of some parameter such as an expansion, deformation or thermoelectric potential. Devices such as thermocouples, bolometers and Golay cells fall into this category. None of these devices possess the required frequency response (e.g. 10^4 Hz corresponding to 1^o CA interval at engine speed of 1750 rpm) for engine work, because of their dependance on their thermal inertia.

The second category of detectors contains those in which the energy of the absorbed photon causes a direct change in the electrical state of electrons within a crystal. Most of these devices can be categorised as semi-conductors in which the absorption of a photon moves bound electrons, from the valence electron band of the material into one of the conduction electron bands and thereby greatly changes the electrical character of the material. This change in the electrical nature can then be measured by a variety of means,

such as measurement of resistance change in a photoconductor or voltage output from a photovoltaic cell.

The frequency response of these photon detectors is associated with the electron mobility within the crystal lattice of the material. The time constant in these devices ranges between 1 to 100 μs, which is quite suitable for engine work. The signal level for photon devices is also high when linked to amplifiers with good impedance matching. The one problem with photon detection devices is that their output is a function of photon arrival rate and not their power (i.e. response to short wavelength (high energy) photons is similar to their response to long wavelength (low energy) photons). To eliminate this problem a device to separate the photons on a wavelength basis must be used to identify the power input to the detector. This makes the system using a photodetector more complex.

Another type of thermal detector which uses the pyroelectric effect of some ferro-electric materials, has recently emerged. These detectors, which could be made with short time constants (less than 1 μs, Kimmit et al (91)) and still retain a useful sensitivity. This type of detector will be described in more detail below (Section 3.2.5).

3.2.3 Choice of a detector for engine work

To investigate the importance of the radiant component of instantaneous heat transfer in a diesel engine, the detection system must be chosen on the basis of:

i) Spectral range important in such heat transfer.

ii) Overall accuracy and sensitivity.

iii) Frequency response required.

In the following text, each of these topics will be discussed briefly in relation to the choice of the final detector.

Flynn et al (34) reported peak radiant heat fluxes in a diesel engine of the order of 1200 kW/m^2. If this fact was considered along with the range of temperatures that could occur in the combustion chamber (up to 2300°K, Myers et al (42)), then boundaries can be drawn for the requirements of the sensing system as far as spectral range and sensitivity are concerned.

It is desirable to be able to detect and identify with some accuracy, heat transfer rates of the order of 20 kW/m^2. This heat transfer was used to define a minimum apparent radiating temperature as follows:

$$\dot{q}_R = 20 = \epsilon_a \sigma T_2^4 \quad kW/m^2$$

Solving for an apparent lower limit temperature from the above equation (assuming an apparent grey body emissivity of 0.5), 900°K was obtained as a minimum important temperature. The upper temperature (flame temperature) observed in different diesel engines appears to be similar (Section 6.10.2) and is of the order of 2200°K.

Considering Planck's distribution function (Section 2.2) for radiant emission, it can be shown that 90.4% of the emission from a grey or black body falls in the spectrum such that λT is greater than 2100 micron degree Kelvin. Also 90.2% of the radiation falls into the spectrum such that λT is less than 9440 micron degree Kelvin. With these boundaries on λT and the potentially important temperature range, the boundaries on the spectrum containing approximately 80% of the power emitted by a black or grey radiation source were:

At 2200°K	0.95 - 4.2 micron
At 900°K	2.3 - 10.5 micron

The required frequency response for a system to measure radiation was determined from examination of the time span in which it was desirable to detect a change in measured radiation. If the engine operated at 1750 rpm (maximum test speed) and it was desirable to be able to define radiation in terms of what was happening within one crank angle degree of engine rotation, calculations could yield a required time constant of the order of 100 μs. With the criterion outlined above, it was possible to consider various types of detectors.

Most photon detectors are known (58, 90) to be useful in the range 0.5 to 7 micron (which falls short of the spectral limit 10.5 micron, important at the lower limit temperature 900°K in the diesel engine) and possess time constants in the range of one microsecond, which is more than adequate for engine work. However, photon detectors with associated amplifiers are rather expensive and are ideal when used with a monochromator for spectral emission measurements because of their high sensitivity. The whole system, detector-monochrometer, however, becomes complex and a simpler system for overall radiant emission detection (irrespective of wavelength) was considered more useful in the present investigation. The combined advantage of response to wide bandwidth, small time constant (adequate for engine work) and a relatively low cost was found in pyroelectric detectors (91, 92 and 58).

Having defined the spectral characteristics in the diesel engine and chosen a pyroelectric detector (sensitive in range visible 35 microns), the next step was to select a window material to transmit

the radiant energy from cylinder charge to the detector. Considering the strength, spectral characteristics, cost and availability, Kodak 'Irtran 4' with spectral transmission visible to 21 microns, was chosen as a window material.

3.2.4 The pyroelectric effect

Crystals of single domain structure of materials such as Triglycine Sulphate (TGS) which are ferro-electric, exhibit a large spontaneous electrical polarisation at temperatures below their Curie points, and if the temperature of the material is altered, the degree of polarisation is changed. The change in polarisation (P_s) can be observed as electrical signals if electrodes are placed on opposite faces of a thin slice of the material to form a capacitor. When polarisation changes, the charge induced on the electrodes can either flow as a current through a comparatively low external impedance, or produce a voltage across the slice if the external impedance is comparatively high. The detector will only give an electrical signal when the temperature changes, that is, when the level of incident radiation changes. The magnitude of the signal appearing across a load resistor (R) connected across the crystal in the direction of the polar axis is:

$$\Delta V = AR \frac{d P_s}{dt} = AR \left(\frac{d P_s}{dT} \right) \left(\frac{d T}{dt} \right) \qquad (3.1)$$

providing that the modulation frequency $\omega (= 2\pi f)$ is greater than the reciprocal RC time constant of the crystal load circuit, and R is less than the leakage resistance R' of the crystal. A is the electroded area and $\frac{d P_s}{dT}$ is the pyroelectric coefficient of

the material. Thus ferro-electric crystals may be used as thermal detectors of electromagnetic radiation. They are, however, different from other thermal detectors in that the output signal is proportional to the rate of change of temperature and so does not depend on the crystal reaching thermal equilibrium with the radiation. Consequently, pyroelectric detectors are capable of operating at much higher frequencies, yet retaining the 'black body' response of thermal detectors.

To calculate the pyroelectric detector performance, both the thermal and electrical characteristics must be considered in detail and the sources contributing to the detectors noise must be enumerated. These aspects are discussed in detail by Cooper (92), Putley (58, Chapter 6, page 259) and Glass (93). Also in a departmental report (94).

3.2.5 The present detector and associated electronics

The detector used in the present study was provided by Plessey Components Ltd. The element of the detector (ceramic pyroelectric PBZT) was sensitive in the spectral range, visible to 35 microns wavelength. The element was a chip of 1 mm^2 and 1 micron thick, fixed to the centre pin of a standard BNC plug to facilitate direct attachment to the associated (preamplifier) electronics. Some of the relevant properties of the ceramic pyroelectric material are given in Table (3.1).

The preamplifier is one of the most critical components in the entire system. The primary requirement is for a noise level that is so low that the noise from the detector is the limiting source of noise in the system. A low output impedance is desirable in order to permit the use of low-impedance connecting cables.

The desired voltage gain of the preamplifier depends on the system application, it is affected by the distance from the preamplifier to the rest of the signal processor, the mechanical and electrical environment, and the maximum undistorted output swing of the preamplifier. To maintain a low noise level for the system, a voltage gain of about 10 in the preamplifier will ensure that the noise contribution of succeeding stages is negligible. If other noise sources are anticipated, such as microphonic or cable pick up, the gain should be increased.

Most transistorised preamplifiers begin to saturate when the output exceeds a few volts. A conservative designer will assume a maximum output swing of 1 volt, and about 100 volts for vacuum tubes. The dynamic range of the preamplifier is therefore limited by the detector noise level at its input and the maximum allowable output swing.

A low output impedance of the preamplifier of 100 to 1000 ohms is desirable, in order to minimise the pick up in low noise shielded cables running to the rest of the signal processor. In systems with a high information rate, a low output impedance ensures that the capacitance of the cable will not attenuate the high frequency components of the signal.

In this investigation, where the detector is exposed to fairly severe vibration and audible noise, plus the restricted space available for the detector and preamplifier on the cylinder head of the Ruston 3YWA engine, the use of the vacuum tube was not considered. Therefore the alternative was the use of a transistor preamplifier which exhibits good microphonic performance and requires less space. Field-effect transistors (FET) have proved useful in preamplifiers

because of their low noise factor and high input impedance. Therefore an FET was utilised in order to match the high impedance of the pyroelectric detector used in this investigation. Before the construction of the preamplifier, calculations were carried out for the detector-amplifier system to fulfil the following requirements:-

i) Flat frequency response of the system up to the value that will produce a realistic representation of the high rate fluctuations of radiant flux expected in diesel engines (10^4 Hz, Section 3.2.2).

ii) To produce a high signal to noise ratio at low irradiance levels of about $3 * 10^{-3}$ W/cm^2, estimated at the detector after passing through a small opening and window.

To fulfil these requirements, the circuit shown in Fig. (3.7) was considered. A low noise FET type BF818 and low noise resistors (provided by the Royal Radar Establishment) were used in constructing this preamplifier. A load resistor of 818 kΩ produced an electrical time constant for the circuit of:

$$t_E = RC = 8.18 * 10^5 * 18 * 10^{-12} \qquad (3.2)$$

$$= 15 * 10^{-6} \text{ sec}$$

which is equivalent to electrical cut-off frequency of:

$$f = \frac{1}{15 \times 10^{-6}} = 6.67 * 10^4 \text{ Hz}$$

This is well above the estimated value necessary for engine work (10^4 Hz). The use of smaller load resistors would provide flat response over a wider frequency range, but reduce voltage responsiveness. Thus, the load resistor of 818 kΩ was selected to obtain the responsiveness versus bandwidth trade off that is most appropriate for the present application.

In constructing the preamplifier, the cables between the detector and preamplifier were made as short as possible to add no capacitance which may reduce the time constant of the system and to avoid cable noise. The circuit was built as compact as possible on a rigid frame fixed inside a brass casing. The latter was provided with a male BNC socket at each end, one for the detector attachment and the other for the output. Fig. (3.9) shows the detector, preamplifier casing and viewing window adaptor.

3.2.6 Calibration and performance of the detector

i) Calibration test rig

The black body type source used for calibration purposes have an emissivity somewhat less than unity (probably independent of wavelength).

In 1880, Kirchoff pointed out that the radiation within an isothermal enclosure is black body radiator, therefore if a small hole is cut through the wall of the enclosure, the radiation leaving this hole should closely simulate that from a black body. A typical configuration utilised for black body sources, is the conical cavity characterised by the depth of the cavity L and the diameter of the opening (2r). On this basis, a conical cavity of opening radius r = 1 cm and $\frac{L}{r} = 8$ was fabricated from 18-8 series stainless steel,

which has good thermal conductivity. Heating the surface to above 800°C formed a stable oxide film on the surface, which according to Snyder (58) has an emissivity of 0.85.

If the emissivity of the cavity surface is assumed to be 0.85, the effective emissivity calculated for the cavity is 0.99 (Gauffe (58)).

This core was placed in a muffle furnace which could be heated to 900°C. The temperature was controlled by a variac, chromel-alumel thermocouple combination. The temperature variation near the end of the core was effectively eliminated by shielding with insulating plate. The limiting aperture (simulation of the combustion chamber viewing passage) and the effect of the radiation viewing window were included in the calibration set up.

A variable speed motor was modified to carry a square wave chopper in order to generate the desired waveform of the chopped pulse. The detector was mounted on a rigid stand, and alignment of the detector with the cavity axis was achieved by looking through the muffle furnace from the opposite side (core removed).

A low noise Brookdeal amplifier type LA 350 (Section 4) that permits a choice of upper and lower frequency cut off was used to further amplify the signal. It also incorporated an r.m.s. meter. The amplified signal was then displayed on a general purpose oscilloscope. A schematic diagram of the calibration test is shown in Fig. (3.8).

ii) Calibration test results

In order to avoid inaccuracies caused by the introduction of shape factors due to configuration, the detector-window and opening arrangement in the cylinder head was simulated exactly for the calibration test, as shown in Fig. (3.8). With this arrangement, the outer hole of the passage in front of the window acts as the limiting aperture. The only correction necessary, compared to the engine setting was for the small distance (0.5 cm) between the limiting aperture and the black body source.

In the calibration test, the output signal of the detector-amplifier system at various black body temperatures (chopping frequency constant at 200 c/s) was observed. The effect of chopping frequency on the output signal was also investigated. Table 3.2 gives the observed results.

The emissive power of the black body source is calculated using Kirchoff's law of radiation.

$$w = \epsilon \sigma (T_s^4 - T_{ch}^4) \qquad (3.3)$$

where ϵ = 0.99 the effective emissivity of the source.

T_{ch} = the chopper blade temperature.

The radiant flux density calculated for source temperatures of 800, 1000 and 1200^{o}K were 2.24, 5.547 and 11.565 w/cm^2 respectively.

The radiant flux at the limiting aperture is effectively the same as the emissive power of the source calculated from equation (3.3). A plot of the radiant emittance against the detector-amplifier output is shown in Fig. (3.10). The linear relationship gives a constant factor of 11.2 w/cm^2 heat flux at the limiting aperture per

volt output of the detector-amplifier system. Thus, the corresponding radiant heat flux at the surface of the cylinder head could readily be calculated from the signal output of the detector when fitted on the engine.

On the other hand, to determine the responsiveness of the detector, irradiance at the detector must be calculated, taking into account all the factors causing attenuation of the radiant flux as it passes through the opening and window. This was calculated as follows:

a) Distribution of energy in the spectrum of a black body. The spectral response of the detector is visible to 35 μ, but that transmitted by the window is limited visible to 21 μ. Therefore the fraction of the total radiant power in this region only must be considered. This was determined from the tables giving relative energy below λT.

Therefore for λT =	222 - 9330:	278 - 11 667:	333 - 13 889 $\mu \cdot K$.
% Total power	0.976	0.988	0.991

b) Transmittance of the window material (Irtran 4): The transmittance of this material of thickness 2 mm is approximately 62% (Hudson (58)) over the range 0.5 - 21 μ. The window used in the present work was 1.9 mm thick, and assuming thickness effect to be linear, a transmittance of 65% was obtained.

c) Radiation through openings: In the passage between the limiting aperture and the window, the net radiation energy reaching the window is less than the total energy at the entrance. The net energy reaching the window is given by:

$$q_{net} = F_{1R_2} \; A \; (W_{b_1} - W_{b_2}) \qquad (3.4)$$

where F_{1R_2} = the angle factor between entrance and exit of the opening

A = Cross-sectional area of opening

W_{b_1} & W_{b_2} = radiant emittance at sections 1 and 2.

For openings with $\frac{\text{Diameter}}{\text{Length}} = 0.47$, $F_{1R_2} = 0.37$ chart in Jacob (53), Vol. 2, page 62.

d) Radiation between circular surface (window) and differential area (detector): The net radiant energy at the detector is given by:

$$q_{net} = F_{w_d} \cdot q_{window} \qquad (3.5)$$

where F_{w_d} is the angle factor defined by the angular relationships describing the mutual position of the two surfaces, and is equal to $1.272 * 10^{-4}$.

Hence the irradiance at the detector.

Considering all the above factors, the following table was obtained for radiation levels from the source to the detector.

Radiation source temperature ^{o}K:	800	1000	1200
Radiant emittance w/cm^2:	2.24	5.547	11.565
Net radiant energy at window W:	0.5875	1.455	3.033
Net radiant energy through window W:	0.263	0.659	1.378
Net radiant energy at detector w:	3.345	8.383	$17.53 * 10^{-5}$
Irradiance w/cm^2:	3.345	8.383	$17.53 * 10^{-3}$
Irradiance (r.m.s) w/cm^2:	1.505	3.772	$7.889 * 10^{-3}$
Detector output (r.m.s) volts:	0.1	0.24	$0.48 * 10^{-3}$
Responsiveness V/w:	6.6	6.4	6.2

The responsiveness of the detector as a function of chopping frequency is described by Fig. (3.11). The maximum chopping frequency was limited by the motor used. However, by extrapolation of the curve to the high frequency region, one may conclude that a reasonably flat response up to the design frequency is not unexpected.

As mentioned before, the configuration and the detector view of the radiating agent was kept the same for both the calibration and engine tests. Therefore, by keeping the detector-amplifier system set up condition constant, a direct conversion of the system output (volts) to heat flux at the cylinder head surface is possible with the calibration curve of Fig. 3.10. Hence:

$$\text{Instantaneous radiant heat flux} = 112 \times E \quad kW/m^2$$

where: E = instantaneous voltage output of the detector-amplifier system.

112 = calibration constant in kW/m^2/volts.

The time constant provides a convenient number to describe the speed with which a detector responds to a change in incident flux. For many detectors the variation of response with frequency can be described by:

$$R_f = \frac{R_o}{(1 + 4\pi^2 f^2 t^2)^{\frac{1}{2}}} \tag{3.6}$$

where R_f = responsiveness at frequency f.

R_o = responsiveness at low frequency.

t = time constant.

Taking f_1 as the frequency at which the responsiveness is 0.707 times its low-frequency value, the time constant is given by:

$$t = \frac{1}{2\pi f_1} \tag{3.7}$$

From the frequency response curve of the present detector (Fig. 4.18), the test frequency was limited, but if it is assumed that $R_f = 0.707$, its maximum value at about 3000 Hz, the calculated value of t is 50 μsec. This again is well below the suggested design requirement of 100 μs in order to respond to changes in radiant emission within 1^o CA at 1750 rpm.

TABLE 3.1

Some properties of the PBZ pyroelectric ceramic element of the radiation detector.

Pyroelectric coefficient P	$3.5 * 10^{-8}$ Columb/cm^2 ^oK
Resistivity (20^oC)	$5 * 10^9 - 7 * 10^{12}$ Ohm.cm
Dielectric constant e (50 kHz)	260 - 300
Volume specific heat c'	2.2 J/cm^3 ^oK
Grain size	1 micron
Curie temperature T_c	190 - 210^oC

TABLE 3.2

Observed results of the infrared-detector calibration test (chopping frequency = 200 c/s. Frequency band 3 Hz to 10 kHz).

Blackbody source temperature ^oK:	800	1000	1200
Output peak/peak volts:	0.25	0.53	1.06
Output r.m.s. volts:	0.10	0.24	0.48
Approximate chopper blade temperature ^oC:	50	60	70

Effect of Chopping Frequency

(Black body temperature = 800^oK

Frequency c/s:	10	25	50	100	250
Output P/P volts:	0.24	0.25	0.25	0.24	0.24

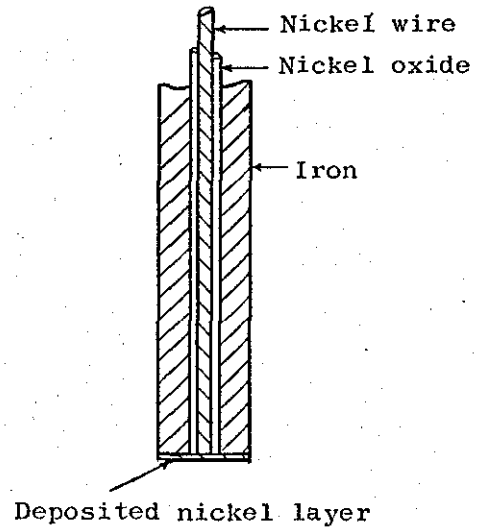

Fig. (3.1) Essential element of Hackemann surface thermocouple

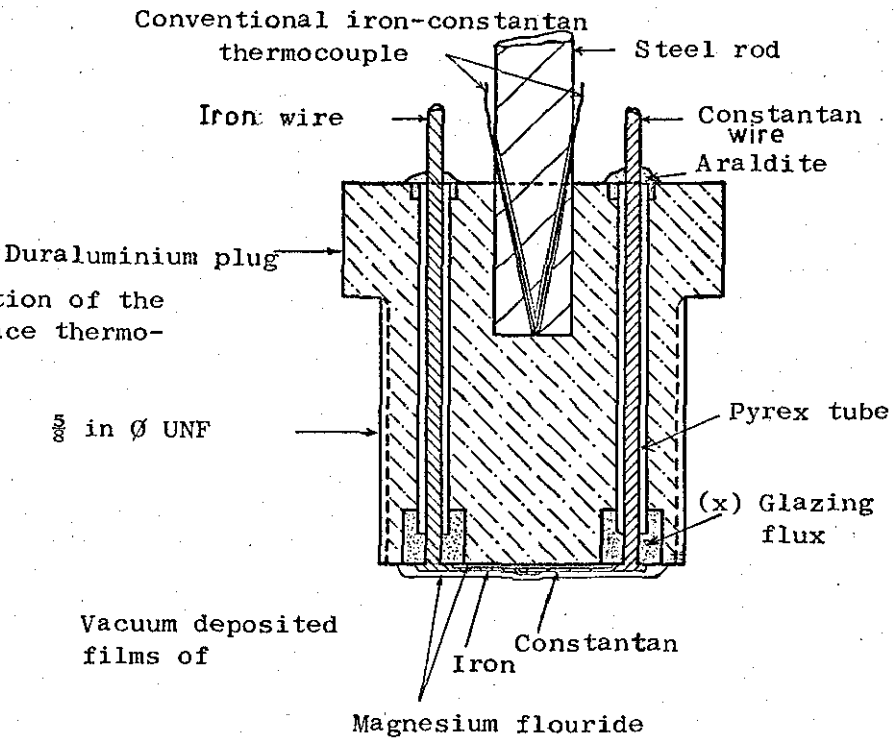

Fig. (3.2) Construction of the new surface thermocouple

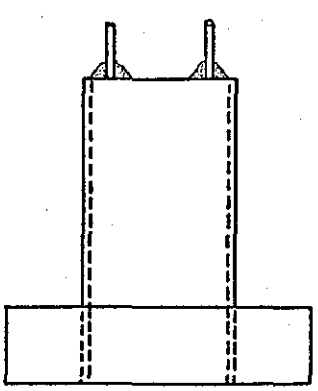

Fig. (3.3) Piston thermocouple plug and mount for polishing process

Fig. (3.4) A Thin Film Surface Thermocouple used for Measurements on Cylinder Head

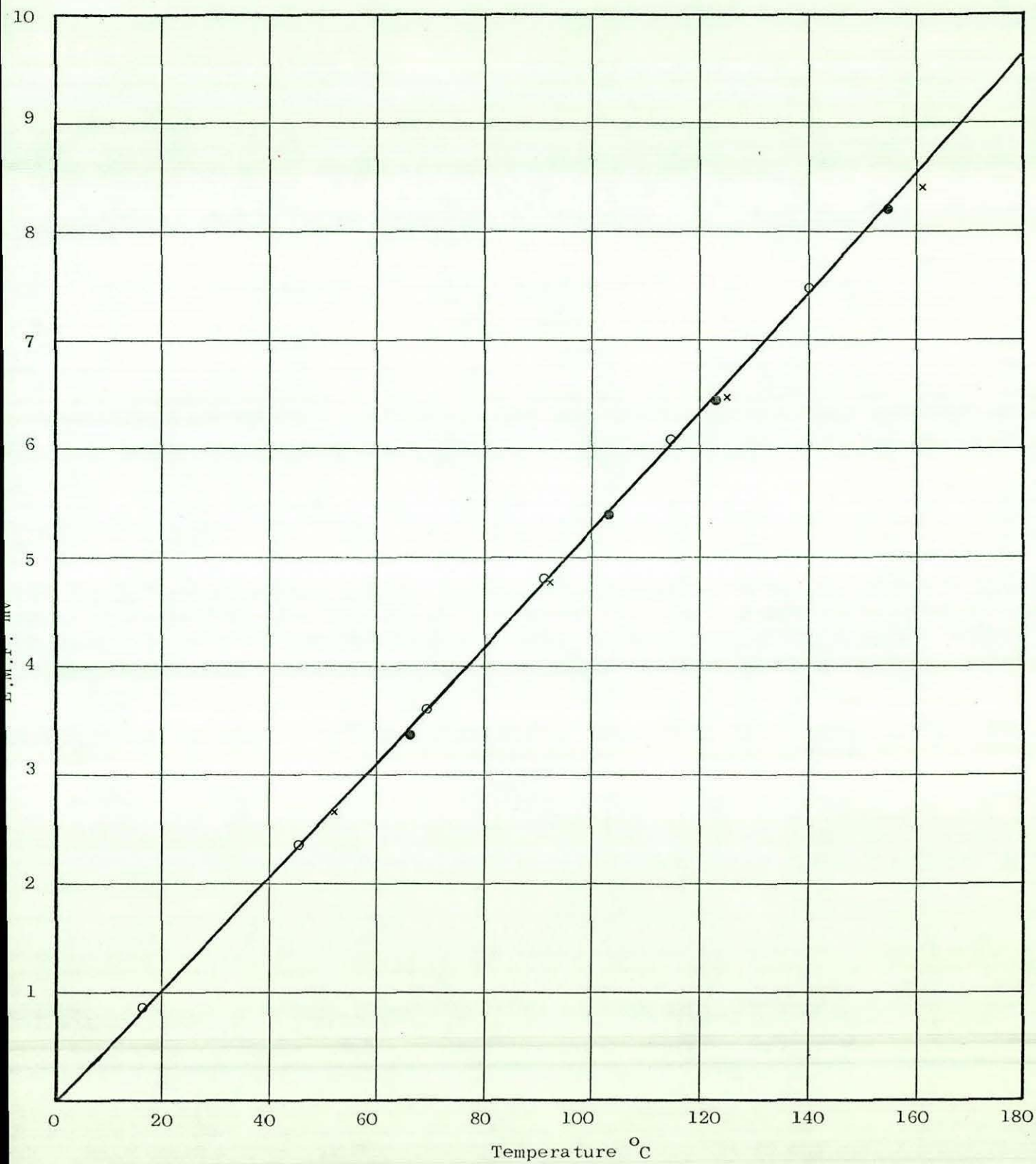

Fig. (3.5) Surface thermocouples calibrations compared to temperature-E.M.F. curve for standard iron-constantan thermocouple.

——— Standard iron-constantan thermocouple curve

× Batch of nine surface thermocouples for cylinder head

● Batch of nine surface thermocouples for cylinder head

○ Batch of nine surface thermocouples for piston.

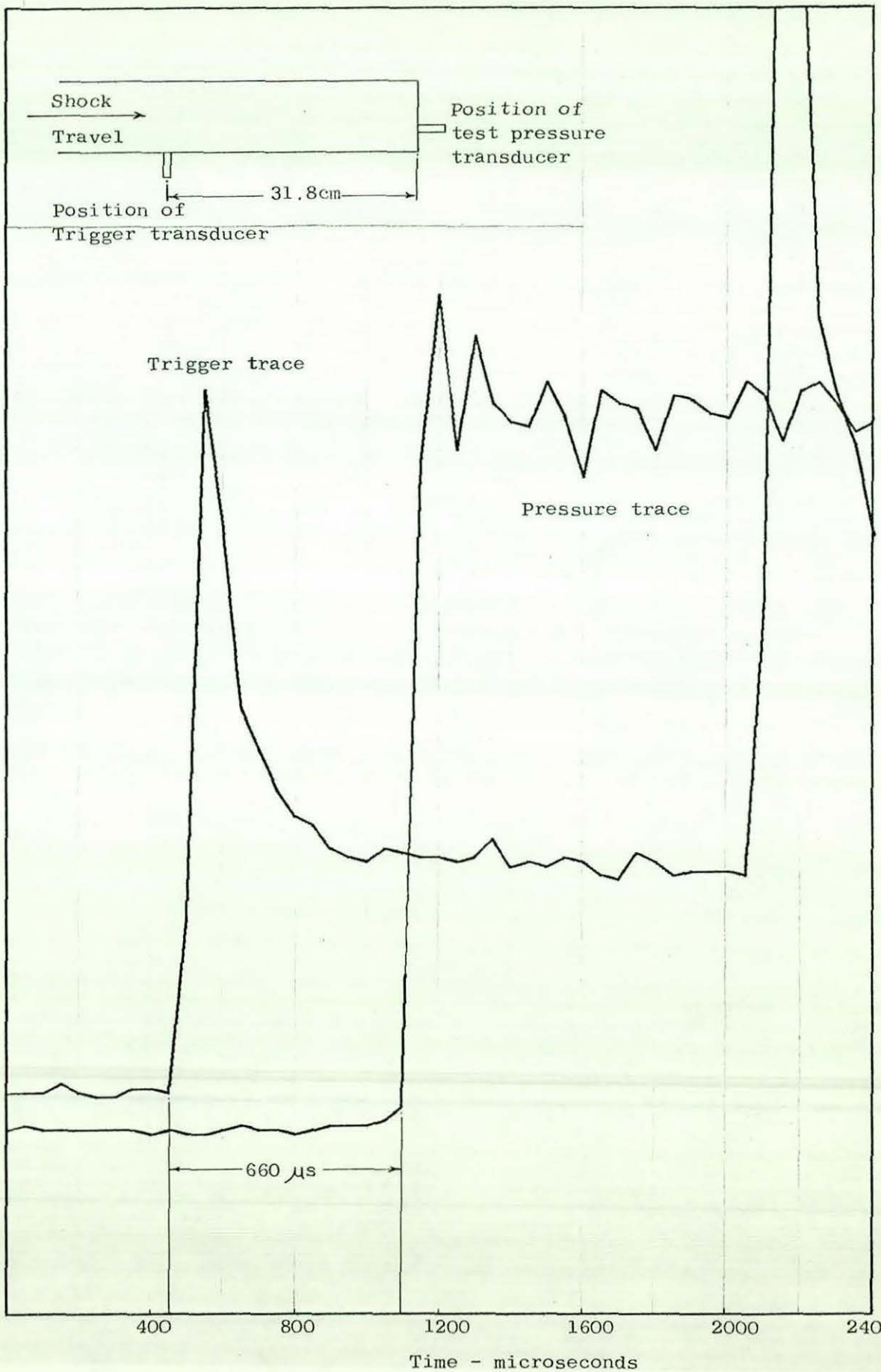

Fig. (3.6a) Shock wave speed indicated by two pressure transducers placed 31.8 cm apart

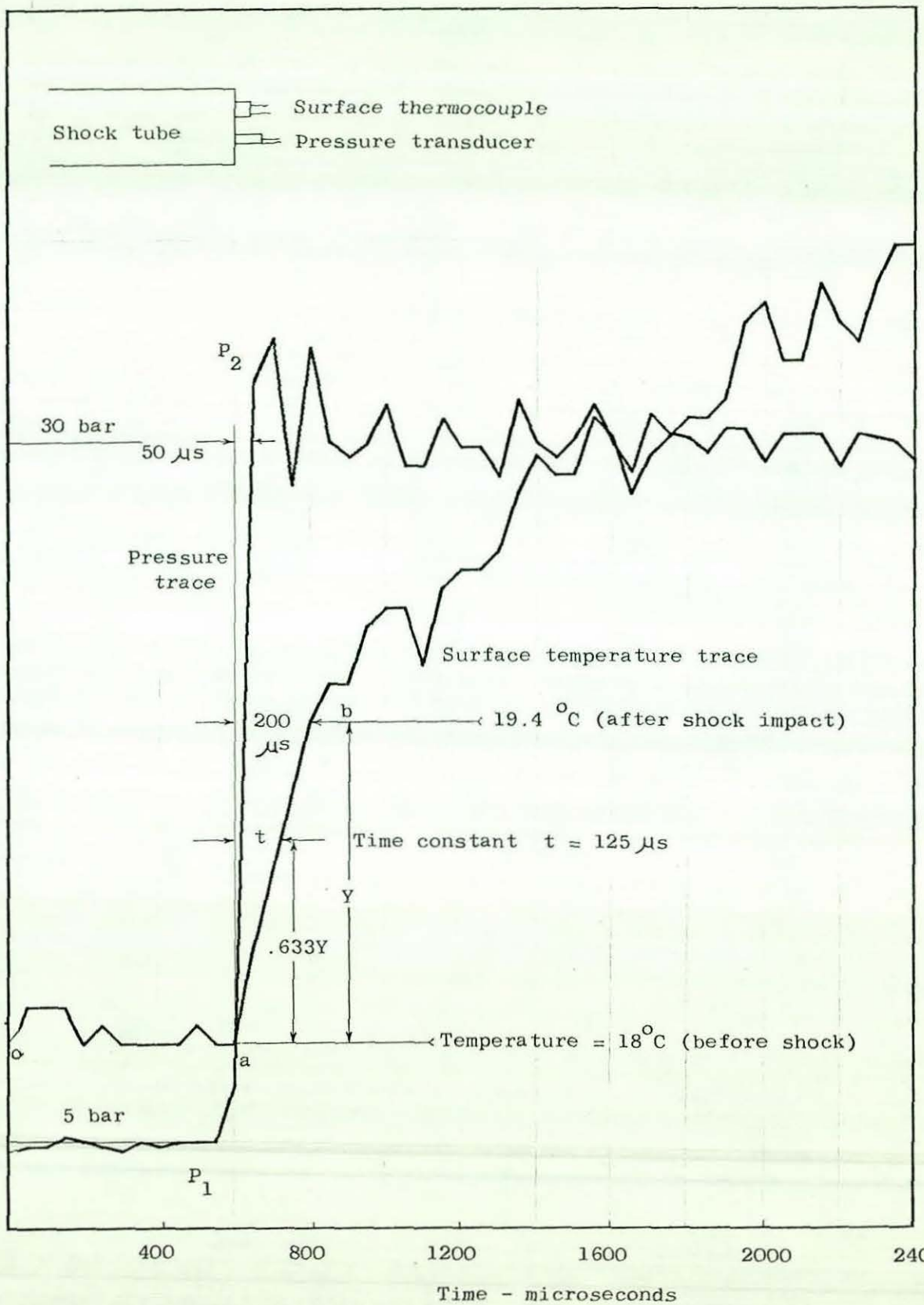

Fig. (3.6b) Surface thermocouple and pressure transducer response at stagnation point of a cylinder in the shock tube (shock produced by pressure ratio of 10 across a diaphragm)

oa surface temperature before shock
ab surface temperature change caused by shock impact
bc surface temperature change by slow conduction from the compressed gas
P_1P_2 change of pressure in shock tube

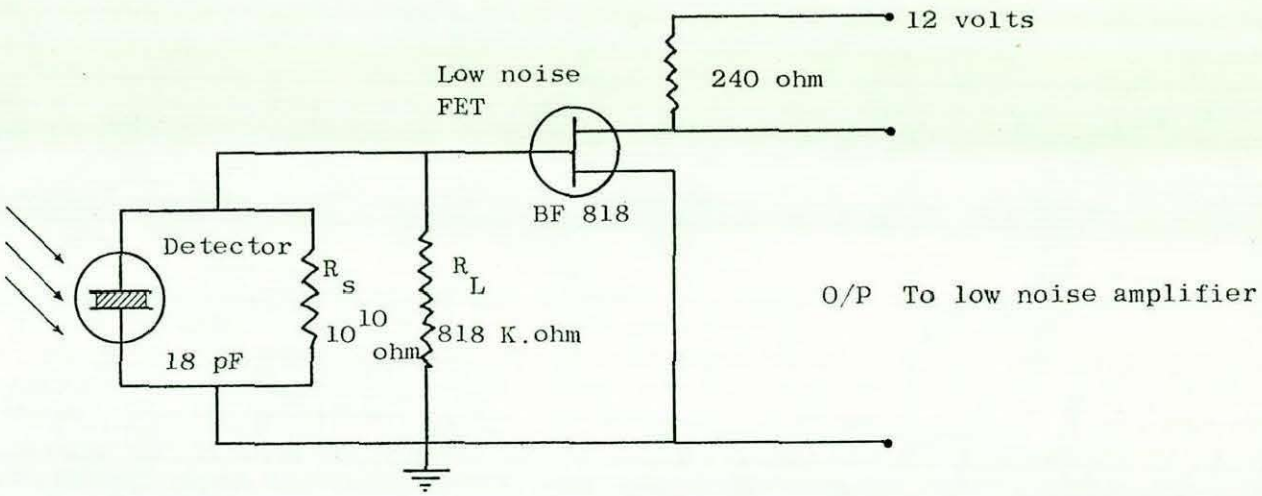

Fig. (3.7) Circuit diagram of preamplifier used with ceramic pyroelectric detector

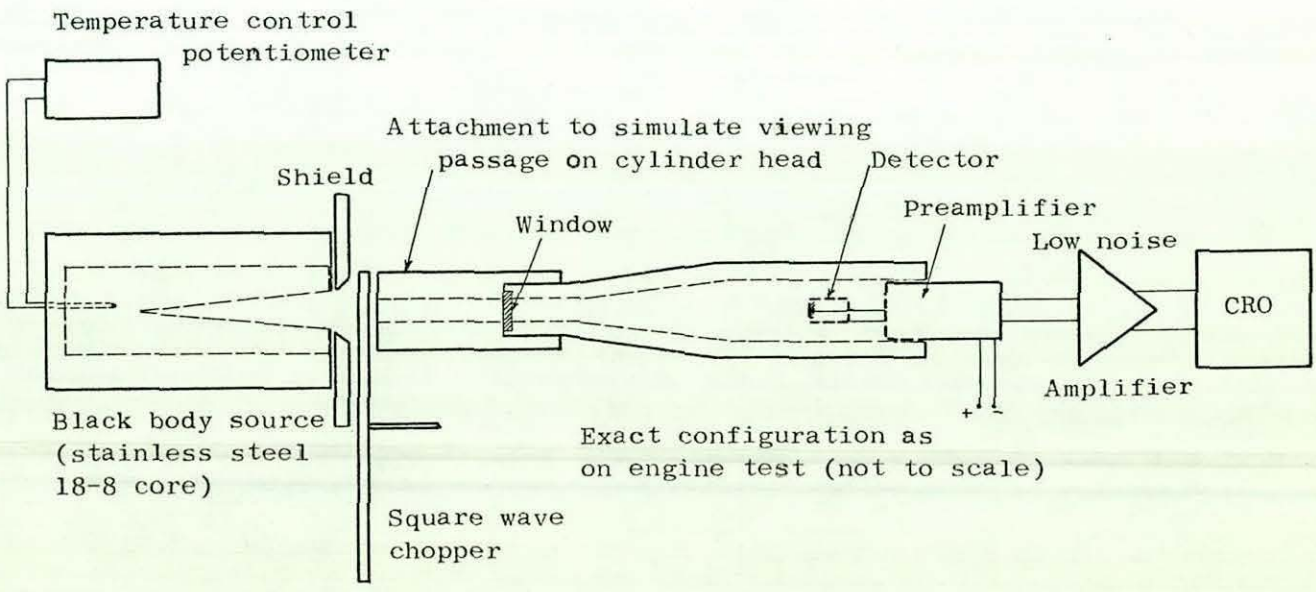

Fig. (3.8) A schematic diagram of the basic test set for the calibration of the infrared detector.

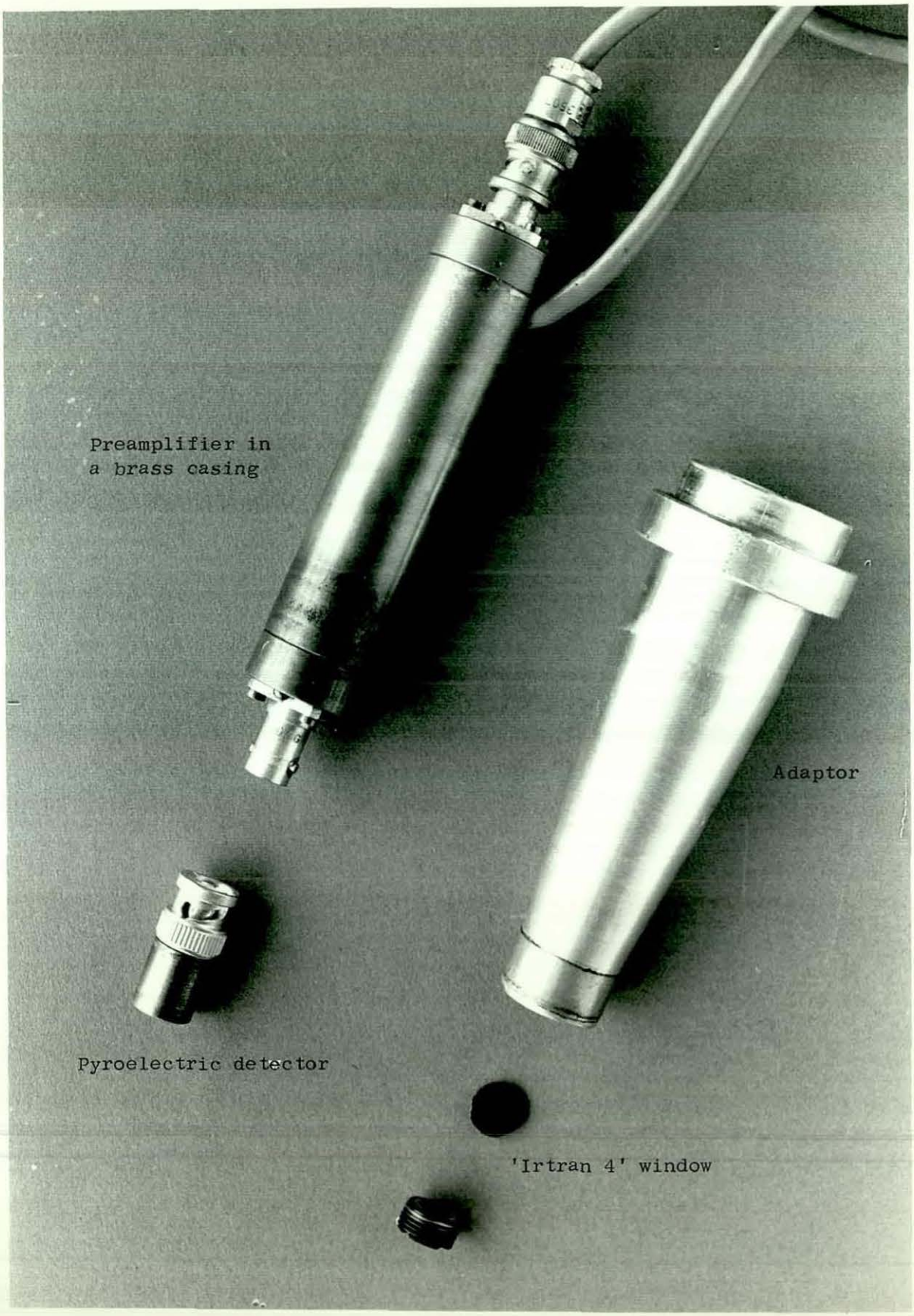

Fig. (3.9) Radiation Detection System

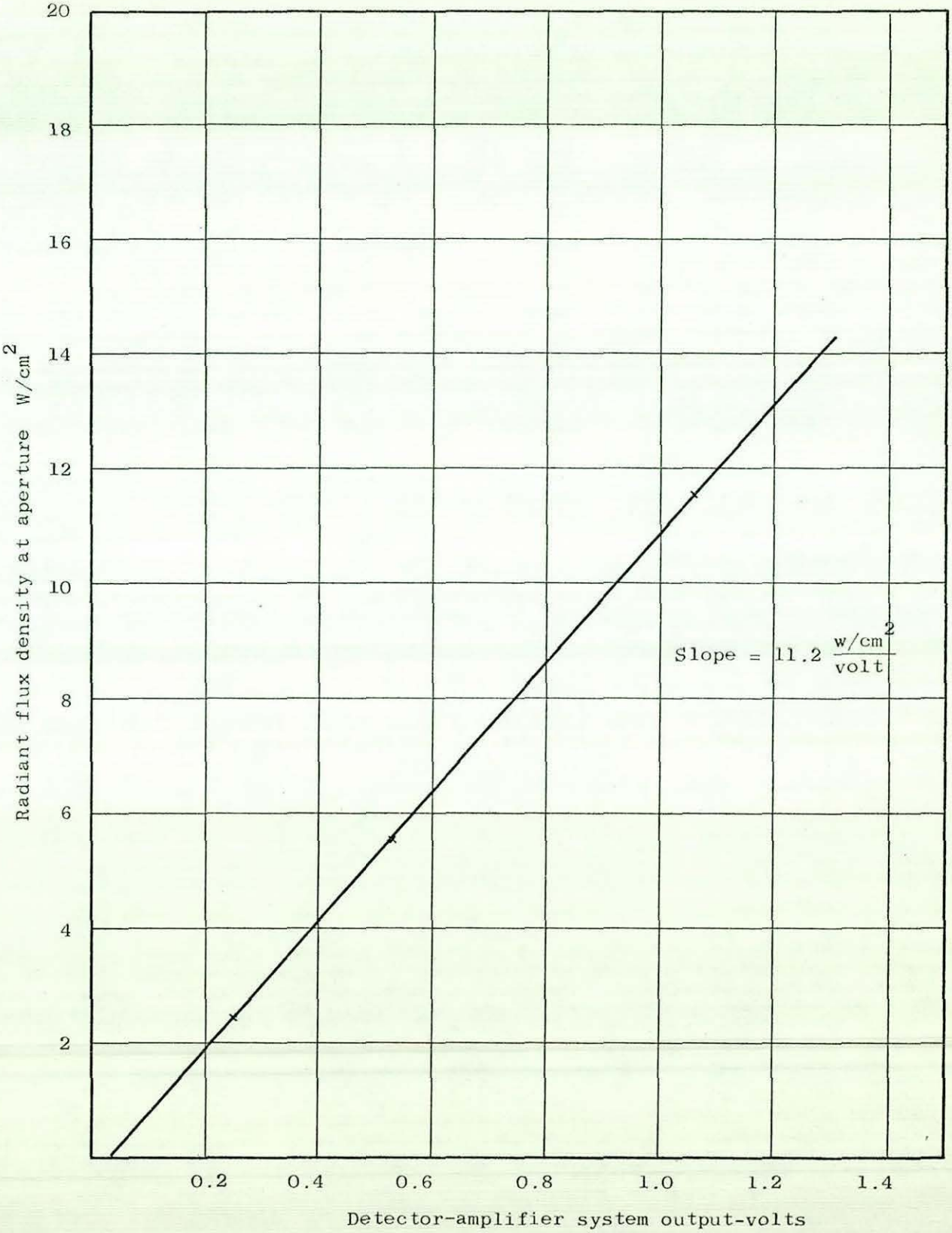

Fig. (3.10) Calibration curve of the infrared detector

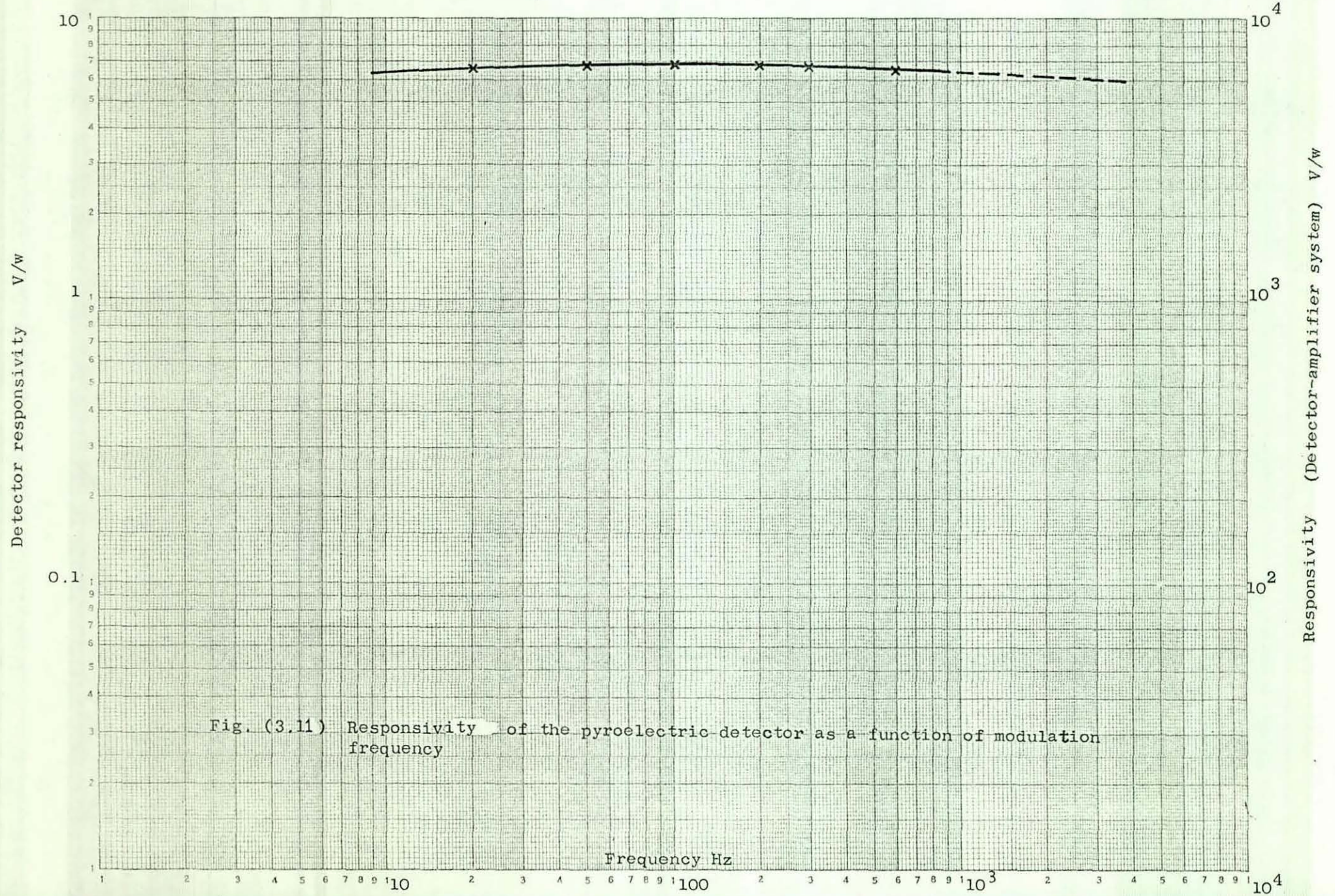

Fig. (3.11) Responsivity of the pyroelectric detector as a function of modulation frequency

CHAPTER 4

EXPERIMENTAL EQUIPMENT AND MODIFICATIONS

4.1 The Test Engine

The engine chosen for use in this investigation was a Ruston and Hornsby 3YWA, three cylinder, direct injection, air cooled, four stroke open chamber diesel engine. The engine was the same as that used by Derham (44) for measurements of instantaneous air motion within the cylinder under motored conditions. A view of the engine and the arrangement of the display and recording systems is shown in Fig. (4.1). Some of the technical data of the engine are as follows:

Bore x stroke	102 x 104.8 mm
Piston displacement (one cylinder)	849 cu.cm.
Connecting rod length	213 mm
Compression ratio (present)	15.3:1
Inlet valve opening	16^{o} BTDC
Exhaust valve closing	15^{o} ATDC
Inlet valve closing	36^{o} ABDC
Exhaust valve opening	45^{o} BBDC
Nozzle tip	4 hole
	0.27 mm diameter holes
	150^{o} spray cone

4.2 Engine Modifications

In order to adapt the engine for use in determining the instantaneous total and radiative heat transfer, it was necessary to modify it to allow access for mounting of the instrumentation. The modifications were carried out for the centre cylinder of the engine which was used as the test cylinder.

4.2.1 Cylinder head and piston crown

The existing cylinder head was modified to allow installation of three $\frac{5}{8}$"in diameter surface thermocouple plugs, and the pressure transducer (Kistler type 628B). The choice of the locations for the thermocouples was limited by the space available, and an attempt to keep to regions of one dimensional heat flow. The facility to mount the pressure transducer was provided such that replacement by a radiation window and detector adaptor could be made when required. A view of the modified cylinder head showing positions of three surface thermocouples, pressure measurement vent and injector location is shown in Fig. (4.2).

The initial planning of radiation measurements in the centre of the combustion chamber, required displacement of the injector (1.3 cm) from the original position. To minimise the effect of this displacement on the combustion process, the piston with the offset bowl was rotated through 180^{o}, thus bringing the injector towards the centre of the combustion bowl. Measurement of radiant heat flux at a second location, required the use of another cylinder head which was also modified to accommodate the radiation window-detector system.

The measurement of instanteous heat transfer on the piston was achieved by use of a "false" crown which carried the surface thermocouples. Fig. (4.3), illustrates the modified combustion chamber, cylinder head and piston thermocouple positions. Note that the radiation measurement location (R2) was actually provided on a second cylinder head because of space limitation on the modified cylinder head.

Facility for fixing a special 4-pin plug was made on the underside of the piston crown as shown in Fig. (4.4). The 4-pin plug which fitted a corresponding socket fixed on the piston skirt was connected via leads on a linkage (Section 4.2.2) leading to the amplifying-recording system. This arrangement of the piston crown, would reduce the amount of labour involved in installing the thermocouple plugs to the piston locations and avoid repeated removal of the entire piston and connecting rod assembly from the engine. Because of limited space on the piston crown, it was necessary to use thermocouple plugs of smaller size ($\frac{3}{8}$" diameter) than those used on the cylinder head.

4.2.2 Swinging link mechanism

Mounting the probes on the piston crown also involves the extraction of the leads via some mechanism to the engine casing. The higher speeds found in modern engines offer distinct problems in instrumenting pistons. Consequently an L shaped link, similar to that used by Furuhama and Enomoto (66), was designed which could be attached between the piston and the extended engine case. The details of the method of leading thermocouples and linkage dimensions are shown in Fig. (4.5). The link ③ is fixed to the lower part of the piston skirt ②. One end ④ of the L link ⑦ is inserted in the link ③ and moves rectilinearly with the piston for a piston stroke. The other end ⑤ placed at an appropriate position, would limit its movement to about 4 mm only for one stroke of the piston.

The reason the L-link is divided into two parts, separated at ⑨, is to enable the insertion of the piston into the cylinder, after the L-link without part ⑩ is fixed to the piston. In ideal

cases, the length of swing link (11) and position of the stationary point (6) are determined after consideration of the L-links strength (Furuhama and Enomoto (66)). Extension of the engine case (12) supported the stationary point (6), and a slider (13), fixed to the crank case, kept the link in the same plane. Two major problems were faced with the link device. One of them is the method of passing the thermocouple wires along the link and to the piston from joint (4). The wires were cast with Araldite in a groove machined on the side of the L-link. To continue the leads at joint (9), a pin and socket arrangement was utilised as shown in Fig. (4.6). Initially, it was planned to pass the leads at end (4) of the L-link in the form of a coil, through the joint pin (4). However, the small space (5 mm) available between the joint (4) and the connecting rod was not enough for the leads curvature. Instead, the thermocouple wires, wound together and protected by a rubber compound (14) are passed around the collar of link (7) and fixed to it. Then it loops before passing through a nylon tube in a hole in link (3), to prevent its rubbing with the metal. In one stroke, the bending of the wires is very small to cause any damage. At joint (5), the wires, protected by rubber compounds, looped from the side of the link (10) through pin (5) and into pin (6) which lead the wires to the outside of the engine case. The actual link mechanism and wire leads are shown in Fig. (4.6).

The other problem is that the L-link may break at the corner. The tests carried out showed smooth operation at 1500 rpm for more than half an hour. Operation at 1050 rpm caused no problems for many prolonged tests, but in excess of 1250 rpm, electrical noise interference was observed on the surface thermocouple signal.

The linkage was made of duraluminium, which exhibits high strength to weight ratio. Complete fulfilment of the design conditions, described by Furuhama (66), could not be achieved because of the limitations imposed by the space available in the crank case for the linkage mechanism to operate. The electrical interference on the signal from the piston thermocouples at speeds exceeding 1200 rpm was puzzling. It was mainly associated with the high acceleration and deceleration at TDC and BDC. Perhaps at these instants, excessive stress was caused at the wires or in the vacuum deposited metal films of the thermocouples.

4.2.3 Engine adaptation for radiation flux measurement

As indicated before, two adaptors, one for the pressure transducer and the other for holding a window and accommodating the radiation detector, were required to fit the same location on the cylinder head. Fig. (4.7) shows the detail of the two adaptors. Derham (44) proved that the small passage ($\frac{1}{8}$ inch diameter) in the pressure transducer adaptor, had no effect on the recorded pressure.

A second adaptor was prepared for radiation measurement at position (R2) to fit another cylinder head, because of space limitation on the modified cylinder head. The viewing configuration relative to the detector was kept exactly the same as in the first adaptor in order to maintain the same calibration coefficient of the detector.

The window chosen for use was Kodak's "Irtran 4", the spectral and physical characteristics of which are given by Hudson (58). The thickness of the window was 2 mm, which for unsupported diameter of $\frac{1}{4}$ inch, would stand the peak working pressures (58 bar) with a

safety factor of 3. The window being at about 10 mm from the inner cylinder head surface provided a pocket of air which protected it from soot deposition. The transmission calibration after half an hour engine running under medium load, showed a reduction in peak to peak radiation signal from a black body source of less than 10%.

4.2.4 Engine motoring and firing arrangements

The engine when used for gas velocity measurements (44), was coupled via a reducing pulley system to a D.C. motor. Thus to operate the engine under fired conditions, it was necessary to modify the motor to work as a generator coupled directly to the engine. The output was absorbed by supplying several immersion heaters with electric power.

In order to run the test cylinder under both motored and/or fired conditions, a simple mechanism consisting of a pin actuated by a spring was designed to lock the fuel pump plunger at the maximum displacement, while the engine was running. The release of the plunger, by pulling the pin out, induced fuel pumping and immediately firing commenced in the test cylinder. A separate fuel supply and measurement system was provided for the test cylinder. Therefore for motored operation testing the two end cylinders were used as the driving cylinders and for fired tests, all three cylinders were driving the generator.

4.2.5 Transducers and amplifying system and the recording equipment

4.2.5.1 Timing pulse

Accurate timing reference was essential for the present work where the instantaneous results derived from pressure signals are

very sensitive to random phase shift. The TDC crank position (beginning of the induction stroke) was sensed by a magnetic pick up conditioned with a high frequency Schmidt trigger circuit which converted the output to a square wave pulse. This square wave provided a definite voltage level for use in data sampling.

4.2.5.2 Total heat flux probes and signal amplifier

The output of the surface thermocouples, described in Section (3.1) were utilised for calculation of total instantaneous heat flux from the working fluid. A Hewlett Packard type DY-2461-A-M1 (wide band 350 CP_s - 25 kc, high gain chopper-stabilised of all transistor design) amplifier was used for signal amplification. Hassan (37) investigated the frequency response of the amplifier at high gain and reported excellent characteristics for surface temperature signal conditioning.

4.2.5.3 Radiation flux probe and signal amplifier

A ceramic pyroelectric radiation detector, described in Section (3.2) was used. The detector output was amplified by a Brookdeal Model LA-350 low noise amplifier. The frequency range of the amplifier was 3 Hz to 300 kHz with total harmonic distortion of less than 0.075% at 1 Hz for 2 volts r.m.s. The input impedance of the amplifier is selectable to match high and low source impedance.

4.2.5.4 Cylinder pressure

Fired and motored engine pressure were obtained using a Kistler type 628B capacitive pressure transducer and the associated charge amplifier type 5001.

4.2.5.5 Fuel line pressure and needle lift

Fuel line pressure was measured by a Kistler fuel line transducer located 23 cm from the injector nozzle (measured along the fuel line path). The injection time was derived from needle lift measured by a 'Distec 915', non-contacting, inductive displacement transducer which was calibrated prior to the tests. Upper frequency of the displacement transducer was 20 kHz, and hence the short rise time at the beginning of the injection could be effectively monitored.

4.2.5.6 Signal recording system

The nature of the present investigation required simultaneous recording of the different instantaneous signals in order to obtain a realistic inter-relation of these parameters. The 'Racal Store 4' FM tape recorder was used to record the various sensor signals after appropriate conditioning. A tape speed of 15 inches per second, which represented an upper frequency limit of 5 kHz, was used. This frequency limit was adequate for all engine data collected under the present test conditions.

4.2.6 Other measurements and equipment

i) Air flow rate. Direct reading of the air flow was made from a calibrated inclined manometer incorporated with a large surge tank and a standard orifice plate. A correction for the ambient conditions of the measured flow was necessary.

ii) Fuel flow rate. Timing the consumption of 50 cc of fuel under operating conditions provided the fuel flow measurement. The commercially available diesel fuel was used for this investigation.

iii) Engine speed - was measured by a tachometer.

iv) Steady surface temperature. A multichannel 'Kent' recording potentiometer was used to record the steady output of the thermocouples. A 'Cambridge' potentiometer was used to check the mean output of the surface thermocouples and to provide calibration voltages for the recorded surface temperature signal.

v) Smoke concentration. a "Hartridge' smoke meter was used for measurements in the exhaust manifold.

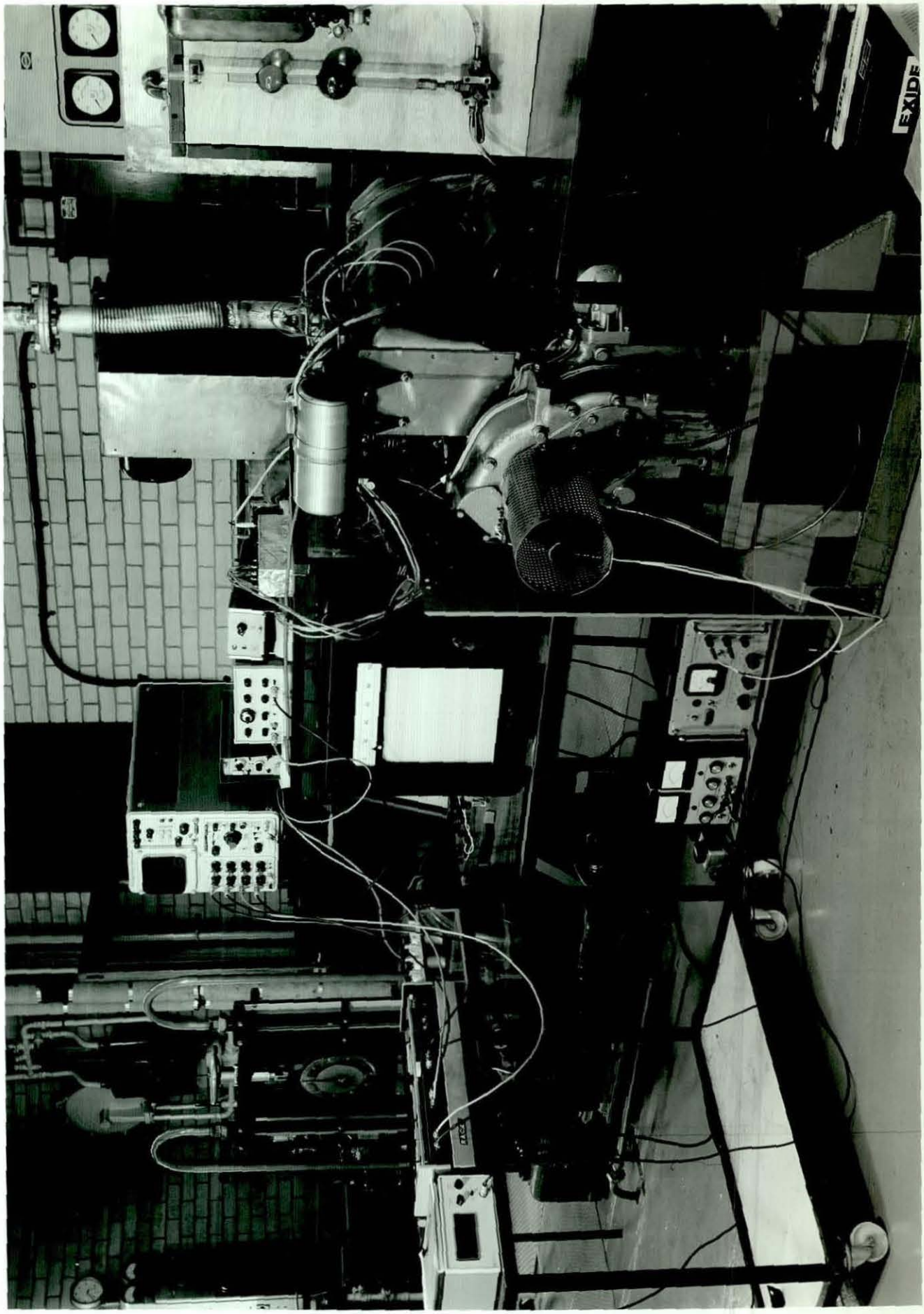

Fig. (4.1) Test Engine and Other Experimental Equipment

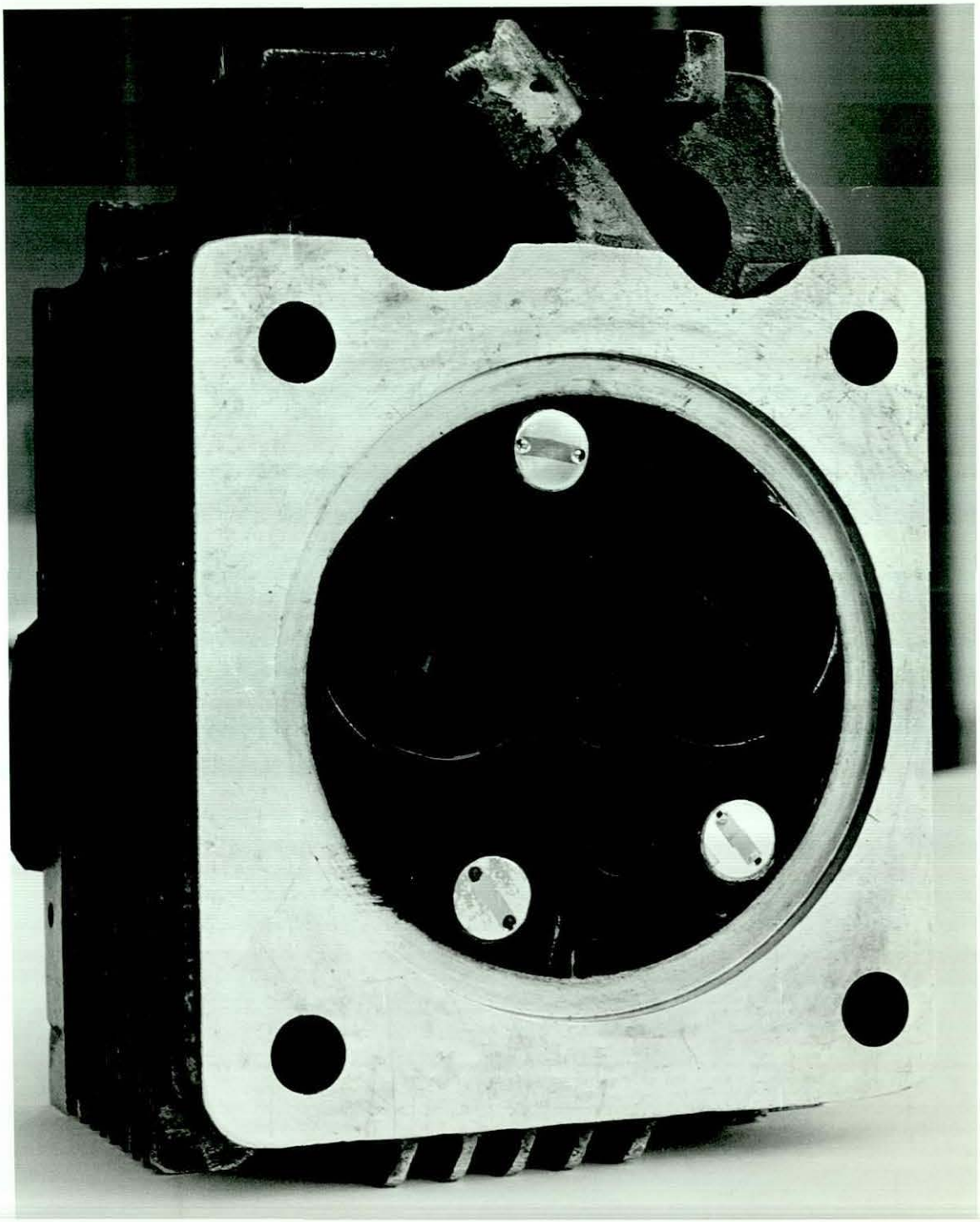

Fig. (4.2) A View of Cylinder Head fitted with Surface Thermocouples and showing Pressure (or Radiation) and Injector Vents

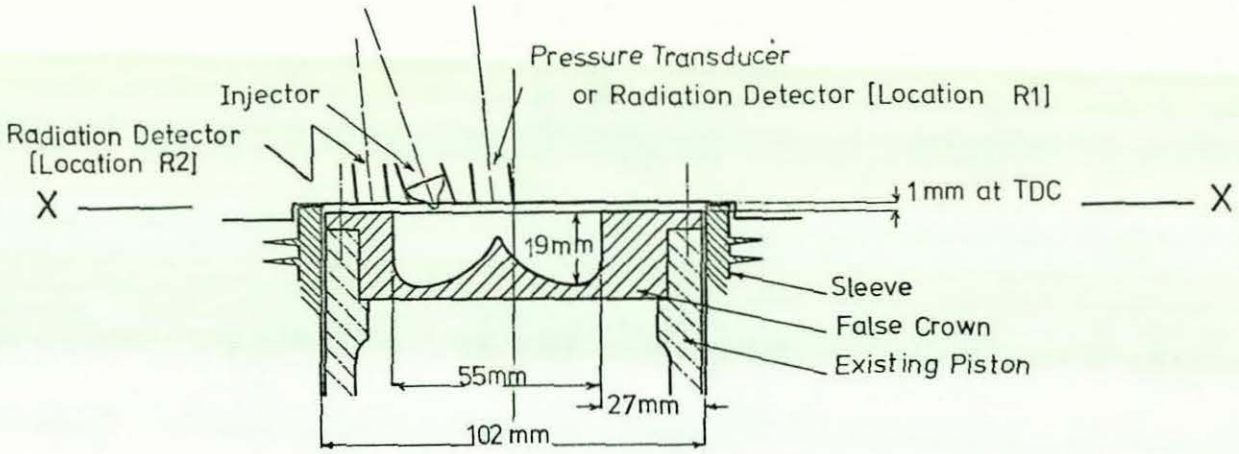

Combustion chamber configuration

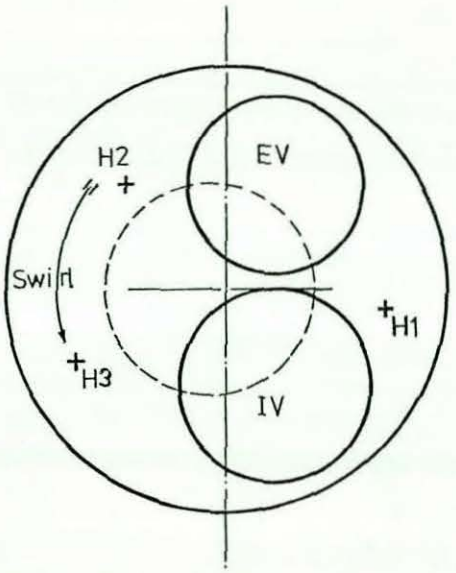

Thermocouple	Radius from cylinder axis mm
H1	42
H2	38
H3	41
P1	36
P2	36

Plan XX showing thermocouple positions on cylinder head

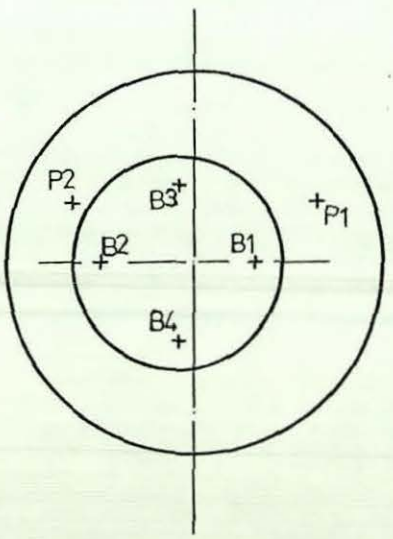

Thermocouple	Radius from bowl axis
B1	20
B2	20
B3	20
B4	20

Plan XX showing thermocouple positions on piston

Figs. (4.3) Combustion chamber configuration and heat transfer measurement locations

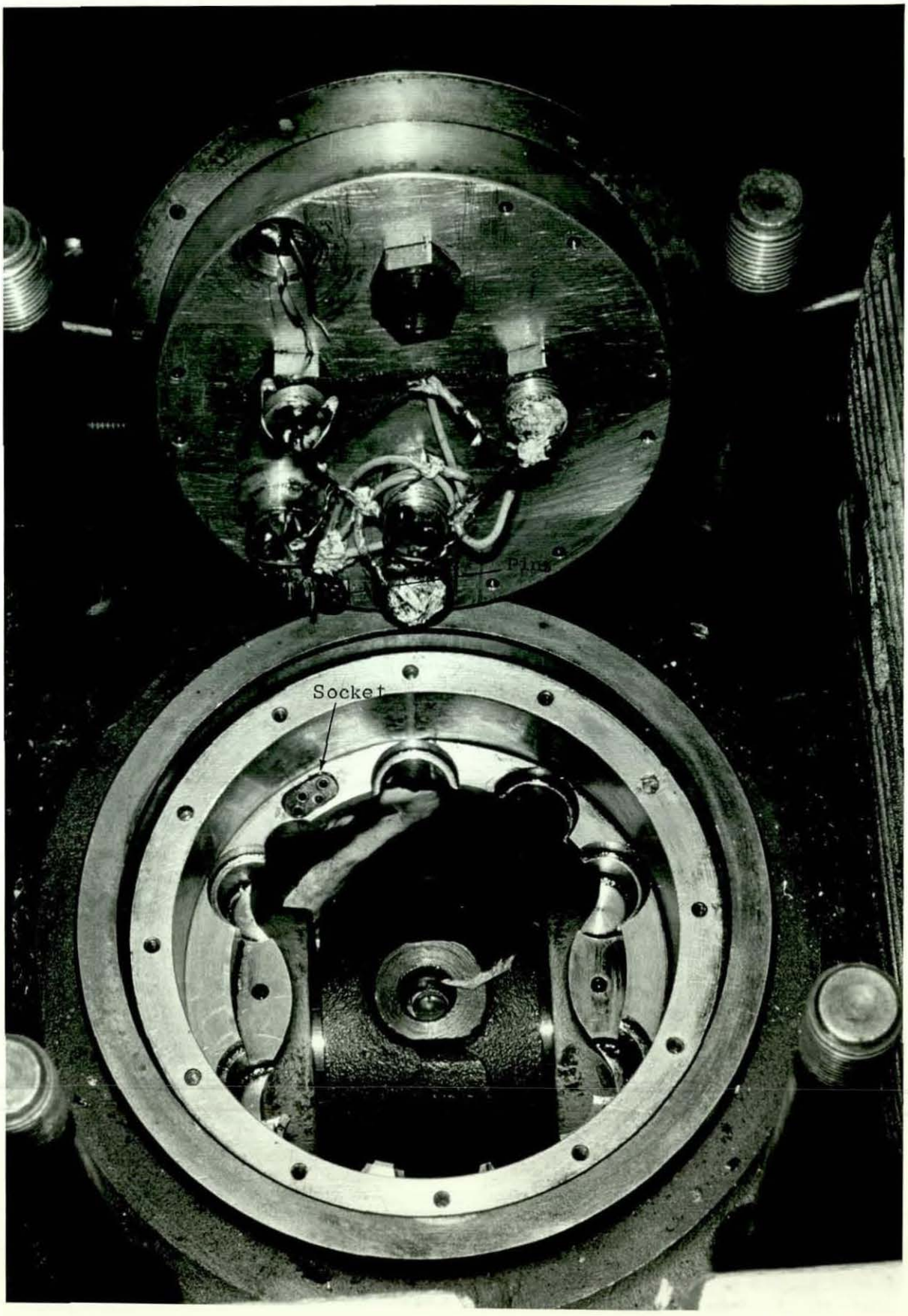

Fig. (4.4) False Piston Crown and Machined Piston Top Showing 4-pin and Socket Arrangement for Thermocouple Leads

A	104	H	72.5	R_1	12
B	198	I	5	R_2	25
C	203	J	12	R_3	51
D	114	K	13		
E	33	L	25		
F	38	M	9,5		
G	10	N	12,7		
		P	19		

[Dimensions in mm]

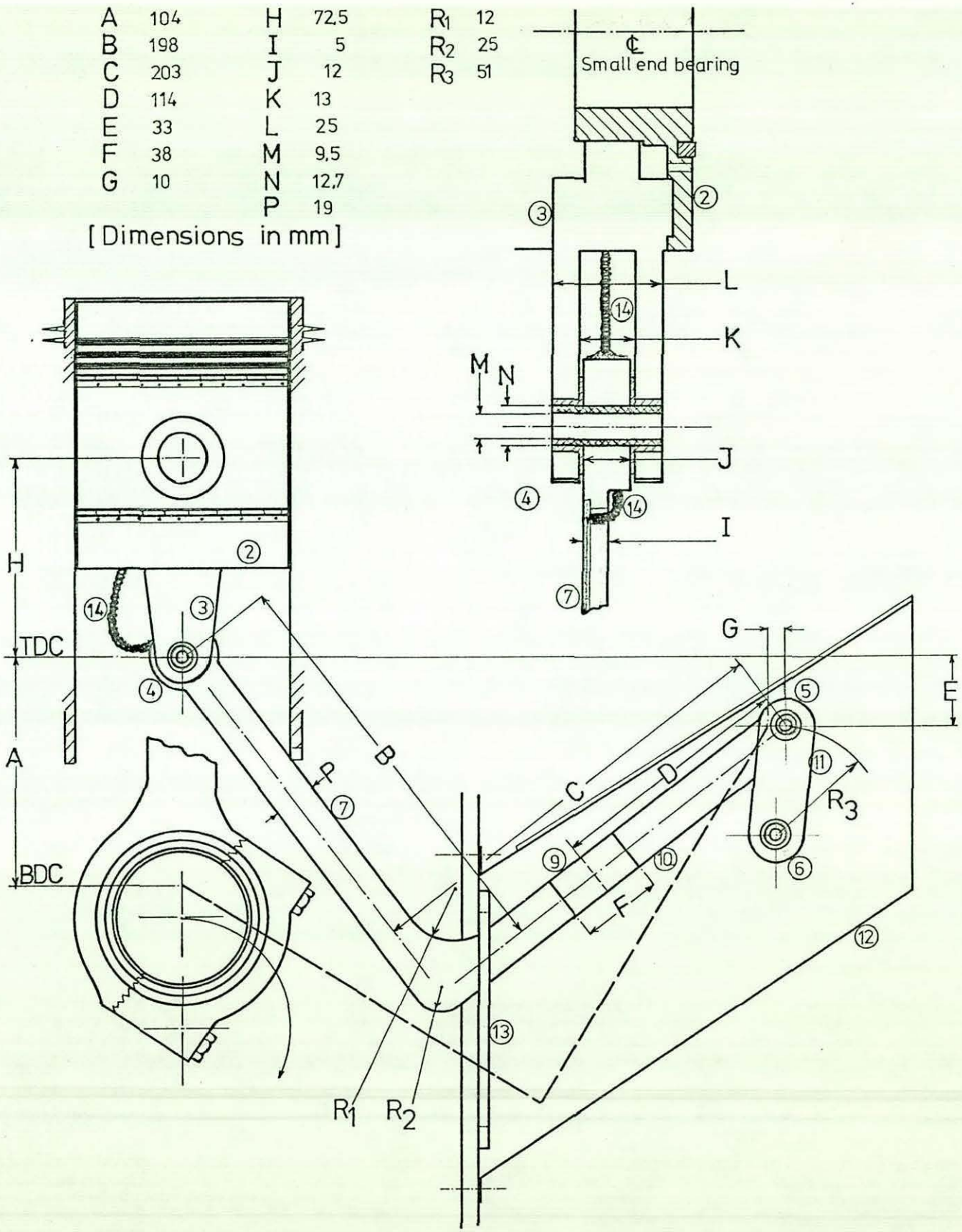

Fig. (4.5) "L-link" device for leading piston thermocouple wires and a section view of piston joint

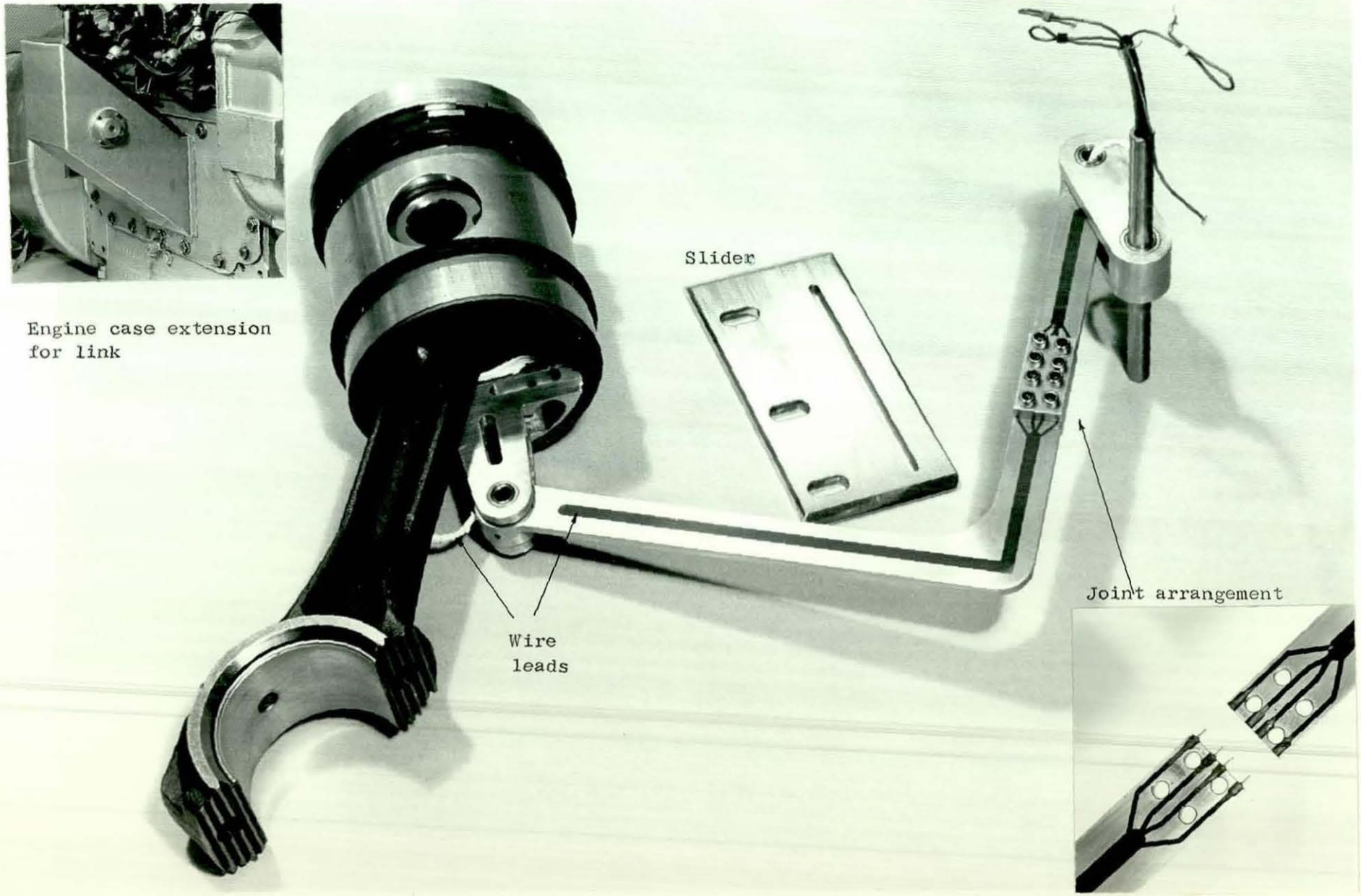

Fig. (4.6) Piston Link-Mechanism

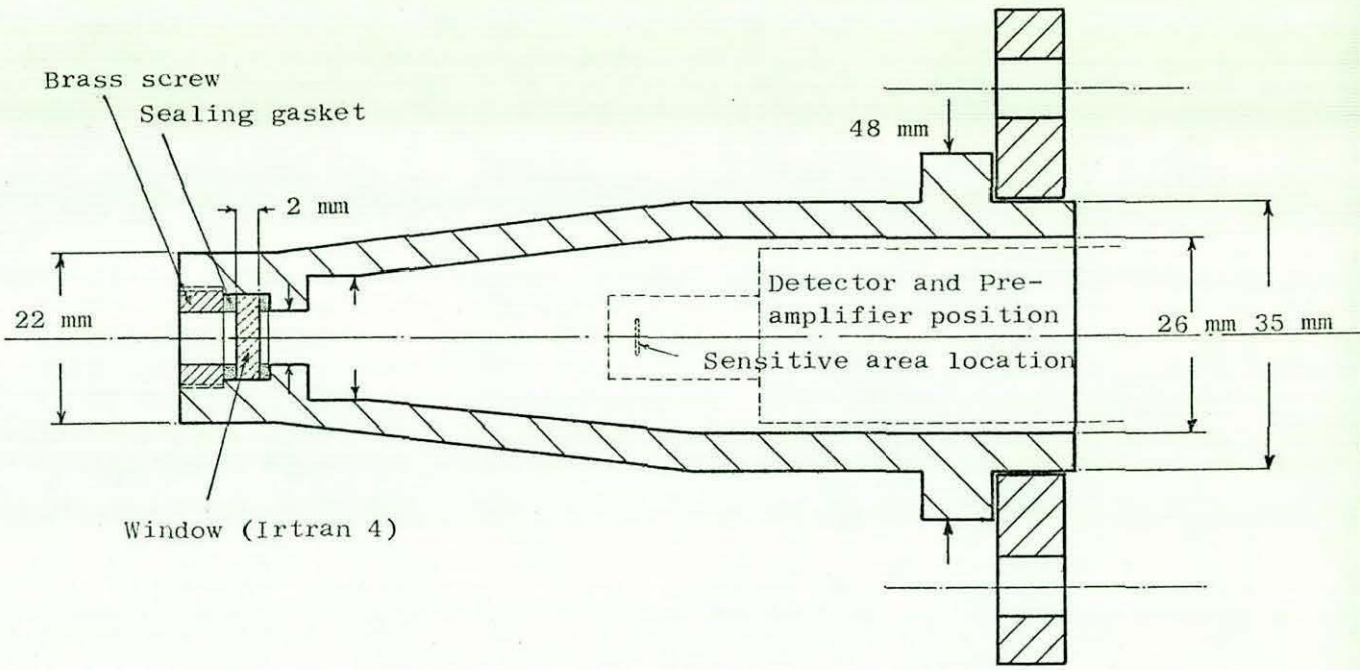

Radiation window and detector holder

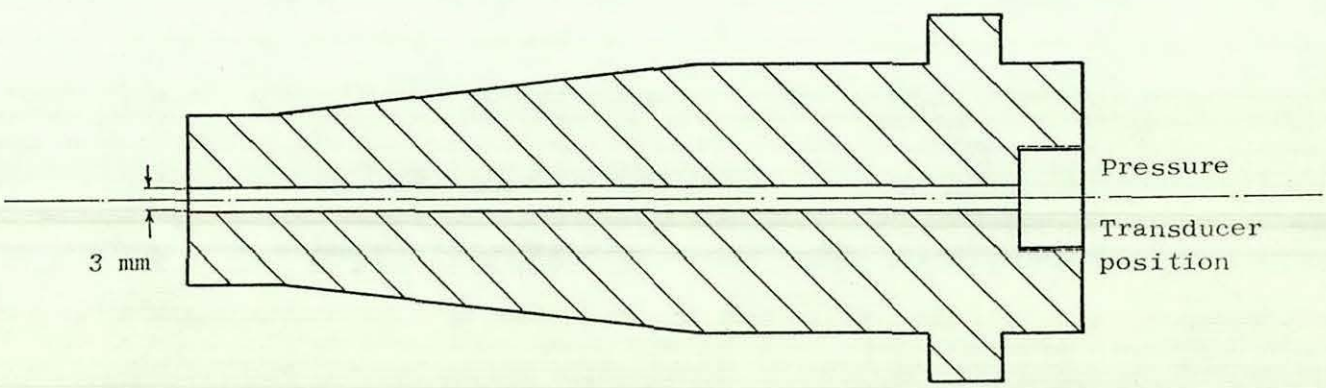

Pressure transducer adaptor

Fig. (4.7)

CHAPTER 5

EXPERIMENTAL PROCEDURE AND DATA ANALYSIS

5.1 Test Programme

In response to the success achieved in the preliminary tests of the constructed surface thermocouple, in respect of its rigidity and high sensitivity at all speeds, a rigorous test programme was planned to obtain fundamental data on the transient heat transfer in a diesel engine. The tests fall into three categories according to operating conditions and objective sought as follows:

a) Motored operation tests, where the variable of chemical reaction is eliminated and radiation is absent, to investigate the convective component of instantaneous heat transfer.

b) Fired operation tests to investigate the total instantaneous heat transfer.

c) Fired operation tests to investigate the radiative component of instantaneous heat transfer and its relative importance in the test engine.

All test conditions covered are listed in Table (5.1). As the experiments involved items of certain life expectancy, notably the surface thermocouples under fired conditions and the link work mechanism with flexing leads, most tests were repeated several times in order to obtain all the required measurements.

5.2 Installation of Surface Thermocouples

The prepared surface thermocouples were fitted with extreme care to the cylinder head or piston crown of the test cylinder.

High torque on fitting was not applied in order to avoid stress of vacuum deposited surface films. All surface thermocouple wires were screened individually and brought to a low noise multipoint switch, where they could be separately directed to the amplifier-recorder system. This reduced the high noise level experienced in the earlier stage of work to an acceptable level. Some attempts made to eliminate the high frequency hash present on the trace by filtering, resulted in attenuation of the signal as shown in Fig. (5.1). Hence it was decided to use unfiltered signals for analysis.

The wall backing temperature directly behind the sensitive junction at a depth of 1.3 cm were measured by conventional iron-constantan thermocouples attached to the plugs prior to installation. All the thermocouples measured the temperature relative to melting ice. Fig. (5.2) shows a schematic diagram for temperature measurements.

5.3 Motored and Fired Test Technique and Associated Problems

A test procedure was adopted to provide the maximum amount of data per test run. Cylinder head thermocouple results were first obtained without the instrumented piston and link work, this reduced the time required for a test, especially as auxiliary equipment (amplifiers, recording channels, etc), were not sufficiently numerous to deal with all records required simultaneously. The tests were to be repeated later with the instrumented piston to obtain piston temperatures, and then for radiation measurements under the same conditions.

In the tests under motored conditions, the gas side surface temperature usually reached a steady state in about 10 minutes. As the surface thermocouples would operate indefinitely in the motored engine, 20 minutes was usually allowed before the signals were recorded. One problem faced in the motored tests, was the formation of a thin oil layer on the surface thermocouple, which attenuated the signal as will be shown in the following chapter. A special oil scraper ring was fitted which reduced this problem but did not cure it completely. Hence most of the results were obtained with a thin oil film on the surface of the thermocouple.

In the fired engine, soot formation has been a troublesome problem during the test run. It was found that at some locations (namely H3), as the carbon was gradually built up over the surface thermocouple junction, the temperature response became slow and the swing diminished. As the analysis of heat flux was based on the assumption of the existence of a clean surface, it was highly important that the experimental results should be taken before the carbon deposit became excessive. To reduce carbon deposition, the test cylinder was first warmed up under motored conditions after which it was fired by releasing the fuel pump plunger. Signals were recorded as soon as the steady component of surface temperature had attained reasonably invariant conditions. The effect of continuous build up of carbon on the thermocouple junction was further reduced by completing the tests at the three load conditions at a fixed speed in two runs. The FNL and F40%L tests were first carried out in one run, after which the cylinder head was removed and the thermocouples cleaned. The heavy load test was carried out immediately after this process while the engine was still warm. The surface thermocouples could be cleaned with some care using acetone and a soft paint brush.

The number of test runs for data acquisition from the piston crown were increased because of the limited number of signals that could be transmitted through the link mechanism. Only two surface temperature signals from the piston crown could be recorded simultaneously. On the other hand the engine speed range was limited to 1200 rpm, by electrical noise interference on the temperature signal. The mean temperature gradient in the piston crown, to determine the steady heat transfer, was obtained by repeating the tests and using a conventional differential thermocouple, built on plugs similar to the surface thermocouple plugs.

During the course of the work, thermocouples were installed in three locations in the cylinder head and six locations on the piston crown. The locations are shown in Fig. (4.3).

In receiving the radiant component through the viewing window, soot accumulation was a problem over periods of engine running greater than half an hour, particularly under heavy load conditions. It was assumed that the high swirl in the test engine which improves air-fuel mixing was the main factor in producing less soot accumulation on the window than reported by previous workers (32, 33, 34). However, as radiation heat transfer is expected to be less dependant on steady conditions, the radiation detector signals were recorded as soon as the cylinder fired and engine speed and load adjusted. It was found that reliable radiation results could be obtained by recording radiation data for FNL and F40%L conditions in one run, and the heavy load test in a second run immediately after cleaning the viewing window.

5.4 Data Recording and Reduction

In order to obtain a reliable representation of the engine transient heat transfer data, modern recording systems, analog-to digital converter and high speed digital computer facilities were utilised. Fig. (5.3) shows the data processing sequence for a single voltage trace and associated timing pulse channel. The signal was conditioned by the amplification stage and a D.C. voltage bias such that the maximum and minimum voltages of the trace lay within the acceptance band (zero to $\pm$ 3 volts) of the 'Racal Store 4' frequency modulating recorder. On completion of the data recording process, known calibration voltages were also recorded and hence modified by the same circuitry.

The recorded signal was then replayed to the input channel of a high speed A/D converter on a Hewlett Packard 5451A computer. A small computer program was used to average any required number of input traces. Origin of the time scale on individual sample traces was maintained constant by using a magnetic pick up output as a triggering voltage on the A/D converter unit. Hence a typical, or mean voltage time trace was generated and stored in the computer data core, with sampling ordinates at intervals as defined by the A/D converter setting. The averaged trace was thenoutput via a high speed paper tape punch.

The engine data recording system was used to record a large number of consecutive cycles over approximately 20 feet of magnetic tape for each load condition. Data recorded included gas-side surface temperature, cylinder pressure, engine TDC position, radiation emission, needle lift and injection pressure. A typical set of the recorded signals are shown in Fig. (5.4).

In the case of the transient heat transfer analysis, two paper tapes corresponding to the voltage-time traces averaged over 15-20 cycles of the surface temperature, were therefore created for each measurement location. Voltage levels on the paper tape did not represent actual test voltages due to the bias and amplification process. Therefore the similarly recorded calibration voltages were also digitised onto paper tape. Signal paper tapes and associated calibration level paper tapes, were then processed by an ICL 1904 digital computer using a simple conversion program to relate the 'punched' voltages on the paper tape to 'actual' voltages from the calibration levels. 'Actual' voltage-time traces thus generated were output on punched card and therefore formed data for the relevant processing program.

For the purpose of the transient surface heat flux analysis, Overbye et al (14), Knight (16) and Hassan (37), who used the Fourier series representation of the time-surface temperature, showed that the use of 72 harmonics was a compromise between accuracy and practicality. In the present investigation, the averaged surface temperature signal over one cycle was represented by 150-250 ordinates for motored tests and 200-350 ordinates for fired tests, with harmonics increasing for high speed.

The instantaneous heat flux was calculated by a method of harmonic analysis of the surface temperature record (Overbye (14)). The method and the computer program used are given in Appendix (A).

5.5 Calculation of Gas Bulk-Mean Temperature

Most of the analysis by past workers in connection with heat transfer has utilised the concept of bulk mean gas temperature. The instantaneous gas mean temperature during the compression and expansion strokes may be calculated from a knowledge of the trapped mass, the instantaneous gas pressure and volume by application of the gas law:

$$PV = m R T_g \qquad (5.1)$$

where m = trapped mass.

The trapped mass could not be determined from the measured air flow because of inlet and exhaust valves overlap. A reasonable approximation was obtained by supposing the cylinder pressure at IVC equal to the ambient pressure. Then assuming the gas temperature at this point is such that a volumetric efficiency of 0.9-0.85 (estimated from literature on similar air cooled engines) is achieved for no-load and full load conditions respectively.

For the compression stroke and later parts of the expansion stroke it seems plausible to suppose that the temperature will be fairly uniform and will be satisfactorily represented by the mean so calculated. For combustion phase such a calculation is unrealistic and for this reason a simplified two-zone temperature distribution was considered in order to represent the driving temperature for heat transfer for this phase (see Results).

It was found that for motored operation, the polytropic relation PV^n = constant (n = 1.35) produced good agreement with the measured pressure, assuming the pressure at IVC equal to the ambient pressure. Therefore the polytropic relationship was used to predict

the gas temperature in the motored engine assuming gas temperature at IVC of magnitude to produce $\eta_{vol} = 0.94$ (60).

5.6 Gas Composition and Properties

In any analysis of heat transfer in internal combustion engines, the thermodynamic properties and composition of the working fluid must be known. Attempts to represent the working fluid in the fired engine as having the properties of air throughout the cycle are inadequate, simply because air is not representative of the working fluid in an engine. Furthermore, because of chemical reaction, the chemical species concentration comprising the working fluid changes continuously during the cycle. Knowing that the major constituent is always nitrogen, the assumption of a simple triangular combustion rate (over 35-40^{o} CA) with peak at mid-point (Lyn (61)) is considered adequate for estimating products constituents. The dissociation and re-association processes usually occurring in combustion engines was not considered in the present investigation as any effect would be swamped in the unreality of the assumption of uniformity of properties throughout the combustion space. The working fluid thermodynamic properties and equilibrium chemical species concentration in the engine at any temperature and pressure can be determined following the method outlined by Annand (6).

The gases to be considered are air, nitrogen, carbon dioxide, water vapour and fuel vapour. For the individual gases comprising the mixture which forms the working fluid, the specific heats C_p were correlated with fifth degree polynomials:

$$C_p = C_0 + C_1 T + C_2 T^2 + C_3 T^3 + C_4 T^4 + C_5 T^5 \quad K \text{ cal/kg}^{o}K \quad (5.2)$$

and the expression used to represent the viscosity in:

$$\mu = \mu_o \, T^{0.645} \quad \text{kg/m.s.} \tag{5.3}$$

where μ_o is the constituent viscosity at zero temperature.

For mixtures of n gases, if the molar fraction of the jth component is X_j, the mean properties are:

$$C_p = \sum_n (X_j \; M_j \; C_{pj})/M \tag{5.4}$$

$$M = \sum_n (X_j \; M_j) \tag{5.5}$$

$$\mu = \frac{\sum_n (X_j \, \mu_j \, \sqrt{M_j})}{\sum_n (X_j \, \sqrt{M_j})} \tag{5.6}$$

where M = molecular weight.

The mean thermal conductivity is estimated from the relationship:

$$k = \frac{C_p \mu}{(P_r)} \quad \text{kW/m}^{\circ}\text{C} \tag{5.7}$$

In view of the predominance of air or nitrogen in all likely mixtures, it seems adequate to take Prandtl number $(P_r) = 0.7$ for the calculation of k.

All the properties were evaluated at the bulk-mean temperature calculated from the measured pressure. In certain cases, where the effect of temperature zoning was indicated by the measurements, the local gas properties are evaluated at the relevant zone temperature. The computer program used for evaluating the working fluid composition and properties and the prediction of instantaneous heat fluxes is given in Appendix (B).

TABLE 5.1

Test Conditions Investigated

a) Equivalence ratio and (fuel consumption gm/s) for range of engine speed and load conditions studied

Engine speed rpm / Load condition	600	1050	1500	1750
Motored	0.0	0.0	0.0	0.0
Fired no load (FNL)*	0.278 (0.122)	0.289 (0.142)	0.283 (0.2)	0.285 (0.23)
Fired 40% load (F40%L)	0.323 (0.134)	0.369 (0.175)	0.378 (0.26)	0.367 (0.29)
Fired 80% load (F80%L)	0.405 (0.161)	0.474 (0.22)	0.512 (0.34)	0.487 (0.38)

b) Measured mode of heat transfer, location and range of conditions covered

Heat transfer mode	Area of Measurement	Range of test conditions
Total heat transfer	Cylinder head (3 locations)	All conditions in Table 5.1a plus super-charge (MOT) of 0.34 & 0.69 bar at 1050 rpm
Total heat transfer	Piston crown (4 locations in bowl and 2 locations on flat rim	All conditions at 600 and 1050 rpm
Radiant heat transfer	Position R1 Position R2	All except 600 rpm All except 1750 F80%L

* It should be noted that engine running under fired no load (FNL) condition represented no useful power from the engine-generator system, but under the condition the inertia and friction load of armature was imposed on the engine. F40%L and F80%L conditions corresponded to similar percentages of the maximum power output of the generator. The indicated mean effective pressure for each condition is given in Section 6.

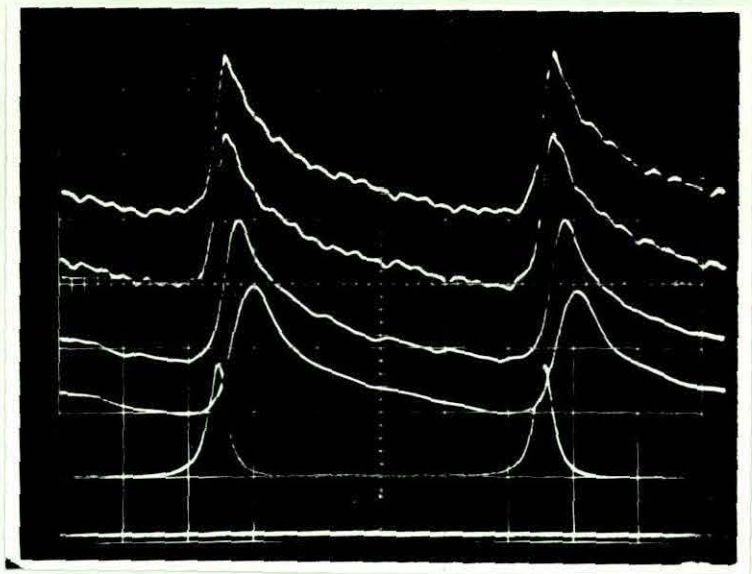

Fig. (5.1) Effect of electronic filtering on instantaneous surface temperature signal

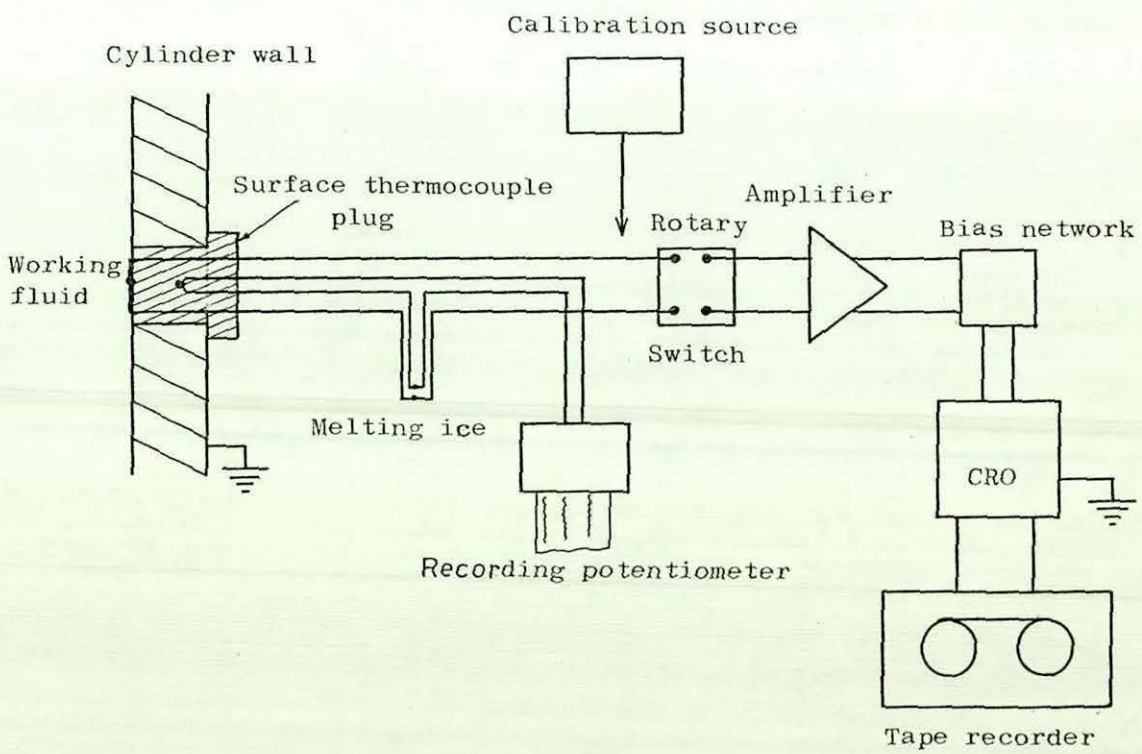

Fig. (5.2) Thermocouple schematic and instrumentation for surface temperature measurement

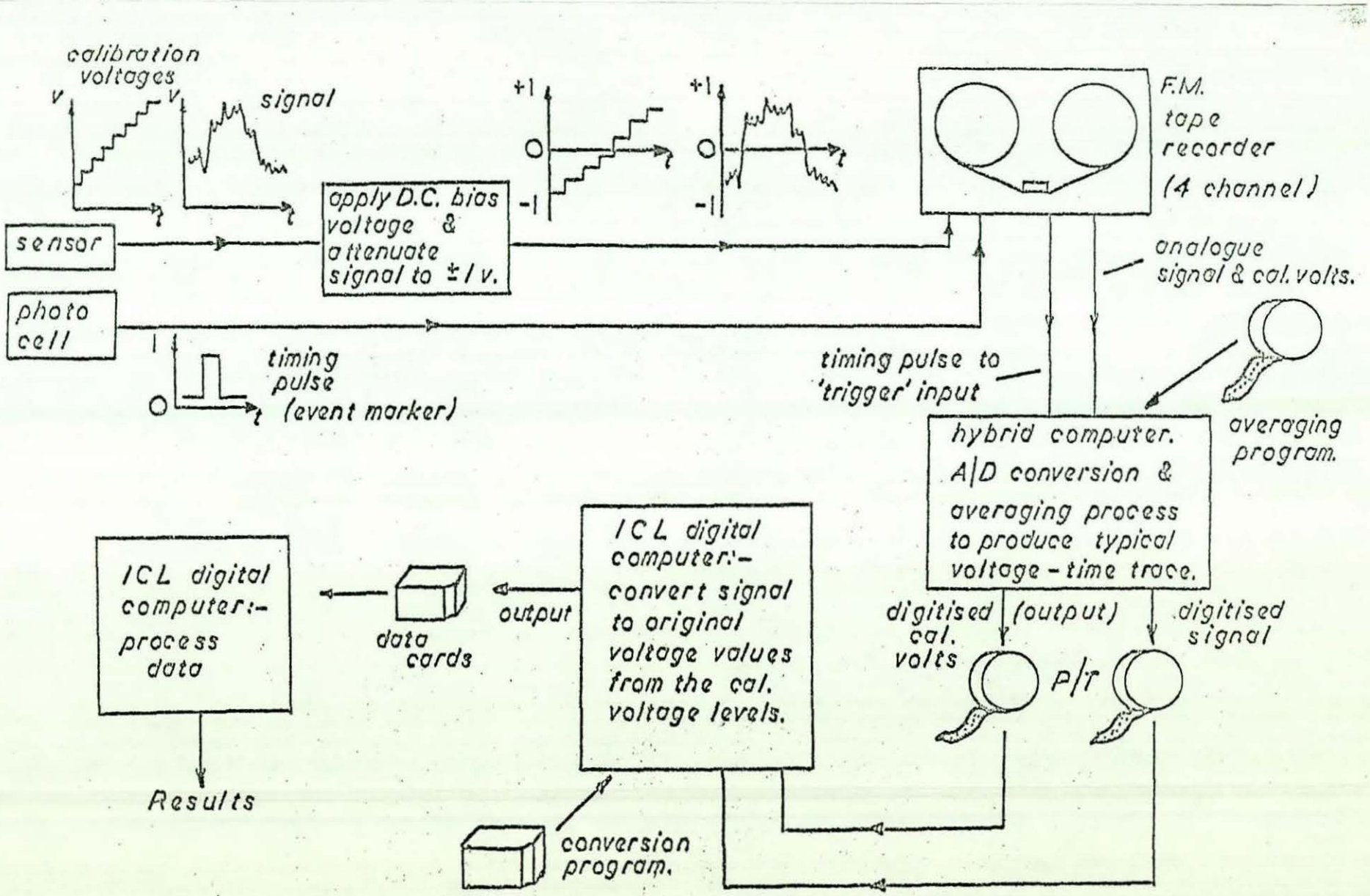

Fig 5.3 Data Processing Sequence for Transient Events.

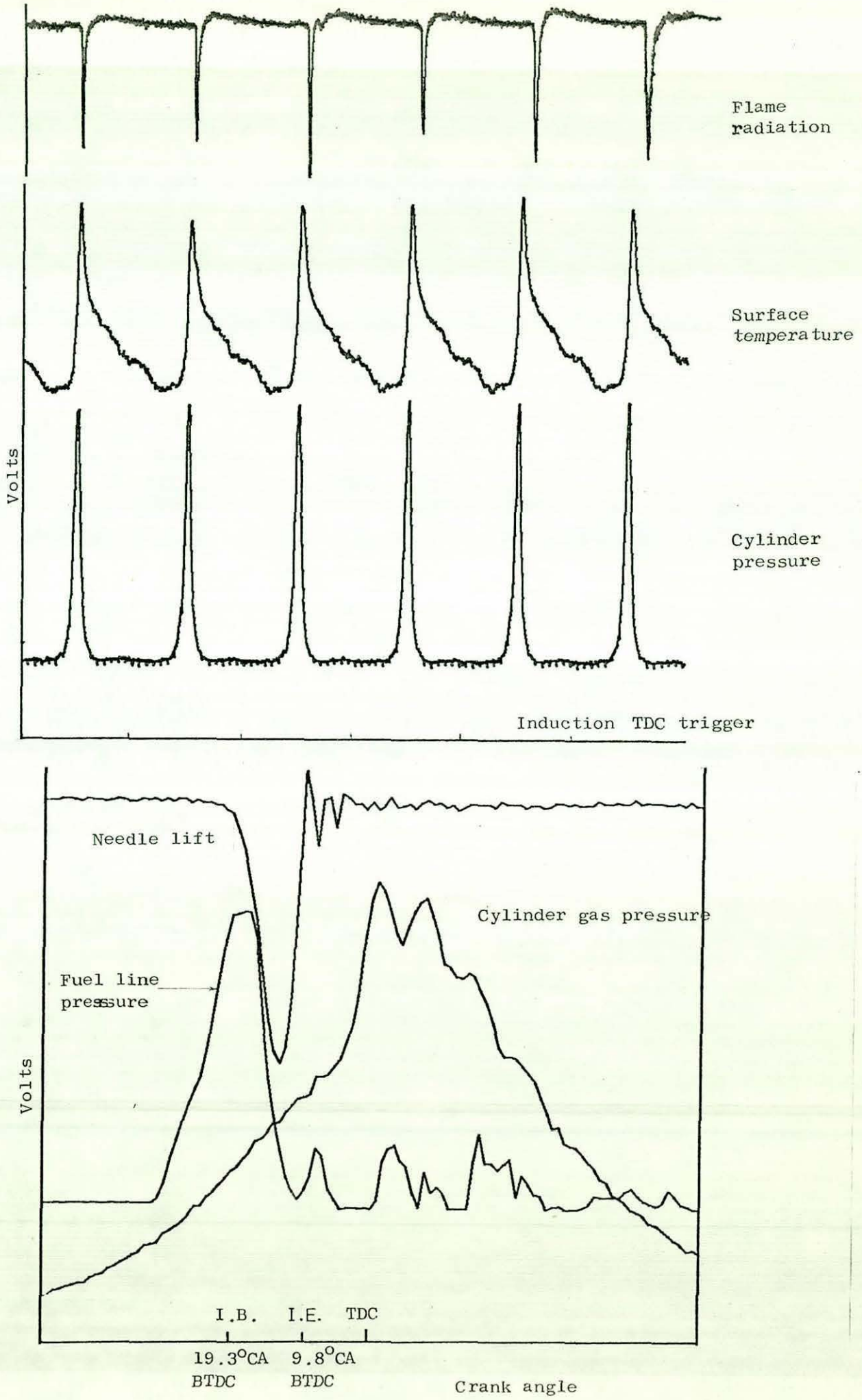

Fig. (5.4) A typical set of signals recorded

CHAPTER 6

RESULTS AND DISCUSSION

6.1 Previous Work on the Test Engine

This project was an extension of a previous study (44) on the measurement of gas motion in a high swirl diesel engine.

Derham (44) measured the gas velocity during the induction-compression stroke and up to 40° ATDC, under motored conditions. The gas motion was found to become orderly at about 90° CA BTDC in the compression stroke, thus forming a solid vortex. Fig. (6.1) shows the measured mean swirl for three engine speeds. These curves were the result of directional measurements at many locations on the piston crown. Theoretical analysis based on momentum conservation led to a model for prediction of swirl in the engine.

The measured gas velocity and the forced vortex behaviour of the flow, were combined with the equation for the forced convective heat transfer to a flat surface (modified to account for changes in heat transfer with radial location) to predict local heat fluxes under motored and fired conditions of engine operation.

6.2 Preliminary Tests to Explore the Validity of the Prepared Surface Thermocouple

The failure of many prepared prototype surface thermocouples led eventually to one (built on 1" plug) suitable for engine use.

The thermocouple was fitted to a cylinder head which was used previously to accommodate a similar plug for holding anemometer probes for gas velocity measurements, the sensitive junction was at 4 cm radius from the cylinder axis. The thermocouple was suitably shielded and grounded (88). The signal output from the thermocouple

together with cylinder pressure and TDC trigger signal, were recorded on a four channel, FM Analog tape recorder over an engine speed range of 600, 1050, 1500 and 1750 rpm. The Fourier analysis of these records produced the instantaneous heat fluxes shown in Fig. (6.2). The instantaneous and time averaged surface heat fluxes generally showed an increase with increasing engine speed as would be expected. Table (6.1) summarises the results obtained.

TABLE 6.1

Some results of the preliminary motored tests obtained by a thermocouple 4 cm from cylinder axis

Engine speed	560	1050	1500	1750	RPM
Peak heat flux	793	1243	1692	1872	kW/m^2
Mean heat flux	74	126	155	183	kW/m^2
Surface temperature swing	5.04	5.9	6.4	6.55	^oC
Peak flux position	363	360	362	363	^oCA
Peak surface temperature position	386	384	383	380	^oCA

Since the gas temperature and pressure histories on a CA basis are not significantly affected by variation in engine speed, the increase in heat transfer with speed must be mainly attributed to gas velocity and rate effects. The rate of compression of the boundary layer is obviously proportional to the engine speed.

Kim Dao (40) showed that heat flux varied in an approximately linear manner with air swirl (Chapter 1). Similar trends were also observed, in the present investigation (Fig. 6.3(a)).

6.3 Reproducibility of the Results

6.3.1 Effect of surface condition on total heat transfer

In the early motored engine tests the observation of the peak-to-peak value of the surface temperature signal of a newly fitted (clean surface) thermocouple was found to reduce by about 5% after a period of 5-15 minutes engine running and remained constant at the reduced level. The cause for this was found to be the formation of a thin layer of oil on the surface. Although special oil control rings were fitted, data were obtained with a very thin oil layer on the sensor. The heat fluxes at location H2 (see Fig. 6.9) for both clean and oiled surface and at two engine speeds are shown in Fig. (6.4). The oil layer attenuates the flux and results in a phase lag. The phase lag is significant ($\simeq 10^{o}$ CA) in the compression stroke and almost non-existent in the expansion stroke. The explanation is that the oil film on the surface will get thinner by the rapidly increasing swirl as TDC is approached, until its effect becomes negligible during the early stages of expansion stroke. However, the peak heat flux cannot be attained because of the reduced heat transfer to the wall due to the thick layer earlier in the compression stroke. The cleaning of the surface thermocouple with alcohol, usually reproduced the original peak temperature signal under similar conditions.

6.3.2 Reproducibility of motored data

In order to establish the repeatability of the experimental data and the consistency of the surface thermocouples, three identical tests under motored conditions with an engine speed of 1050 rpm were made. Each time a different thermocouple was fitted

to location H1. The measured heat flux for the three runs are shown in Fig. (6.5). Note a maximum change of nearly 20% in peak value. The repeatability is good when considering the many factors, such as oil layer formation and its thickness, small change in engine speed and possible difference in thermocouple response due to difficulties involved in controlling thermocouple film thicknesses during manufacture.

6.3.3 Carbon formation effect under fired operation

At the end of the motored tests, several tests were conducted to study the behaviour of the thermocouples under fired operation. As indicated earlier, the thermocouples were coated with a protective coating ($M_g F_2$) to avoid corrosion by the severe conditions and catalytic reaction at the film surfaces. During these tests carbon deposition proved a problem. However, this was confined to certain areas of the chamber, such as location H3, and to a lesser degree at H2. At location H1 the carbon formation was negligible for runs up to one hour duration. As deposits affect the temperature response of the thermocouples and hence the calculated heat flux, it is important to assess the results from this effect. The surface temperature at location H2 was recorded under motored operation at 1500 rpm, first with a clean surface and then with the surface coated with carbon accumulated during a period of half an hour engine running under fired half load condition. Fig. (6.6) shows the calculated heat fluxes for the clean and sooty thermocouple. An attenuation of 19% in peak heat flux is observed with a phase lag of about 12^{o} CA in peak position.

It is interesting to note the effect of carbon deposit on the phase lag throughout the cycle compared to the effect of the oil layer which is significant during the compression stroke only. This observation supports the hypothesis of oil thinning by increased gas motion near TDC.

6.3.4 Reproducibility of fired data

The previous test indicated the importance of recording the fired results before the carbon deposit became excessive. This was achieved by a quick check of the peak surface temperature signal under the same motored operation, before and after a fired test (with engine mean temperature levels the same in each case). If a significant attenuation was observed, the cylinder head was removed and the thermocouples cleaned in position with Isopropyl alcohol.

To test the reproducibility of the fired data, a single thermocouple was utilised for heat flux measurement at H2 under two test conditions (fired no load and fired 40% load, both cases at 1050 rpm). The observed data for these tests compared with results obtained three months later by the same thermocouple, for nominally the same operating conditions, show good agreement (Fig. 6.7). Ignoring the small change of equivalence ratio (which occurred unintentionally), the trend of the results indicated that reliable data are possible with careful control of engine operation and carbon deposition on the thermocouples.

6.3.5 Cycle-by-cycle variation of instantaneous surface temperature and heat flux

The character of cyclic variation of the recorded surface temperature is represented in Fig. (6.8), where seven consecutive cycles are shown for a range of running conditions. Note that the cyclic variation in the motored engine is negligible compared to the fired engine records, and analysis of individual motored cycles yields the same heat flux as an averaged cycle. In the fired engine, although there is a random variation of the surface temperature records obtained on the cylinder head (Fig. 6.8(c)), the steep gradient leading to the peak are in general so similar that the computed heat fluxes vary little from one another, and all are in good agreement with the averaged cycle obtained from 15-20 cycles. On the other hand, the surface temperature records of the piston bowl show a larger cyclic variation (Fig. 6.8(d)), which reflects the varying environment in the region of fuel spray-air mixing and the random ignition position in the diesel engine. Therefore averaging over 20 cycles was necessary to minimise the effects of cyclic variation.

6.4 Motored Results

The motored engine, where the variable of chemical reaction is eliminated, is ideal for the study of convection heat transfer in I.C. engines. Therefore, a series of tests were conducted to investigate the effect of location, engine speed and manifold pressure on instantaneous heat fluxes.

6.4.1 Effect of location on measured instantaneous heat flux

The instantaneous heat fluxes at three locations H1, H2 and H3, on the cylinder head (indicated in Fig. (6.9)) were measured. The results obtained for two engine speeds are shown in Fig. (6.10). It was anticipated that due to the presence of an approximately solid body type of rotational motion of gas, the heat fluxes would be the same at the same distance from the cylinder axis. The heat flux was also expected to increase away from the cylinder axis where the gas velocities are high. The results indicate the opposite, note the peak heat flux is greater at H2 (nearest to the axis) than at H1 (farthest from the axis). The difference between the local heat fluxes is also seen to be greater at higher engine speeds. However, the results may have been affected to some extent by the fact that the piston bowl is not symmetrically positioned with the cylinder axis. Thus the thermocouples H1, H2 and H3 being at 4.2 cm, 3.8 cm and 4.1 cm from the cylinder axis respectively, fall at 1.8 cm, 0.6 cm and 1 cm from the piston bowl edge. The offset of the piston bowl must therefore cause some irregular gas motion when TDC is approached. Nevertheless, the low heat fluxes observed at the largest radius (where gas velocity is greater according to the observed solid swirl by Derham (44)), is more likely to result from decreased temperature of the thin gas layer compared to the central part of the cylinder, because of the high surface/volume ratio and low thermal capacity of the gas in the annular space.

The small increase in peak heat flux at H1 (largest radius) with engine speed compared to that observed at H2 and H3 is in line with the above argument, in that at higher gas motion, heat loss will be greater, and therefore cause larger temperature drop of gas in the

annular space, which in turn induces lower peak heat fluxes as observed.

On the piston crown, the results were again not as anticipated, but still in line with the observations on the cylinder head. The measured heat fluxes at locations B1 and B2 in the piston bowl, and locations P1 and P2 on the flat surface of the piston crown are shown in Fig. (6.11). The locations in the piston bowl which were at the same radii (2 cm from the bowl centre) indicated the same heat fluxes at 600 rpm, but different peak values (1019 and 873 kW/m^2) at 1050 rpm. In the annular region, P1 and P2, both at 3.6 cm from the cylinder axis, the same heat fluxes were measured, but only slightly greater than in the bowl for the same conditions. Knowing that the gas velocity is greater at larger radius, which is contradictory to the observed heat fluxes, the effect of the other major factor (gas temperature) influencing heat flux was examined. It was interesting to find that the temperature drop of the gas in the annular region, because of heat loss, ranged between 100-150^{o}C over the interval 10^{o} CA BTDC to TDC. The estimate was made on the basis of a constant mass in the annular region and using an average recorded heat flux over the period considered. Such a drop in gas temperature would account for about 20% drop in peak heat flux in the annular region.

Accepting the foregoing argument, then the similar peak fluxes observed in the bowl and annular region suggest greater gas velocities (20% or more) at P1 and P2 than at B1 and B2, which is roughly of the same magnitude as suggested by the measured velocities in the two regions by Derham (44).

The lower heat fluxes measured on the piston crown at P1 and P2, compared to those measured on the cylinder head cannot be explained, unless the local variations observed on the cylinder head are ignored for a moment. Then it may be said that the smaller distance of P1 and P2 from the cylinder axis, compared to H1, H2 and H3 is responsible for the low heat fluxes obtained on the piston crown. Otherwise, only a large temperature gradient between the gas near the cylinder head and the layer adjacent to the piston crown would explain the results obtained. Table (6.2) gives the measured peak and mean heat fluxes for the different locations under motored conditions.

TABLE 6.2

Measured peak and mean heat fluxes at different locations in the engine cylinder under motored conditions.

Engine Speed rpm	Heat Flux kW/m^2	Location								
		H1	H2	H3	B1	B2	B3	B4	P1	P2
600	Peak	717	858	803	622	660	621	688	718	769
	Mean	103	100	104	98	96	94	98	75	78
1050	Peak	1103	1577	1296	1019	873	890	971	1016	1050
	Mean	141	155	143	125	118	121	121	81	75

In an attempt to avoid the disturbances of gas motion caused by the toroidal piston crown, a false crown with concentric cylindrical cavity was used. The instantaneous heat fluxes measured at the centre of the cavity and at 2.2 cm from the centre are shown in Fig. (6.12). The results do not show the expected difference

caused by velocity distribution in a solid body swirl motion.

Although these observations are in line with the findings of Kim Dao et al (40) (Section 1.21), in observing equal fluxes on cylinder head near the centre of the cavity and deep in the annular region under swirl conditions of gas, it is suspected that errors caused by two-dimensional heat transfer (unaccounted for) contribute to the higher fluxes recorded in the centre of the bowl. There is also the possibility of radial velocity components in the central region close to the wall.

6.4.2 Effect of engine speed on instantaneous heat flux

Fig. (6.13) shows the local instantaneous heat fluxes for the engine speed range of 600 to 1750 rpm. At each location, the instantaneous and time-averaged surface heat flux increased with increasing engine speed. This trend is most evident near TDC during compression and expansion processes.

Since the gas temperature and pressure histories on a CA basis are not significantly affected by a variation of engine speed, the increase in heat transfer with speed must be attributed to increased air motion. The measured gas velocities by Derham (44) in this engine, at different speeds (shown in Fig. (6.1)) are certainly in agreement with the present findings. The same trend was obtained on the piston crown as shown in Fig.(6.11). In this case the results obtained were limited by the linkage induced electric noise interference on the signal at engine speeds exceeding 1200 rpm.

The results obtained for the cylinder head, show a negative heat flux during the induction stroke at an engine speed of 1750 rpm.

This is expected when the gas temperature is less than the cylinder wall temperature, as the direction of heat transfer would be from the wall to the gas. At low engine speeds, negative heat transfer was not observed. Application of pipe flow heat transfer to the induction process of the engine, simulated on the computer, showed that the trapped mean gas temperature at IVC changed by no more than 6°C (31°C to 37°C) under motored conditions as engine speed increased from 600 rpm to 1750 rpm. Therefore, a negative heat transfer is more likely at high engine speeds when wall surface temperatures are higher (73°C at 600 rpm and 102°C at 1750 rpm measured on the cylinder head). Negative heat fluxes were observed by Le Feuvre (34) on the cylinder liner of a moderate swirl engine, but not on the cylinder head which led to the conclusion that the bulk-mean gas temperature is not representative for heat transfer calculations over at least part of the cycle during fired operation.

The effect of engine speed on instantaneous heat flux seemed less pronounced at location H1 than at H2 and H3. The peak heat flux measured at H1 was 717 kW/m^2 at 600 rpm and 1605 kW/m^2 at 1750 rpm, while the corresponding measurements at H2 were 858 kW/m^2 and 2700 kW/m^2, i.e. twice the rate of change with speed as at H1. This behaviour was shown previously to be related to the larger radial distance of H1 in the annular space,where gas conditions are affected by a decrease in the driving temperature caused by heat loss to the cooler walls (large surface/volume ratio) and also by expansion of gas in annulus by blowby.

For the piston crown, the tests were limited to engine speeds of 600-1050 rpm, the maximum observed increase in peak heat flux over this speed range was 397 kW/m^2 at location B1 compared to the maximum increase over the same speed range of 719 kW/m^2 at H2

on the cylinder head. Therefore the rate of change of peak heat flux with speed on the piston crown was half that on the cylinder head, which indicates different behaviour with speed of the parameters controlling heat transfer at the two surfaces.

Although the cyclic variation of the measured parameters in the motored engine were negligible, an accurate estimate of the dependance of crank angle position and peak heat flux on engine speed was not possible. This was because of the uncontrollable oil layer formation on the surface and its continuously variable effect on the phase lag. In general, the peak heat flux occurred earlier as speed increased. The change in crank angle position of peak flux (averaged for all the motored records obtained) over the speed range 600 - 1750 rpm was about 4^{o} CA earlier at higher speed. The increased gas velocity and higher rate of change at high speeds must be responsible for the advance. Another interesting point was that, peak heat fluxes on the cylinder head usually occurred after TDC except at high engine speeds. In contrast most of the peak heat fluxes on the piston crown occurred at or before TDC, generally about $3\text{-}5^{o}$ CA before cylinder head peak position.

Plots of peak heat flux versus engine speed for piston and cylinder head surfaces are shown in Fig. (6.3a), which are of similar trend to the plots given by Kim Dao (40) as shown in Chapter 1.

6.4.3 Effect of manifold pressure on heat transfer

The effect of manifold pressure conditions on instantaneous heat transfer in the motored engine was also investigated. Fig. (6.14) shows this for an engine speed of 1050 rpm and three manifold conditions.

(Inlet pressure = ambient, 0.345 bar and 0.69 bar gauge). It will be noted that the change in the peak heat flux caused by increase of inlet pressure from ambient to 0.345 bar (gauge) was more significant than the increase resulting from a further increase of 0.345 bar in inlet pressure. This effect of inlet pressure was noticed in Kim Dao's (40) results as shown in Chapter 1. As the higher manifold pressure has little effect on the bulk mean gas temperature, it may be deduced that heat transfer coefficients increase as a result of increased swirl velocity (Fig. (6.1)) and of course by the higher gas density. At the high supercharge conditions, peak heat fluxes as high as 3378 kW/m^2 were recorded at location H2, and a negative heat transfer was observed during the induction stroke. The later observation checks the earlier hypothesis about negative heat flux. The average measured surface temperature on the cylinder head was 103^{o}C under supercharged conditions and 81^{o}C naturally aspirated, while the trapped gas temperature is expected to be more or less the same in both cases. Therefore heat transfer from the wall to the gas is more likely under supercharged conditions as observed. A plot of peak heat flux versus manifold pressure is shown in Fig. (6.3b), and Table (6.3) gives other observations under the supercharge condition.

TABLE 6.3

Observations related to heat transfer at different manifold pressures

Manifold Pressure	Location	Peak & (mean) heat flux. kW/m^2	Surf.Temp. Swing ^oC	Position of peak flux & Peak surf. Temp. CA degree
Ambient	H1	1103 (141)	4.94	369 (380)
	H2	1577 (155)	6.04	360 (380)
	H3	1296 (143)	5.4	369 (379)
0.345 bar (gauge)	H1	2257 (238)	9.5	360 (380)
	H2	3024 (264)	11.7	363 (383)
	H3	2326 (233)	9.4	366 (380)
0.69 bar (gauge)	H1	2671 (242)	10.5	364 (380)
	H2	3378 (273)	13.5	364 (376)
	H3	2761 (232)	12.5	356 (380)

6.5 Fired Engine Results

6.5.1 Local heat flux variation

The observation of varying local heat fluxes at similar radii under motored operation, suggests that even larger local variation in surface heat fluxes would occur during firing. The measured local heat fluxes at 1050 rpm under fired no-load and fired 80%-load conditions are shown in Fig. (6.15). The instantaneous heat flux is greater at location H1 than at H3. This situation is the reverse of the motored engine case. The suggested explanation is that H3 being downstream of two fuel jets, partial fuel spray impingement may occur, thus causing surface cooling by evaporation. At location H2, as in motored operation, the largest peak heat flux was registered, and also a greater negative heat flux was noticed during induction compared to other locations. The closer location of H2 to the combustion chamber (piston bowl) would result in this thermocouple feeling the earlier influence of the hot combustion products expanding from the combustion bowl, while a later influence on the other two locations when the gas is cooled by expansion of hot products on the account of compression of cooler air zone and by mixing with it. Considering the character of fuel distribution in the diesel engine, followed by a random and complex combustion process in the cylinder, the local variation of instantaneous heat fluxes on the cylinder head is not large. The peak heat fluxes occurred between 9-15 degrees after TDC, coinciding with, or a few degrees later, than position of peak driving temperature (peak bulk mean gas temperature) for heat transfer.

The local instantaneous heat fluxes at four positions in the piston bowl shown in Fig. (6.16), are for two engine speeds under fired 40%-load conditions. The similarity in magnitude and shape of the heat flux curves was not surprising, because the locations were at the same radius from the bowl centre, and were all in the proximity of fuel sprays. The odd result obtained at B2 for 1050 rpm cannot be explained, except that this location is between two jet impingement zones. The mean and instantaneous heat fluxes recorded in the piston bowl were generally higher than on the cylinder head and other parts of the piston surface. The marked difference in the shape and magnitude of the heat flux diagrams obtained in the piston bowl and other surfaces, therefore clearly demonstrates the predominant influence of the burning fuel jets in the piston bowl. The rapid rise of heat flux in the bowl with peaks occurring long before those observed on the cylinder head reflects the direct influence of the rapid early heat release by combustion of the premixed charge. It was hoped that the crank angle position where the heat flux starts rising and the peak position would indicate when and where the premixed flame occurs. Unfortunately the small difference in the position of the thermocouples relative to fuel jets, did not allow this point to be investigated.

However, the heat flux curves obtained at B2, B3 and B4 indicate the influence of a second hot zone at about 380^{o} CA which may result from presence of more than one flame region, i.e. one corresponding to each fuel jet.

6.5.2 The effect of engine speed and load condition

The similarity of induction-compression strokes in both motored and fired engines suggest that the gas motion would also be the same during this period. Ohigashi (50) confirmed this by swirl measurements during induction-compression strokes in a diesel engine under both motored and fired operation and found only marginally greater swirl for the fired engine. Therefore, the effect of engine speed on instantaneous heat fluxes for induction-compression is expected to be as found for motored engines. Figs. (6.17) and (6.18) show the measured instantaneous heat fluxes for locations H1 and H2 respectively. At each engine speed, three load conditions were investigated. Loading the engine produced greater local instantaneous heat fluxes which was obviously the result of higher bulk mean gas temperatures due to increased fuel injection. Unfortunately higher load (or air:fuel ratio < 29) could not be tested because of excessive carbon deposition on the combustion chamber surfaces under such conditions.

Accepting the findings of Ohigashi (50) of similar swirl in induction-compression strokes of motored and fired engines, the influence of engine speed on heat flux in the fired engine could be explained. Fig. (6.17) indicates results for heat flux at position H1 at various conditions. At similar loads the increase in peak heat fluxes when the engine speed varied from 1050 rpm to 1500 rpm, is of the same order as for the motored engine. However, further increase in speed did not result in higher peak heat fluxes although mean heat fluxes were still rising. Similarly for location H2 as shown in Fig. (6.18) the influence of engine speed is less

significant in the fired engine than under motored conditions. No logical explanation could be given at the time and it was not until some radiation measurements were carried out, that a plausible explanation could be given for the above behaviour. The radiant flux measured at positions R1 and R2 (see Fig. (6.9) for location) are also shown in Figs. (6.17) and (6.18) for comparison. A glance at the radiant flux curves would reveal contrary effects of engine speed at the two locations. Increased flux from the bowl centre (R1), but reduced flux from the annular region (R2) with increased speed. This appears to suggest increased concentration of combustion process in the piston bowl at high engine speeds, with less time available for expansion of still very hot products to the annular region. Hence, the convective flux would also be less in the annular region at high engine speed, as recorded at H1, H2 and H3. Cine film study of combustion by Morris (65) showed that high swirl conditions, constrain the combustion products in the piston bowl longer.

An interesting argument may also be reached from the rapid drop of heat flux in the expansion stroke at H1 for 1500 rpm and 1750 rpm. The trapped air mass in this section of annular space of maximum width, seems to have a dominant effect in quenching the hot products flowing to the region early in the expansion stroke.

Data obtained for piston crown locations P1 and P2 are shown in Fig. (6.19). It must be pointed out that the engine when running at 600 rpm under fired conditions, was unstable and difficult to control. It was only attempted to obtain extra results from the piston (because electrical noise interference through the linkage system prevented tests at engine speeds exceeding 1200 rpm).

At 600 rpm, loading the engine had a small effect on instantaneous heat fluxes. No reason can be advanced for registering higher fluxes at P1 than P2 with low engine speed, but at 1050 rpm, the measured heat fluxes at P1 and P2 followed the same trend as observed at nearby locations (H1 and H2) on the cylinder head. The heat fluxes were as for the motored engine, lower than those observed on the cylinder head surface. P1 and P2 are at smaller radius, but this alone does not explain the discrepancy. The answer could only be in a greater influence on the piston surface of the trapped air in the annular region.

In the piston bowl, negligible local variation was observed, therefore the load and speed effect for one location (B1) is shown in Fig. (6.20). Note the significant effect of engine speed on the instantaneous heat fluxes, which again reflects the influence of gas motion on heat transfer. An additional effect on heat transfer would also result from a more efficient combustion under high swirl conditions. The effect of load on increasing heat flux was approximately the same at both engine speeds and is explained by the higher average charge temperature of the products and air mixture. At 600 rpm, the results for 80% load was not obtained for B1, but a drop of about 3% in the peak heat flux occurred at B2 and B3 under 80% load condition. This is supported by the longer combustion period due to more wall burning observed by Morris (65).

At 1050 rpm, a peak heat flux of 4416 kW/m^2 was recorded at B1 which was $1\frac{1}{2}$ times the maximum value recorded on the cylinder head.

Mean heat fluxes recorded in the bowl, also increased with increasing engine speed and loading condition, and were much higher

TABLE 6.4

Fired Engine Total Heat Transfer Data

Engine Speed	Condition (IMEP) Bar	Peak Flux/Mean Flux. kW/m^2			Position CA.Peak(Flux/S.T)			Surface Temp. Swing °C		
		H1	H2	H3	H1	H2	H3	H1	H2	H3
1050	FNL (3.5)	1759 216	2169 240	1417 205	374 389	376 395	374 405	7.9	9.5	6.2
	F40%L (4.3)	1942 238	2668 266	1436 240	373 399	372 386	380 397	9.24	11.5	6.4
	F80%L (5.5)	2391 240	2868 312	1976 293	369 396	376 392	376 395	9.6	12.3	7.6
1500	FNL (3.6)	2167 265	2540 246	1680 228	382 396	382 405	380 396	9.3	10.4	6.6
	F40%L (4.6)	2424 302	2557 274	1753 270	378 401	392 414	387 410	9.4	11.56	6.9
	F80%L (6.0)	-	2996 301	1967 294	-	392 405	369 405	-	12.2	7.3
	MOT	1334 178	1883 184	1487 170	380 426	366 389	378 405	5.8	7.5	5.8
1750	FNL (3.7)	2042 275	2767 284	2555 264	365 376	370 387	378 395	4.5	9.6	9
	F40%L (4.5)	2247 300	3024 331	2671 311	368 373	378 395	383 399	4.4	9.8	8.7
	F80%L (5.7)	-	-	-	-	-	-	-	-	-
	MOT	1617 210	2375 232	2268 223	365 376	360 381	362 388	4.1	7.5	8

Table 6.4 (continued)

PF = peak flux, MF = mean flux, PFP = PF position, PSTP = peak surface temperature position, DSTS = dynamic surface temperature swing

Engine Speed	Condition (IMEP) Bar	Measured Parameter	LOCATION					
			P1	P2	B1	B2	B3	B4
600	FNL (3.0)	Peak flux	1095	748	1955	1812	2120	1895
		Mean flux	283	192	270	249	265	271
		PF position	360	362	367	377	356	360
		PST "	396	382	379	383	371	390
		DST swing	6.2	3.3	6.9	8.5	6.4	7.4
	F40%L (3.8)	PF	1247	872	2235	2257	2211	1920
		MF	200	207	322	290	311	334
		PFP	380	360	367	367	364	363
		PSTP	413	376	376	386	375	371
		DSTS	5.9	3.7	6.9	9.4	7.3	7.8
	F80%L (4.8)	PF	1265	958	-	2224	2164	-
		MF	220	219	-	314	413	-
		PFP	364	364	-	372	362	-
		PSTP	396	378	-	388	382	-
		DSTS	7.2	3.8	-	9	7.4	-
1050	FNL	PF	1300	1959	3148	1436	2543	1900
		MF	200	207	320	295	354	351
		PFP	378	375	368	363	360	366
		PSTP	384	384	377	375	369	375
		DSTS	47	7.1	7.6	5.3	5.4	5.9
	F40%L	PF	1604	2125	3728	2267	3913	4364
		MF	213	233	335	280	412	408
		PFP	380	381	368	365	362	362
		PSTP	382	390	377	380	370	370
		DSTS	5.4	8.1	9.1	7.4	8.4	9.5
	F80%L	PF	1752	-	4416	2540	-	-
		MF	244	-	340	305	-	-
		PFP	367	-	370	367	-	-
		PSTP	379	-	380	380	-	-
		DSTS	5.9	-	11.1	8.0	-	-

than the mean flux measured at other surfaces of the engine cylinder. Table 6.4 summarises the fired engine data obtained.

6.6 Measured Radiant Flux in Diesel Engines

In view of the complexity of the theory and the associated uncertainty in the calculated values of gas emissivities, total radiation measurements are still in many respects the most reliable source of information with which to design heat transfer equipment and to evaluate the relative importance of radiation heat transfer in internal combustion engines. Therefore to further our knowledge of heat transfer in diesel engines, the instantaneous radiant flux was measured at two locations (R1 and R2) on the cylinder head as shown in Fig. (6.9). Position R1 was directed at the centre of the piston bowl and R2 directed at the flat surface of the piston just outside the bowl when the piston is at TDC position.

6.6.1 Reproducibility of measured data and cycle-to-cycle variation

In order to establish the repeatability of the experimental data, the test run at 1500 rpm 40% load condition was repeated at the end of the collection of radiation data from position R1. Results of the two tests are compared in Fig. (6.21a), in the form of the recorded voltage. The repeatability is very good considering the many factors that affect the radiation heat transfer. It must be pointed out that these traces are the average of 15 cycles and that comparison of single cycles is meaningless. The large cyclic variation of radiation signal observed at R1 under different conditions is shown in Figs. (6.21b)

Although soot deposition on the viewing window was not a problem over short periods of running (e.g. 10 minutes under medium load conditions), the repeatability of the data was ensured by first cleaning the viewing window at the beginning of each test and again before the heavy load test. Secondly, the engine operating condition was maintained at a stable state during the entire data collection process to allow for reliable averaging of a large number of cycles. The calibration of the detector was also checked several times throughout the engine tests.

6.6.2 Effect of engine load (equivalence ratio) on radiant flux

Plots of the measured radiant flux at positions R1 and R2 are shown in Fig. (6.22) and Fig. (6.23) respectively. Note at each engine speed tested, the highest peak emissions were recorded for the highest equivalence ratio run. This finding was in agreement with the average flux results obtained by Flynn (34), discussed in Section (1.2), but not with the peak emission trend. Flynn stated that the drop in peak emission after exceeding a certain equivalence ratio was unexpected and explained the behaviour by:-

1) Possible decrease in reaction zone temperatures caused by the higher overall F/A, or by significant formation of carbon particles which may have masked the view of the hotter particles in the reaction zone.

2) Penetration of the fuel spray in the viewing passage, which was away from the influence of the air swirl and might have burned in a different manner than those in the main chamber.

In the engine used here, the swirl is high (17 000 rpm mean

swirl or 34 000 rpm peak swirl at 1500 rpm engine speed) compared with that of Flynn's engine (4000 rpm mean swirl at an engine speed of 2000 rpm) and hence the problem of over-richness would not arise. Therefore the results as expected, showed an increase of instantaneous radiant emission with greater equivalence ratio. The trend of the variation of radiant flux with increasing load could be explained by;-

a) Increased fuel injection would lead to larger flame size, hence increased radiation. The literature shows no change in flame temperature with increasing F/A ratio.

b) Rich mixture zones are expected with increased fuel injection which tends to form more soot in the reaction zone followed by combustion with increased flame luminosity causing higher radiation. In general, the high swirl would result in efficient combustion.

The high F/A run produced exhaust smoke. Whether this smoke production is directly related to the higher radiant emission values is unknown.

Radiant emission started rising more or less at the same crank angle, but peak emission position occurred later (3-5^{o} CA) as engine load increased from no-load to 80% load. The shift was most likely caused by the accompanying increase in ignition delay with changed mode of combustion at rich mixtures. The peak radiant emission recorded in the present work occurred between 365-375^{o} CA, compared to Flynn's (34) recorded peak emissions between 360-370^{o} CA. The early detection of maximum emission by Flynn may have been related to the viewing window which was looking into fuel spray plane where combustion is started. The viewing field at R1 was into the

centre of the piston bowl, away from the rich mixture zone near the combustion bowl wall where combustion starts according to the work of Morris (65).

6.6.3 Effect of engine speed on radiation heat transfer

The effect of engine speed on measured radiation was different for the two locations of measurement. Therefore, the results obtained are discussed separately for each position.

i) Measured radiant flux at position R1

Data in Fig. (6.22) shows the radiation flux observed at position R1. When the engine speed was increased, holding other factors constant (note the slight change in equivalence ratio), both peak and total radiant emission increased. This effect of engine speed was not unexpected because in the test engine, measured gas swirl was shown to increase from 10000 rpm to 34 000 rpm as engine speed varied from 600 rpm to 1500 rpm. Such increase of gas motion is expected to improve air-fuel mixing and results in more efficient combustion. In addition to this, it is thought from Morris' photographic studies (65) that the higher air swirl conditions tend to constrain the combustion products in the piston bowl longer. Thus increased engine speed may lead to concentrated and more complete combustion at the centre of the combustion chamber because of more fuel vapour driven to the centre by radial (squish) velocity components which increased from about 9 m/s to 34 m/s as the engine speed increased from 500 rpm to 1500 rpm (Derham (44)). In other words increased engine speed affected the geometry of the flame in the cylinder.

A change in position of peak radiant emission was observed with increasing engine speed (about 5^{o} CA/500 rpm). Also, the decay of the radiant heat flux on a crank angle basis was slower as speed increased. These effects would be expected if one associated a more or less fixed time interval for combustion and carbon particle formation and destruction process.

ii) Measured radiant flux at position R2

Fig. (6.23) shows the measured radiation heat flux at location R2. The instantaneous radiant flux increased first with engine speed up to 1050 rpm and then dropped as the engine speed increased further. This trend was not observed at location R1. At low engine speeds (600 and 1050 rpm) the heat flux at R2 indicates the expansion of the flame and combustion to the detector viewing field (annular region). At higher engine speeds with less time available near TDC, the expansion of the hot products to the measurement region, may not be significant. The foregoing would be in agreement with the observation at R1, which indicated concentrated combustion in the bowl. The concentrated combustion in the bowl must be related to the high swirl-squish velocities induced at high engine speed.

The shape of the radiant heat flux curves obtained are unique for each location of measurement. At R1, a smooth radiant flux curve with a single peak, indicates a gradual increase in temperature and size of radiating body. In contrast a fluctuating curve with two peaks was obtained at R2. The first peak appeared to be associated with the first stage of rapid combustion resulting the expansion of the flame into the annular region. The second peak,

occurring later (380-400° CA) must be associated with uncovering by the piston of the hot gaseous products in the combustion bowl.

The time averaged radiant heat flux rates could not be measured directly by the radiation detector. However, the integrated values obtained for locations R1 and R2 are given in Table 6.5

TABLE 6.5

Time-averaged radiation heat flux considered over the compression–expansion stroke only.

Location	Load Condition	Mean Heat Fluxes in kW/m^2 Engine Speed rpm			
		600	1050	1500	1750
R1	FNL	-	4.88	12	21
	F40/L	-	6.76	19.5	30
	F80/L	-	13.2	32.6	53.6
R2	FNL	15	14.4	8.6	17.2
	F40/L	22.5	23.4	16	18.8
	F80/L	26	45.4	39.1	-

6.7 Relative Importance of Radiant Heat Transfer in High Swirl Diesel Engines

A visual comparison between the measured instantaneous radiation fluxes at positions R1 and R2 and the total instantaneous heat fluxes measured at H1 and H2 were presented in Figs. (6.17) and (6.18) respectively. Considering the position of measurements, radiant flux at R1 should be compared with the measured total flux in the piston bowl. It will be seen that the peak radiant flux for engine speed at 1050 rpm is less than 8% of the measured total peak flux in the bowl. It is expected that at higher engine speeds, the radiant/total percentage will not change significantly or may be reduced due to better air-fuel mixing and less carbon formation and by increased convective components, (No data of total heat flux was obtained in piston bowls at higher engine speeds). Peak radiant fluxes at R1 are between 15% to 20% of the total peak fluxes obtained at H1. On the other hand, peak radiation flux at position R2 is 16% of the total peak flux at H2 for 1050 rpm, heavy load condition. Smaller percentages are observed at higher engine speeds, decreasing to about 5% at 1750 rpm, medium and low load conditions.

Comparison on the basis of measured (integrated) mean fluxes during the compression-expansion strokes, shows that radiant flux at R1 represents 5% of the total flux measured in the bowl under heavy load conditions (1050 rpm) and does not exceed 16% of the mean flux measured on the cylinder head, both obtained for 1750 rpm heavy load condition. A comparison on the basis of mean fluxes obtained over one whole cycle, the radiant flux will represent no more than 7% of the total heat flux under the most favourable conditions. Therefore, the percentage values of radiant flux/total flux obtained

in the present high swirl engine falls short of values of up to 45% reported by Ebersole (32) for low swirl 2-stroke diesel engine, 15% - 33% by Oguri (33) for large low swirl engines, and about 20% by Flynn (34) for moderate swirl engine. Because the measured radiant and total heat transfer are critically dependant on location of measurement, the above mentioned relative magnitudes of radiant and total heat fluxes will not be representative for the whole cylinder surfaces. In addition, the small interval (near TDC) during which the radiant heat transfer becomes significant. However, the difference between the gas motion in the present high swirl engine and the low swirl engines tested by Ebersole (32), Oguri (33) and Flynn (34) is likely to be the major cause for differing fractions of radiant/total heat transfer. Firstly, the intense gas motion will improve air-fuel mixing which in turn will reduce carbon formation and radiant heat transfer. Secondly, the intense gas motion will lead to increased convective component of heat transfer. Hence the overall effect results in smaller radiant/total heat transfer.

6.8 Prediction of Instantaneous Heat Flux Using Bulk Mean Gas Temperature

6.8.1 Bulk mean gas temperature

Most of the analyses carried out by past workers in convective heat transfer in I.C. engines have utilised the concept of bulk mean gas temperature calculated from the measured pressure. The bulk mean concept does not allow for spatial variation of temperature in the combustion space. It is quite certain, however, that temperature gradients exist in the gas space, particularly during the early stages of combustion, this is confirmed by cine film studies of the combustion

process, which indicates that combustion in a diesel engine is initiated at several independent zones of burning, which merge later in the combustion period. The system will be further complicated in the presence of air swirl where the tendency is for the hotter and less dense products to convect upwards and/or towards the central region of the swirl flow. These considerations show that the bulk mean concept cannot be expected to give anything more than an approximation to the resultant heat transfer calculated for any particular area. The error introduced into the instantaneous predicted heat fluxes will be greater of course because of strong spatial temperature distributions in the combustion chamber. However, in motored engines, it is expected that bulk mean gas temperature would represent the local gas temperature accurately.

The measured pressure and the calculated bulk mean gas temperatures under motored and fired (different load) conditions at an engine speed of 1050 rpm, 600 rpm and 1500 rpm are shown in Figs. (6.24) to (6.26) respectively.

6.8.2 Prediction of local convection heat flux in motored engines

The foregoing experimental data showed considerable variation in the surface heat flux over the cylinder head and piston areas. Variation was observed under motored operation and to a larger degree in the fired engine, which suggests a temperature gradient in the gas between the two surfaces.

The modified flat plate forced convection equation described in Section (2.1) was used to predict the local heat transfer

coefficient for each of the conditions tested. Note that none of the previously proposed correlations predict local heat fluxes in the cylinder except that of Le Feuvre (20) which also shows wide discrepancy with experimental results. The bulk mean gas temperature and the local surface temperature were used to obtain a driving temperature for heat transfer. All gas properties were calculated on the basis of the measured pressure and the bulk mean gas temperature (calculated from the measured pressure, trapped mass and instantaneous volume) in the manner suggested by Annand (6). The measured local instantaneous gas velocity was used in the calculation of Reynolds number. Fig. (6.27) shows the calculated and measured local heat fluxes on the cylinder head, under motored conditions. Peak calculated heat fluxes coincide with TDC because peak swirl and maximum gas temperature occurred at TDC, unlike the measured peak flux which shows a phase shift. In general, the measured results are greater than the calculated local heat fluxes, and this was especially significant at the smaller radius location H2. The agreement for location H1 is quite good in the compression stroke, but not so during expansion. The swirl velocities used in the calculation, which are the mean value of measurements at many locations, are unlikely to be responsible for the discrepancy. Squish velocities near the bowl edge which were neglected, may have greater influence than expected and perhaps as much as indicated by the measured flux at H2.

It can be seen that deduction of a steady component of heat flux from the measured heat flux curve would improve the agreement with the calculated values of heat flux. The steady component difference is about 200 kW/m^2 for H2 and 100 kW/m^2 for H3. Such

discrepancy could not be compensated by local gas temperature variation, which is not expected to be large in a motored engine, but errors caused by two-dimensional heat transfer in the measured mean value may account to some extent for the discrepancy.

The predicted heat flux curves for piston surface are shown in Fig. (6.28) compared with the maximum and minimum measured flux curves obtained for different locations at the same radius. In the piston bowl, again the predicted flux was less than measured, but good agreement was obtained for the piston surface in the annular region.

Similar discrepancy was observed at other engine speeds, but in general the difference was less at the higher engine speed (e.g. 1500 rpm). An explanation for this behaviour can be found in the gas velocity measurements made by Derham (44) in the test engine. It was found that squish velocities were significant in the interval 350 to 360^{o} CA with peak values reaching 60% of swirl component at low engine speeds (500 rpm), and 30% of swirl at high speeds (1500 rpm). These radial velocities would enhance the resultant gas velocity by about 18% at 500 rpm and by 6% at 1500 rpm near TDC (350-360^{o} CA). Therefore, as radial velocities were not considered in the prediction, it seems that this could be the reason for higher measured fluxes than predicted values, particularly at low engine speeds.

6.8.3 Prediction of local heat flux in fired engines

The 3YWA Ruston engine is a type where it is now suspected that bulk mean gas temperature under fired conditions is not at all representative of the local variations in gas driving temperature for heat transfer. This suspicion is particularly strong in

consideration of the experimental flux variations measured in the piston bowl and at other surfaces. However, it is interesting to ignore such considerations for the present and to inspect the result of a heat transfer prediction made on the basis of bulk mean gas temperature. This is done at this stage because it is thought that a comparison of the predicted results with those actually measured, will be more informative with regard to the suitability of the bulk mean gas temperature in the present heat transfer situation. In addition to the above, the radiation effects are expected to augment the predicted heat flux in the fired engine. Fortunately the measured radiant component of heat transfer was not large enough to have a significant effect on the predicted convective heat transfer.

Therefore as for motored engines, the modified flat plate equation combined with the information on motored gas velocities, gas properties evaluated at bulk mean temperature and measured pressure and measuredlocal surface temperature, were used to predict the local heat transfer in the fired engine. The measured and predicted heat flux curves are presented in Figs. (6.29) and (6.30). In order to facilitate comparison, the measured heat fluxes for no-load and 80% load conditions for each location are presented with the corresponding predicted values. Good agreement during the compression stroke was followed by a large discrepancy during the combustion period and expansion process. This is thought to result from the inadequate representation of the local gas temperature. Inspection of data from the cylinder head and piston annular region locations, indicates that the driving gas temperature (bulk-mean) used for prediction of heat transfer in the annular region is high

for the early combustion period (up to 20° CA ATDC). The gas in the annular region is expected to be predominantly air. In the expansion stroke, however, the reverse occurred. The low predicted heat fluxes indicated that the gas temperature near the cylinder head becomes higher than the calculated bulk mean temperature. This suggested the expansion of combustion products into the annular region, and the convection of the hotter products upwards, which remained adjacent to the cylinder head surface throughout the expansion stroke.

The measured and predicted heat fluxes in the piston bowl (Fig. (6.30)), also supported the above explanation. As shown, the measured values were generally higher than predicted values, this time indicating that actual gas temperature in the bowl is greater than the calculated bulk mean gas temperature. These results in general suggest two-zone temperature effects.

6.8.4 Prediction of local area-mean heat flux

To avoid confusion, local area-mean heat flux is the average value obtained for different sections of the cylinder, e.g. the cylinder head, piston bowl and piston annular region. The bulk-averaged flux is the overall average obtained for the whole chamber surface which will be discussed in section (6.9.4).

i) Prediction of local area-mean heat flux in the motored engine

Having failed in the prediction of local heat fluxes on the basis of bulk mean gas temperature, an attempt was made to predict area-mean heat fluxes, where the assumption of bulk mean gas temperature is perhaps a more realistic proposal. The area-mean

heat flux curve for the cylinder head was obtained by calculating the instantaneous arithmetic-mean heat flux for the three locations H1, H2 and H3. Note that although the thermocouples were far apart on the cylinder head, they fall on circles with small differences in radii. Thus the predicted heat flux was calculated for the mean radius of the three positions of measurement.

It was noted previously that most proposed correlations predict a single heat flux-time curve for the cylinder head or the whole chamber area. Therefore a comparison with the most popular correlations was also possible. The extent to which Annand's equation 1.4 , Woschni's equation 1.12 and the present correlation predict the experimental area-mean data under motored engine are shown in Fig. (6.31) for the cylinder head. The values of the empirical constants in Annand's equation were selected in the range suggested by Annand (6 and 15) as suitable for high swirl diesel engines. ($a = 0.8$, $b = 0.7$, $a' = -0.2$ and $c = 1.5\sigma$) (σ = Boltzman constant). Similarly, Woschni's equation was used with the suggested constants and expression for gas motion. None of the correlations provide a good fit of the experimental data. The modified flat plate equation (to account for radial changes of gas velocity and heat flux) is seen to provide the better prediction, particularly at high engine speed. Under all conditions the discrepancy is larger in the expansion stroke, suggesting a higher driving temperature for heat transfer especially on the cylinder head. Here again the relatively high influence of squish velocities (ignored) at low engine speed explains the discrepancy observed at 600 rpm. Better agreement at high engine speed is obtained because of negligible influence of squish velocities.

Fig. (6.32a) shows the predicted and measured mean-instantaneous fluxes for piston bowl and piston annular region at 600 rpm and 1050 rpm. Similar discrepancy as for the cylinder head is observed, with the best fit of the predicted and measured heat flux obtained for piston crown annular regions at 1050 rpm. The instantaneous mean heat fluxes obtained from Woschni's equation are very low in the motored engine, with little response to the change in engine speed. Annand's equation gives better prediction at low engine speed and for the central region of the cylinder (piston bowl), where gas motion is low. However, as Annand's equation and Woschni's equation were derived for application to fired engines, the discrepancy is justified. The prediction of instantaneous mean heat fluxes by the flat plate equation is different by up to 50% of the measured mean flux at low engine speed. Improved agreement obtained at high engine speed suggests two possible causes:

a) Smaller errors involved in the assumption of one-dimensional heat transfer in the analysis of transient heat flux from surface temperature record, because of shorter time available for heat transfer parallel to the surface. At the same time, any errors made in the measurement of steady component of heat flux (also assumed one-dimensional) has a smaller percentage effect on the high transient fluxes recorded at higher speeds.

b) Smaller errors involved by ignoring squish velocities near TDC (350 - 360^{o} CA) in the prediction of heat flux. Ignoring squish velocities leads to a reduction in resultant gas velocity of 18% for 600 rpm and 8% for 1050 rpm.

The above argument concerning the smaller effect of errors involved in measurements when the measured parameters are large, is supported by the improved prediction of mean instantaneous heat flux on the cylinder head at 1050 rpm. 1.69 bar manifold pressure shown in Fig. (6.32b). The squish velocities under supercharge conditions were not measured by Derham (44), but are expected to be higher than naturally aspirated conditions which will be enough to account for discrepancy between measured and predicted, near TDC.

ii) Prediction of local area-mean heat flux in the fired engine

In the fired engine, poor agreement between the measured area-mean heat fluxes and the predicted values was observed under all conditions. Fig. (6.33) shows the results obtained for cylinder head surfaces at 1050 rpm and three load conditions. Inspection of the heat flux curves indicates the same trend in the discrepancy, with both Annand's equation and flat plate equation (ignoring Woschni's equation for a moment) giving greater heat fluxes than measured during early combustion period, but less for the remainder of the expansion stroke. The trend again indicates the inadequate use of bulk mean gas temperature as the driving temperature for heat transfer.

Note that as the measurement positions on the cylinder head fall in the annular region, away from the early combustion in the bowl, the gas in this region is mainly pure air and will be at a temperature lower than the bulk mean.

Calculations on the basis of two-zone temperature distribution will be presented in the following section to clarify the above argument.

A comparison of the measured and predicted heat fluxes for the cylinder head at 1500 rpm and different load conditions are shown in Fig. (6.34). In this case an even larger discrepancy than for 1050 rpm is observed, suggesting wider difference between calculated bulk-mean and actual gas temperatures in the annular region during combustion. This behaviour is in agreement with the decreasing radiation flux, measured in the annular region (R2) at high engine speed as shown in Fig. (6.23). The larger discrepancy at high load is caused by higher calculated bulk mean gas temperatures, due to more fuel injected.

For the piston crown, results for fired conditions were obtained at speeds of 600 rpm and 1050 rpm. Comparison of measured area-mean and predicted mean instantaneous heat fluxes were obtained for the piston bowl and the flat annular region of the piston surface separately. The comparisons are shown in Figs. (6.35) and (6.36). In the annular region at 600 rpm, all the predictions differed widely from the measured heat flux. Only the flat plate equation predicted peak heat flux values with an acceptable margin. It is obvious that in Annand's and Woschni's predictions, where piston mean speed is used to represent the gas motion, the effect of piston speed exceeds the actual magnitudes of gas motion at low engine speed. Note that in the present engine, the ratio swirl/engine speed changed from 1.3 at 600 rpm to 2.3 at 1500 rpm. Therefore, the use of piston mean speed for gas motion, overestimates and underestimates this effect at low and high engine speeds respectively.

At an engine speed of 1050 rpm, the flat plate equation gives good agreement with the measured fluxes during compression and expansion strokes, but again predicts high values near TDC during the combustion period. This trend, as in the case with cylinder head

results, will be described by the inadequate representation of the driving gas temperature, particularly during combustion. The corresponding predictions by Annand's equation and Woschni's equation are the same as in Fig. (6.33). Annand's prediction is also affected by the temperature distribution, while the weakness of Woschni's prediction is the late increase and early decrease of heat fluxes, caused perhaps by its sensitivity to gas temperature. The latter behaviour is obvious from Woschni's prediction of relatively low heat fluxes for the supercharged condition, Fig. (6.32b) where pressures are high, but gas temperatures are similar to the naturally aspirated engine.

The measured area-mean heat fluxes in the piston bowl are compared with predicted values in Figs. (6.37) and (6.38). The sharp high peaked characteristic of measured mean heat flux-time curves, were obviously linked with the sharp heat release characteristic of the initial combustion taking place in the bowl. The possibility of the flame propagating and hitting the surface is not unexpected. The predictions by the flat plate equation, on the basis of bulk-mean gas temperature are low throughout the compression-expansion strokes. Near TDC and during the combustion period, the gas temperature in the bowl is expected to be much higher than the calculated bulk mean temperature. Improved prediction of instantaneous heat flux in the bowl under heavy load conditions was observed when the driving temperature for heat transfer is represented by the adiabatic flame temperature as shown in Figs. (6.37) and (6.38).

Concerning the steady component of the measured heat flux, this was large in the piston bowl (greater than 300 kW/m^2) compared to other positions of measurement on the cylinder head and piston (see Table 6.4). It is now suspected that two-dimensional heat transfer

may have exaggerated these measurements. On the other hand, the predictions on the basis of heat transfer coefficient and application of Newton's cooling law, gives negligible values of heat transfer up to 30°CA BTDC and after 50° CA ATDC. Therefore, some means of estimating a steady component of convection heat transfer must be found, perhaps on the basis of gas-mean temperature throughout the cycle, or during the trapped period.

6.9 Prediction of Instantaneous Heat Flux on the Basis of Two-Zone Temperature Distribution

6.9.1 Two-zone temperature model

The large variation in magnitudes of measured heat fluxes at the different surfaces of the combustion chamber, and the prediction of these fluxes on the basis of bulk-mean gas temperature, all suggest the presence of different temperature zones in the cylinder. The total heat flux results and the radiation flux results, in general indicate the presence of a hot gas core in the piston bowl and a cooler gas in the annular region. The two zones seem to exist up to 400° CA (40° ATDC) and they are better defined at higher engine speeds.

Consider the combustion chamber about 15° CA BTDC when the fuel is injected. The piston-cylinder head clearance at this point is only 2 mm, which results in all the fuel being injected into the piston bowl, if at this stage the following assumptions are made:

a) The fuel injected forms a chemically correct mixture with a portion of the air in the bowl to form a so called mixture-zone, and

b) That the remainder of the air in the cylinder forms the air zone, assumed not to mix with the mixture-zone, therefore occupying the volume above the mixture, and includes the annular region.

If this system is to be equivalent to the actual cylinder conditions, then the following may be deduced from application of gas laws to the different zones.

Apply gas laws to the actual cylinder conditions (as usual assuming a homogeneous mixture), therefore:

$$PV = m\,RT \tag{6.1}$$

For the air zone:

$$P_a\,V_a = m_a\,R_a T_a \tag{6.2}$$

and for the chemically correct mixture zone:

$$P_m\,V_m = m_m\,R_m T_m \tag{6.3}$$

It may be assumed that pressure is the same everywhere in the cylinder, i.e. $P_a = P_m = P$ (measured) and:

$$V_m + V_a = V \tag{6.4}$$

Therefore, combining the above equations, it can be shown that the chemically correct mixture temperature is given by:

$$T_m = T + \frac{m_a\,R_a}{m_m\,R_m}\left[\,T - T_a\,\right] \tag{6.5}$$

which reduces to: $T = T_a$ during compression.

In equation (6.5), it was further assumed that the gas constant for the chemically correct mixture ($\frac{air}{fuel} \simeq 15$) of fuel vapour and air is the same as that for pure air. Such an assumption was found to cause no more than 3% error in the calculated mixture temperature. Therefore, the combustion zone (c.c.m. zone) temperature was calculated by the simplified equation:

$$T_m = \frac{m.T - m_a T_a}{m_m} \tag{6.6}$$

where m = total mass of charge in the cylinder

m_m = mass of fuel and air forming a chemically correct mixture

m_a = mass of excess air in the cylinder.

T, T_m & T_a are bulk-mean, mixture (combustion) zone and air zone temperatures respectively.

The bulk mean gas temperature T is calculated as usual, from the measured pressure and initial trapped conditions using gas laws. The air temperature T_a, may be assumed to follow a polytropic process, hence:

$$T_a = T_i \left(\frac{p}{p_i} \right)^{\frac{n-1}{n}} \tag{6.7}$$

where T_i and P_i could be the temperature and pressure of air at IVC.

Knowing the mass of the trapped air at IVC (m_i) and the amount of fuel injected per cycle m_f, the mass of the mixture in the

combustion bowl, mass of remaining air and total charge mass can be calculated. Hence the mixture zone temperature T_m follows at each instant after combustion has started. The burning-zone temperature and the pure air-zone temperatures calculated for different test conditions are shown in Figs. (6.24) to (6.26).

The rate of expansion of the mixture zone calculated by applying gas laws, shows that at 1050 rpm no-load condition, the mixture which initially occupies one third of the bowl volume, starts leaving the bowl at 380^{o} CA due to expansion. Under 80% load, with the mixture initially occupying half the bowl, it starts leaving the bowl at about 370^{o} CA. Outsquish velocities caused by the expansion are of the order of 3.0 m/s under no-load and 9.4 m/s at 80% load condition for an engine speed of 1050 rpm, and a corresponding outsquish velocity of 6.7 m/s to 15.3 m/s at an engine speed of 1500 rpm. Table 6.6 summarises some relevant results obtained from the two-zone temperature model.

If the outsquish is slightly directed towards the cylinder head as is expected, the displaced cooler air would move downwards over the flat part of the piston which would explain the low measured fluxes obtained from the later surface. The cool air would move into the piston bowl due to its larger density as shown by the sketch (6.A). Alternatively the cool air may be forced to a rotary motion by further expansion from the bowl which with the swirl component would form a helical motion in the annular region.

6.9.2 Combustion induced swirl increase

In internal combustion engines, random gas motion is expected to result by the combustion process. This combustion generated gas

TABLE 6.6

Rate of radial spread in the annular region and outsquish velocities of hot products from piston bowl obtained from two-zone model.

Radial spread cm from bowl centre/outsquish velocity m/s

CA°	1050 rpm			1500 rpm		
	FNL	F40%L	F80%L	FNL	F40%L	F80%L
360						
370			2.25/9.4		2.25/5.4	2.3/15.3
380	-/3.1	2.67/4.8	3.75/2.3	2.25/6.75	2.85/6.75	4.0/2.5
390	2.8/3.2	3.44/1.8	4.1/0.9	3.0/4.3	3.6/3.2	4.28/1.1
400	3.3/1.0	3.7/0.9	4.26/0.25	3.48/1.8	3.96/0.7	4.4/ -
410	3.47/0.9	3.84/0.9	4.3/0.25	3.66/1.3	4.0/0.5	4.4/ -
420	3.6/ -	3.99/ -	4.34/ -	3.75/ -	4.1/ -	4.45/ -
		600 rpm				
	FNL	F40%L	F80%L			
360						
370						
380		1.37/5.9	2.75/3.1			
390	2.8/1.66	3.0/1.2	3.6/1.1			
400	3.24/0.94	3.3/1.0	3.9/0.7			
410	3.5/0.1	3.6/ -	4.1/ -			
420	3.52/ -	3.6/ -	4.1/ -			

motion would have an additional effect on heat transfer and was considered by Woschni (2). It was assumed to be proportional to $(T_{fired} - T_{motored})$. Therefore, in high swirl engines, an increase in swirl component as well as random motion is expected to result from combustion. The following approach is made in order to approximately estimate combustion influence on swirl.

Consider first the unburned charge moving at swirl ω rpm. Then at any instant during combustion, imagine two adjacent portions of gas, one burned and the other unburned, separated by an imaginary boundary.

The mass flow/unit area-unit time in direction of swirl of the fresh charge $= \rho_u \; U_u$ and of the burned charge $= \rho_b \; U_b$

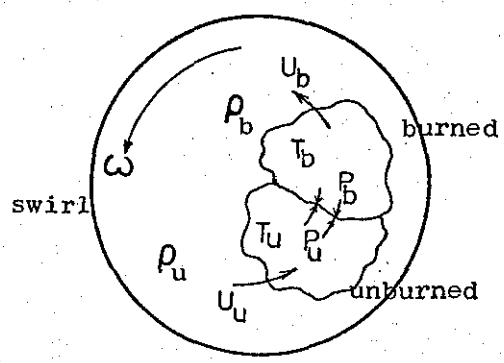

Sketch (6.A)

where U = velocity, ρ = density, subscripts u and b stand for burned and unburned gas.

The momentum flux transported by the fresh charge in the direction of flow $= \rho_u \; U_u . \; U_u$ (6.8)

Hence application of conservation of momentum in the direction of flow along with assumption of a uniform pressure field and negligible frictional effect results in:

$$\rho_u \; U_u^{\,2} = \rho_b \; U_b^{\,2} \qquad (6.9)$$

i.e. velocity of burned gas $U_b = U_u \sqrt{\frac{\rho_u}{\rho_b}}$ (6.10)

OR in terms of swirl $\omega_b = \omega_u \sqrt{\frac{\rho_u}{\rho_b}}$ (6.11)

Calculations on the basis of two-zone temperature in the cylinder, at different operating conditions, produced values of $\sqrt{\frac{\rho_u}{\rho_b}}$ of 1.2 – 1.4 during the expansion stroke, and therefore an increase in the motored swirl of 1.2 - 1.4.

6.9.3 Predicted heat fluxes by two-zone model

The prediction of heat transfer on the basis of the two-zone temperature distribution concept was complicated by finding when and where each zone became effective. In the present case, this was decided by the estimated expansion rate of the burning products as shown in sketch (6.B). Therefore, the mixture zone temperature would be the driving temperature in the bowl during the important period of heat transfer (10° CA BTDC to 30° CA ATDC). On the other hand, in the annular region where cylinder head and piston thermocouples were located, the pure air zone temperature is the effective temperature until the hot products reached the measurement position. Over the rest of the expansion stroke, a hot zone is assumed to remain adjacent to the cylinder head by nature of its low density, while a bulk mean temperature is assumed to be effective on the flat part of the piston surface caused by the outsquish mixing with cooler air in the annular region before passing over the piston surface. The increase in swirl was assumed to be complete when combustion was near completion (at about 390° CA) estimated from measured pressure diagrams. Therefore the

predictions of the heat fluxes were corrected for both two-zone temperature effects and the increase in gas motion.

Figs. (6.39) and (6.40) show a comparison of the predicted mean instantaneous heat fluxes for cylinder head surface by the two-zone approach, with the measured and the previous prediction based on bulk mean gas temperature. Inspection of the heat flux curves for 1050 rpm engine speed, Fig. (6.39), suggests that in the measurement region, the air-zone temperature is the effective driving temperature for heat transfer up to 370° CA. The effective temperature between 370° CA and 390° CA (during which the hot zone expands to the annular region) varies continuously from the air temperature towards the hot zone temperature, but in a manner which is unpredictable. Note that predicted heat fluxes during this period using either hot-zone temperature or air-zone temperature, are too high or too low respectively, compared to the measured flux. At 400° CA and beyond, the effective driving temperature seems to be the hot-zone temperature. At engine speeds of 1500 rpm, the same trend is observed, except that the unpredictable driving temperature interval stretched beyond 380° CA to 400° CA. At 410° crank and beyond, the hot-zone temperature was the driving temperature for heat transfer.

According to the two-zone model considered, the rate of spread of the hot mixture-zone into the annular region depends upon the running conditions (see Table 6.5). Of course, in the actual case, the hot products will probably enter the annular region earlier than the model suggests, because of fuel mixing with excess air in the bowl but the temperatures would not be as high as calculated by the model.

Therefore in the crank angle interval, when the measurement region falls between the two temperature zones, (370 - 390° CA for 1050 rpm and 380 - 400° CA at 1500 rpm) the driving temperature for heat transfer is difficult to predict. It was found that the driving temperature in the annular region, changed gradually from air-zone temperature to hot mixture zone temperature with intermediate values represented by the bulk mean temperature and then by arithmetic mean of hot zone and air zone temperature as follows:

Engine Speed	Driving temperature for heat transfer			
	Air Zone	Bulk Mean	Arithmetic Mean	Hot Zone
1050 rpm	Up to 370° CA	At 380° CA	At 390° CA	390-EVO
1500 rpm	Up to 380° CA	At 390° CA	At 400° CA	400-EVO

Note the gradual change of driving temperature from air-zone to hot product zone temperature, as the arithmetic mean temperature is greater than the bulk mean temperature.

Similar predictions for piston annular region are shown in Figs. (6.41) and (6.42). For an engine speed of 1050 rpm, the air temperature is used up to 370° crank, beyond which the bulk mean temperature, plus the correction for combustion induced swirl, give good agreement with the measured flux. At 600 rpm the calculated heat flux based on air temperatures were low, again because of ignoring the relatively significant squish velocities. During expansion, a correction for increased swirl with use of bulk mean gas temperature produced acceptable agreement with the measured values. It is interesting to note the driving temperature (bulk-mean) on the piston surface is lower than the temperature applicable for cylinder head surface (hot zone), which suggests the hot zone

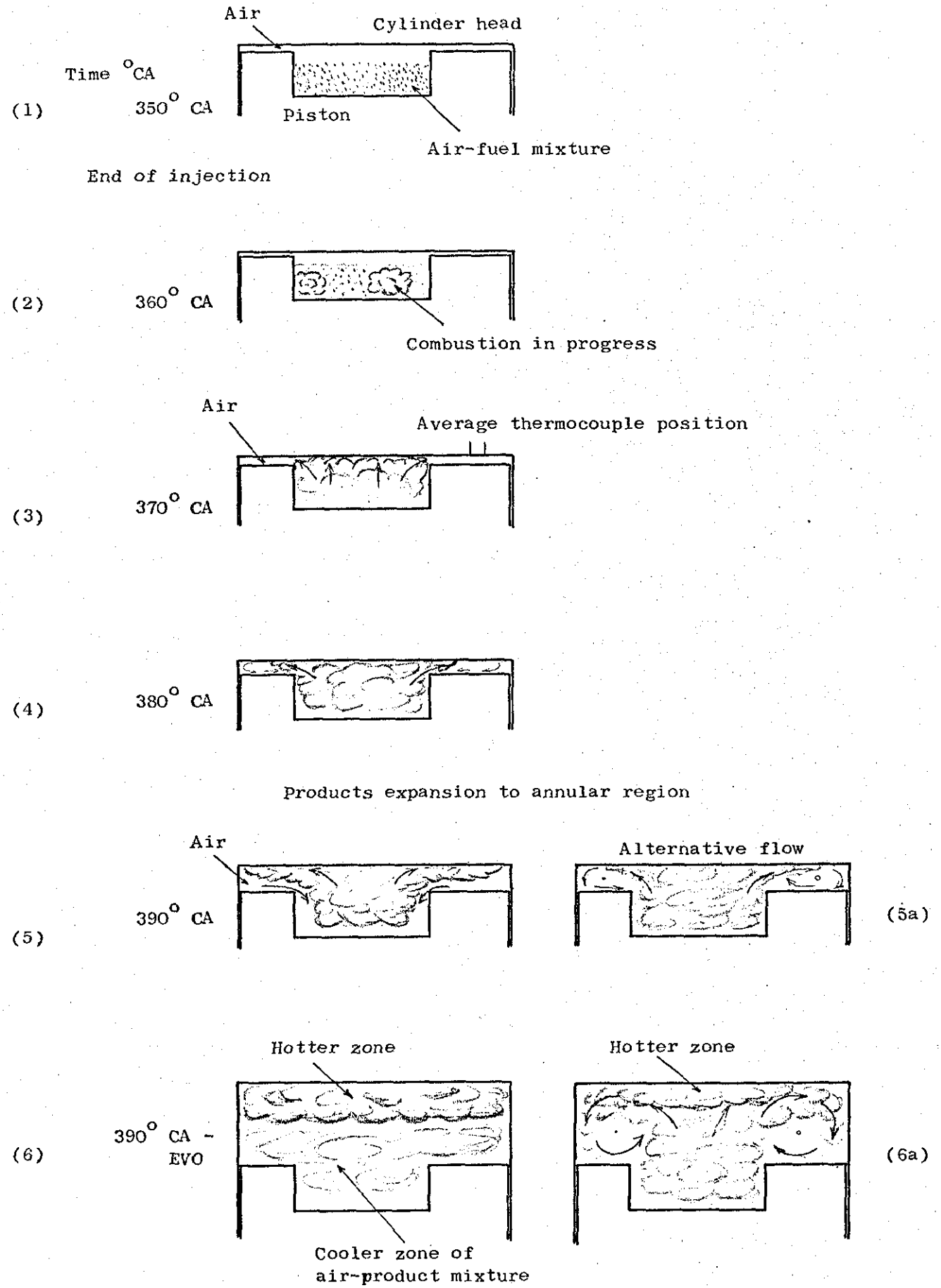

Sketch (6.B) Two-zone temperature field and flow profile expected in the engine cylinder

being cooled by mixing with air and passing over cool walls before flowing over the piston surface as shown in sketch 6.B.

The predicted and measured mean instantaneous heat fluxes in the piston bowl are shown in Figs. (6.43) and (6.44). The new prediction for 1050 rpm, on the basis of the hot-zone occupying the bowl is seen to be higher than the measured value at the low load condition, but low at heavy load condition. The discrepancy in the low load condition results could be explained by the fact that the actual gas temperature in the bowl will be less than calculated from the two-zone model because of dilution by excess air. On the other hand, the heavy load behaviour may be explained by presence of gas regions reaching adiabatic flame temperature in the actual engine, i.e. higher than the hot-zone temperature calculated from the model (adiabatic flame temperature $\simeq 2500^{\circ}K$ compared to maximum calculated two-zone temperature of $2300^{\circ}K$ at 1050 rpm).

The latter argument would also explain the discrepancy observed at 600 rpm between the measured instantaneous heat flux and that predicted on the basis of the two-zone model. Another likely cause of low heat fluxes predicted at low engine speed, is the ignoring of gas motion components other than that due to swirl.

6.9.4 Prediction of convection heat flux on bulk-averaged basis

A final attempt was made to examine the area-averaged flux variation, taken over all measuring surfaces (accounting for the relative area each region represents) in relation to the bulk mean gas temperature variation in the charge. The predicted instantaneous surface mean heat flux variation obtained from equation (2.5), gives

reasonable agreement with the measured area-averaged flux, particularly near peak values as shown in Fig. (6.45). Prediction of heat flux was improved in the expansion stroke by accounting for combustion-induced swirl increase, but still the large mean components of heat transfer measured on the cylinder head and piston are partly responsible for discrepancy late in the expansion stroke. Note that the above prediction considers the cylinder head and piston surfaces only. Inclusion of the cylinder liner, usually with lower steady and transient components of heat transfer (average heat flux recorded at one inch below cylinder top was $\frac{1}{4}$ heat flux measured on the cylinder head under fired conditions), will reduce the surface mean heat flux. Therefore, calculation of surface mean heat flux on the basis of bulk mean gas temperature will be possible if cylinder liner surface is included.

6.10 Verification of Power Law for Convection Heat Transfer

It was mentioned earlier that no attempt would be made to obtain yet another correlation which will be applicable to a particular engine and a limited number of test conditions. Nonetheless it was thought worthwhile to verify the use of the flat plate equation and the power law usually assumed in heat transfer problems, which is of the form:

$$Nu = a \, R_e^{\,b} \tag{6.12}$$

Reynolds number was formed using $2\pi r$ as local characteristic length, measured local gas velocity with the gas properties evaluated at the bulk mean gas temperature calculated from measured pressure. Heat transfer coefficient h, calculated from the measured local mean flux, the bulk mean gas temperature and local surface temperature is used to form Nusselt number. Fig. (6.46) shows some of the experimental

data (at 10^{o} intervals) during the period 40^{o} CA before TDC to 40^{o} CA after TDC. A comparison with the flat plate equation used, shows a considerable scatter. The evaluation of all properties in Re and Nu at gas bulk mean temperature may be partly responsible for the scatter. An account of the effect of gas properties evaluated at the surface temperature (or intermediate temperature) was possible in a lumped form, according to Kays (97) by the following simple correlation:

$$\text{Nu surface} = \frac{\text{Nu (bulk mean)}}{\left(\frac{T_g}{T_w}\right)^{n}} \qquad (6.13)$$

where $n \simeq .15$ for gases when $T_g > T_w$.

Therefore the corrected Nu with the corrected Re (accounting for combustion induced swirl where applicable) improved the relationship as shown in Fig. (6.47).

Note that the radiation heat flux was not deducted from the total measured heat flux in calculating heat transfer coefficient (h), because the radiant component was negligible. Also the above mentioned correction was not considered in the prediction of heat fluxes presented in this work. However the experimental data in general shows that the convection heat transfer in the diesel engine could be represented by the modified flat plate equation presented in section (2.1.3) which is:

$$\dot{q} = 0.037 \frac{k}{2\pi r} \left(\frac{(2\pi r\omega)\, 2\pi r}{\mu} \right)^{0.8} (P_r)^{0.33} \cdot [\, T_g - T_w \,] \qquad (6.14)$$

6.11 Prediction of Radiant Heat Transfer in Diesel Engines

As stated earlier, the complexity of the combustion process in the high speed diesel engine, and the many unknown phenomena involved, make an accurate theoretical calculation of radiant heat transfer in an engine impossible with our present knowledge. Also the use of simple radiation terms, similar to that suggested by Annand (6), to calculate instantaneous radiation flux on the basis of bulk mean gas temperature is unlikely to represent the temporal trend of radiant flux in the engine. This is because of the large difference between the radiating luminous flame temperature and the bulk-mean temperature in addition to the differing transient variation of these temperatures during the combustion-expansion phase of the engine cycle. Since no basic method is available for obtaining values of apparent radiant temperatures and optical thickness as a function of time during the cycle, the measured radiant flux and measured flame temperature in several diesel engines is first compared. The absorption coefficient of diesel flame and its variation is evaluated, then its use in prediction of radiant flux in other engines is investigated.

6.11.1 Comparison of measured instantaneous radiant fluxes in diesel engines

Measured radiant heat fluxes in three direct injection diesel engines (Oguri, Flynn and present study) are shown in Fig. (6.48). In order to facilitate comparison, the engines configuration and test conditions in each case were as follows:

Engine type and test condition	Flynn et al (34) D.I. 4 stroke	Oguri and Inaba (33) D.I. 4 stroke	Present Study D.I. 4 stroke
Bore x stroke (mm)	114 x 114	150 x 220	102 x 104.8
CR	16.7	22 (estimated)	15.3
Test speed (rpm)	2000	900	1750
Swirl (rpm)	4000 (mean)	No swirl	17000 (mean), 34000 (peak)
Equivalence Ratio	0.44	Not available	0.487
IMEP (bar)	6.5	8.7	5.7
Injection time ^{o}CA BTDC	20	15-20 (est)	18
Fuelling rate (gm/cycle)	0.037	Not available	0.026
Nozzle configuration	5 x 0.25 (mm) - 150^{o} cone	Not available	4 x 0.27 mm - 150^{o} cone
Detector position & view	Cylinder top, across chamber	Cylinder head, bowl edge	Cylinder head, bowl centre

Flynn measured the radiant flux by a lead-selenide photo-conductor; Oguri used a surface thermocouple, whilst a pyro-electric detector was used in the present investigation. Assuming these detectors were adequate in response to detection of instantaneous radiation, the large difference observed in the radiant fluxes in the three engines reflects the influence of some important factors (operating condition or geometry) listed above. The late peak radiant flux measured by Oguri, must have resulted by prolonged combustion in the low swirl engine and perhaps by a slow rate of injection (not reported but expected at low engine speed) which would increase soot formation with delayed peak value (Khan et al (64)).

The high radiant flux measured by Flynn, compared to the flux measured in the present test engine was thought to result from the different path lengths ($L = \frac{3.6V}{A}$) of the two engines. Therefore assuming other factors (radiant temperature, absorption coefficient) being the same, a new value of (TKL) is calculated for the test engine shape, by allowing for the mean beam length. Hence a new apparent emissivity followed from the relationship between apparent emissivity and TKL given by Flynn (34). The estimated radiant flux for the test engine was still greater than the measured values as shown in Fig. (6.48). Thus, the discrepancy between the radiant flux observed by Flynn and in present tests is due to differences in basic factors, such as absorption coeff-icients, injection condition and flame shape. These may in turn be attributed to one or more of the following reasons:

i) Compression ratio - Macfarlane and Holderness (45), showed that for a given equivalence ratio, carbon formation increases steeply with pressure (typically something approaching P^3

for test conditions up to 21 atmospheres) and emphasised the same applicable to higher pressures. Therefore, higher absorption coefficients are expected under the higher compression ratio as for Flynn's engine.

ii) Air-fuel mixing - Khan et al (64) showed that instantaneous soot formation reduced to about one third of its initial level as swirl ratio increased from 1.5 to 3.4. These authors also showed that higher exhaust soot (which reflects the soot formation process) with increased fuelling rate. Therefore higher soot formation is expected in the moderate swirl engine used by Flynn, with greater fuelling rate than in present engine tests. The combined effect of low swirl and high fuelling rate results in fuel-rich zones which enhance soot formation.

iii) Injection time and nozzle configuration - the small difference in injection time (20^{o} BTDC (Flynn) and 18^{o} BTDC (present) is unlikely to cause a significant change in soot formation. According to Khan et al (84) the nozzle used in Flynn's engine (5 hole x .25 mm diameter) will result in more exhaust soot than test engine nozzle (4 hole x .27 mm diameter) with other parameters being the same, this effect being attributed to better air entrainment of the four hole nozzle.

iv) Detector view - another factor in Flynn's engine was the direct view by detector, of the reaction zone, which envelops the core where fuel and air are transported and where heat release and soot formation takes place. In the present tests, combustion products resulting from expansion

of reaction zones (at impingement with bowl wall) was viewed by the detector located near the centre of the bowl.

6.11.2 Effective radiating temperature in diesel engines

A survey of the relevant literature shows that flame temperatures do not vary much with load. It also appears that flame temperature for different types of engines are of approximately the same magnitude. Fig. (6.49) presents the measured flame temperatures in I.D.I. or D.I. combustion chambers of several diesel engines. Flame temperatures obtained in all cases by the two-wavelength principle, developed by Hottel and Broughton (43) are in reasonable agreement with each other, except that due to Belinskiy (23) which are rather high. It is interesting to note the calculated hot zone temperature band for different conditions obtained from the two-zone model (also shown in Fig. (6.49)), is in close agreement with the measured flame temperatures, particularly when combustion is nearly complete, i.e. beyond 370^{o} CA.

It is well known that the calculated bulk-mean gas temperature is much lower than the observed flame temperature, (see Figs. (6.24 - 6.26)), therefore radiation calculations based on bulk mean gas temperature would lead to large errors due to the fourth power law dependance of radiative heat flux. The prediction of radiant heat flux from hot zone temperatures would be convenient, as it makes use of readily available engine data (measured pressure, trapped charge and fuel flow and engine geometry).

6.11.3 Flame absorption coefficients in diesel engines

In section (2.2.5) it was shown that a knowledge of absorption coefficient of radiating flames is necessary in order to calculate the radiant flux at the enclosure. The cyclic nature of diesel combustion leads to a continuous change of the absorption coefficient, therefore a comparison of the temporal variation and magnitude of absorption coefficient in different diesel engines was first required.

The available instantaneous data on radiant heat transfer in diesel engines, are those of Flynn (34) and Sitkei (23). Absorption coefficients K (m^{-1}) were calculated from Flynn's measured radiant flux and flame temperature, accounting for combustion chamber geometry by the procedure outlined in section (2.3.5). The absorption coefficients were obtained by first dividing the gas into a number of cylindrical elements and calculating net (integrated) gas-surface exchange areas as a function of absorption coefficient, using tables of exchange areas for a cylindrical body given by Hottel and Sarafim (52). Secondly, finding the absorption coefficient which satisfies the equation:

$$\dot{q}_R = \sigma T_F^4 \frac{\overline{gs}\ (KL)}{A} \qquad (6.15)$$

where $\dot{q}_R$ = measured radiant flux

$\overline{gs}\ (KL)$ = net exchange area

A = surface element area corresponding to net exchange factor which contains position of measurement.

Similarly, absorption coefficients in the present test engine were calculated assuming the flame temperature as measured by Flynn to exist in the engine.

Sitkei (23) obtained instantaneous absorption coefficients $k_p = K/P$ (m^{-1} atm^{-1}) for various load conditions in the pre-combustion chamber of a diesel engine, assuming flame temperatures as measured by Belinskiy (24). Therefore, to facilitate comparison, the absorption coefficient obtained by Sitkei for two equivalence ratios (0.45 and 0.56) were recalculated on the basis of Flynn's measured flame temperatures. A correction for the cylinder pressure in Sitkei's engine was also included. The calculated absorption coefficients in Flynn's engine, Sitkei's precombustion chamber engine and of the present test engine are shown in Fig. (6.50). The magnitude of absorption coefficients in the three engines may again be explained by the effect of gas motion on air-fuel mixing. Khan et al (64) explained the reduction in smoke levels with increasing swirl by its effect on the rate of air entrainment leading to lower equivalence ratios in the richer zones of the jets and by increased rate of intimate mixing (fuel vapour transport) in the fuel jets. Flynn described the engine as one with moderate swirl, which is expected to affect more soot formation. On the other hand, in a precombustion chamber where swirl is very high, improved mixing will result in lower absorption coefficient. The high overall fuel-air ratio, however, expected in the precombustion chamber will have an opposite effect by increasing absorption coefficient (45). Note that the later factor may be responsible for the difference between Sitkei's data and the present test results for the same overall equivalence ratio. The combustion pressure, according to Macfarlane and Holderness (45) would affect soot formation (by a factor of P^3)

which would be significant in the three engines where compression ratios varied from 18.5:1 (Sitkei), 16.7:1 (Flynn) and to 15.3 (present engine).

To determine the effect of load (equivalence ratio) and engine speed, the absorption coefficients in the test engine were calculated for two engine speeds and several load conditions. The radiant temperature was first assumed to be the calculated hot-zone temperature from the two-zone model, and secondly to be measured flame temperature by Kamimoto (49) obtained in a similar engine. The calculated absorption coefficients are shown in Fig. (6.51). The instantaneous absorption coefficient increased with load as expected, due to increased fuelling per cycle which lead to fuel-rich zones. Peak values of absorption coefficients occurred later at higher speeds as a result of a nearly constant time required for combustion-soot formation and destruction process. The apparent effect of engine speed on the absorption coefficient is thought to be mainly related to the effect of engine speed (swirl and squish) on the shape of the flame by driving it to the centre as explained in section (6.5c) and on combustion process. The latter could be the only explanation possible, because increased speed results in high swirl and increase rate of injection, both of which reduce soot formation according to Khan et al (64). Therefore less radiation (reverse of observed) is expected with increasing speed, unless the reduced soot recorded by Khan et al (64) was on account of more soot burned to form luminous (high radiation) flames.

The calculated hot zone temperature early in the combustion process (near TDC, 360^{o}-370^{o} CA) are too low to account for the radiant fluxes measured. This is not surprising, because the calculated hot zone temperature is a mean value for the whole c.c.

mixture zone, which will be low before combustion is complete. For this reason, the calculated emissivities are not realistic during the early period.

The accuracy of the calculated absorption coefficient in the present engine, is dependant on the flame temperature assumed to exist in the engine. Therefore, if the flame temperature measured by Flynn (34) or by Kamimoto (46) (which are in close agreement) are assumed to occur in other diesel engines of the same type, then the calculated absorption coefficients together with account for area-exchange factors as described in section (2.2.5), could be used to predict radiant heat flux in other diesel engines. Instead of calculating area-exchange factors in order to estimate the radiant flux in a particular engine, a convenient method which will be more adaptable for computer calculations may be adopted if the diesel flame is assumed equivalent to a grey body. In such a case, the integrated equation in the form:

$$\epsilon = 1 - e^{-KLm} \qquad (6.15)$$

can be used, where K indicates the absorption coefficient and Lm represents the mean path length of radiant flame.

The mean beam length for any gas shape can be obtained from the relationship between the standard gas emissivity and the direct-exchange area $\overline{gs}$ as shown in section (2.2.5). However, when interest is in the flux to the entire bounding area of a gas mass of arbitrary shape, $Lm = \frac{3.6V}{A}$, where V is the gas volume and A is the enclosure surface area.

Therefore emissivities for other similar engine types operating under similar conditions can be calculated from the knowledge of absorption coefficients obtained so far, Figs. (6.50) to (6.51).

The gas volume emissivity can then be used to calculate the radiant flux at the surface by:

$$q_R = \epsilon \sigma (T_f^4 - T_w^4) \qquad (6.16)$$

where σ = Stefan-Boltzman constant.

ϵ = calculated flame emissivity.

T_f = flame temperature.

T_w = surface temperature of enclosure.

Following the above procedure, as expected, the measured instantaneous radiant fluxes were reproduced within 3% in the worst case.

6.11.4 Observed emissivities in diesel engines and in other flames

The flame emissivities in the test engine were calculated for two engine speeds and three load conditions. In Fig. (6.52a), the emissivities were evaluated on the basis of calculated hot-zone temperature (two-zone model), while in Fig. (6.52b), they were evaluated assuming Kamimoto's (49) measured flame temperature occurring in the test engine. Again the erroneous behaviour of the calculated emissivities as the case with absorption coefficients obtained on the basis of hot-zone temperatures were observed near TDC. The reason was due to the low temperatures calculated early in the combustion process. The assumption of flame temperatures

measured by Kamimoto, gives a complete picture of the flame emissivity variation. Instantaneous flame emissivities increase with load. At low load combustion ends comparatively early (30-40^{o} CA ATDC) and at high loads, it continues up to 50-60^{o} ATDC. In general, the high emissivity observed at high engine speed is thought to be related to the effect of high swirl-squish on the shape of the radiating flame in the viewing field and more efficient combustion, i.e. concentration of a hot core in the centre of the combustion chamber. Improved combustion and a more confined and homogeneous flame at high swirl, is suggested by cine film studies of diesel combustion by Morris (65).

Kunitomo et al (46) studied luminous flame radiation (spray combustion of liquid fuels) at high pressures (up to 21 atmospheres) and presented correlations for predicting flame absorption coefficients and emissivities. Using his correlation, the following results were obtained for the test engine geometry and pressure conditions.

Equivalence Ratio	Flame Emissivity	Absorption Coefficient m^{-1}
0.86	0.062	1
1.0	0.622	15.4
1.11	0.966	50
1.25	1	328

Note the steep change in emissivity and absorption coefficient as fuel:air mixture changes from just below stoichiometric to slightly rich. It is possible that such conditions occur in the vicinity of fuel spray in diesel engines, but is likely to disperse quickly by the intense gas motion.

Macfarlane and Holderness (45) measured radiation heat flux from liquid fuel (kerosene) flames as a function of equivalence ratio and pressure. Radiant heat transfer increased with pressure, with peak fluxes appearing for equivalence ratio >1.0. At 21 atmosphere, peak flux of 500 kW/m^2 was observed at 1.3 equivalence ratio, but reduced to about 200 kW/m^2 at 0.8 equivalence ratio. This suggests a significant effect of equivalence ratio which are usually low in diesel engines, although local values would be high during the early combustion period.

Maesawa et al (47) working with open flames at ambient pressure, showed that the radiant flux decreased with increasing momentum of the liquid fuel jets which is in line with less soot formation at increased fuelling rate claimed by Khan et al (64). Radiant fluxes of less than 200 kW/m^2 were observed and emissivities of 0.2 - 0.6 were measured at about 0.8 metres from the burner, varying with momentum and little with fuel flow rate. The injection rate is expected to affect flame emissivity at different speeds, but this could not be investigated because of the dominant influence on combustion of the speed dependant gas swirl.

Referring back to the emissivities observed in the test engine, the peak values varied from 0.2 to 0.55 depending on load and engine speed conditions. These were similar to the emissivities observed by Sitkei, but less than observed on Flynn's engine. Note that a direct comparison is not strictly correct, because of its dependance on shape of flame, temperature and pressure. However, the foregoing discussion suggests that the quality of mixture formation and combustion affects the concentration of carbon particles and, as a result, the radiation capacity of the

flame. The quality of combustion affects the radiation period (length) as well. The more ideal the combustion, the shorter the flame radiation period, and the smaller the quantity of heat transferred by radiation. Accordingly it may be assumed that for the present engine (high swirl) the heat transferred by flame radiation is less than in the quiescent chamber diesel engine.

Engine speed affects flame radiation as much as it modifies the quality of combustion.

6.12 Analysis of Radiant Flux at Position R2

The measured radiant flux at position R2 (discussed in section 6.6) were not analysed for two reasons:

i) Low levels of emission recorded at all engine speeds except at 1050 rpm.

ii) The recorded radiant flux at R2 was characterised by high frequency fluctuations and two peaks. The first peak was associated with expansion of hot products which soon cooled by mixing with cooler air in the annulus. The second peak associated with uncovering by the piston of combustion products in the bowl. It was the additional effect of engine geometry on radiant flux at this point that made the calculation of area-exchange factor or mean beam length (required for the analysis) more difficult.

It is interesting to note that radiant flux at R1 under heavy load condition, lasted over a period of 40^{o} CA at 1050 rpm, but remained effective for about 80^{o} CA at 1750 rpm. This behaviour supports the statement of more fuel driven to the centre by higher

squish velocities at higher speeds. On the other hand, the radiant flux at R2 remained effective over about 70 - 80° CA, irrespective of engine speed, suggesting longer time combustion in the fuel-rich (upstream of jets) zone at the piston bowl periphery.

6.13 Prediction of Radiant Flux Using Bulk Mean Gas Temperature

Fig. (6.53) shows the radiant flux predicted by the radiation term ($1.5\sigma (T_g^4 - T_w^4)$) in Annand's equation (15) and the measured radiant flux in the test engine at two speeds. The calculated values correspond to the bulk mean gas temperatures at 1050 rpm. The factor (1.5) multiplied by the black body radiation at bulk-mean temperature was obtained for a low swirl engine (Annand and Ma 15) where radiation heat transfer is expected to be higher than for high swirl engines.

In a recent publication, Annand (69) suggested a new route for prediction of radiative transfer in internal combustion engines, which was in line with the approach made by Sitkei and Ramanaiah (23), but suggested evaluation of flame absorption coefficients by utilising soot concentration. It was pointed out that more information on level of soot concentration in engine flames is needed, and that for effective radiation temperature, reliance must be put on empirical estimates. The analysis of the radiant heat transfer in the foregoing sections, indicates how the flame absorption coefficients varies during the cycle if the radiant temperature is taken as the measured flame temperature in similar diesel engines. Attempts should be made to relate this behaviour with direct measurements of soot concentration, in order to obtain a method for the prediction of flame absorption coefficients in terms of operating parameters. Such information would be valuable for the prediction of radiant heat transfer in diesel engines.

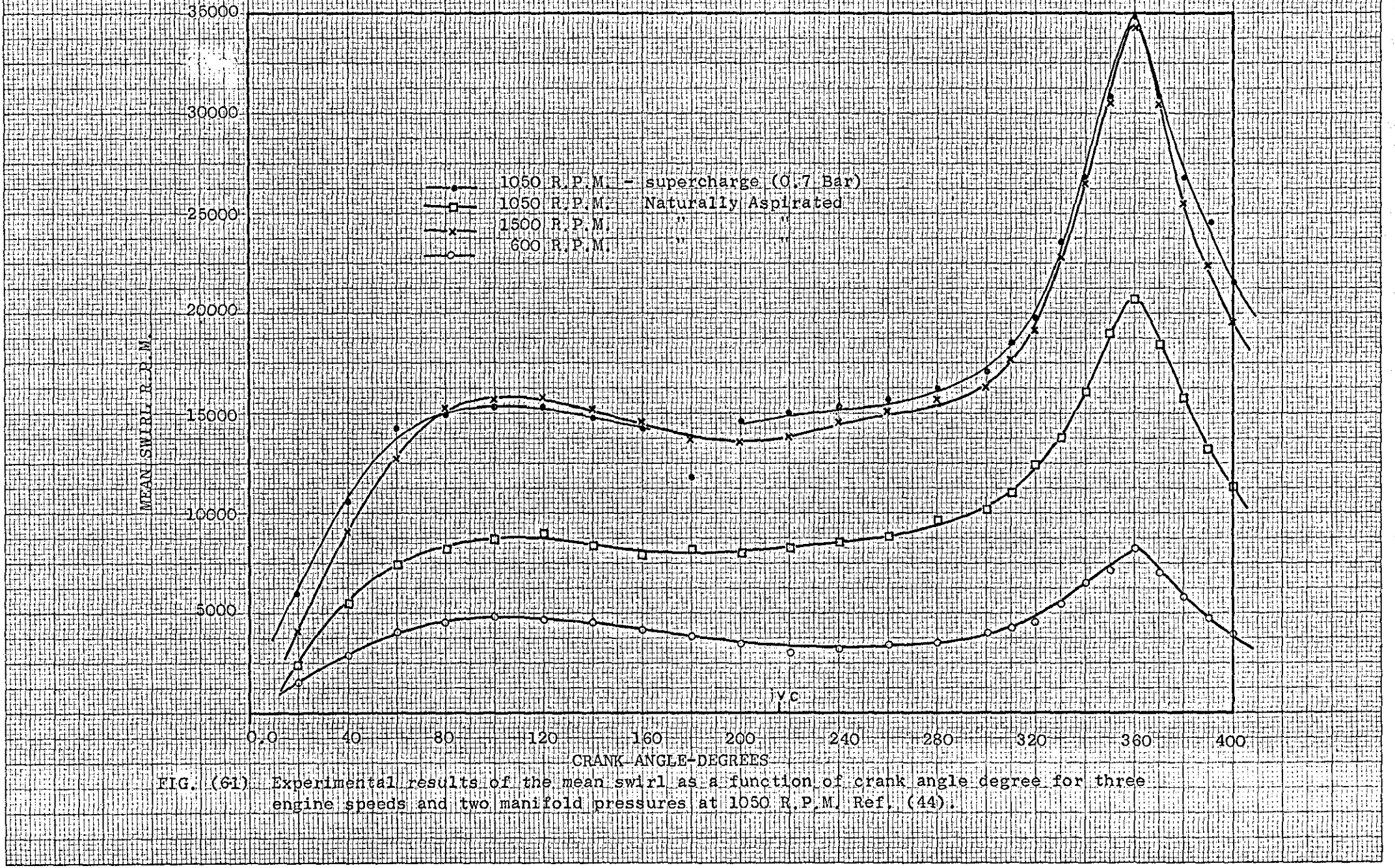

FIG. (61) Experimental results of the mean swirl as a function of crank angle degree for three engine speeds and two manifold pressures at 1050 R.P.M. Ref. (44).

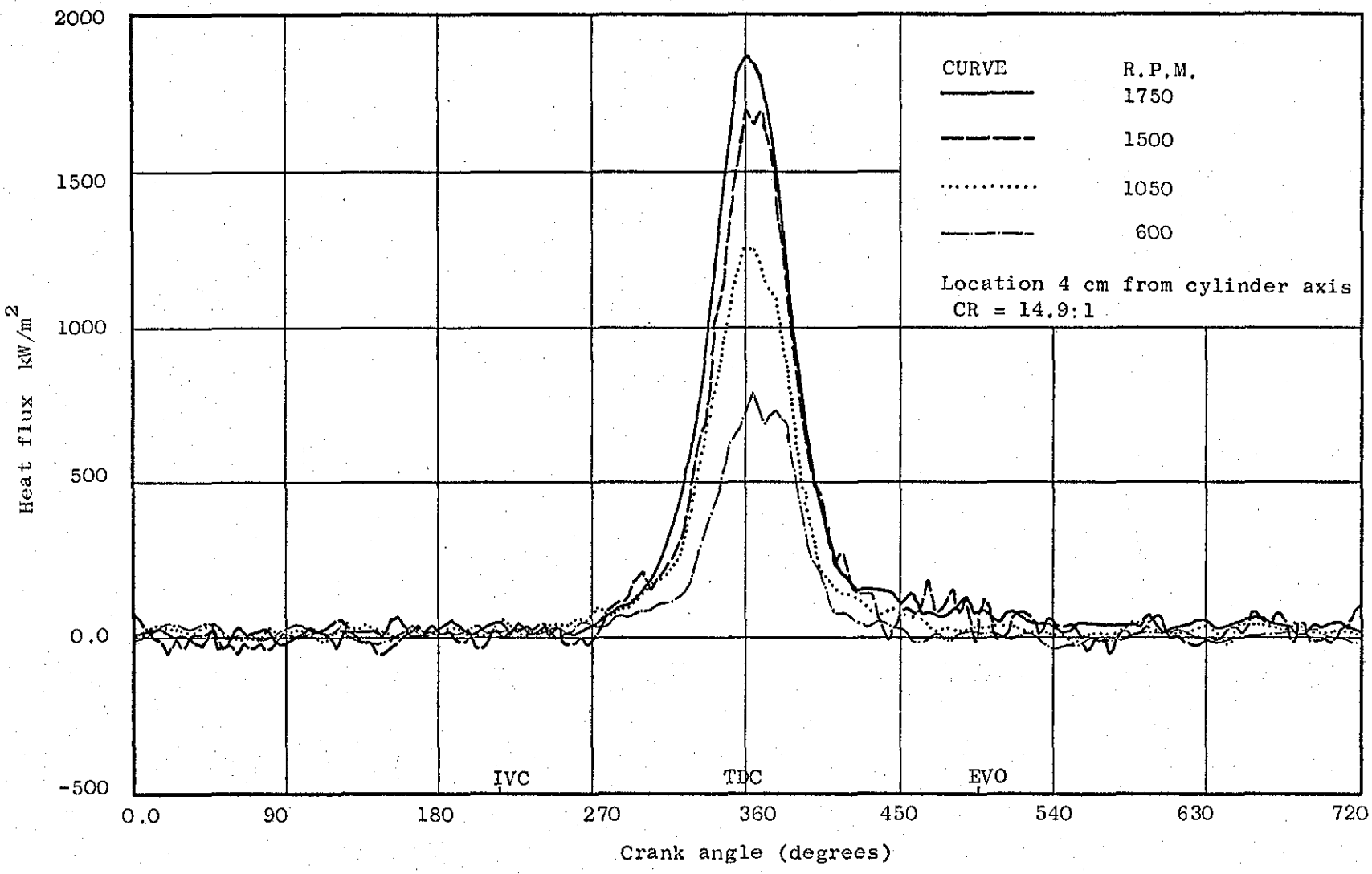

Fig. (6.2) Preliminary test showing variation of cyclic heat flux for motored engine at several engine speeds

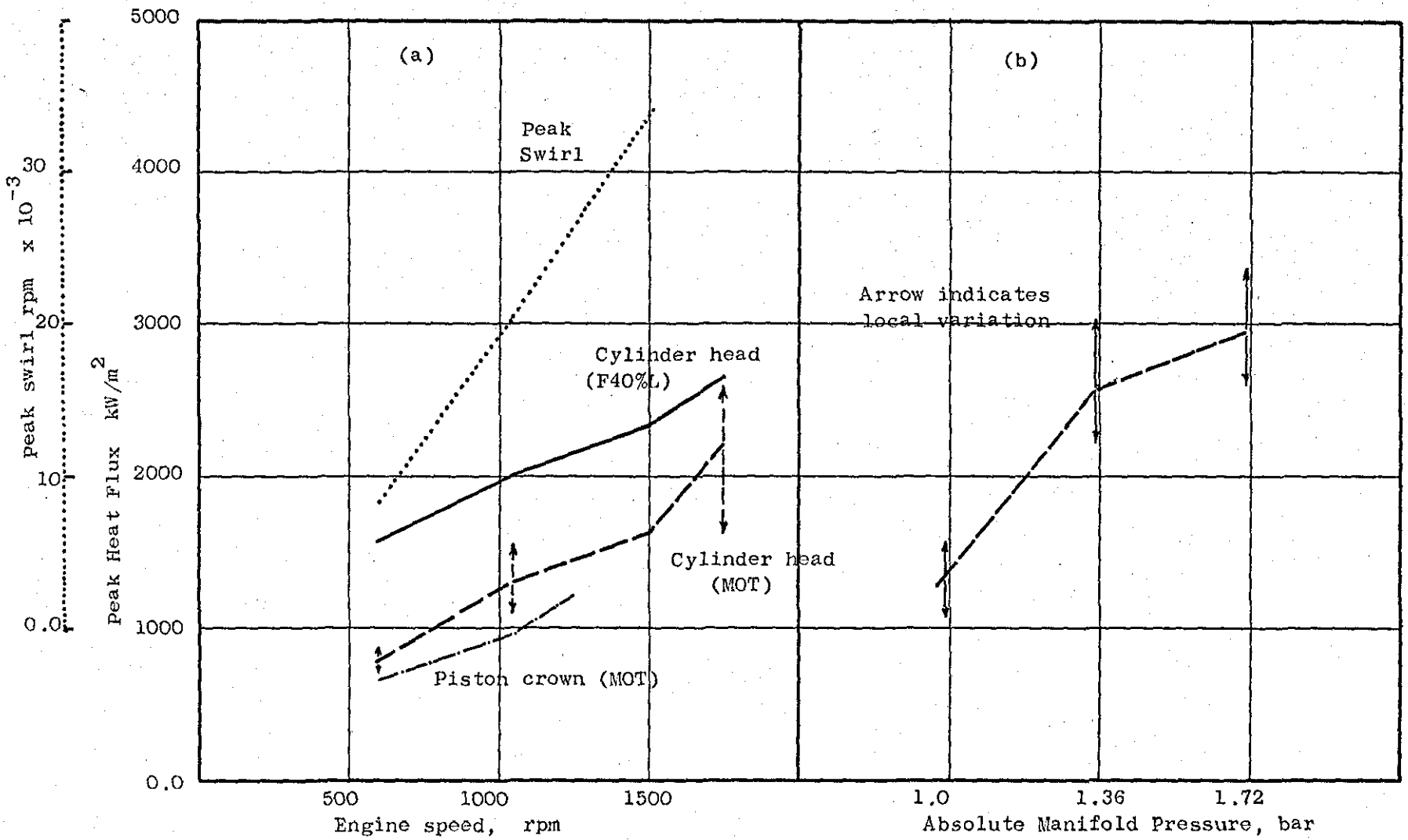

Fig. (6.3) a) Plots of peak heat flux versus engine speed for different conditions and,
b) peak heat flux versus inlet air pressure under motored conditions

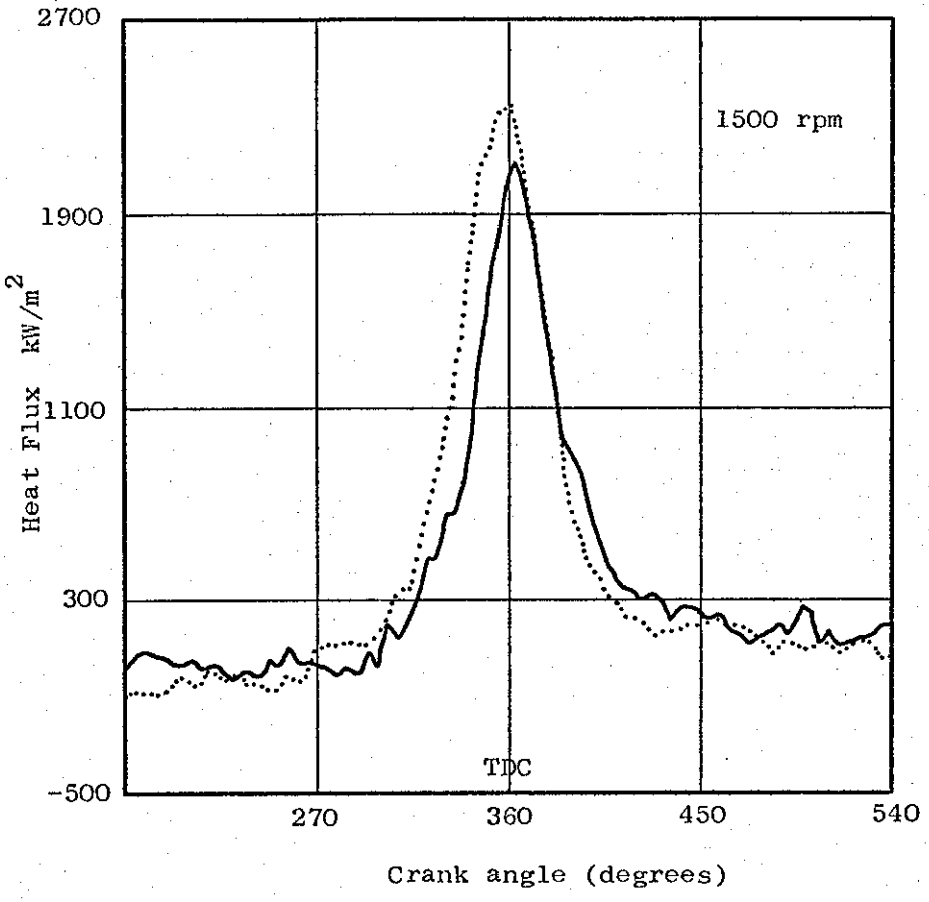

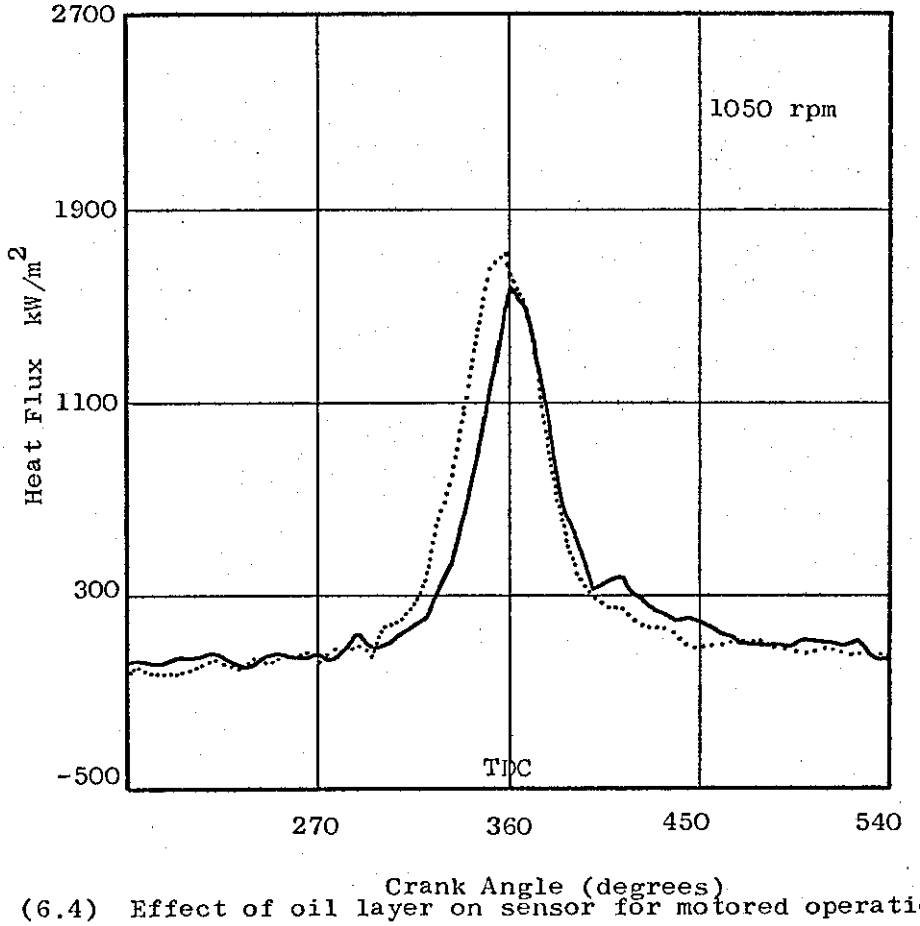

Fig. (6.4) Effect of oil layer on sensor for motored operation at two engine speeds

..... clean sensor ——— oiled sensor

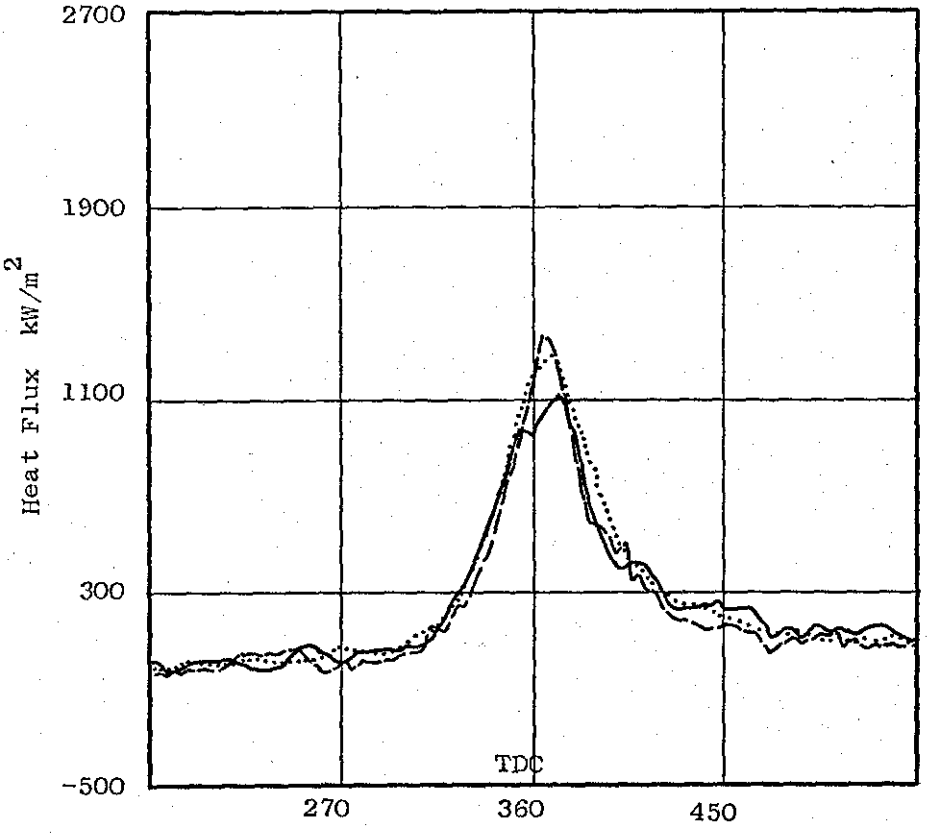

Fig. (6.5) Reproducibility of measured heat flux under motored conditions registered by three different thermocouples at same location (H1) and 1050 rpm

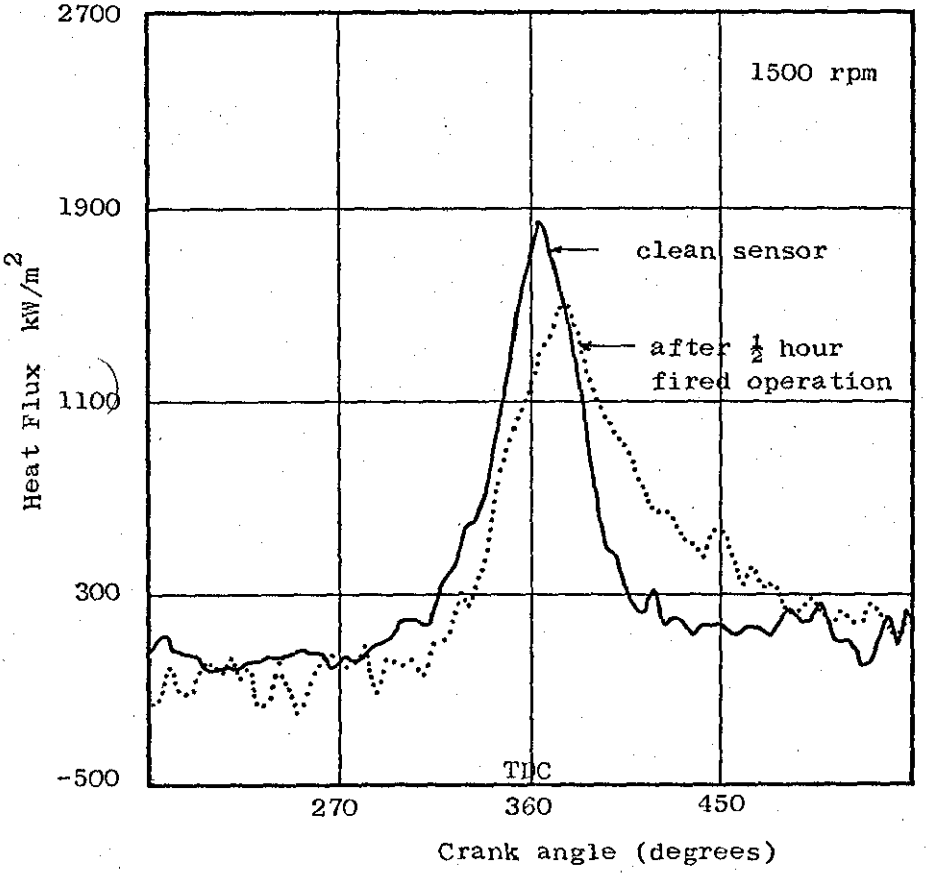

Fig. (6.6) Effect on motored heat flux of carbon deposit on sensor during ½ hour fired operation

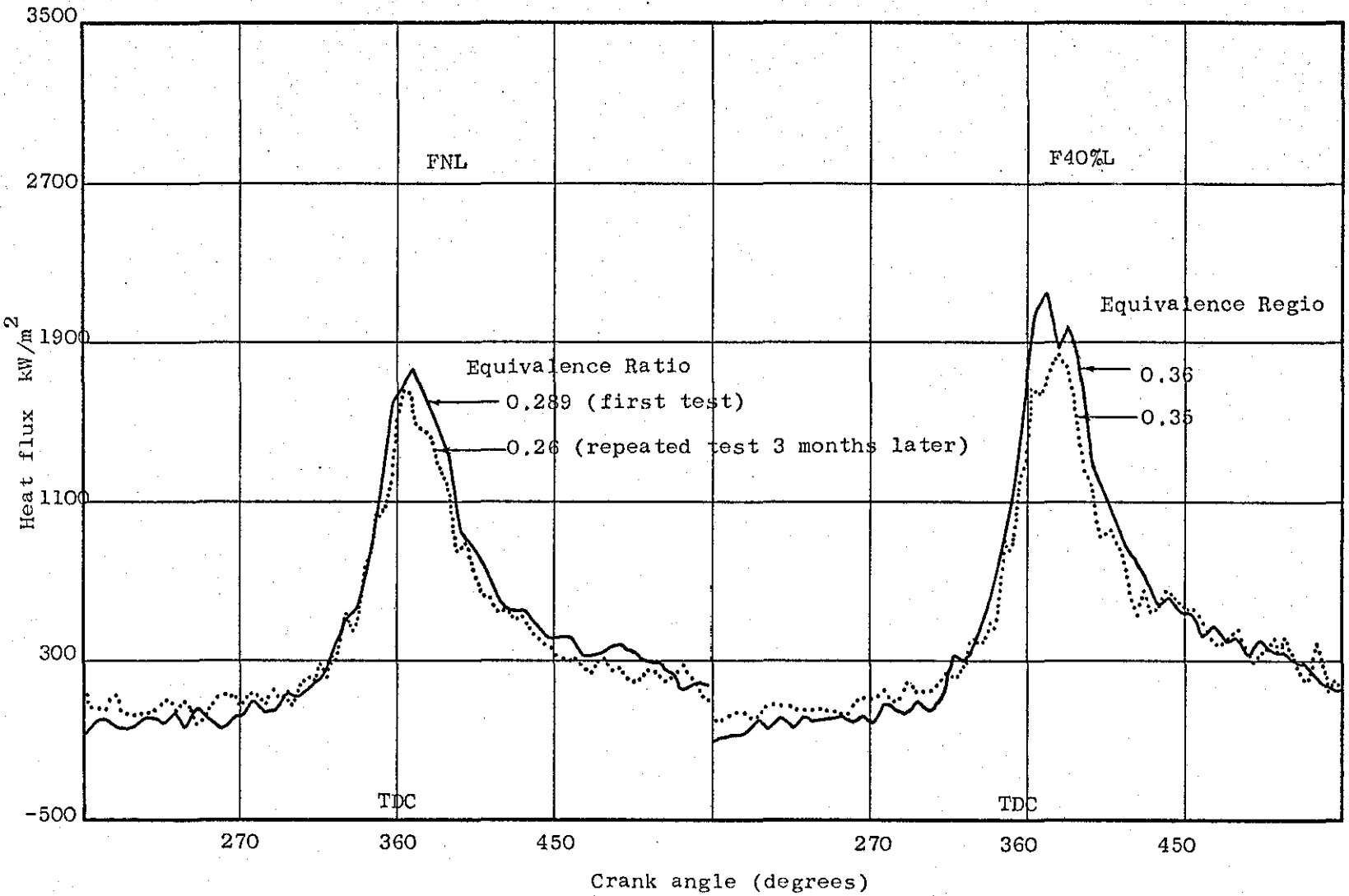

Fig. (6.7) Reproducibility of measured heat flux at location H2 for fired engine at 1050 rpm and two load conditions (note small variation in equivalence ratio)

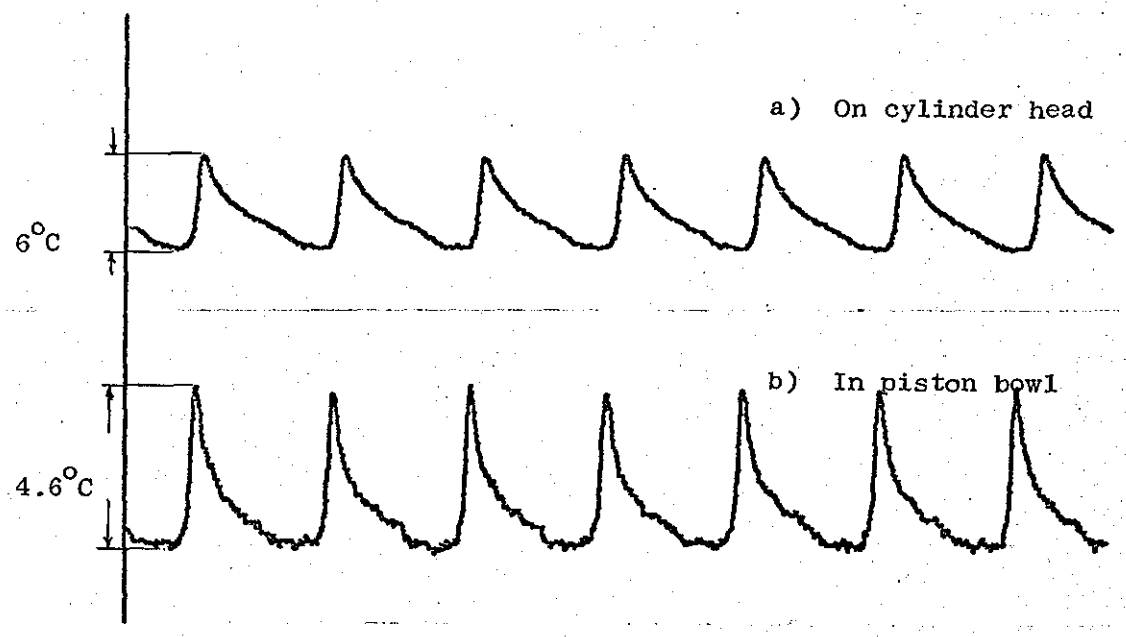

Motored operation

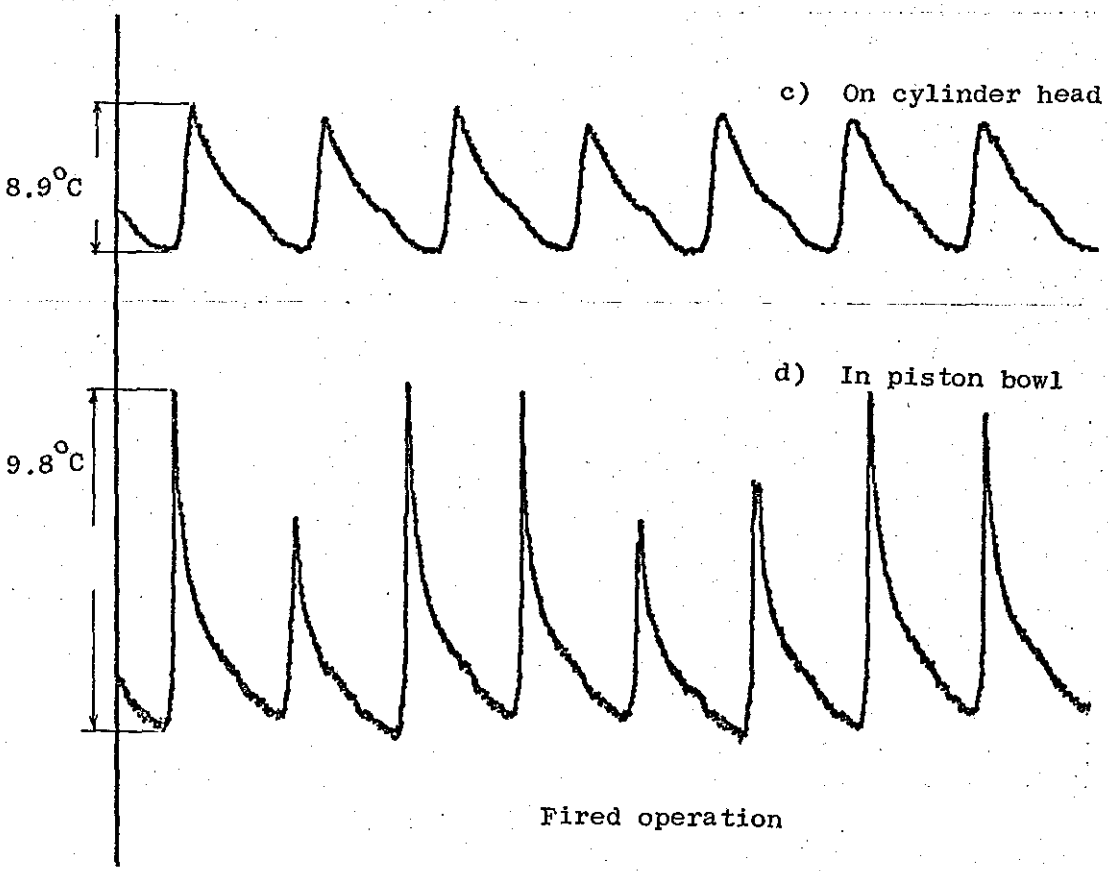

Fired operation

Fig. (6.8) Cyclic variation of surface temperature recorded on cylinder head and piston bowl under motoed and fired conditions (1050 rpm)

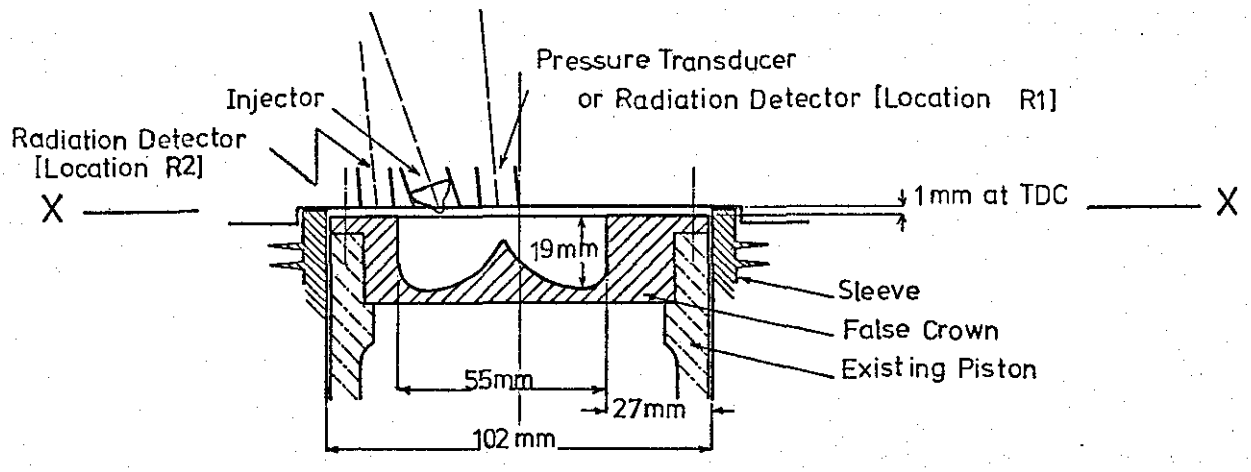

Combustion chamber configuration

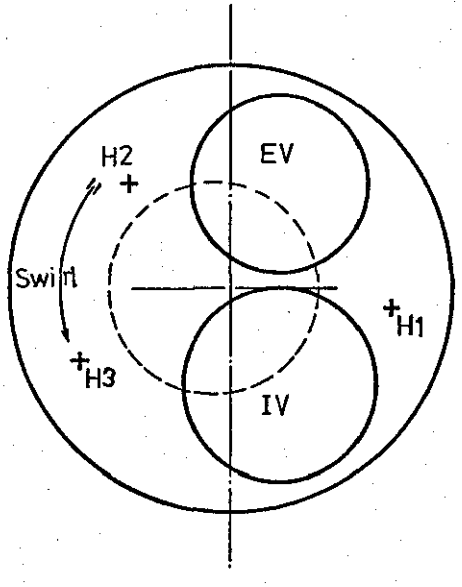

Thermocouple	Radius from cylinder axis mm
H1	42
H2	38
H3	41
P1	36
P2	36

Plan XX showing thermocouple positions on cylinder head

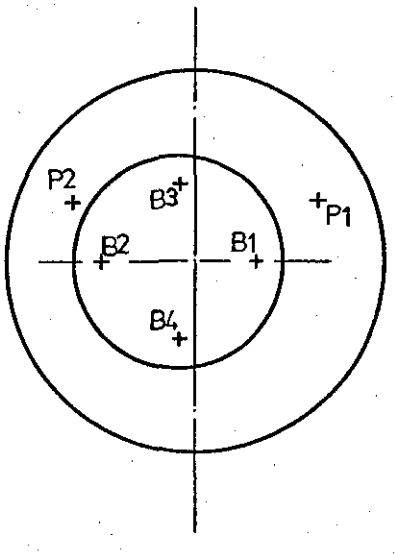

Thermocouple	Radius from bowl axis
B1	20
B2	20
B3	20
B4	20

Plan XX showing thermocouple positions on piston

Figs.(6.9) Combustion chamber configuration and heat transfer measurement locations

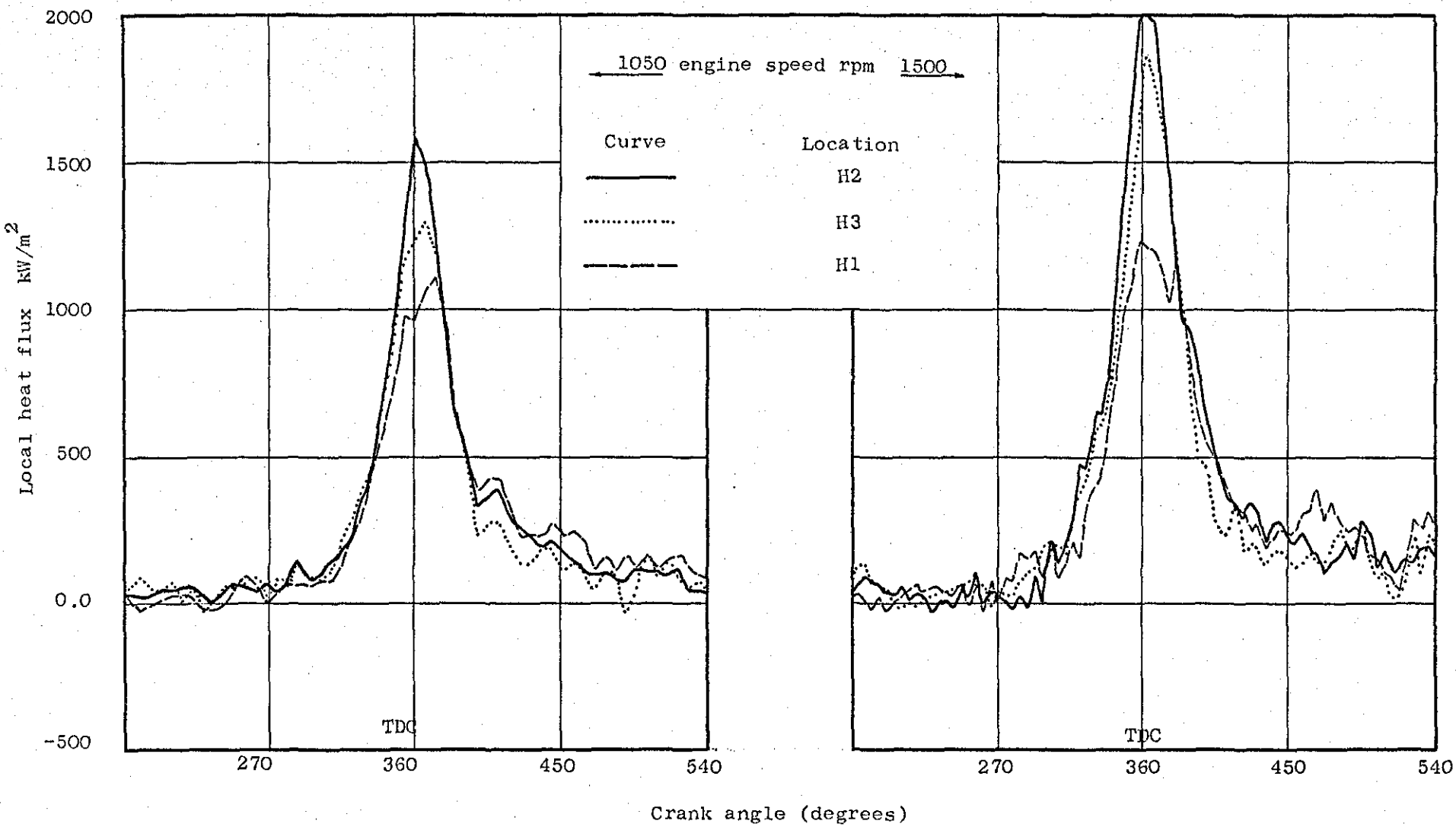

Fig. (6.10) Variation of local heat fluxes for motored operation at two engine speeds

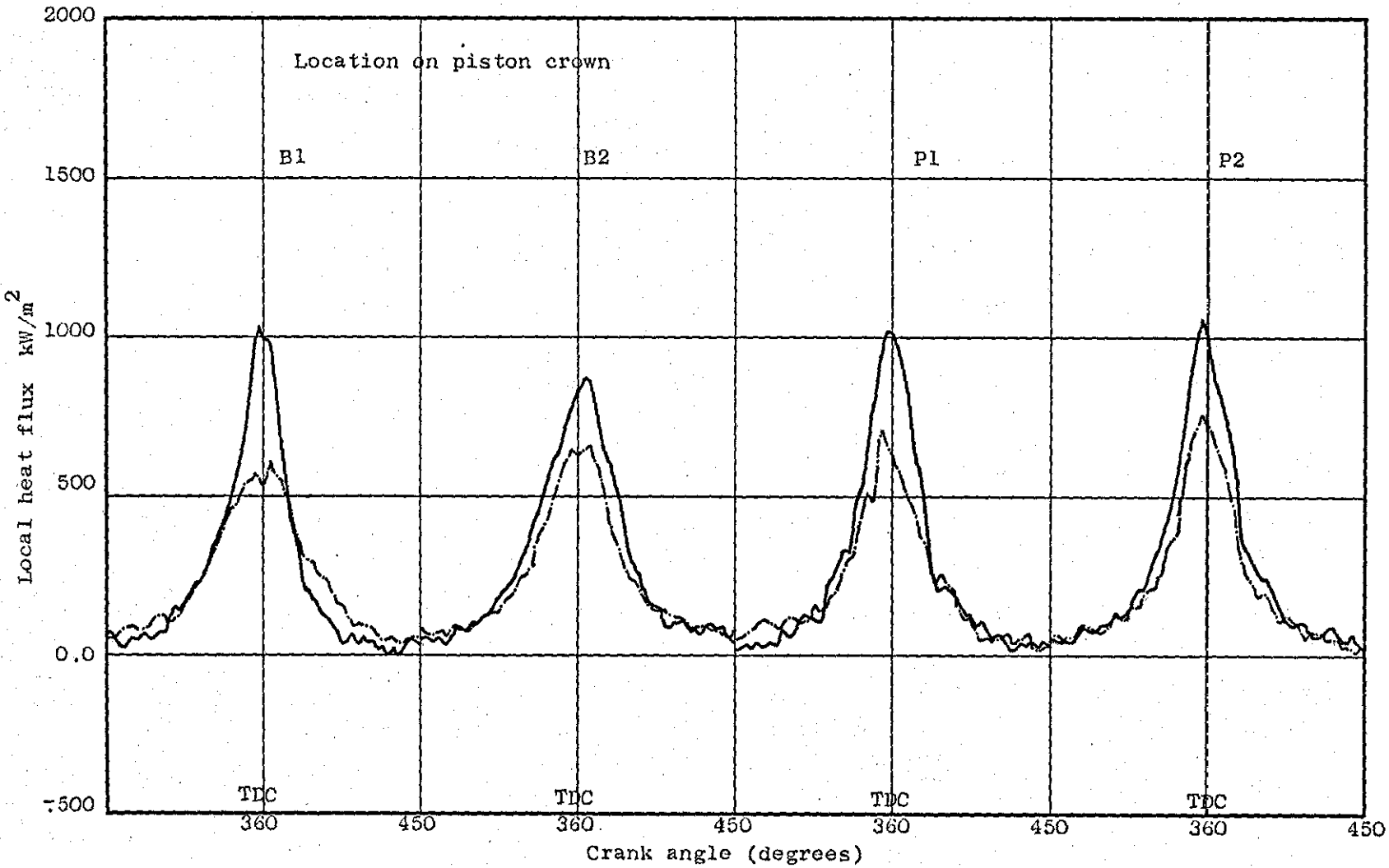

Fig. (6.11) Variation of local heat flux on piston crown for motored operation at two engine speeds ——— 1500 rpm, —·—·— 600 rpm

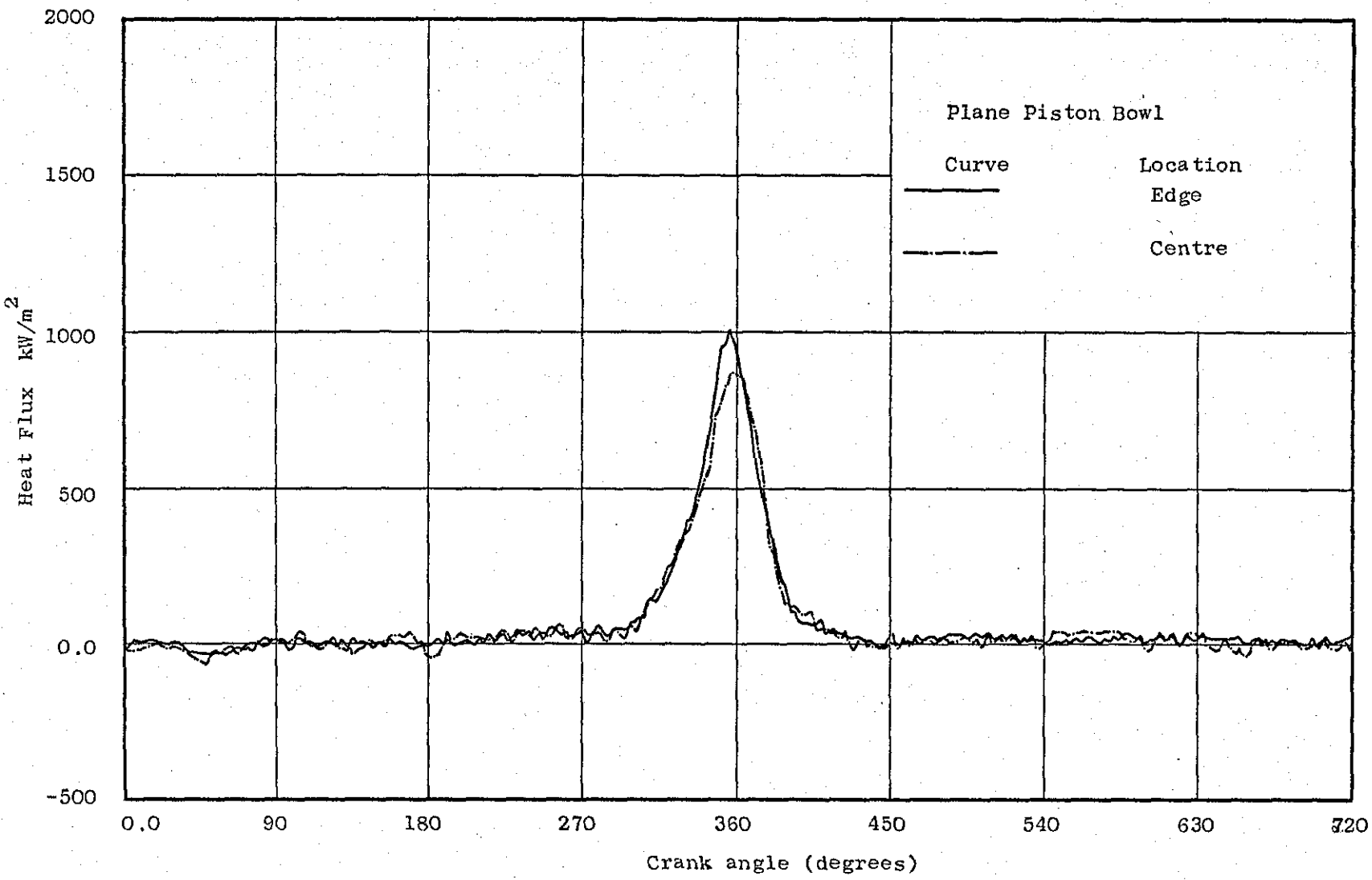

Fig. (6.12) Local heat flux in a plane concentric bowl with engine motored at 1050 rpm

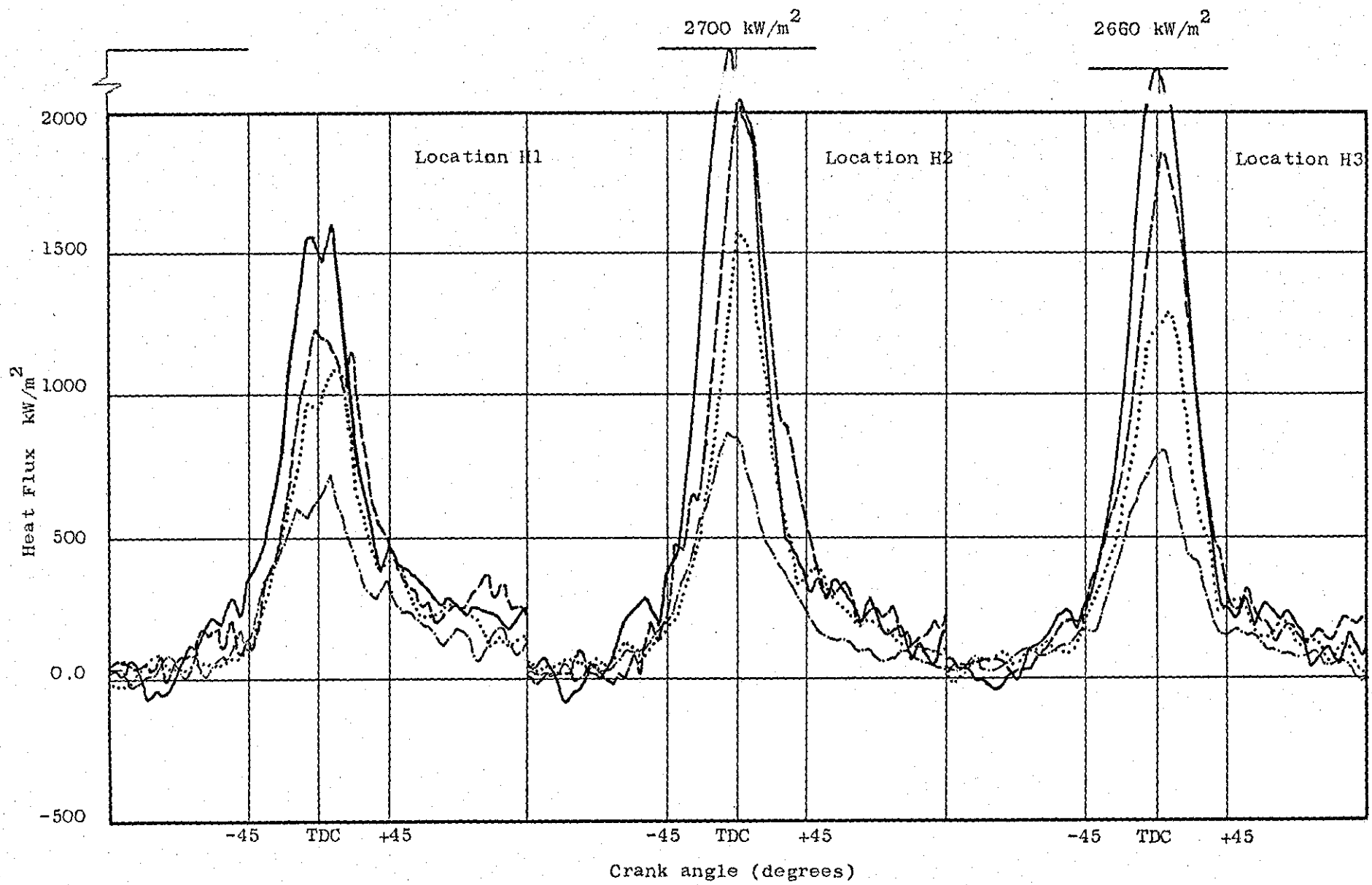

Fig. (6.13) Variation of local heat flux on cylinder head for motored operation at several engine speeds

—·—·— 600 rpm ····· 1050 rpm — — — 1500 rpm ——— 1750 rpm

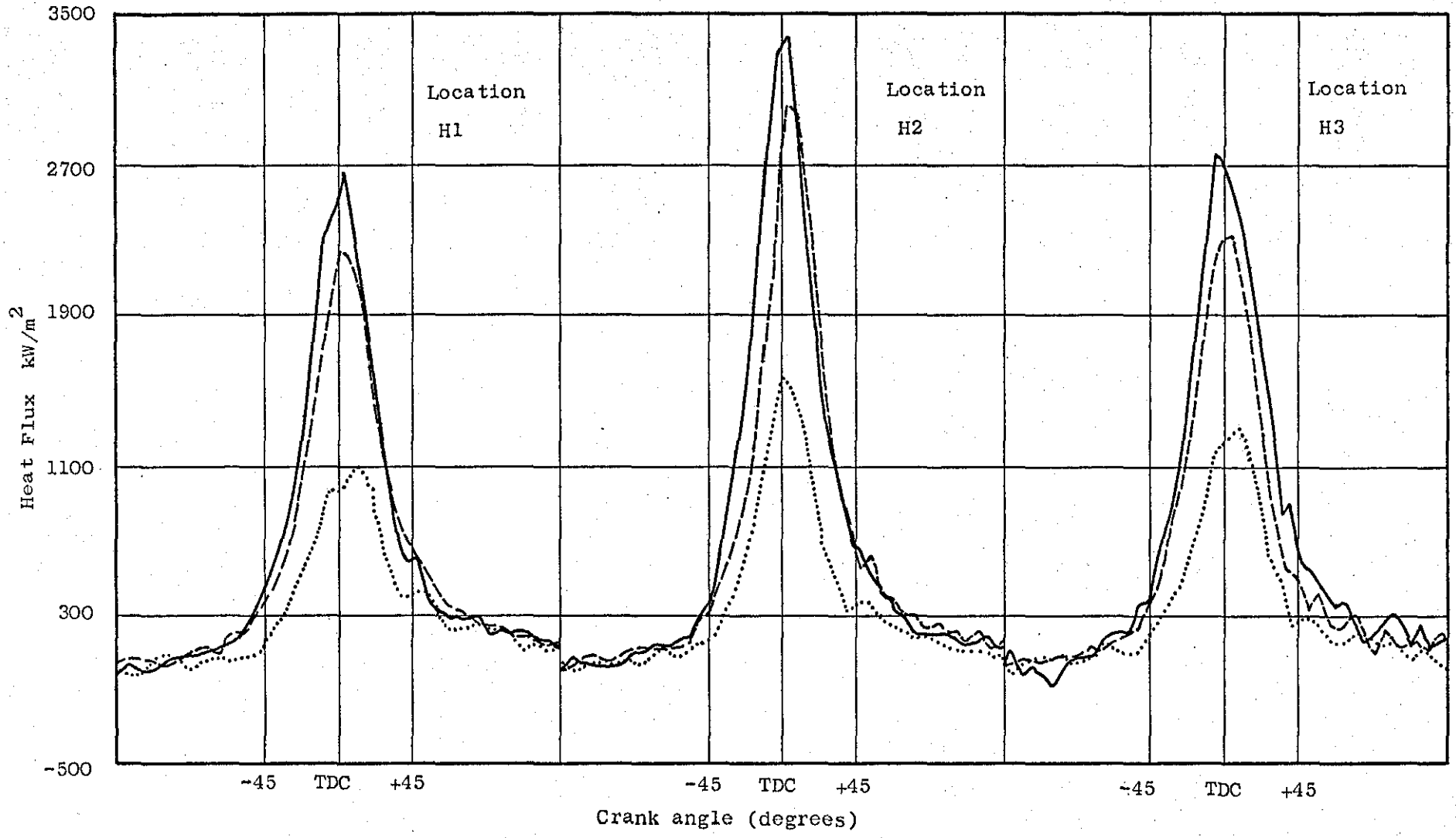

Fig. (6.14) Variation of local heat flux for 1050 rpm under motored operation at several intake pressures (cylinder head locations)

..... naturally aspirated ---- 5 psi gauge —— 10 psi gauge

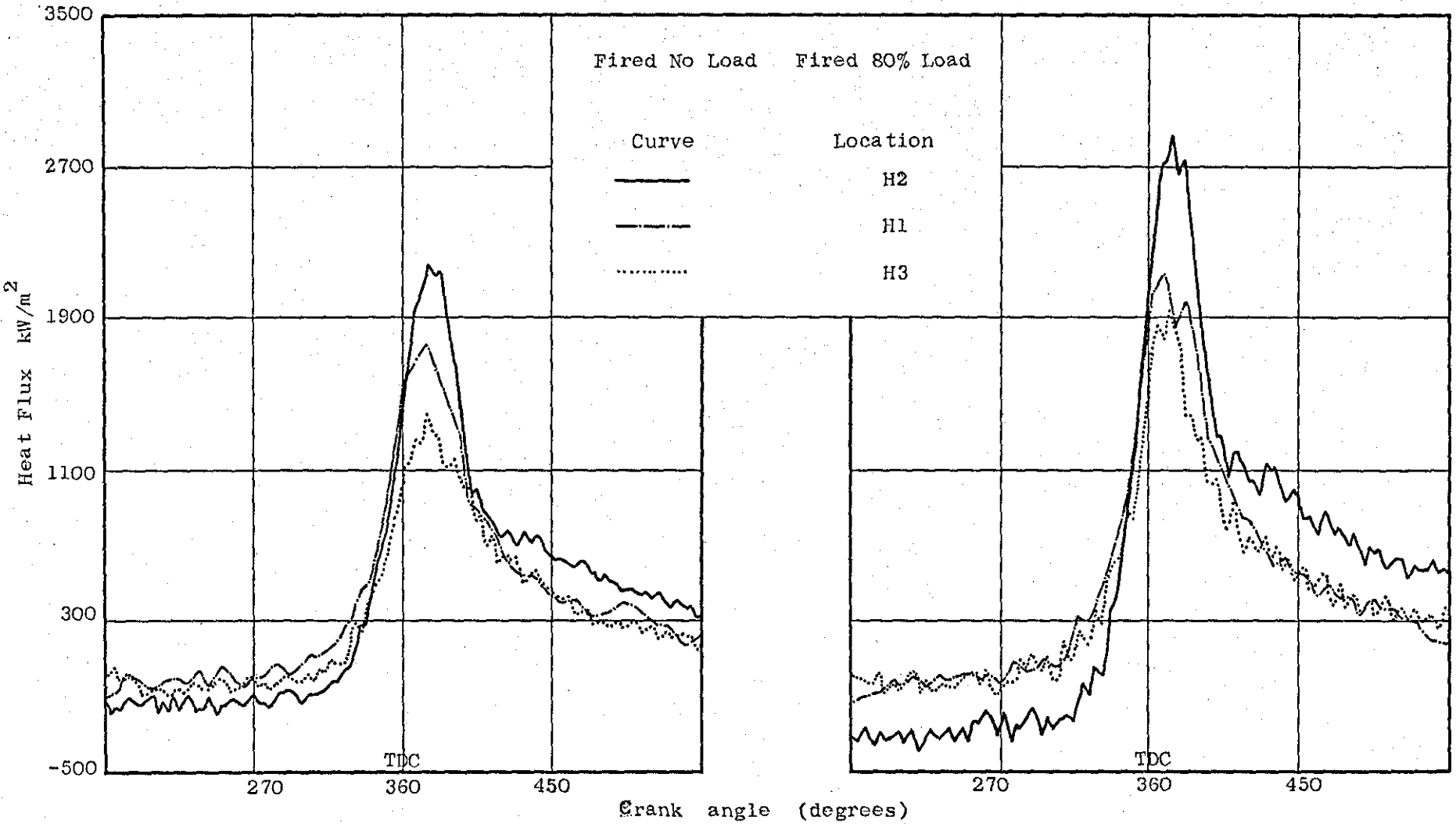

Fig. (6.15) Variation of local heat fluxes on cylinder head for fired operation at 1050 rpm

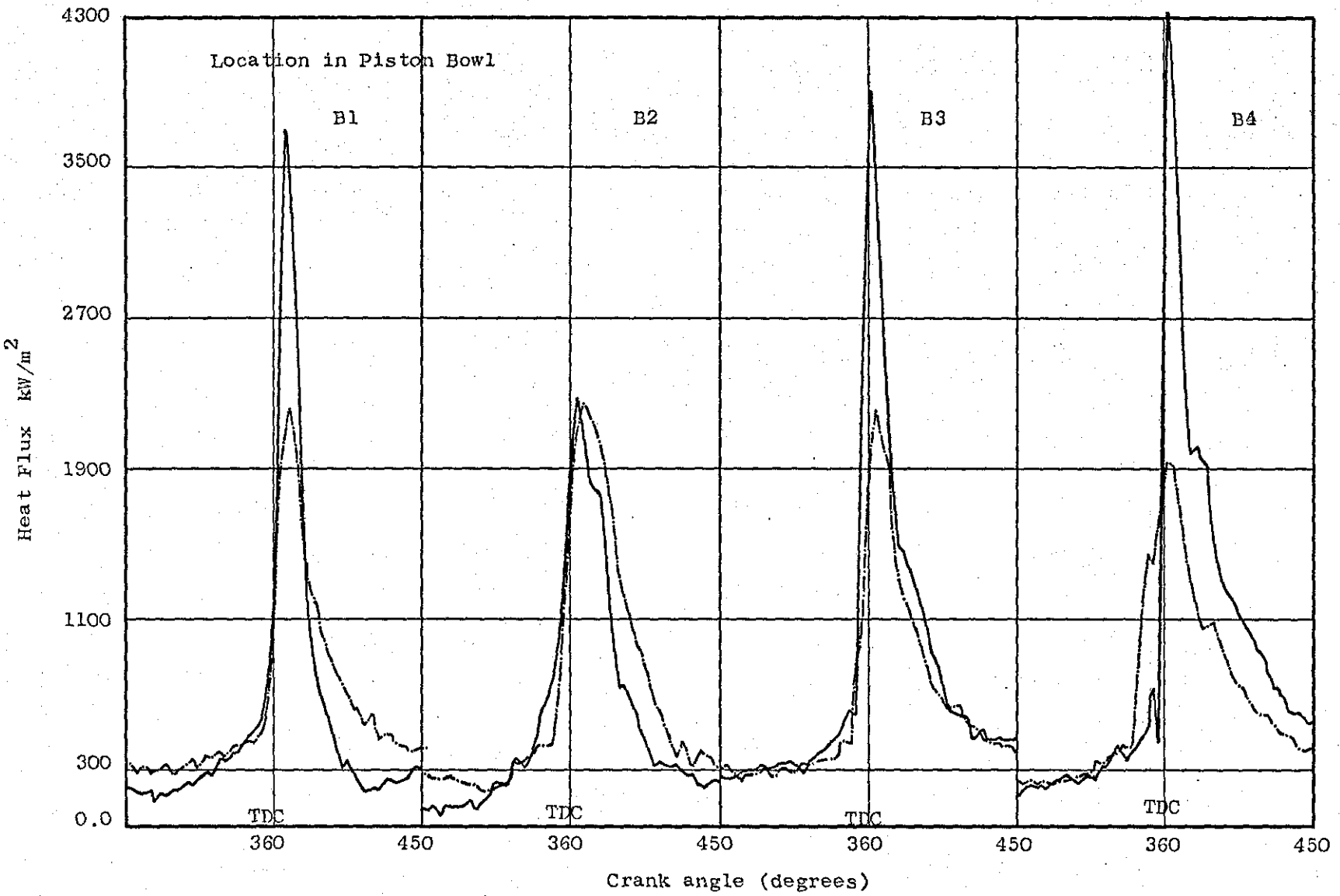

Fig. (6.16) Variation of local heat flux in piston bowl for fired 40% load condition.

——— 1050 rpm -·-·- 600 rpm

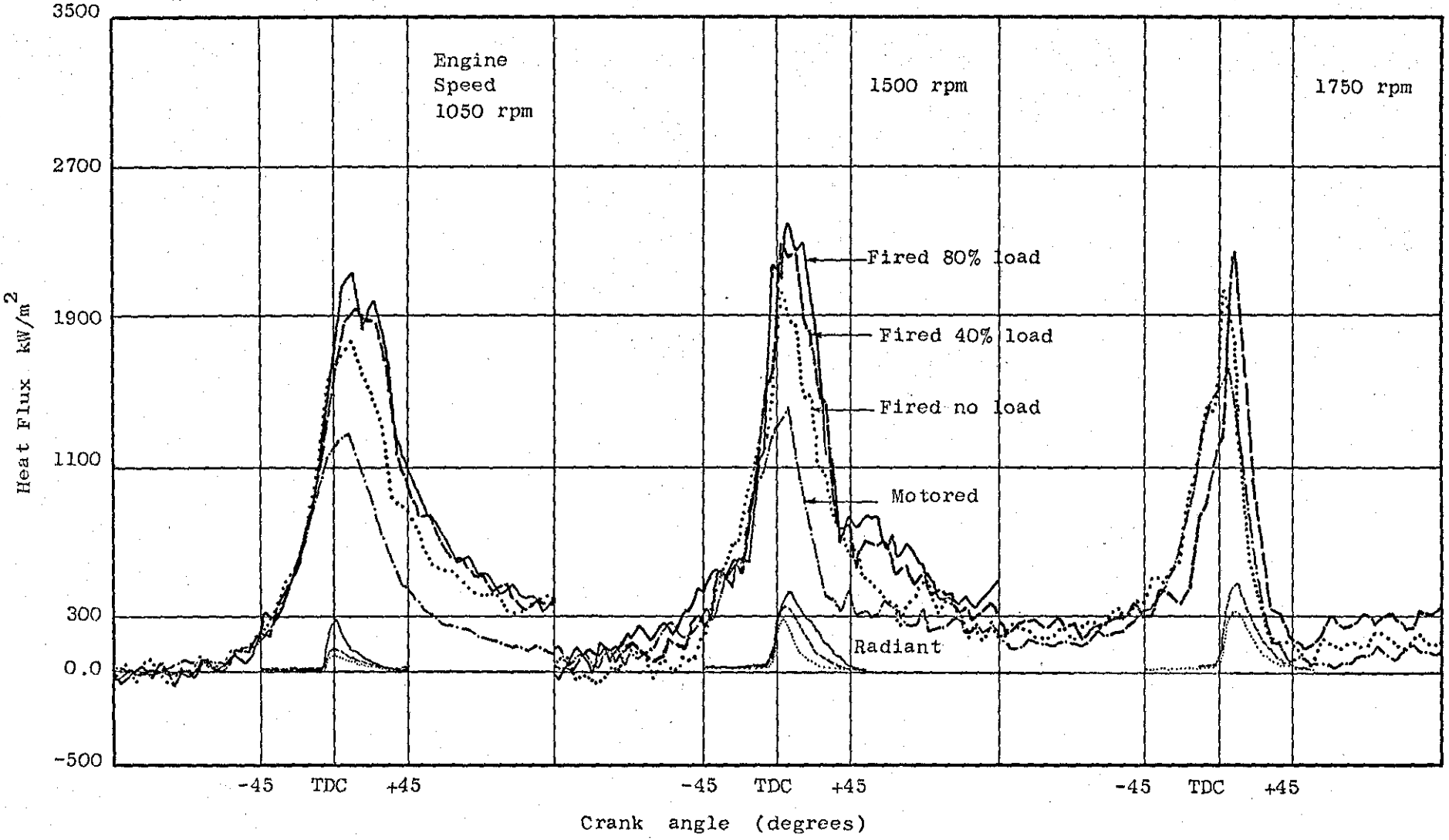

Fig. (6.17) Variation of total heat flux under fired operation with engine speed and load condition for cylinder head location H1. Motored and radiant heat fluxes (positionR1) are included for comparison

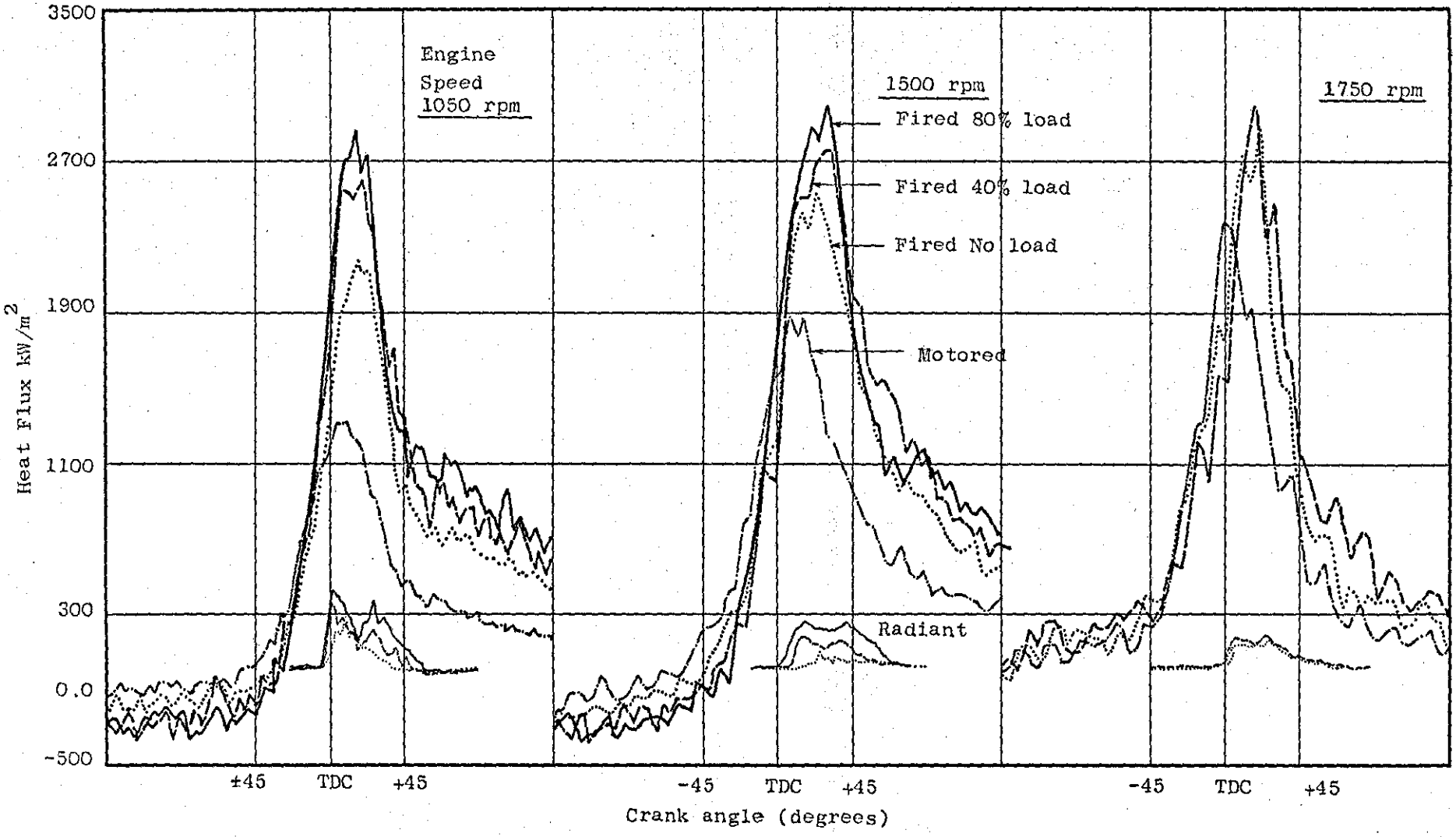

Fig. (6.18) Variation of heat flux at cylinder head location H2 with engine speed and load. Radiant heat fluxes (position R2) are included for comparison

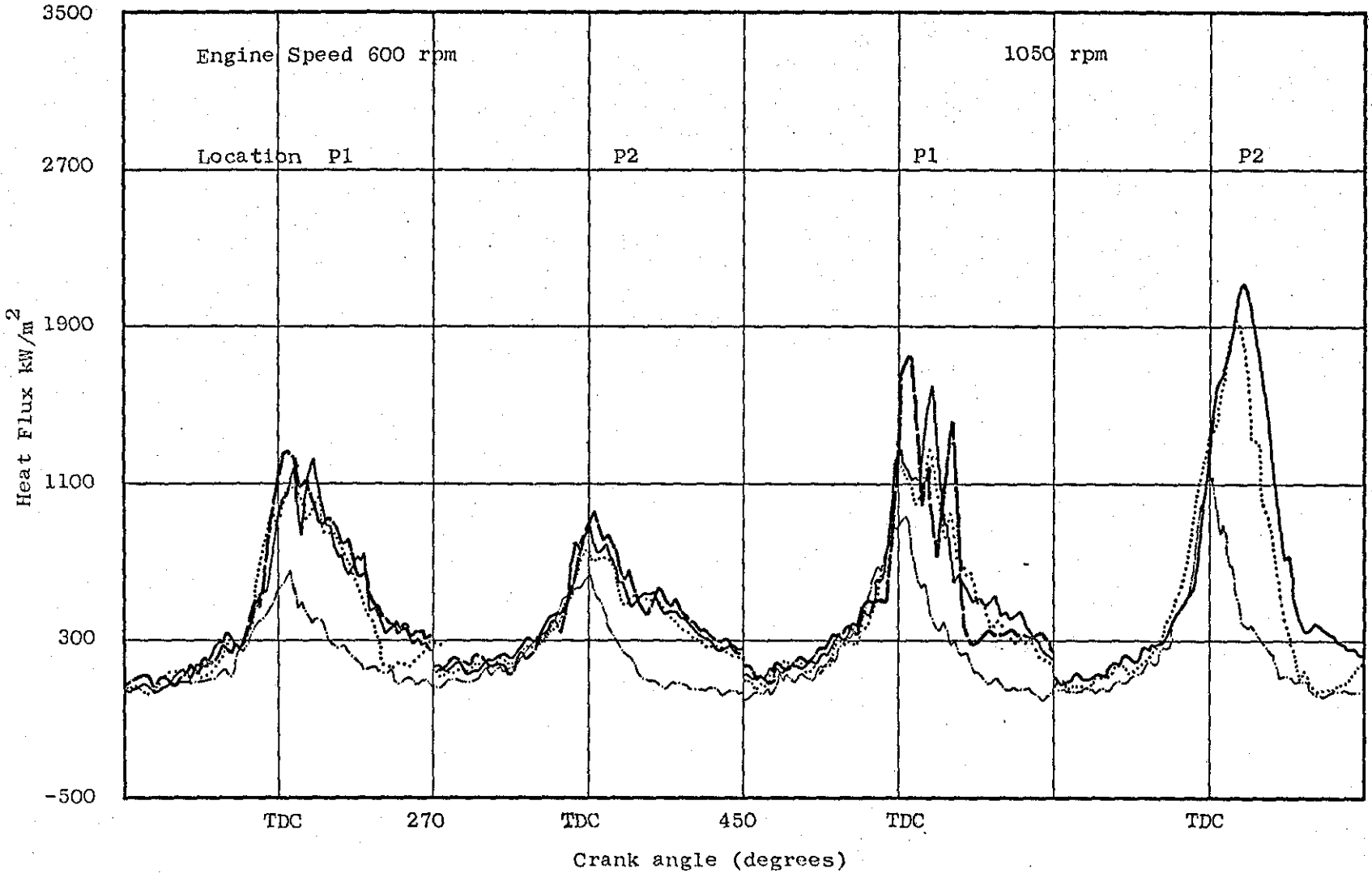

Fig. (6.19) Heat flux variation at two locations on piston crown (annular region) when engine load is varied

——— F80%L ——— F40%L ..... FNL —·—·— MOT

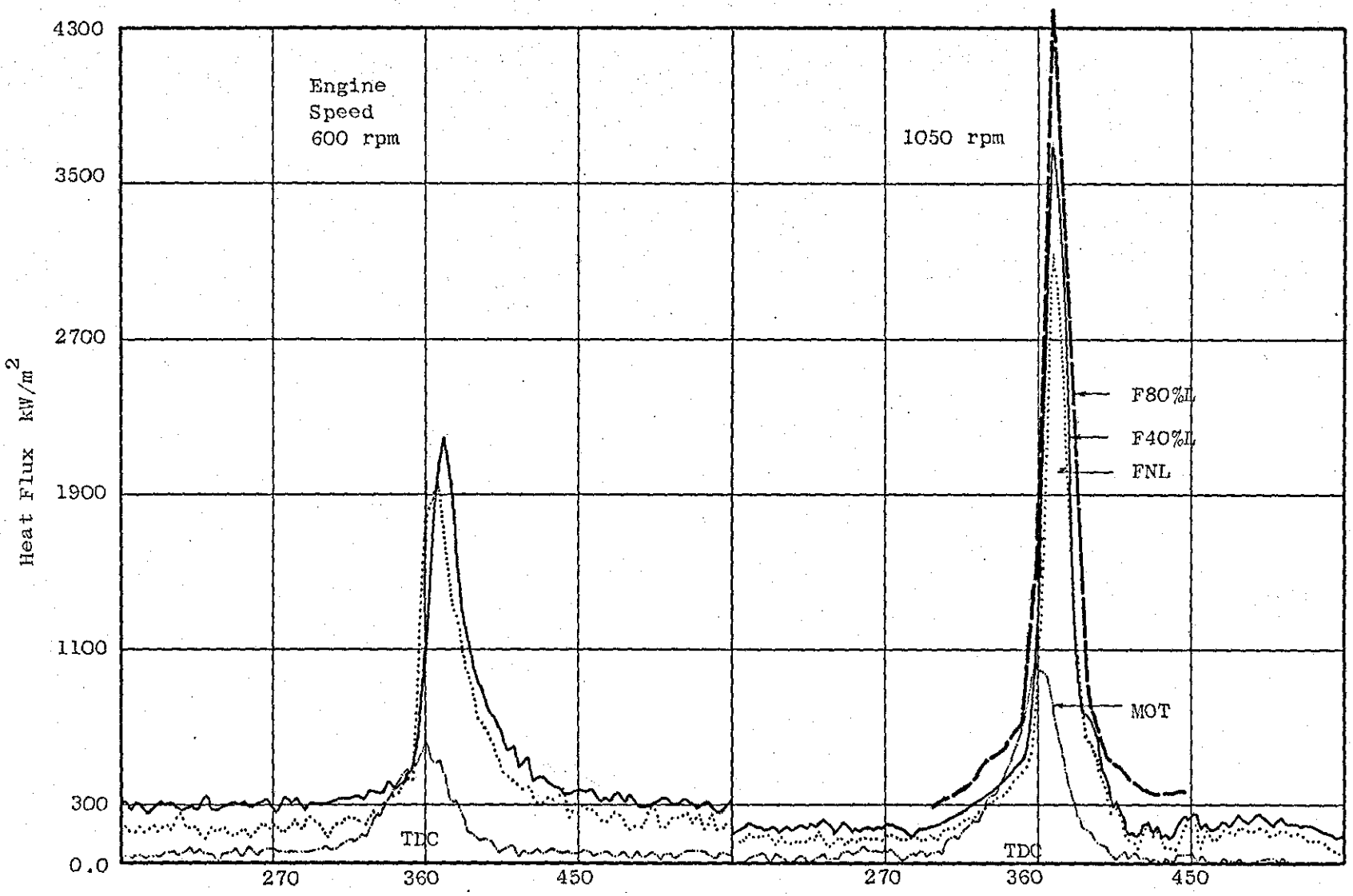

Fig. (6.20) Heat flux on piston crown (location B1) when engine load varied

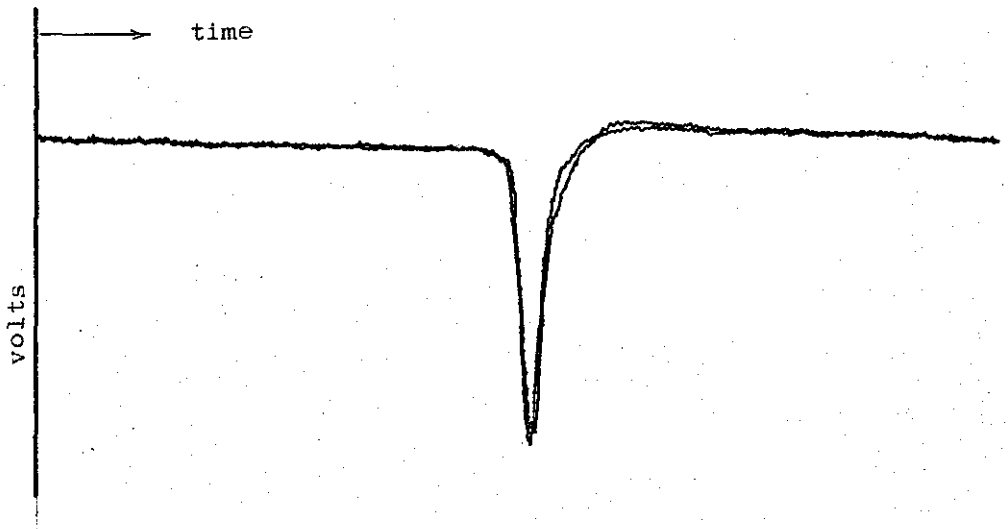

Fig. (6.21a) Repeatability of measured radiant flux at 1500 rpm medium load averaged over 15 cycles

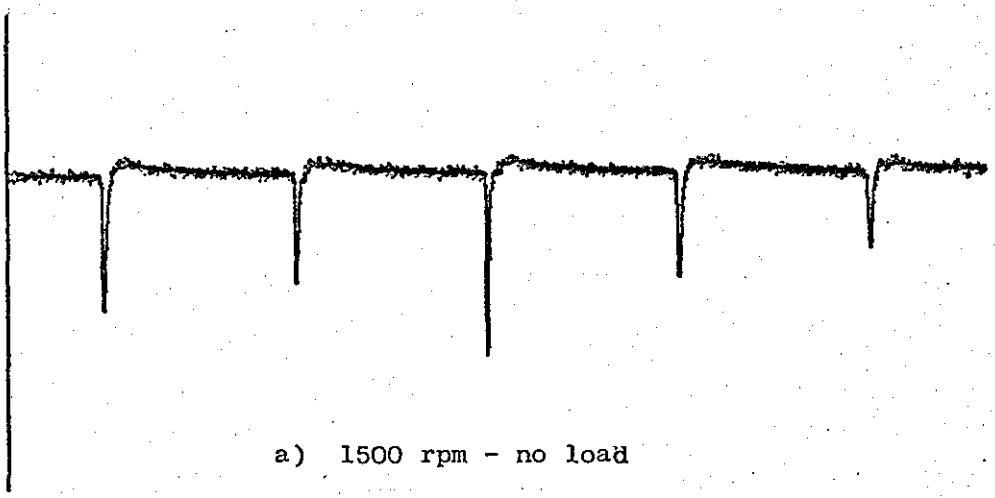

a) 1500 rpm - no load

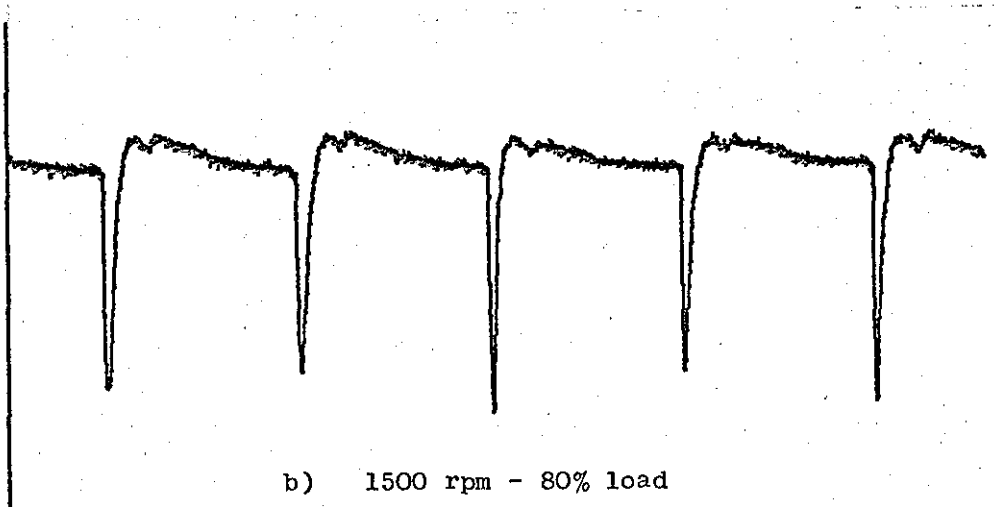

b) 1500 rpm - 80% load

Fig. (6.21b) Cyclic Variation of radiant flux observed at position R1

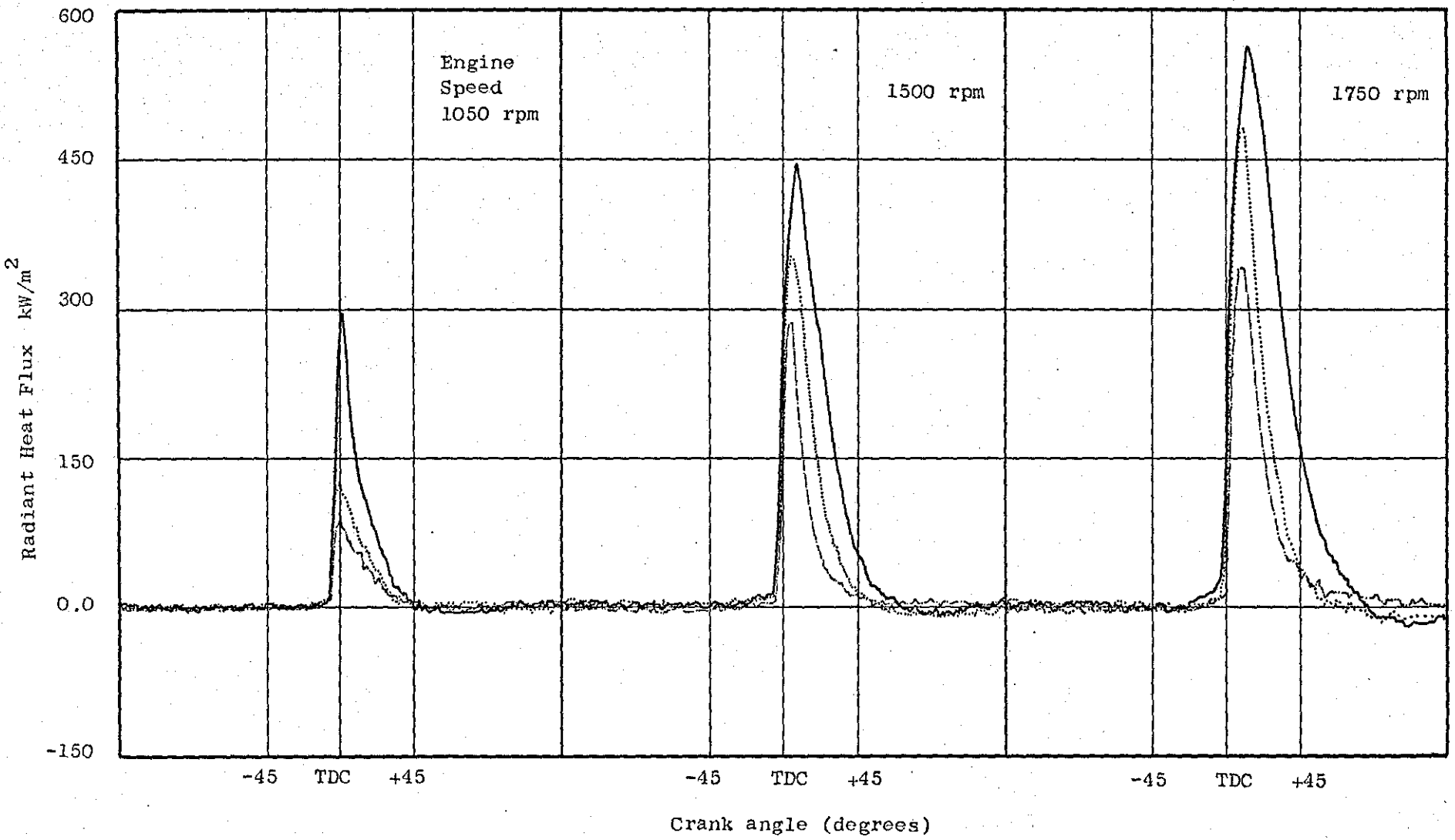

Fig. (6.22) Radiant flux observed at position R1 when load and engine speed varied

Curve ——— 80% load .....40% load —·—·— No load

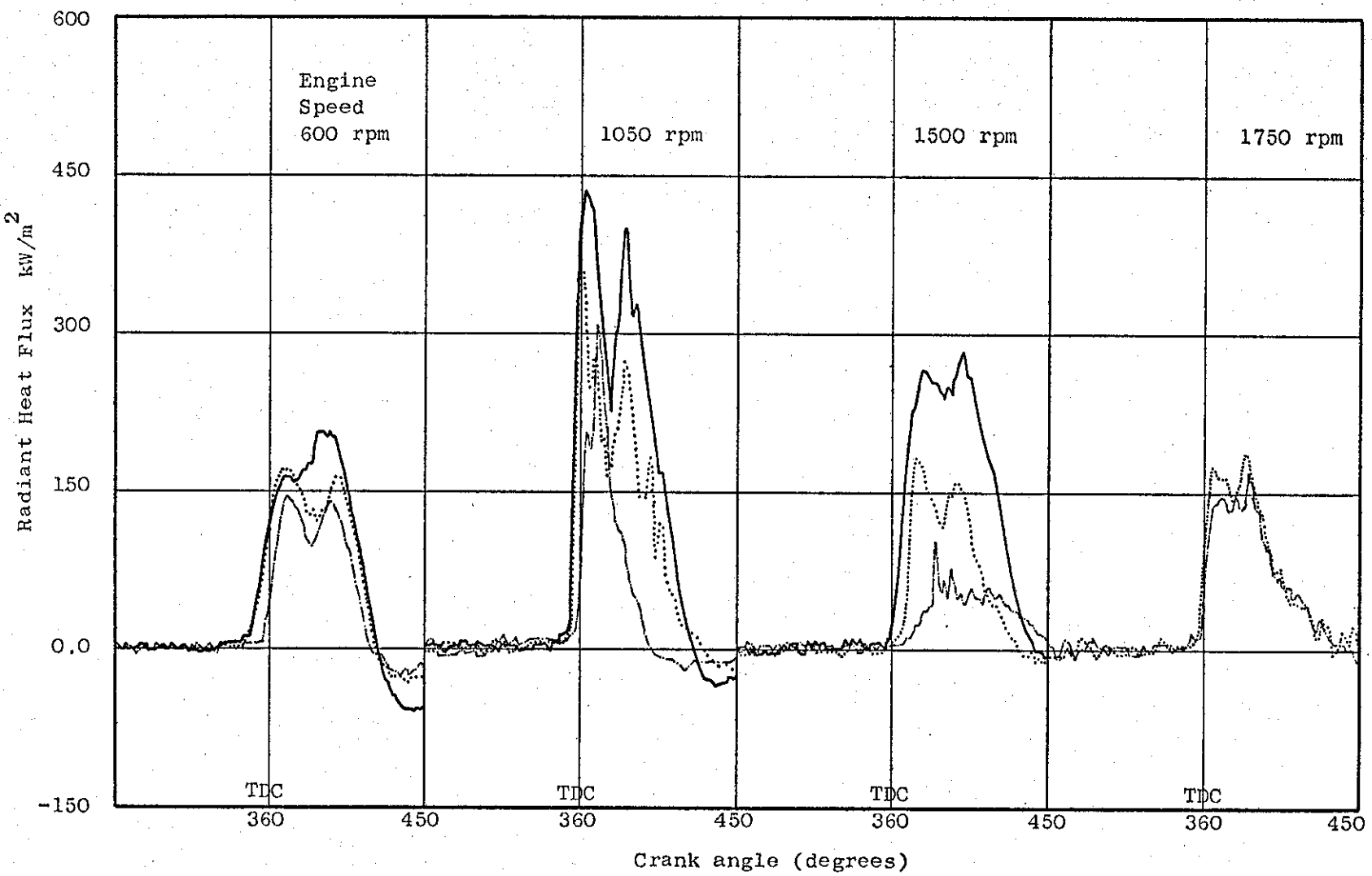

Fig. (6.23) Radiant flux observed at position R2 when both load and speed varied.

Load condition ———80% load..... 40% load-·-·-·- No load

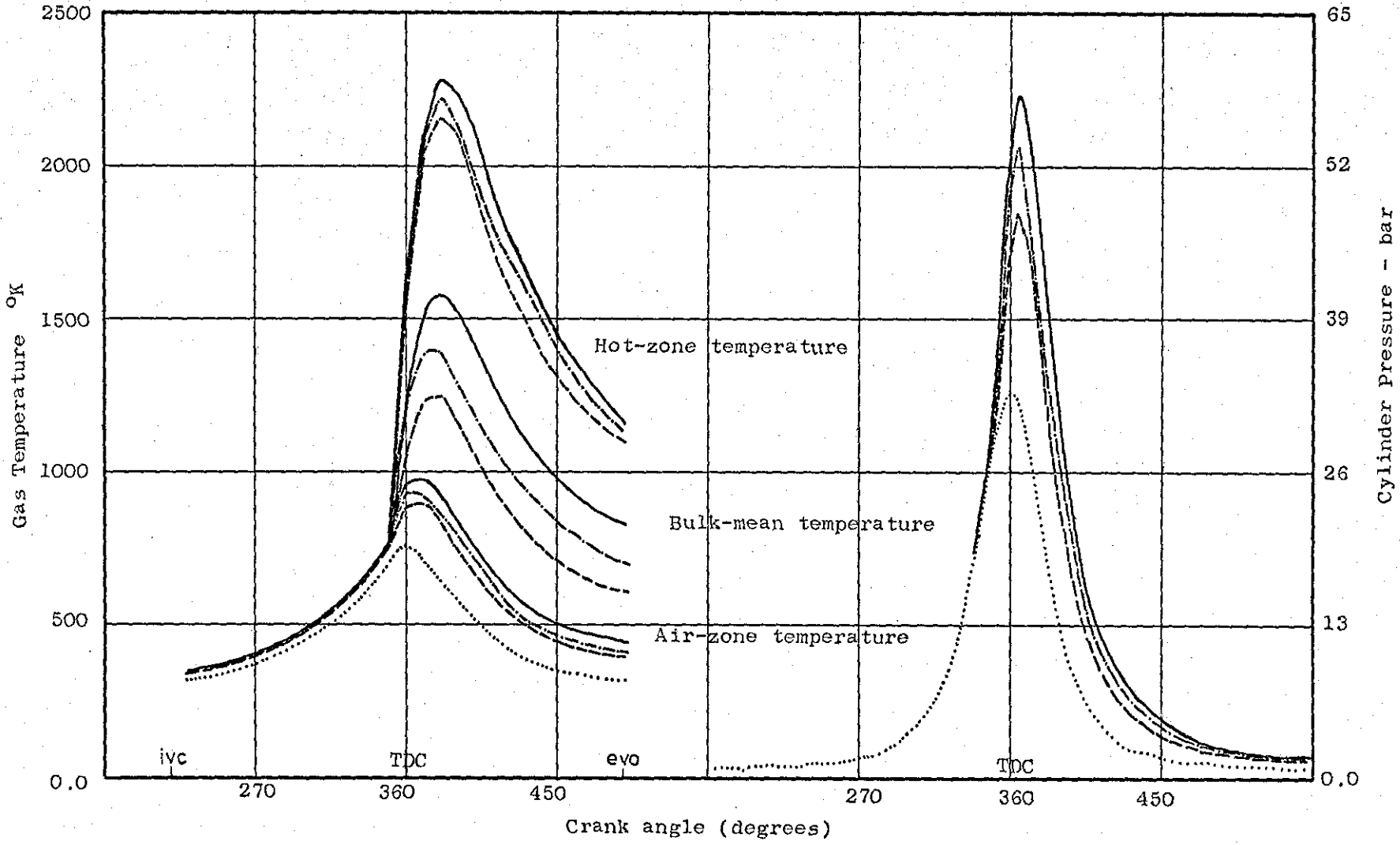

Fig. (6.24) Calculated bulk mean gas temperature and measured cylinder pressure at 1050 rpm under different operating conditions. Also shown are calculated hot-zone and air-zone temperatures from 2 - zone model

MOT ——— FNL ——— F40%L ——— F80%L

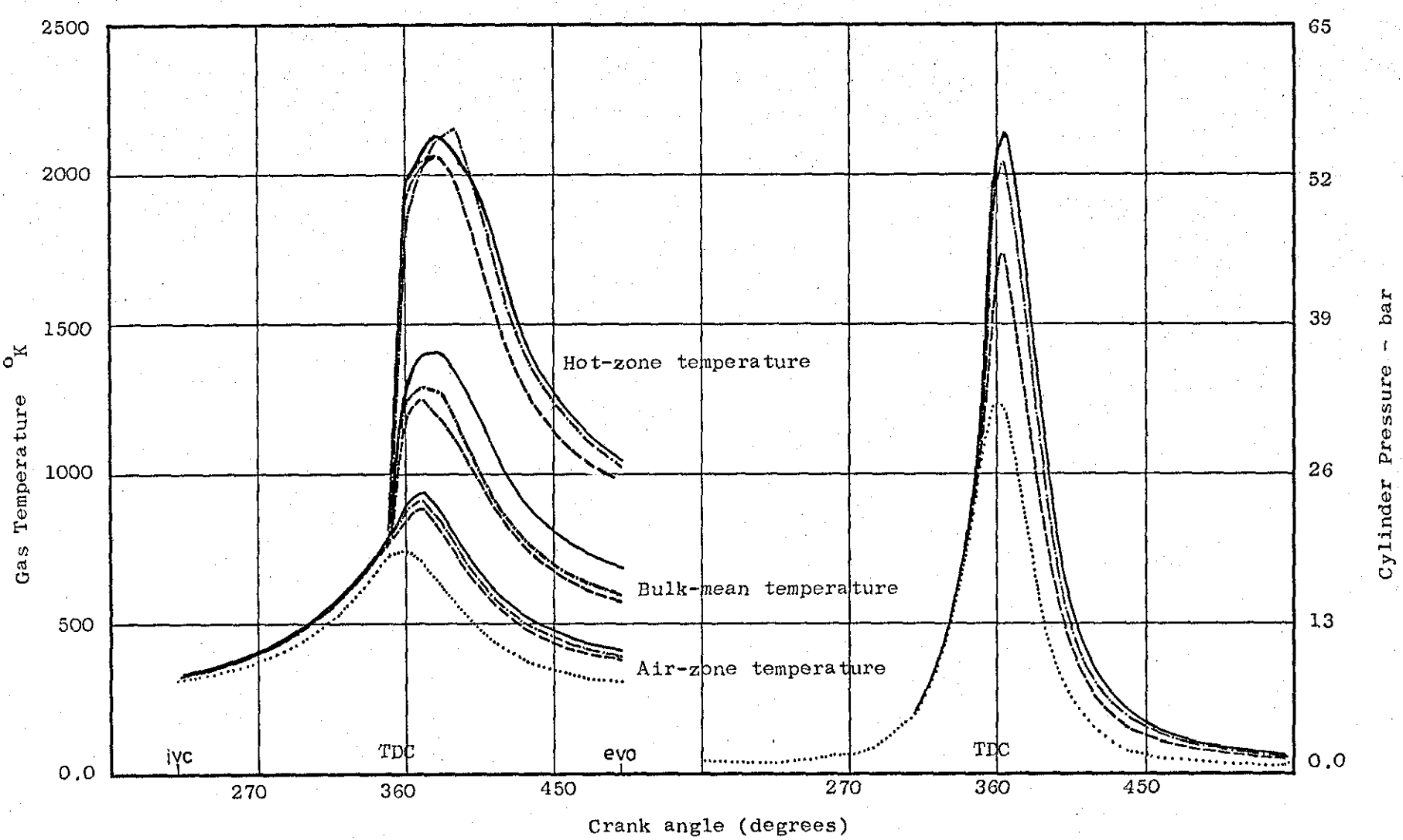

Fig. (6.25) Calculated bulk mean gas temperature and measured cylinder pressure at 600 rpm under different operating conditions. Also shown are calculated hot-zone and air-zone temperatures from 2-zone model

.....MOT ——FNL —·—·—F40%L ——— F80%L

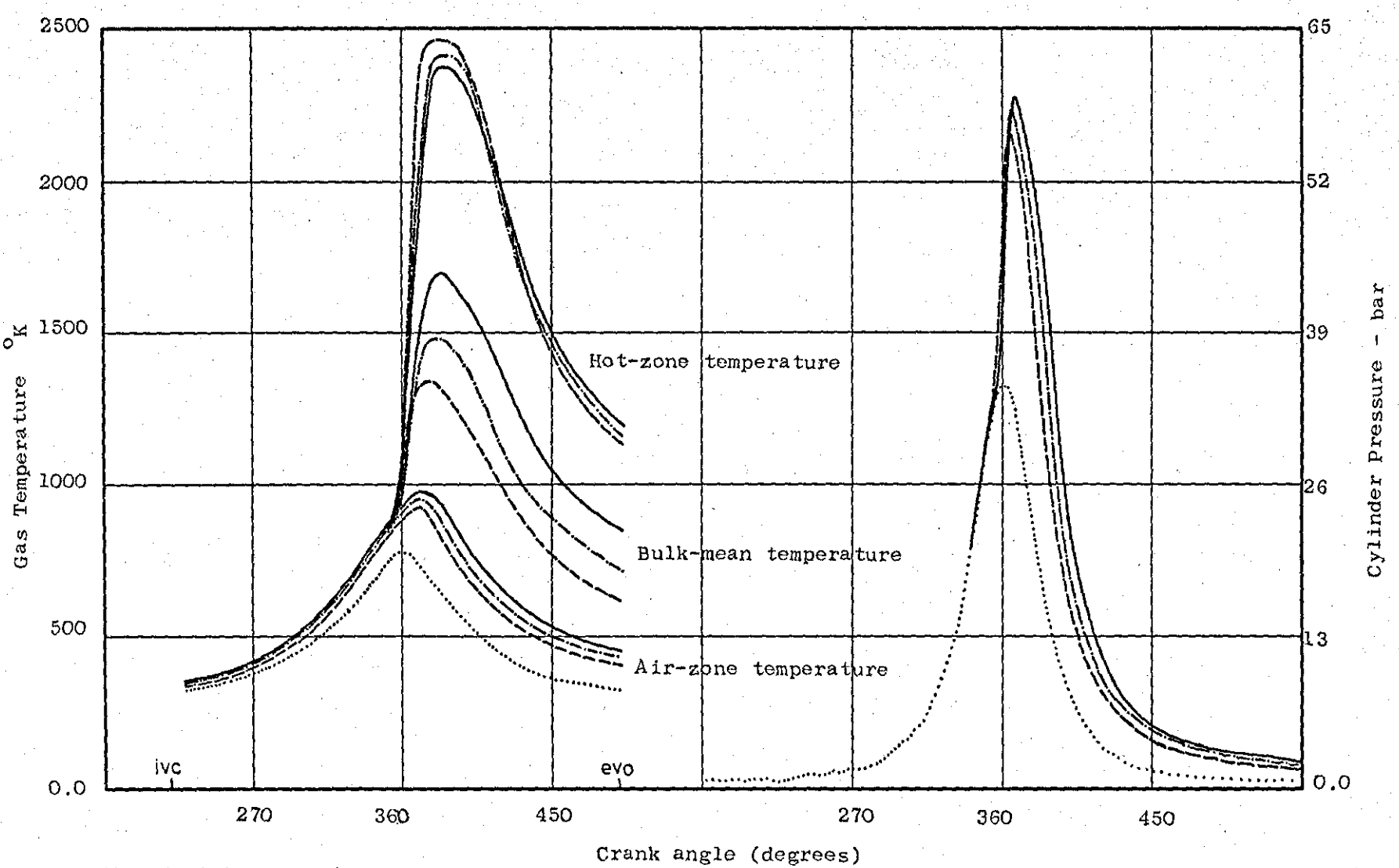

Fig. (6.26) Calculated bulk mean gas temperature and measured cylinder pressure at 1500 rpm under different operating conditions. Also shown are calculated hot-zone and air-zone temperatures from 2-zone model

..... MOT ---- FNL —.— F40%L —— F80%L

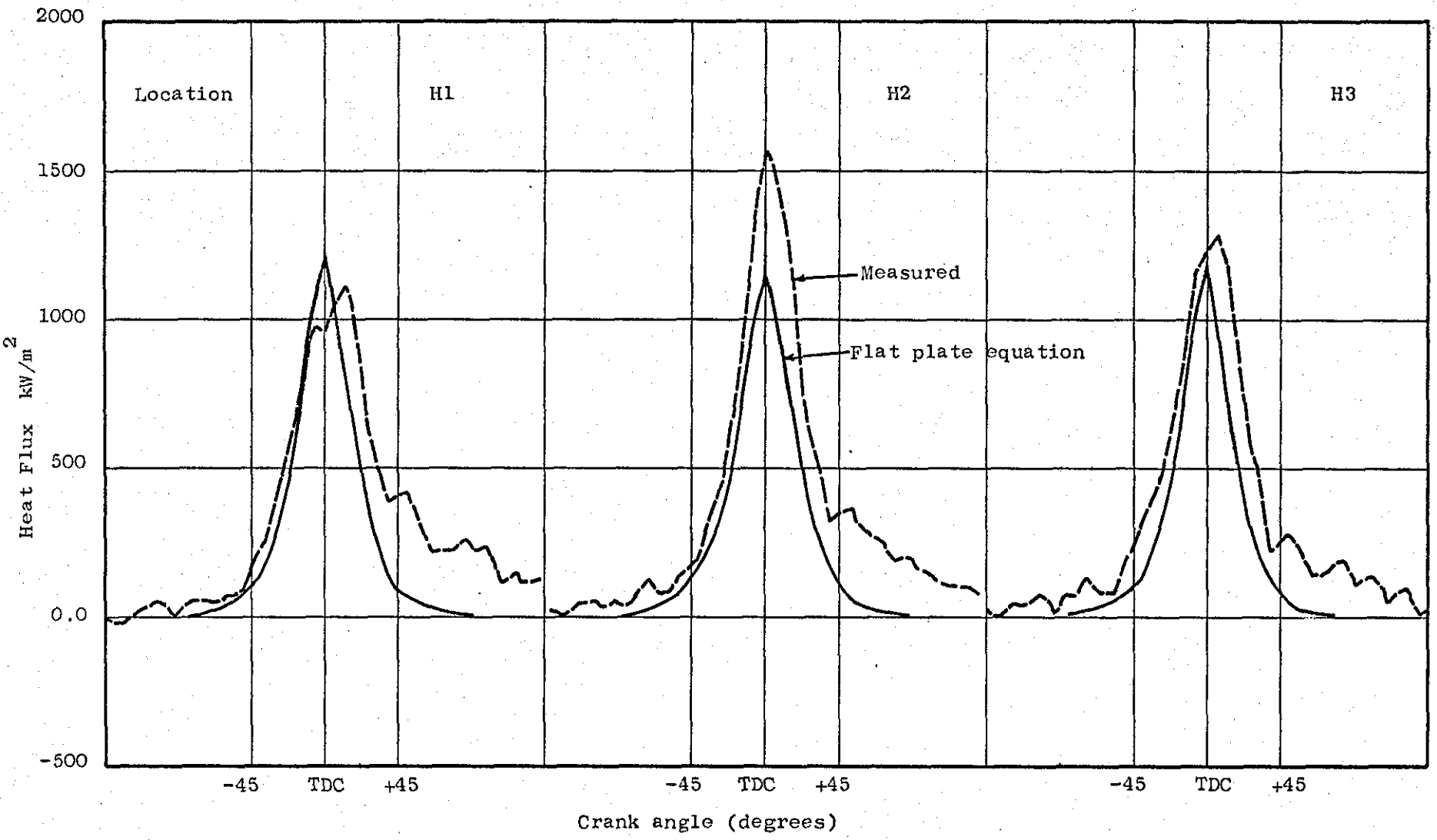

Fig. (6.27) Comparison of measured local heat fluxes on cylinder head at 1050 rpm motored operation with the prediction by the modified flat plate equation and measured air motion

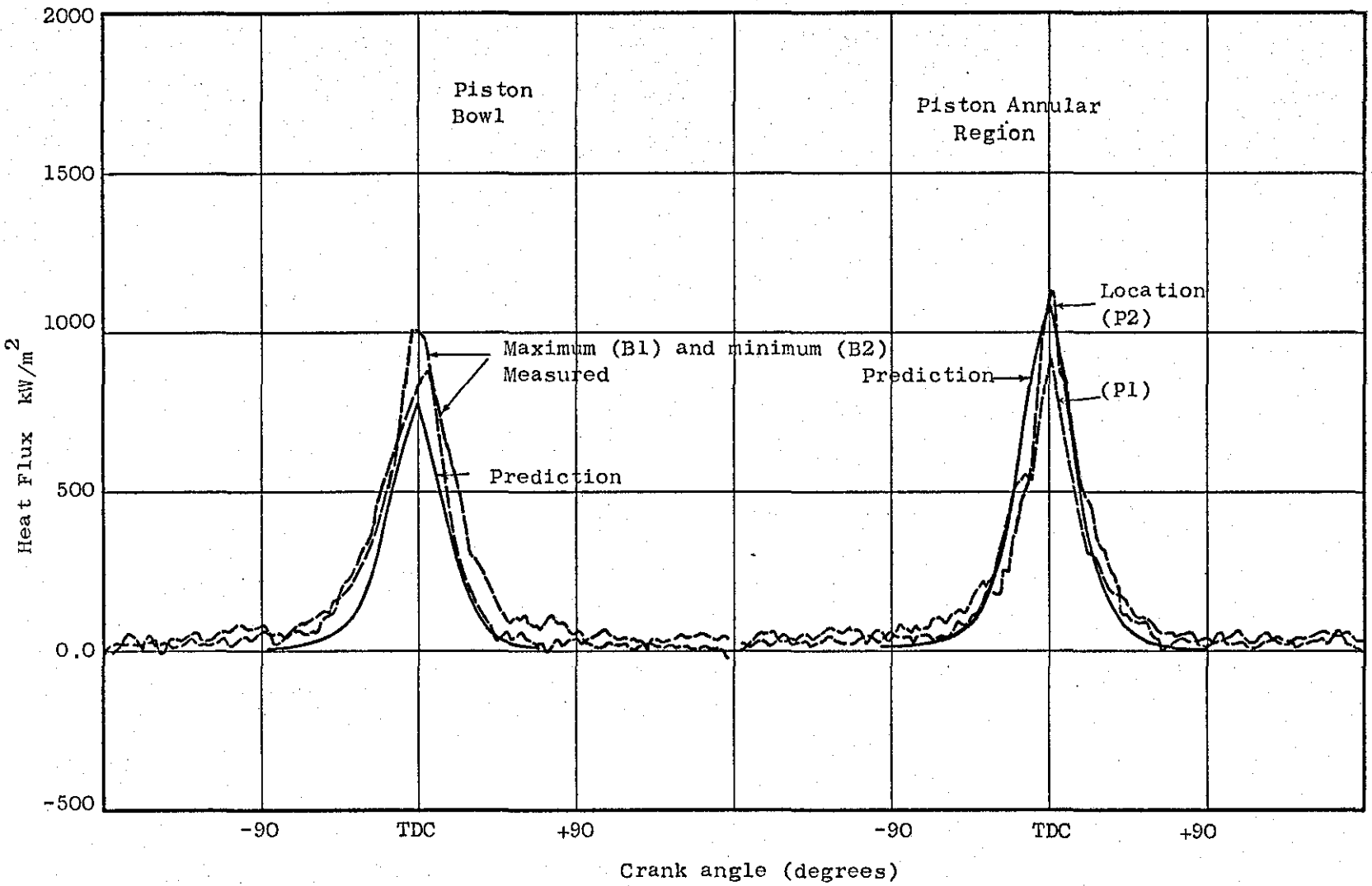

Fig. (6.28) Measured local heat fluxes (minimum and maximum local records) on piston crown at 1050 rpm motored operation with the predicted fluxes using measured gas swirl

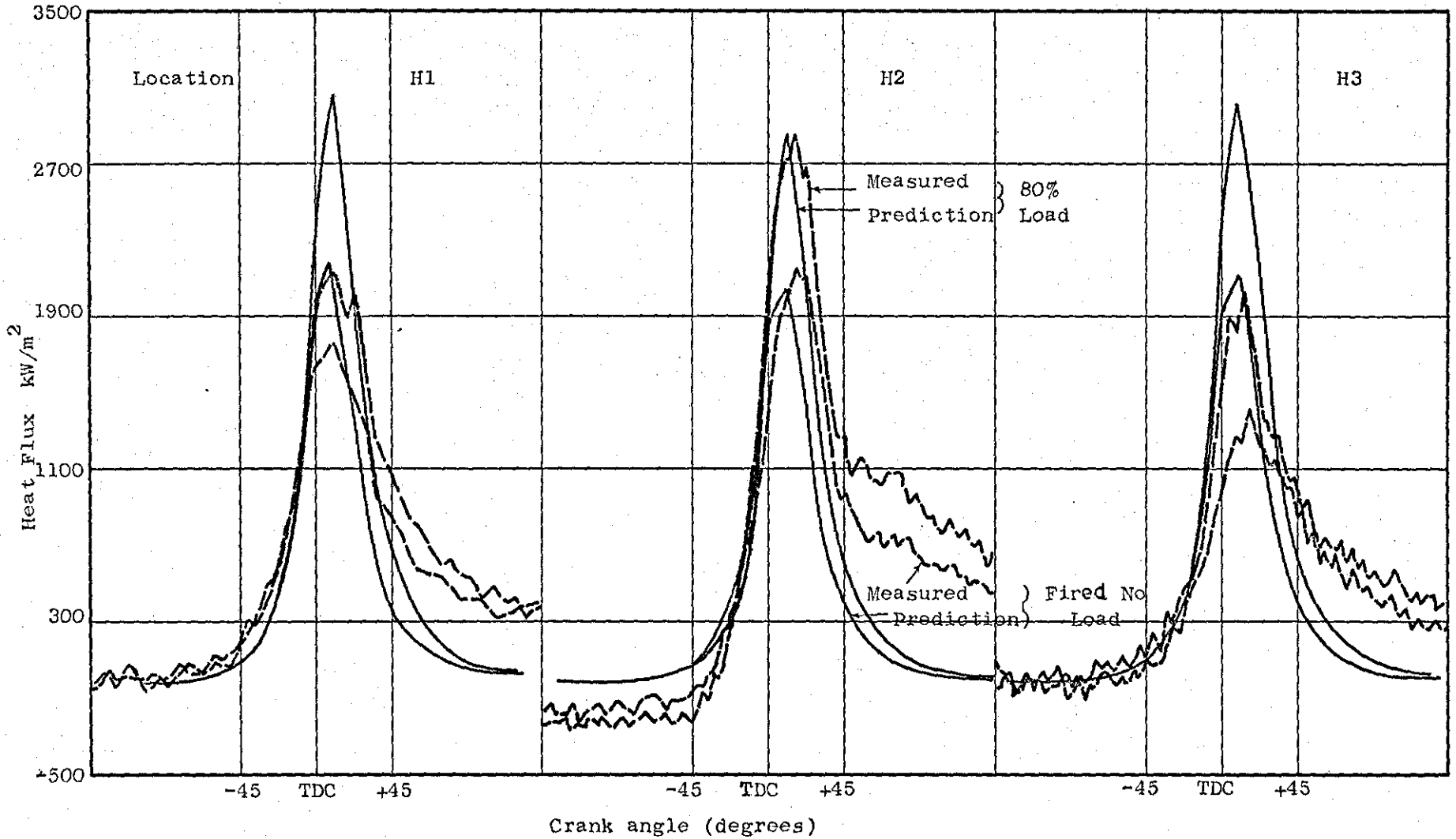

Fig. (6.29) Comparison of the measured local heat fluxes on cylinder head under FNL and F80%L conditions with the corresponding local predictions by the modified flat plate equations for engine speed of 1050 rpm using bulk mean gas temperature

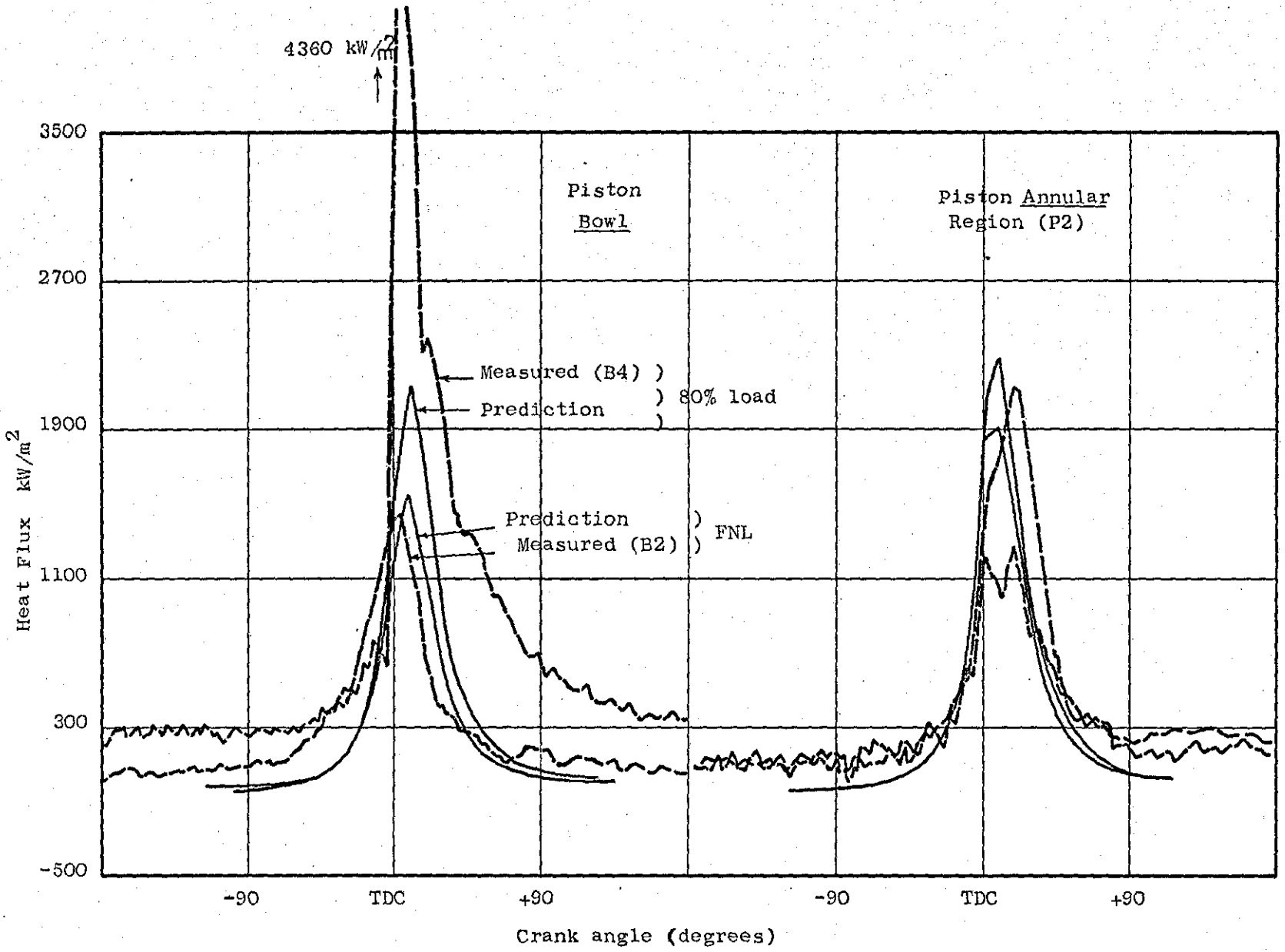

Fig. (6.30) Measured local heat fluxes for 1050 rpm fired no load and fired 80% load conditions with the corresponding predictions using bulk mean gas temperature

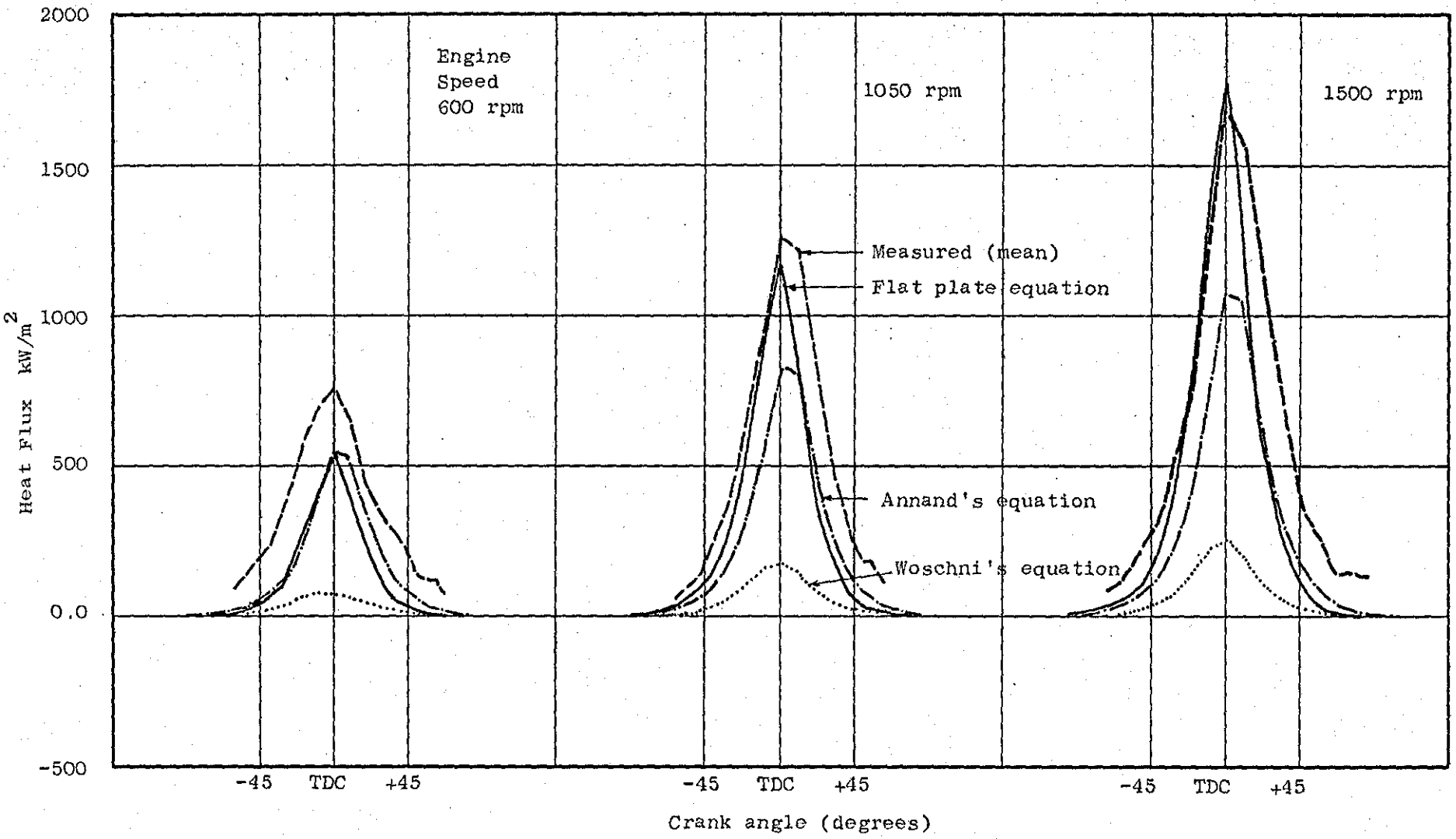

Fig. (6.31) Measured mean heat fluxes on cylinder head for motored operation and prediction by flat plate equation, Annand's equation and Woschnis' equation

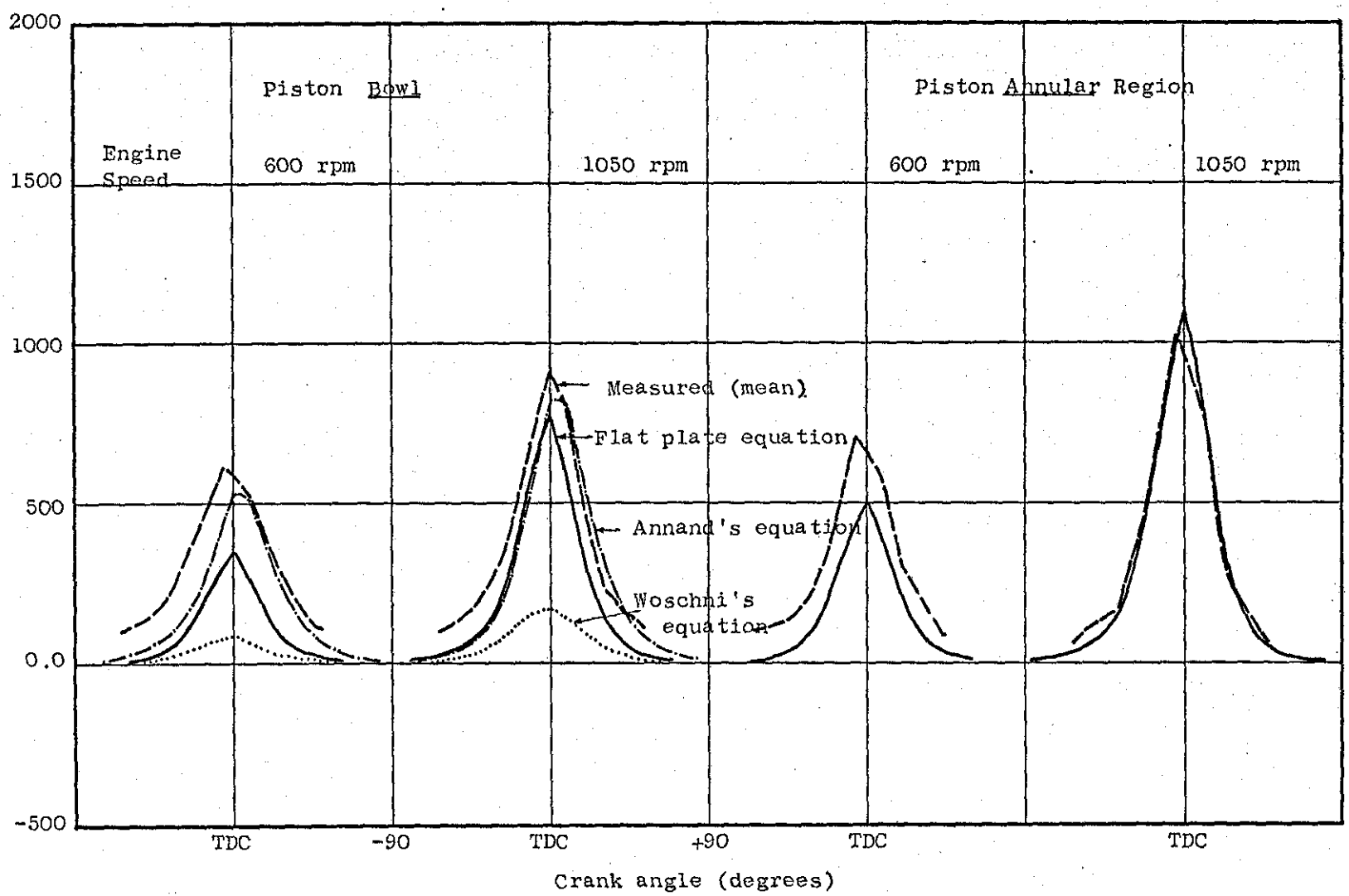

Fig. (6.32a) Measured mean heat fluxes on piston crown for motored operation and predicted fluxes by modified flat plate equation, Annand's equation and Woschni's equation

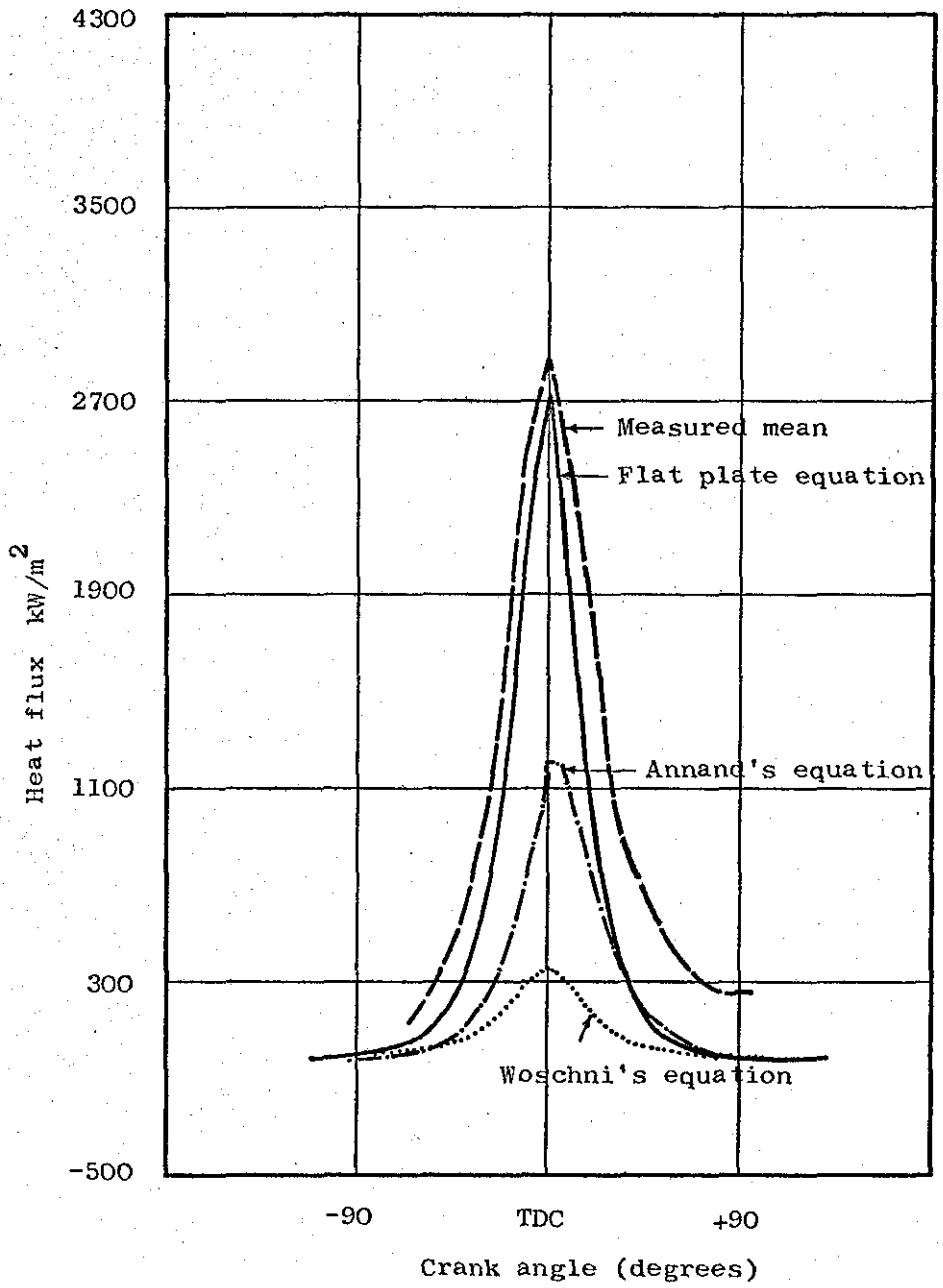

Fig. (6.32b) Measured mean heat flux on the cylinder head at 1050 rpm and 1.69 bar manifold pressure, and the predicted fluxes by flat plate equation, Annand's equation and Woschni's equation.

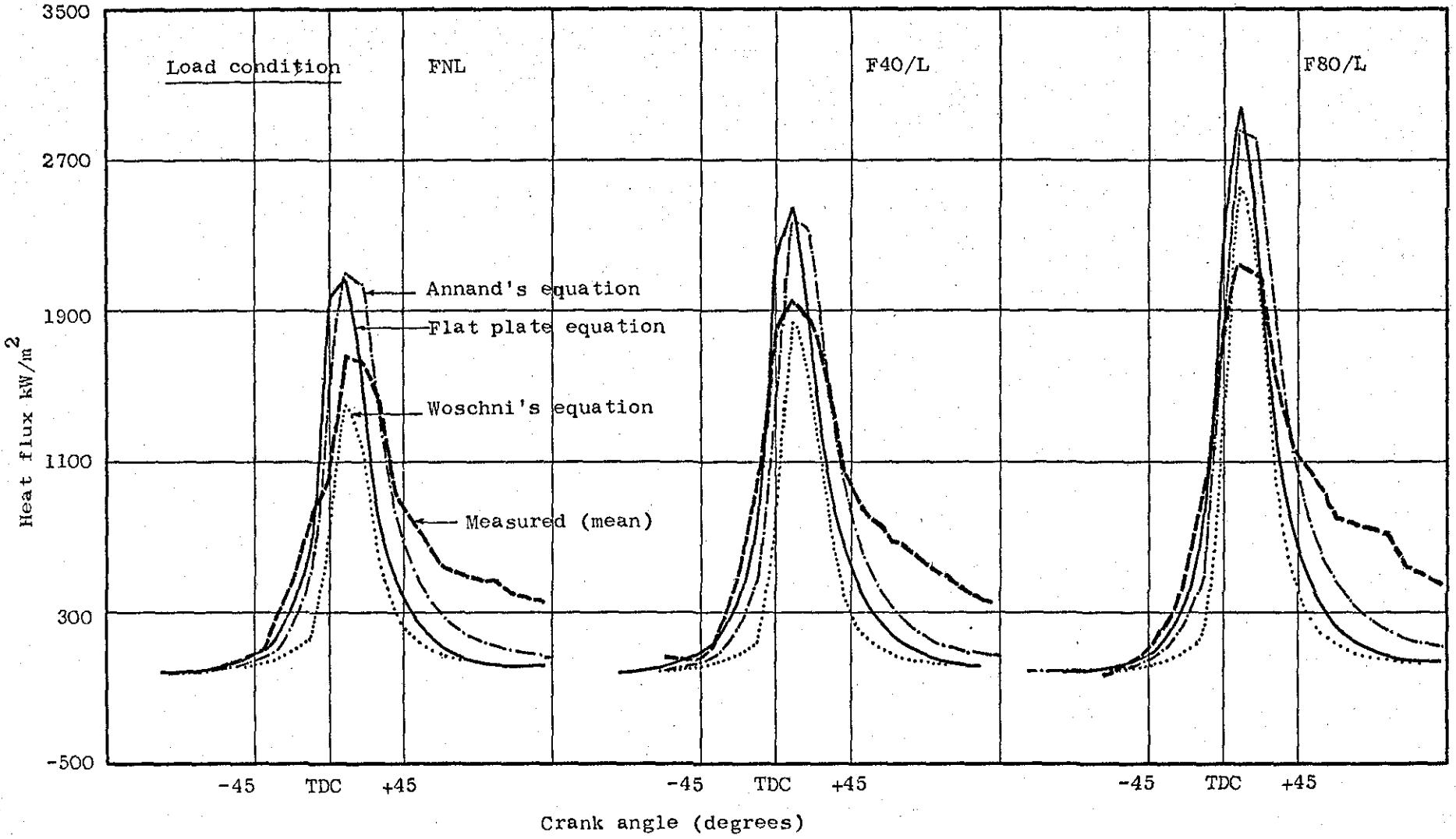

Fig. (6.33) Comparison of measured mean heat fluxes on the cylinder head at 1050 rpm fired operation with predictions by flat plate equation using measured gas motion, Annand's equation and Woschni' equation (using bulk mean gas temperature).

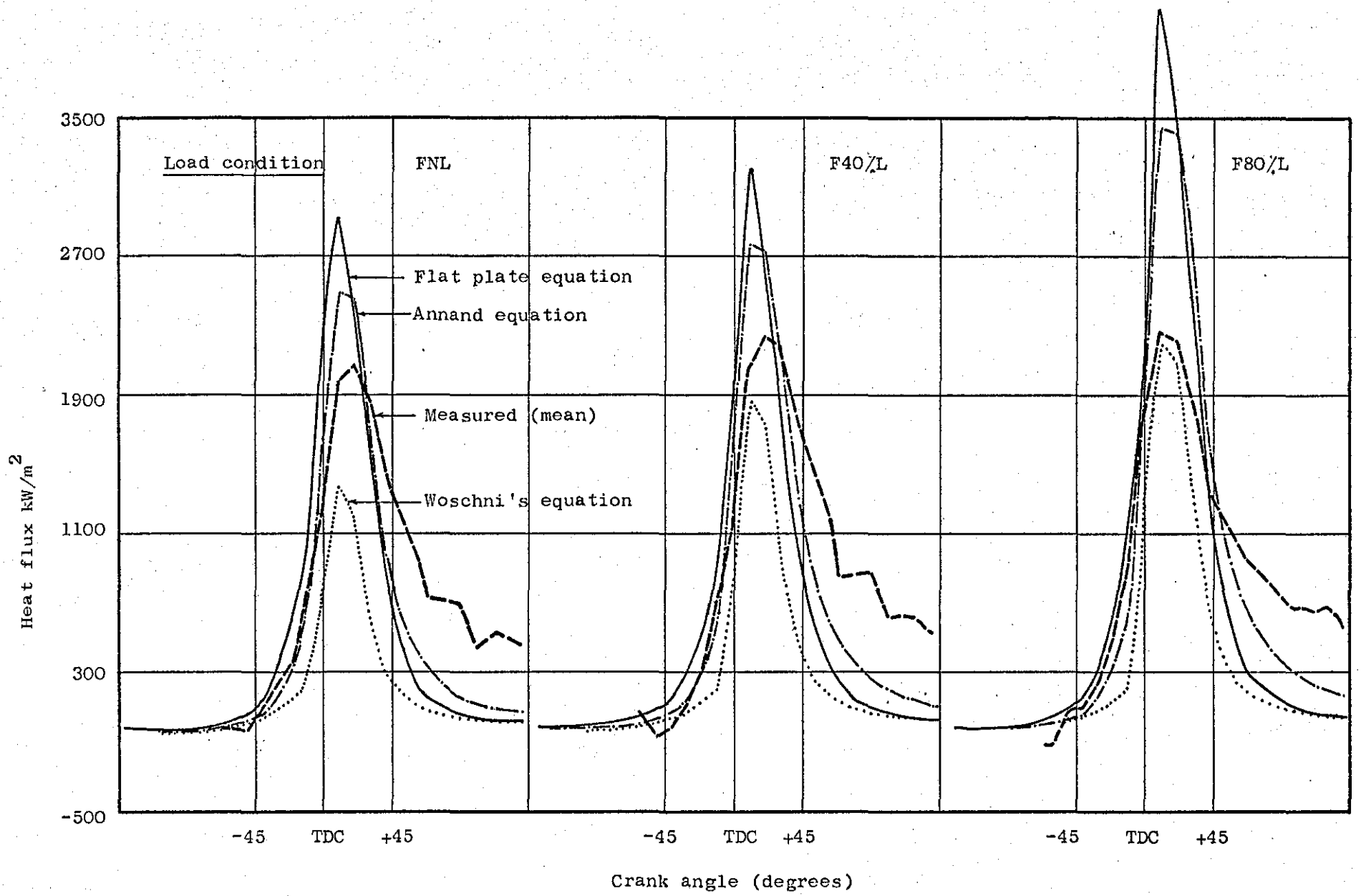

Fig. (6.34) Measured mean heat fluxes on cylinder head at 1500 rpm fired operation and predictions by flat plate equation, Annand's equation and Woschni's equation (using bulk mean gas temperature.

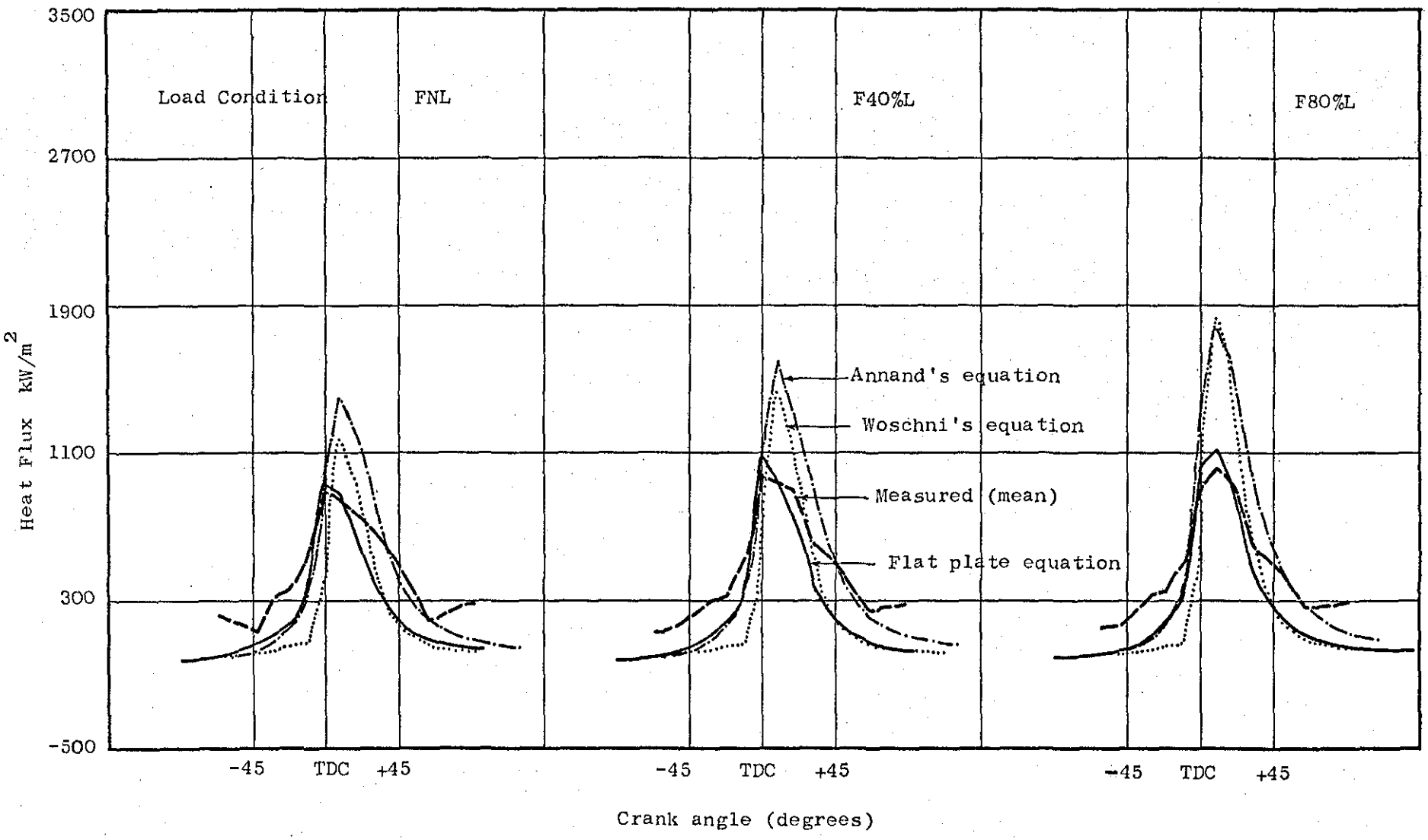

Fig. (6.35) Comparison of measured local mean heat fluxes on piston crown (annular region) with prediction by flat plate equation using bulk mean gas temperature for engine speed of 600 rpm

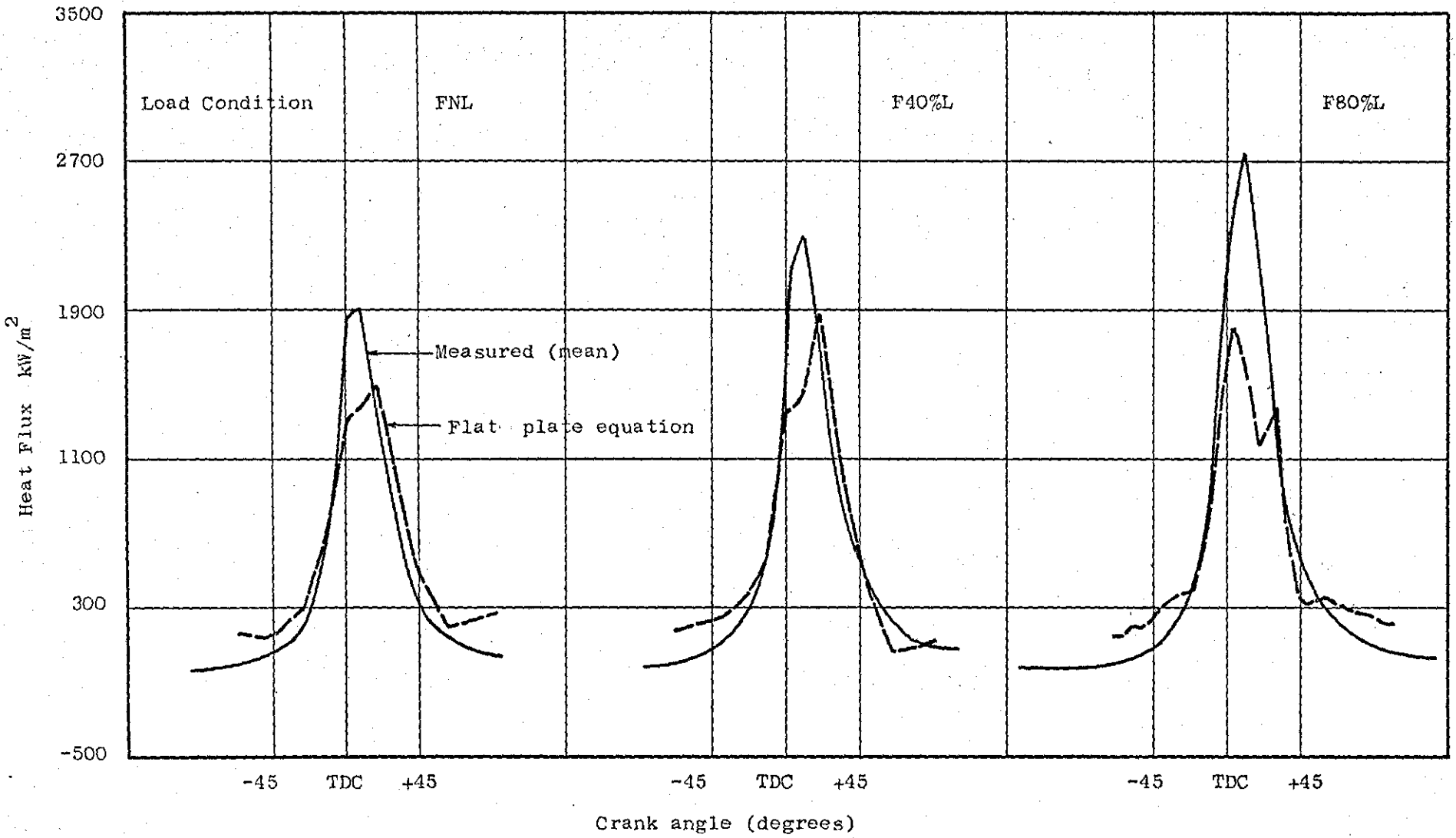

Fig. (6.36) Comparison of measured mean heat fluxes on piston crown (annular region) with prediction by flat plate equation using bulk mean gas temperature at 1050 rpm fired operation

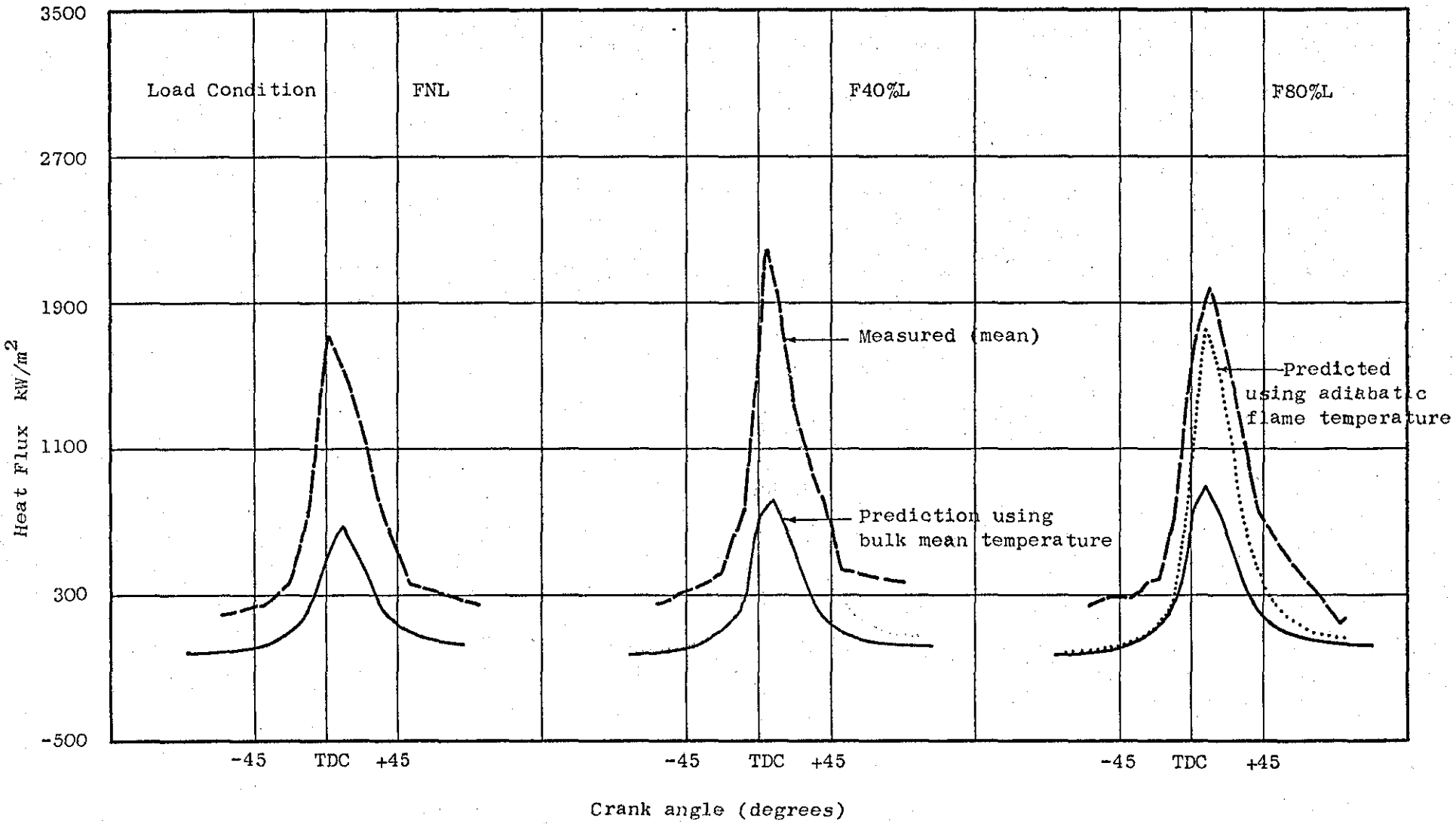

Fig. (6.37) Measured mean heat fluxes on piston crown (bowl region) and prediction by flat plate equation for 600 rpm fired operation

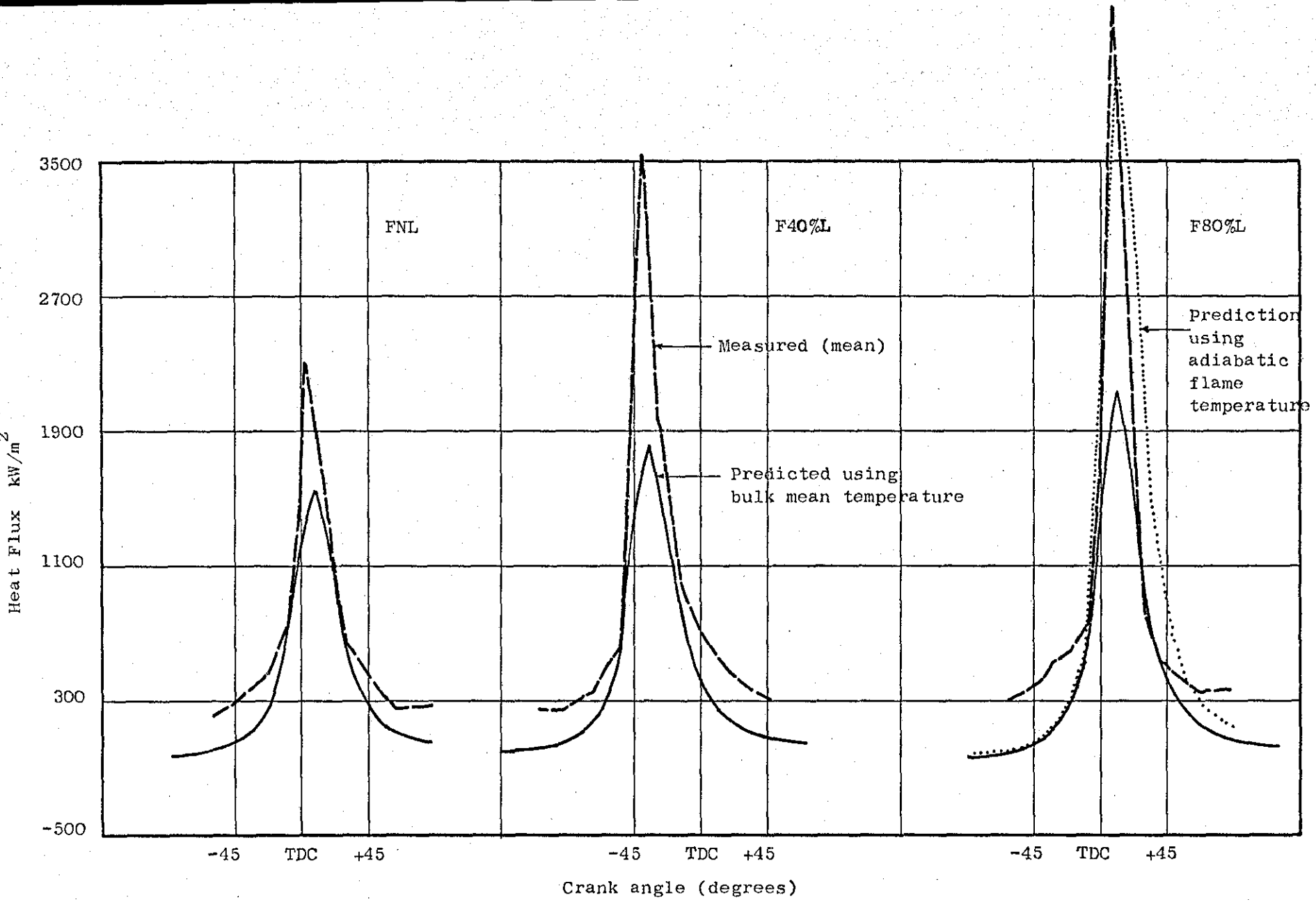

Fig. (6.38) Measured mean heat fluxes on piston crown (bowl) for 1050 rpm fired operation and prediction by flat plate equation

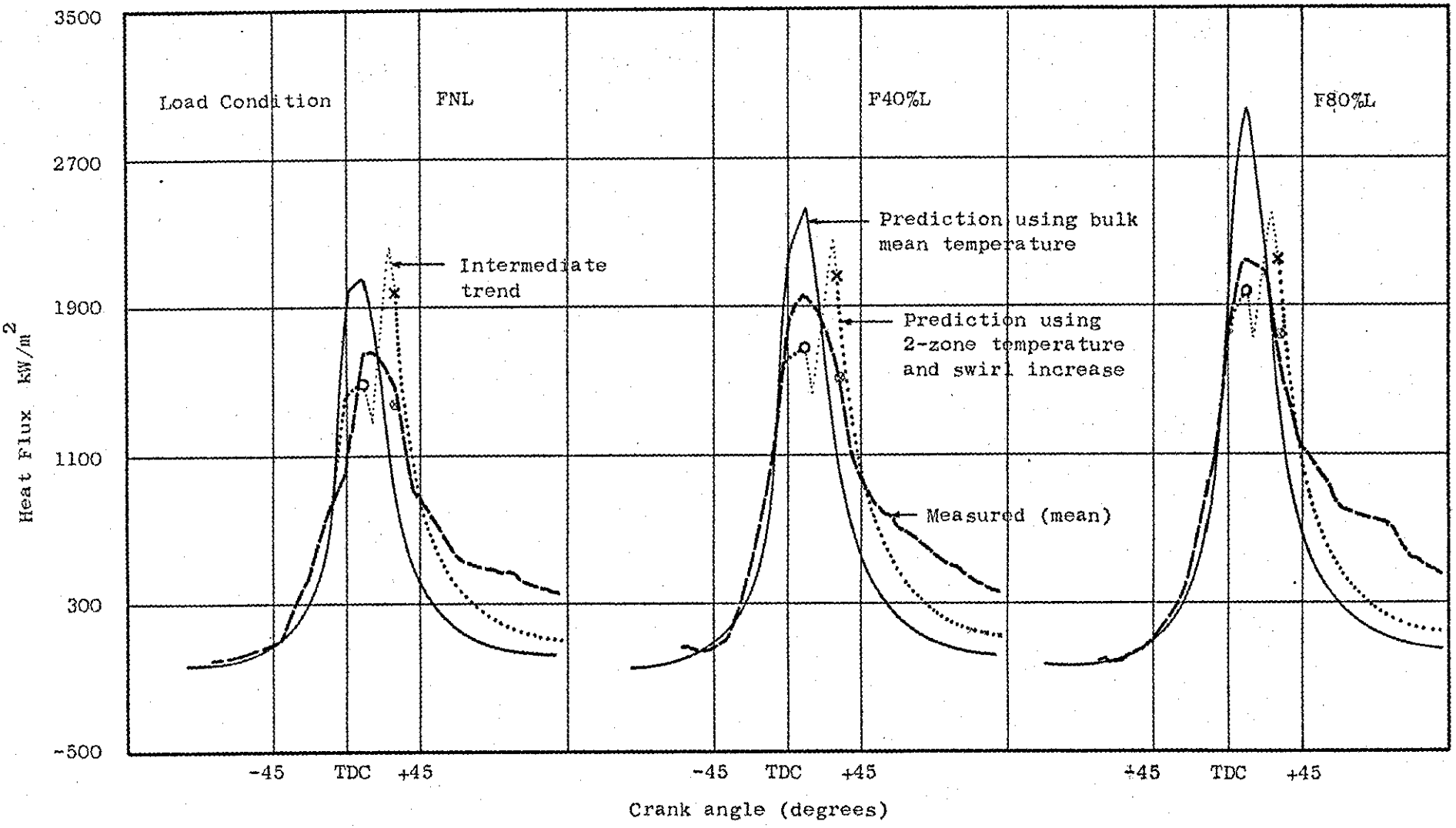

Fig. (6.39) Measured mean fluxes on cylinder head for 1050 rpm fired operation and predictions on basis of bulk mean gas temperature, and on basis of 2-zone temperatures.
o - last point using air zone temperature, × - first point using mixture zone temperature and accounting for swirl increase. ⊗ using arithmetic mean temperature

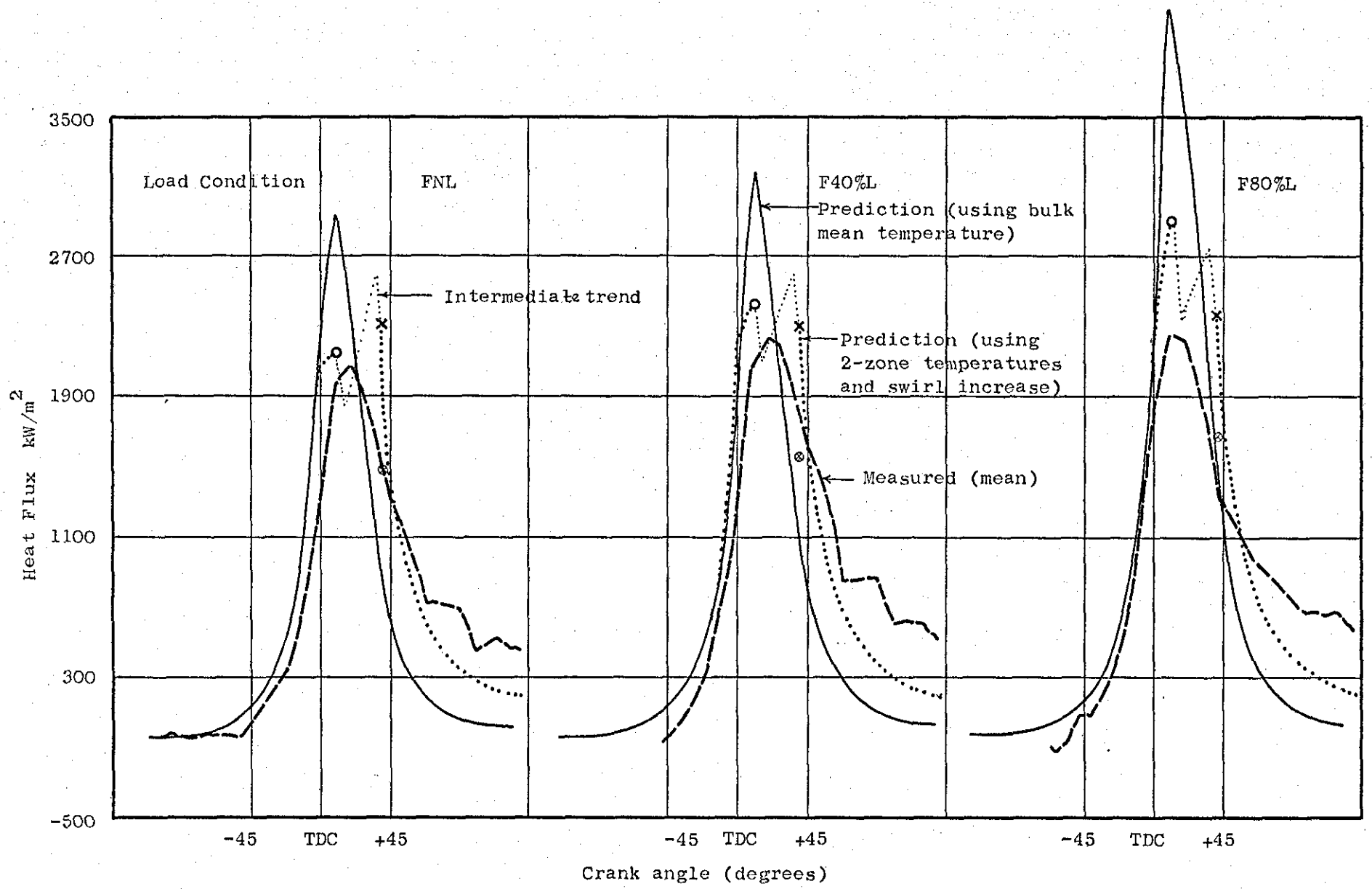

Fig. (6.40) Measured mean fluxes on cylinder head for 1500 rpm fired operation and predictions on basis of bulk mean gas temperature (—), and on basis of 2-zone temperatures. o - last point using air zone temperature, × - first point using mixture-zone temperature and accounting for swirl increase, ⊗ - using arithmetic mean temperature

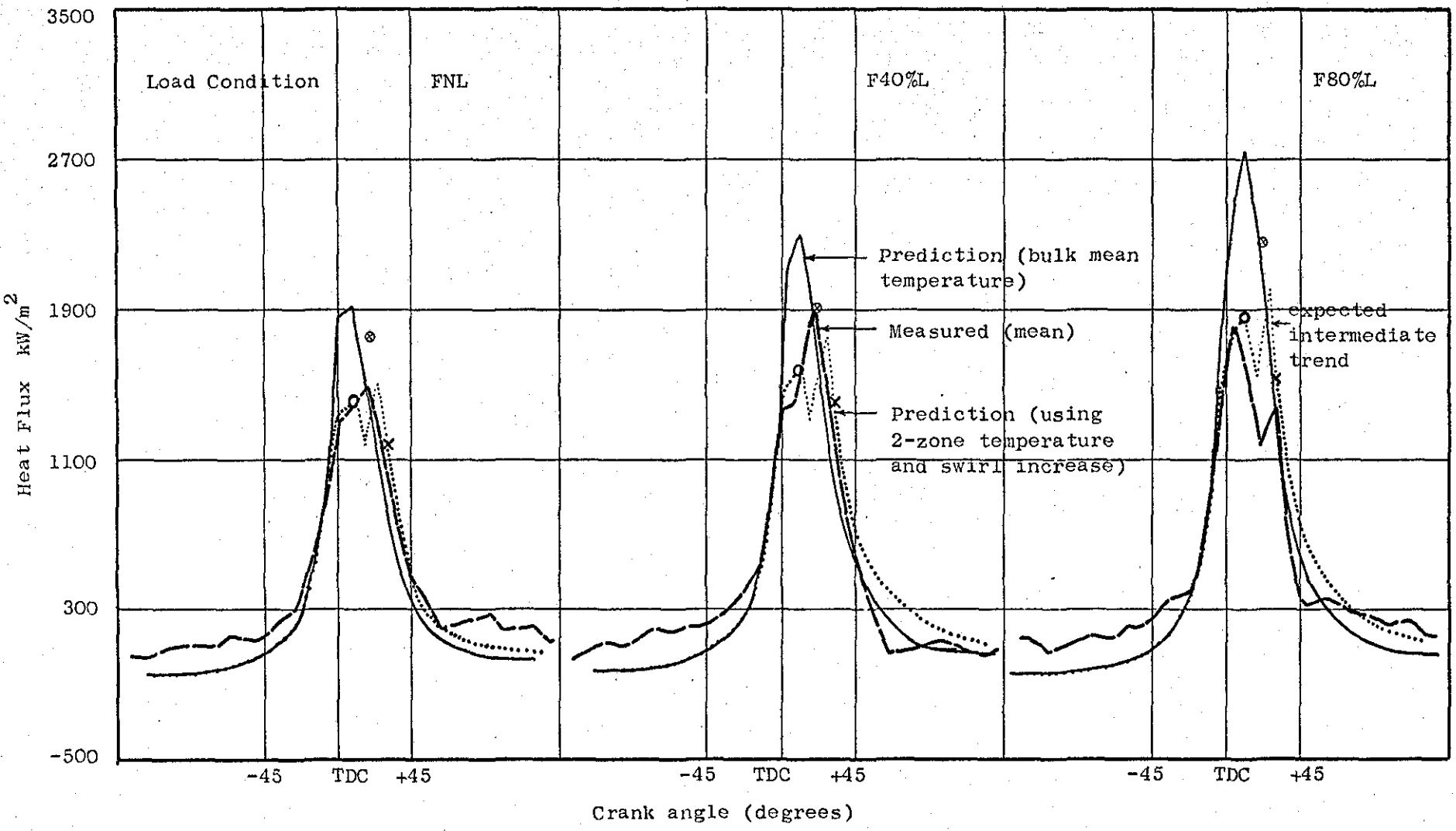

Fig. (6.41) Measured mean fluxes on piston crown (annular region) for 1050 rpm fired operation and predictions on basis of bulk mean gas temperature (—) and on basis of 2-zone temperatures. o - last point using air zone temperature. × - first point using bulk mean temperature and accounting for swirl increase, ⊗ - using arithmetic mean temperature

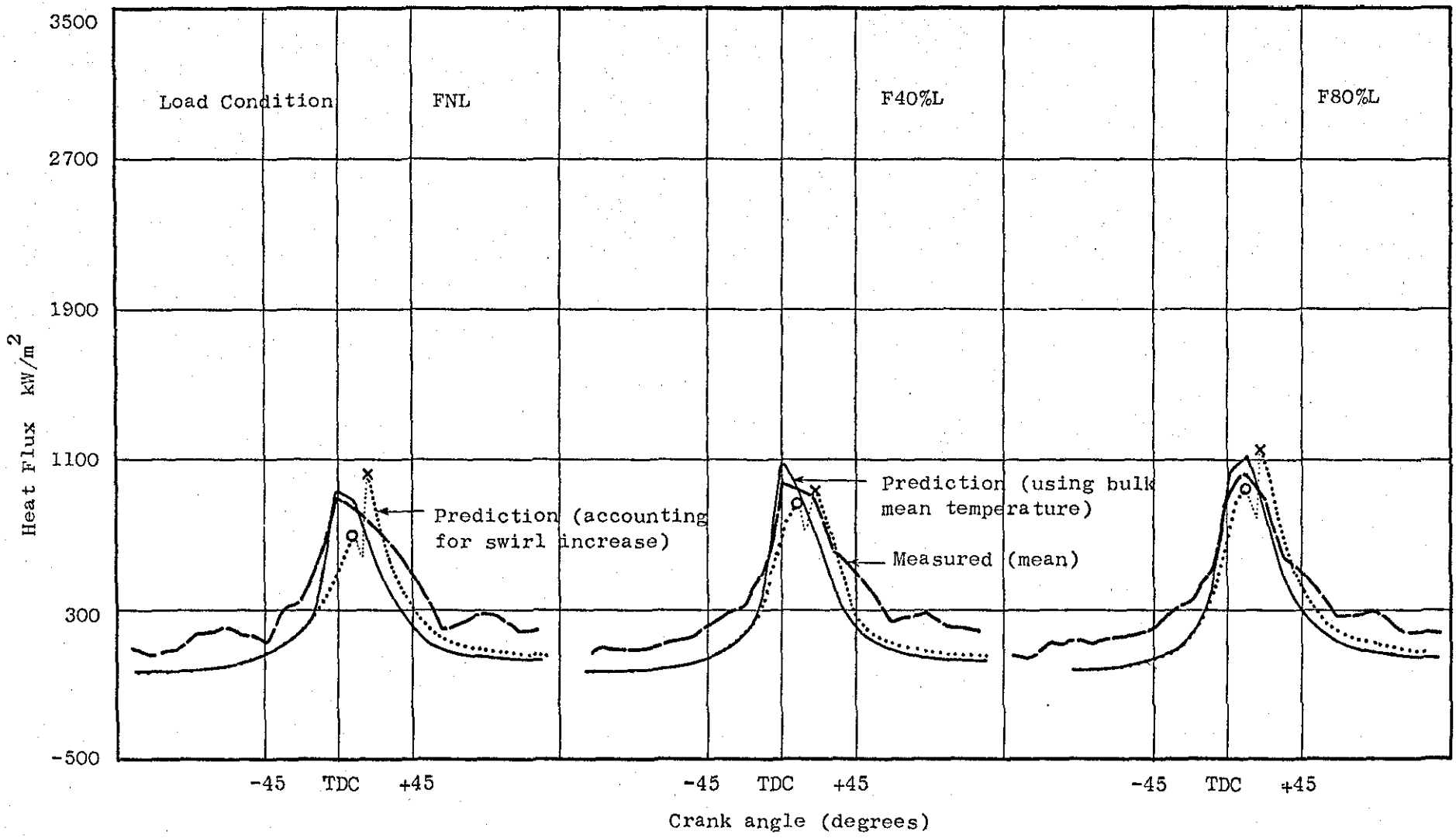

Fig. (6.42) Measured mean fluxes on piston crown (annular region) for 600 rpm fired operation and predictions on basis of bulk mean gas temperature and the same with correction for swirl increase (× first point), o last point using air-zone temperature

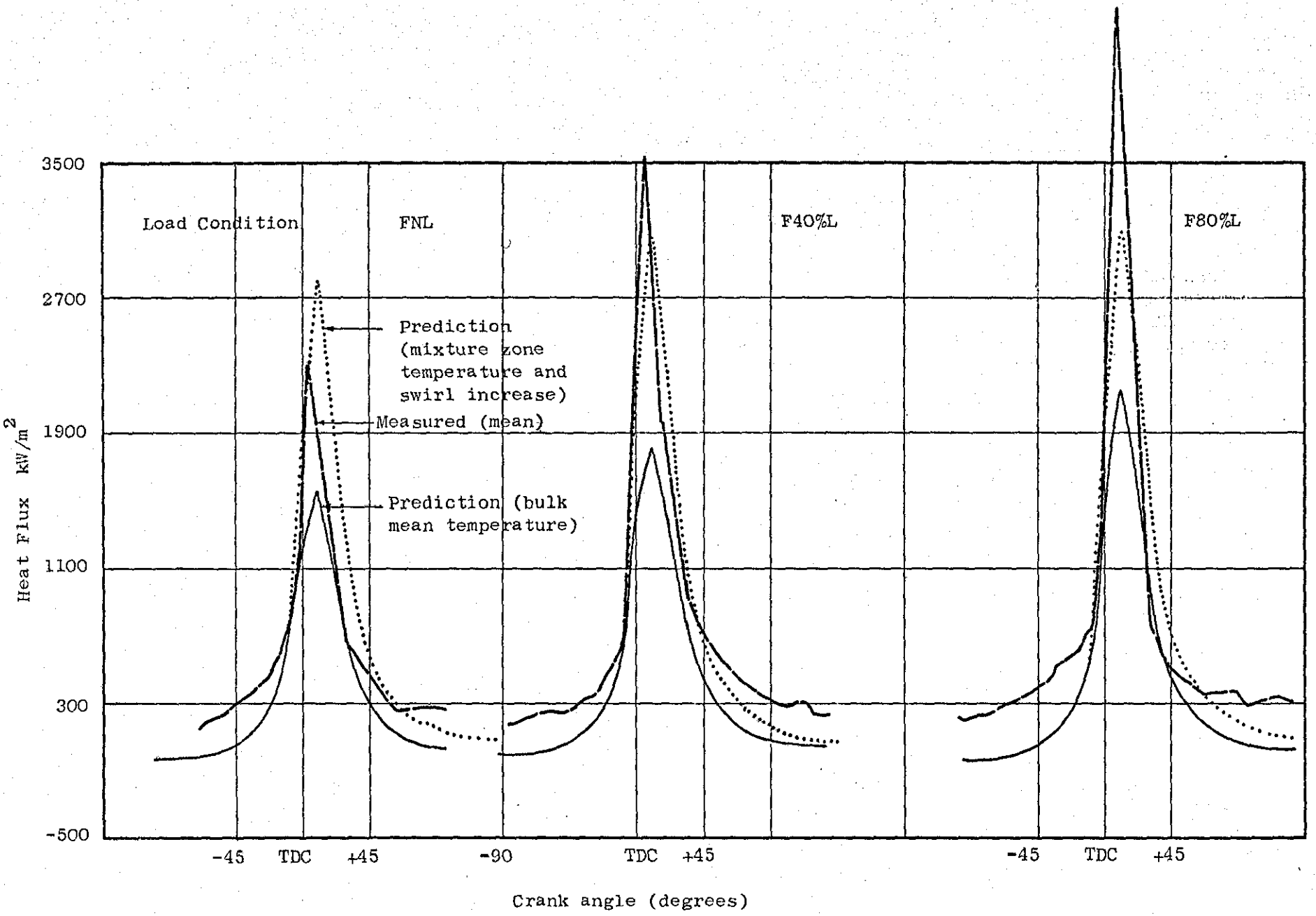

Fig. (6.43) Measured mean fluxes in piston bowl for 1050 rpm fired operation and predictions on basis of bulk mean temperature and mixture zone temperature including swirl increase by combustion

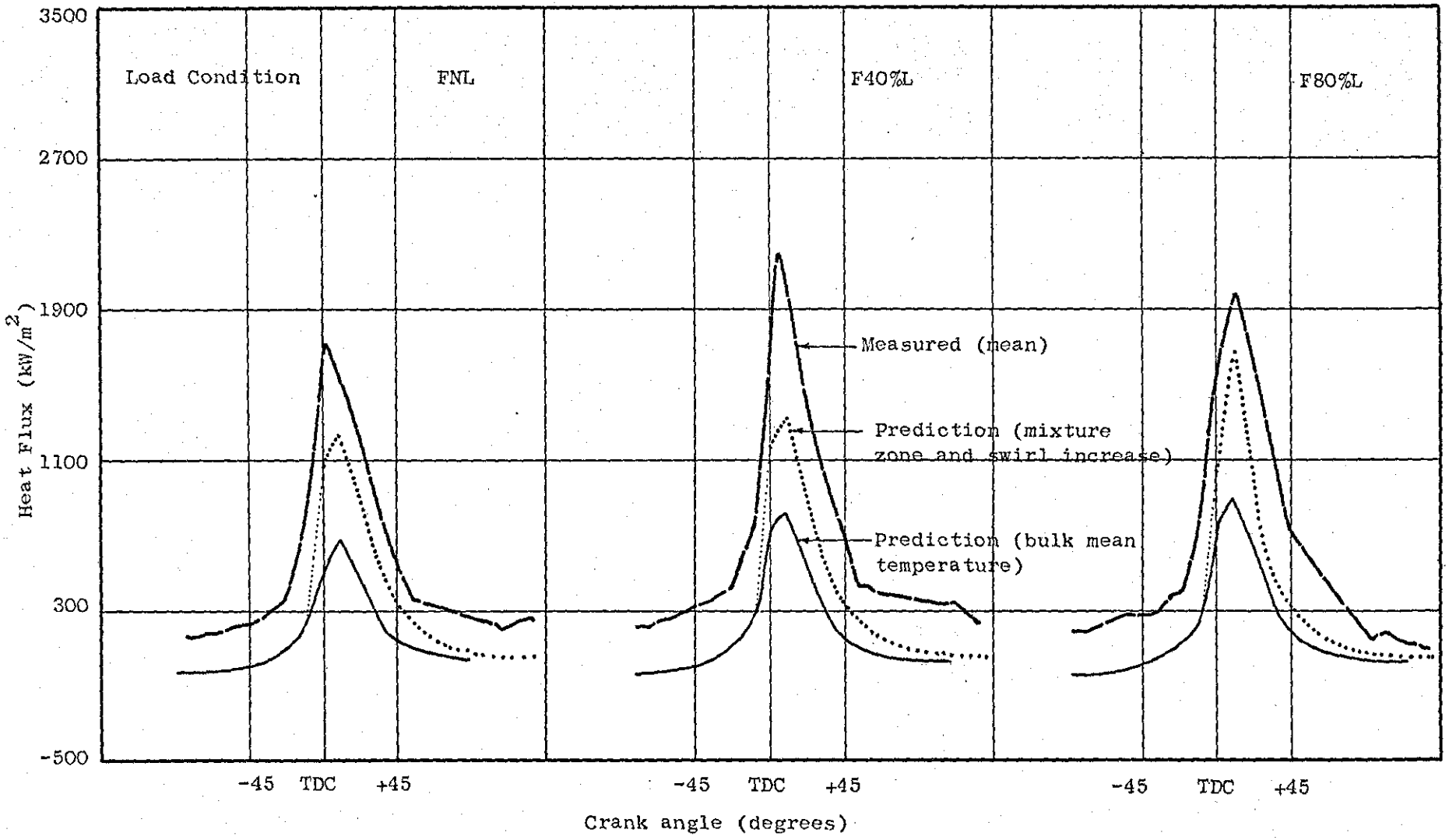

Fig. (6.44) Measured mean fluxes in piston bowl for 600 rpm fired operation and predictions on basis of bulk mean temperature and mixture zone temperature including swirl increase by combustion

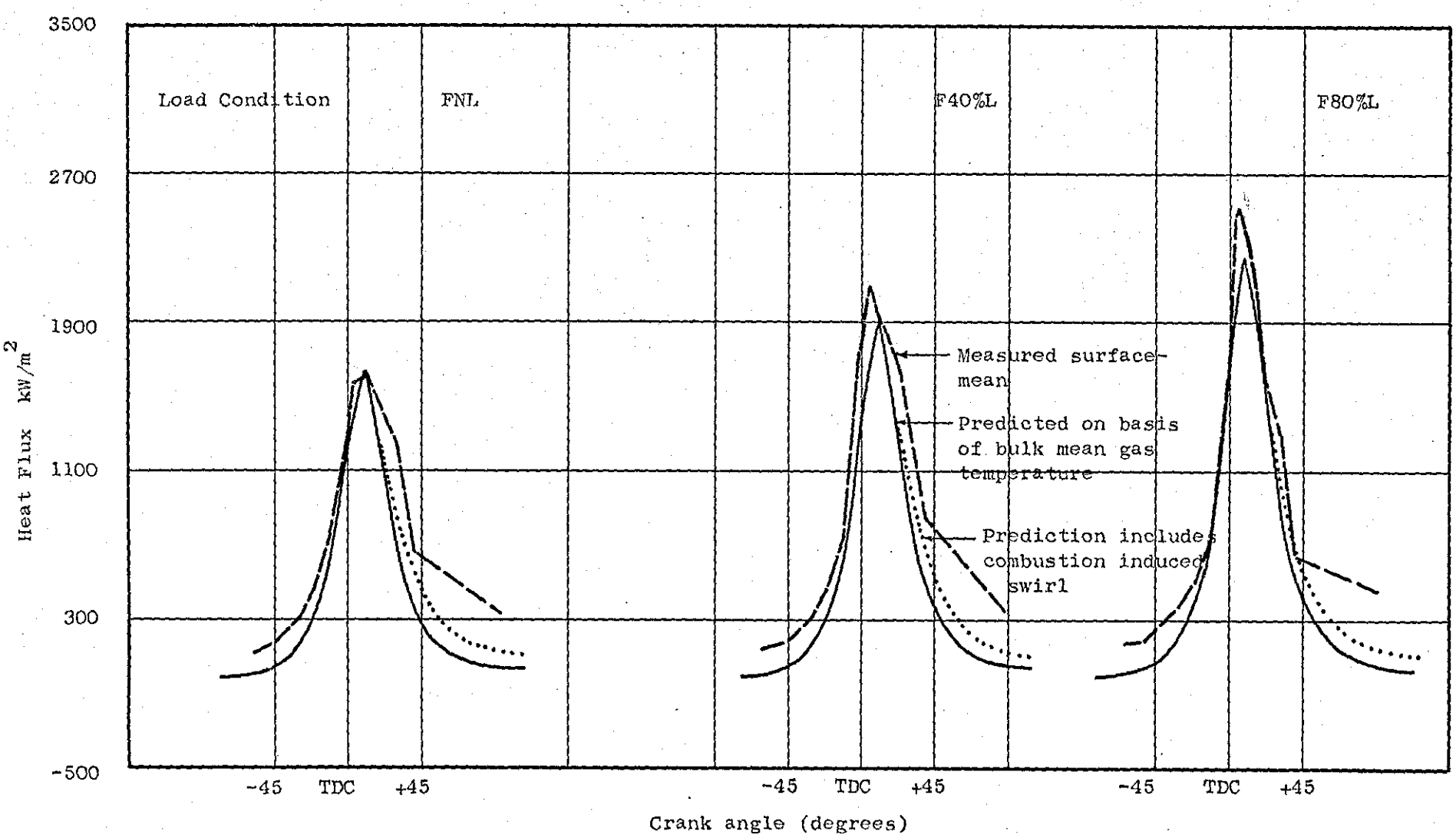

Fig. (6.45) Measured combustion chamber surface mean heat flux for 1050 rpm fired operation and prediction on the basis of bulk mean gas temperature

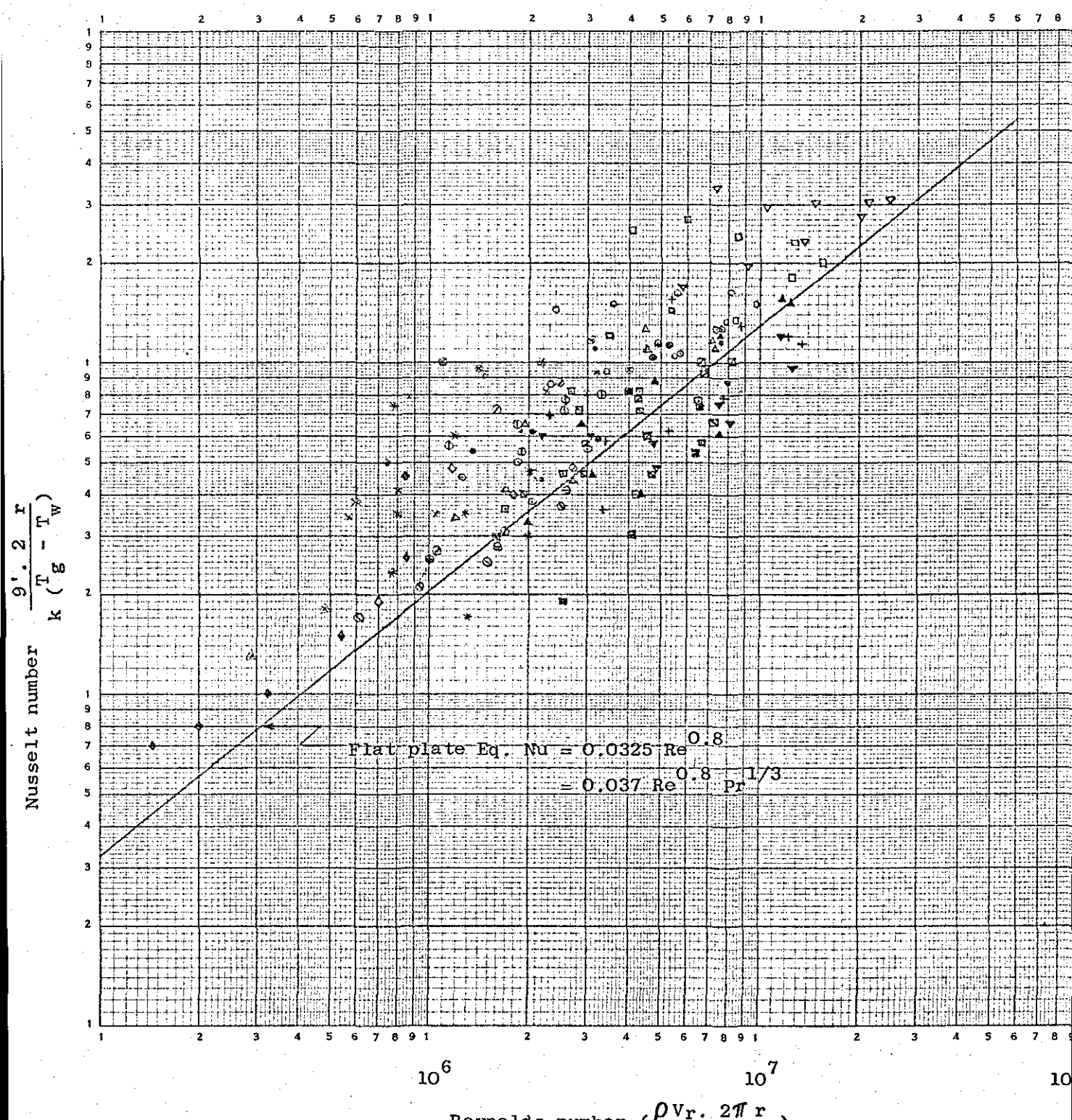

Fig. (6.46) Experimental data during 40° CA BTDC to 40° CA ATDC of motored and fired tests.

Symbols grouped at each speed as for cylinder head, piston bowl, piston (annular)

Speed condition	600	1050	1500
MOT	⊗ ⊠ ⊕	○ * ⊡	□
FNL	◈ ⊘	● ⊡	+
F40%L	⊖	⊙ ⊡	▼
F80%L	▲ ⊘	△ ◇ ■	▲
Supercharge 0.69 bar		▽	

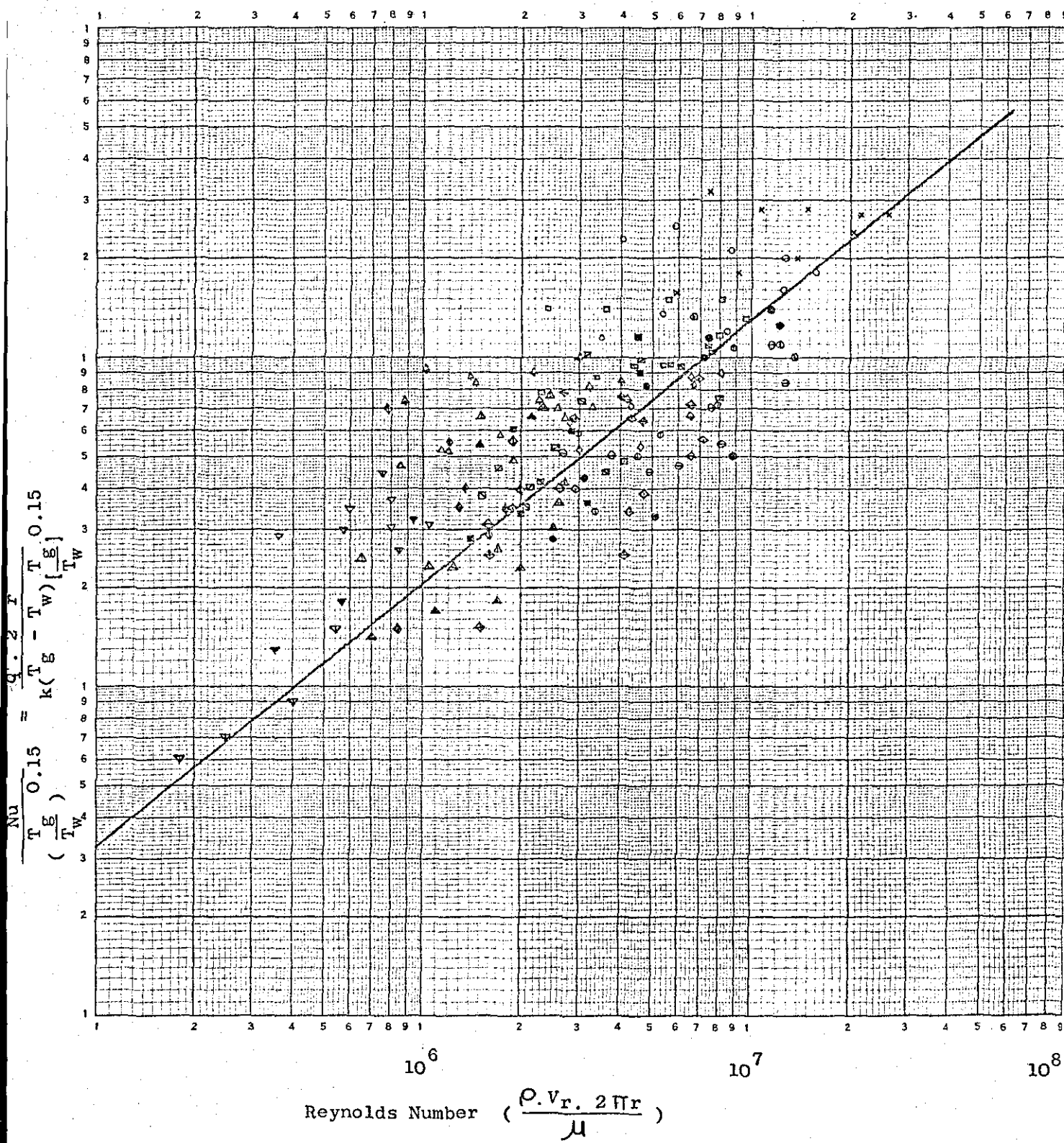

Fig. (6.47) Experimental data corrected for gas properties at gas-wall interface temperature.

Symbols grouped at each speed as for cylinder head, piston bowl, piston (annular).

Speed	600	1050	1500 rpm
Condition			
MOT	▲▽△	□◇◇	○
FNL	▼▲	⧄◈◇	◍
F40%L	△	⧅ ◇	⊖
F80%L	▼▲	■◆◇	●
Supercharge 0.69 bar	×		

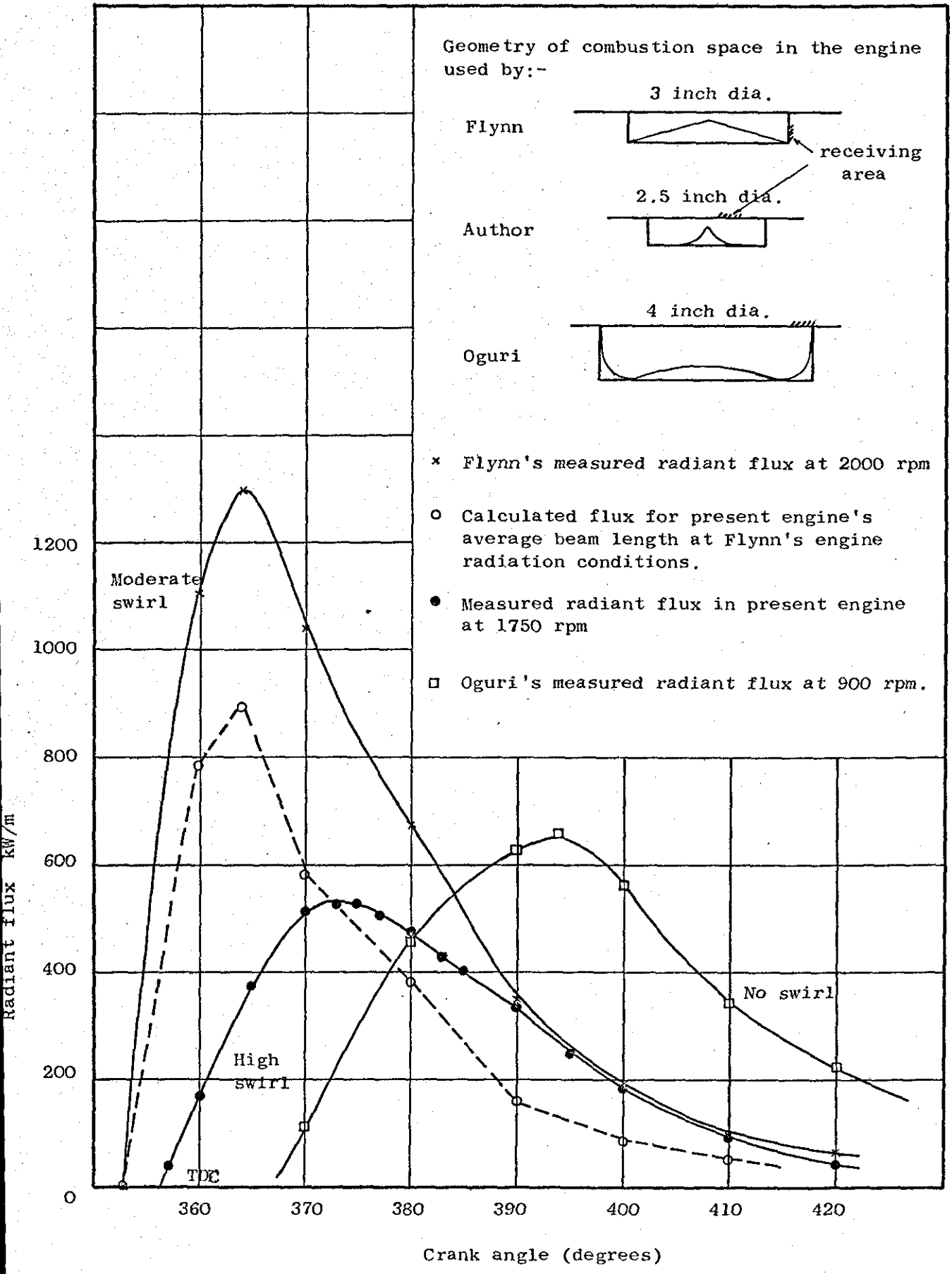

Fig. (6.48) Comparison of measured instantaneous radiant flux in three different diesel engines

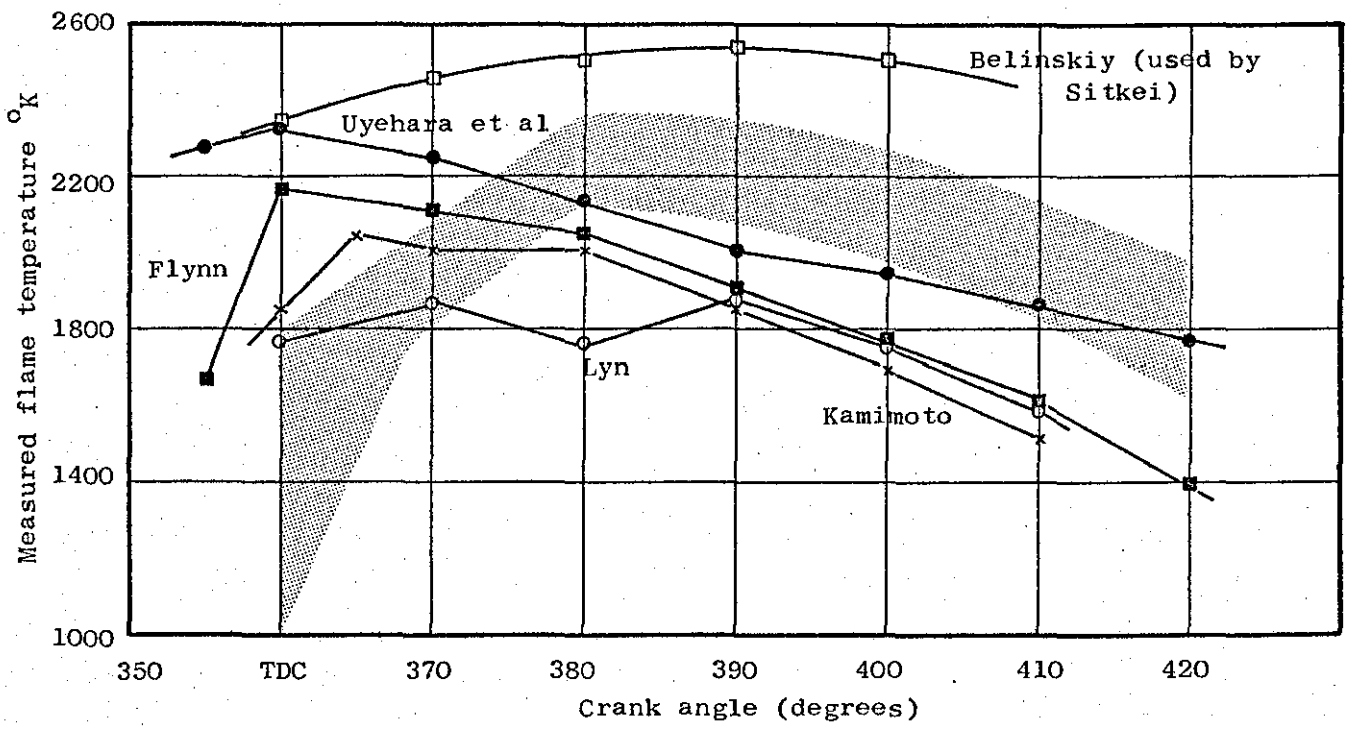

Fig. (6 49) Measured flame temperatures in diesel engines

Hot zone temperature band for different operating conditions calculated.

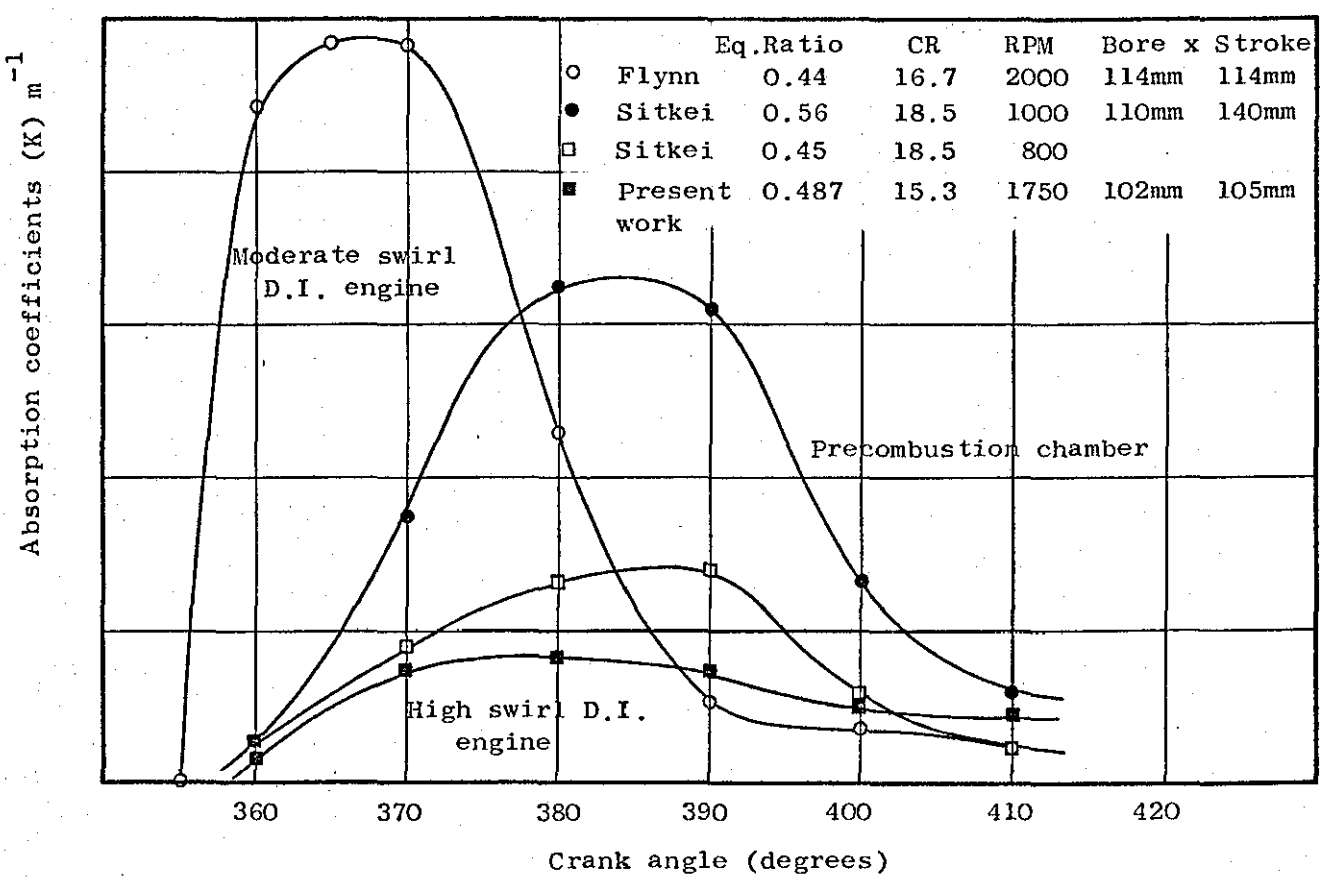

Fig. (6.50) Absorption coefficient in several diesel engines. All absorption coefficients evaluated assuming Flynn's measured flame temperature exists in the engines.

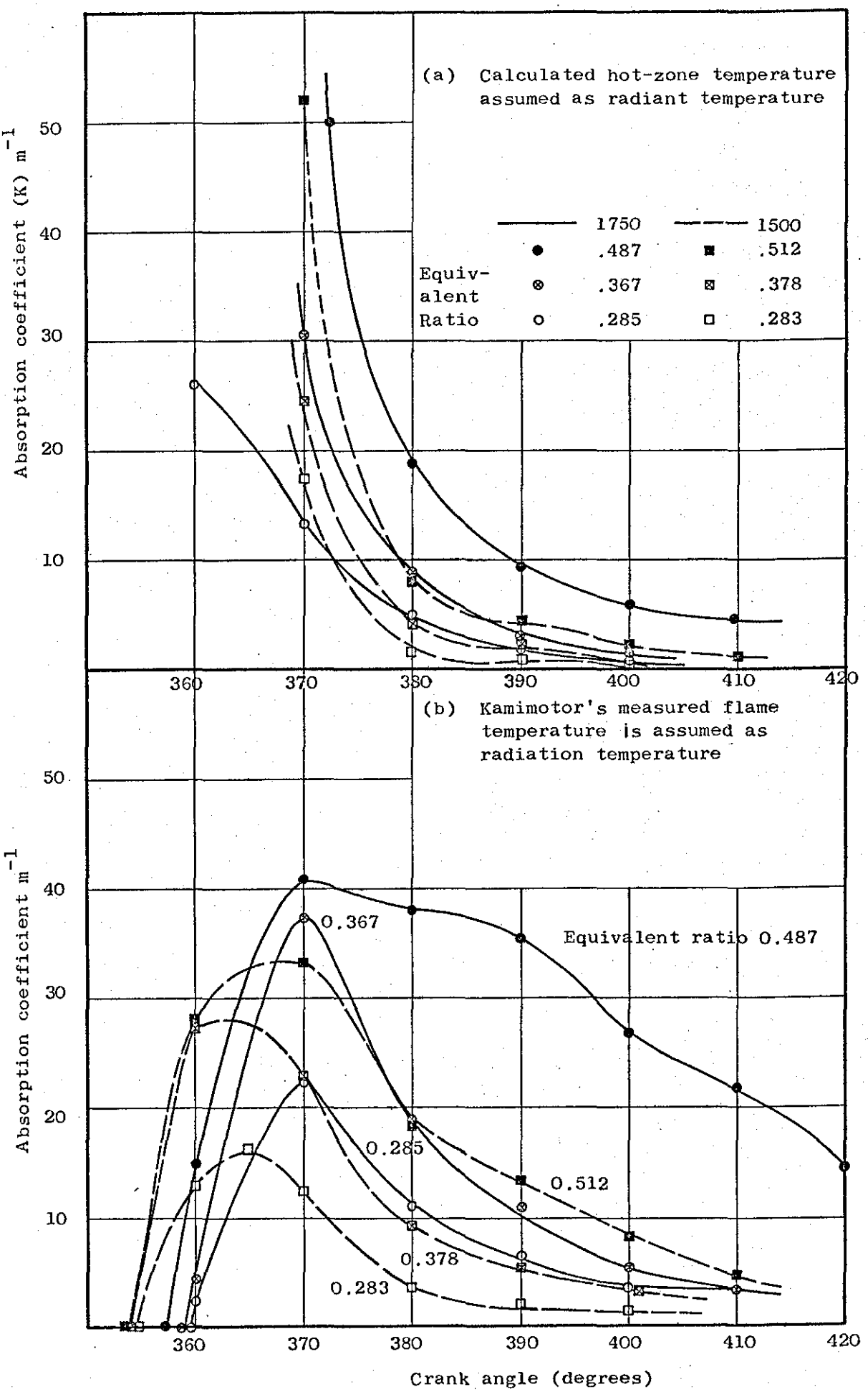

Fig. (6.51) Absorption coefficients in test engine for different running conditions. Obtained on basis of Hottel's interchange areas in a cylindrical enclosure.

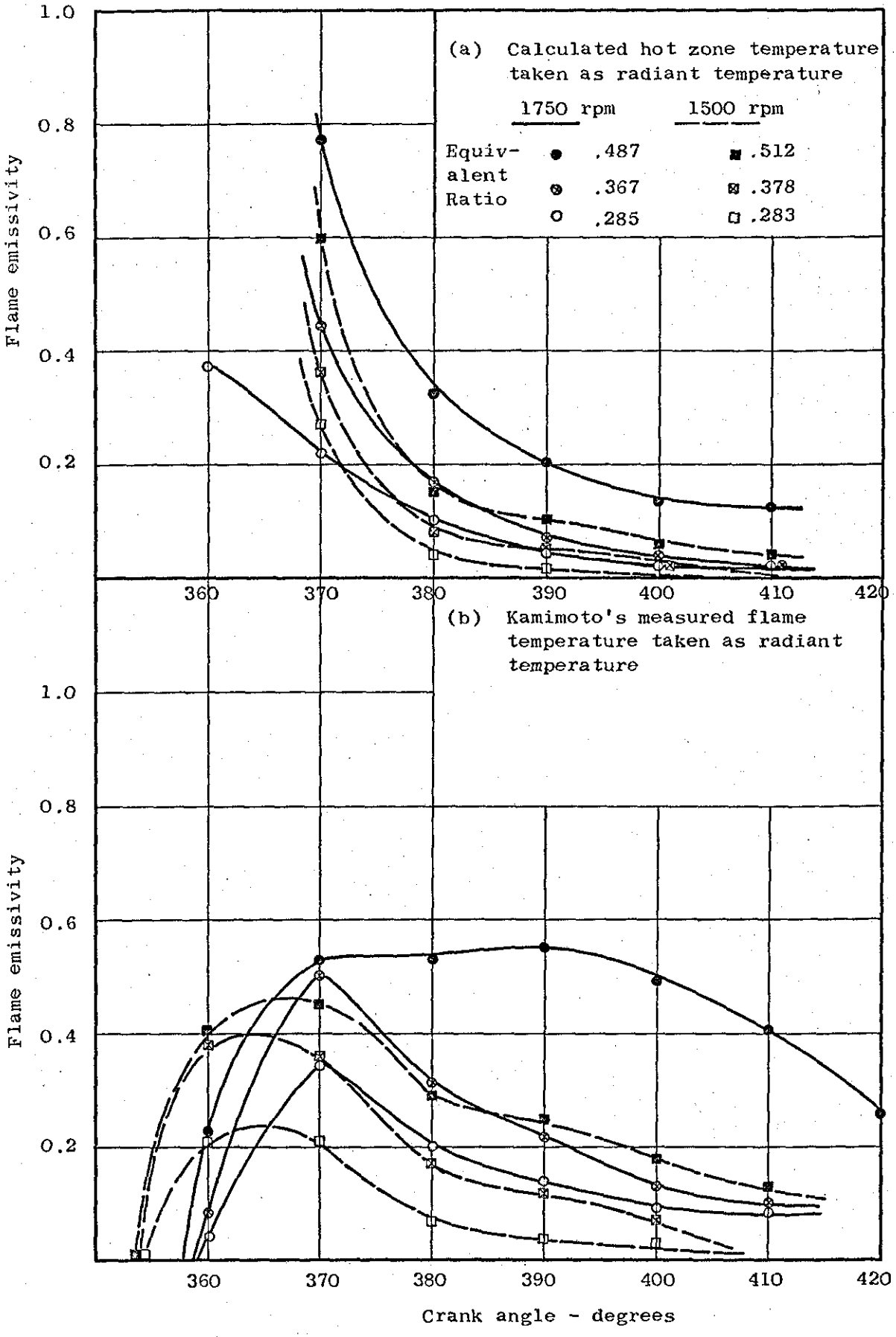

Fig. (6.52) Flame emissivities in the test engine for different operating conditions

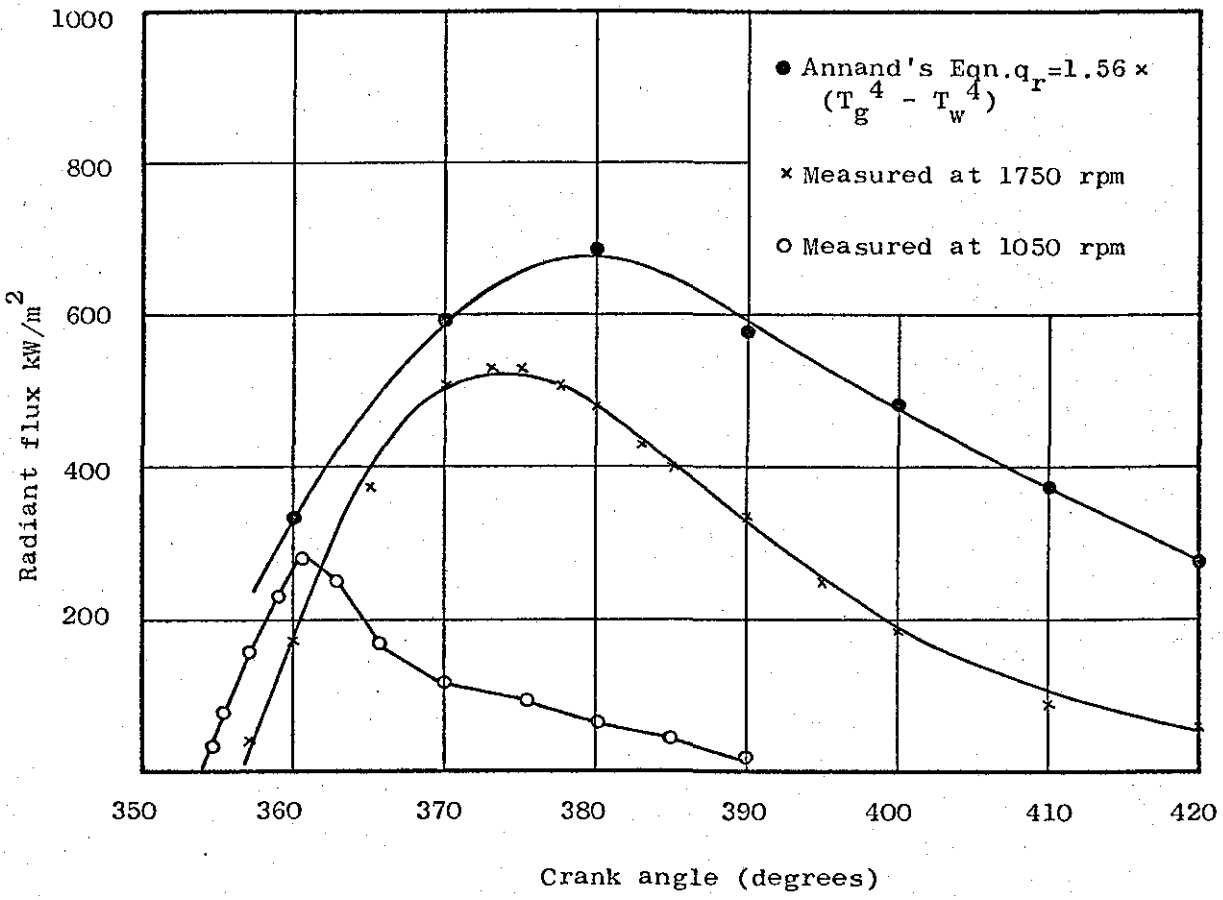

Fig. (6.53) Predicted radiant flux by radiation term in Annand's equation on the basis of bulk mean gas temperature compared with measured radiant fluxes

CHAPTER 7

CONCLUSIONS TO THE PRESENT INVESTIGATION AND SUGGESTIONS FOR FURTHER WORK

7.1 Conclusions for the Present Investigation

In this investigation, the instantaneous total and radiant heat fluxes in a high swirl diesel engine were studied experimentally and attempts made to find methods of predicting these components. In the course of the work, a surface thermocouple, suitable for measurement of instantaneous surface heat flux in the engine cylinder was developed. It was capable of responding to surface temperature changes within a period of two crank degrees at engine speeds up to 1750 rpm. The instantaneous radiant flux was measured by a ceramic pyroelectric transducer incorporated into a special circuit in order to respond to changes in radiant fluxes within a period of 1 crank degree at 1750 rpm.

The experimental observations of total heat flux demonstrate a large variation from point to point in the engine cylinder under both motored and fired conditions. Variations in local heat flux by up to 30% in the motored tests, and by up to 70% in the fired engine, reflect the magnitude of temperature gradient and local velocity variation in the cylinder, particularly under fired conditions.

Engine speed and manifold pressure influenced the measured instantaneous heat flux in approximately a linear fashion. The effect of engine speed was shown to be described by its influence on gas motion as measured by Derham (44) shown in Fig. (6.1). The significant influence of manifold pressure on total heat transfer was obvious from its effect on measured peak flux in the motored engine, which increased from 1600 kW/m^2 when naturally aspirated to 3300 kW/m^2 when at 0.69 bar supercharge. The latter peak flux was

found to be higher than most peak fluxes measured under fired conditions outside the piston bowl. High instantaneous heat fluxes (up to 4300 kW/m^2) were measured in the piston bowl (combustion chamber), compared to generally lower values observed in the annular region (2800 kW/m^2 maximum) on the cylinder head or piston surface. It was also noted that heat fluxes measured on the cylinder head remained high for longer periods in the expansion stroke than on other surfaces. These variations of flux with time and location have been shown to be qualitatively explicable in terms of probable local events during combustion.

The measured radiant heat flux also varied with location. It was found that radiant flux from the centre of the combustion chamber increased with increasing engine speed, but the opposite was observed in the annular region just outside the piston bowl. The results indicated a more efficient and concentration combustion in the central region at high speed (high swirl), with less time available for hot products to expand to the annular space. The high squish velocities measured by Derham (44) at high engine speed would drive more fuel vapour and droplets into the centre of the combustion chamber which is in agreement with the above behaviour.

Measured peak radiant fluxes reached 560 kW/m^2 at heavy load and high engine speed (1750 rpm) which amounted to 15-20% of peak total heat fluxes. Comparison based on the mean fluxes over the whole cycle showed that radiant flux represents no more than 7% of the total flux under the most favourable conditions. The contribution of heat transfer by radiation decreased as the engine speed increased, due to larger increase in convection heat transfer. The results suggest that relative importance of radiant heat transfer in high

swirl engines is much less than in lower swirl diesel engines, which according to previous researchers, obtained values of 40% (Oguri 33), 20% (Flynn 34) of the total heat transfer.

A comparison between the experimental data and correlations of Annand and Woschni showed that these could predict the surface mean heat fluxes accurately, but with adjustment of the constants in the correlations. It was obvious from the comparison that use of average piston speed, cylinder bore and bulk mean gas temperature for instantaneous surface heat fluxes, preclude the prediction of the spatial variation shown by experimental data.

Analysis of the motored data showed that the use of solid swirl motion observed in the test engine (Derham 44) in conjunction with existing heat transfer data for flat plates produced a correlation (section 2.1.3) for prediction of spatial and temporal variation of heat flux. The form of the relationship for flux at radius (r) was:

$$\dot{q} = 0.037 \frac{k}{(2\pi r)} \left(\frac{V_r (2\pi r)}{\mu} \right)^{0.8} (P_r)^{0.33} \left[T_g - T_w \right] \quad (2.6)$$

The prediction of local and area-mean heat fluxes under motored conditions was in good agreement with measured results for both cylinder head and piston surfaces, except at low engine speeds and in the central region of the piston bowl. The later discrepancy was explained by ignoring of radial (squish) velocity components which accounted for up to 60% of swirl components at and engine speed of 500 rpm (Derham 44) and caused a change in resultant velocities by up to 18% at the edge of the bowl.

In the fired engine, the bulk-mean gas temperature was found inadequate for prediction of local heat fluxes. The use of a simple two-zone temperature model based on local events (total and radiant heat fluxes) observed during combustion, produced fairly good estimates (within 15% of peak values) of measured local heat fluxes. The large discrepancy between the prediction and measurements during the expansion stroke was considered to be due to combustion influenced gas motion, which was not accounted for.

A rough estimate of combustion influenced gas motion was made on the basis of conservation of momentum between burned and unburned charge, ignoring both frictional and pressure forces. The following simple relationship was obtained for velocity of burned products in terms of known unburned gas velocity and the unburned and burned gas densities:

$$U_b = U_u \sqrt{\frac{\rho_u}{\rho_b}} \tag{6.10}$$

The value of $\sqrt{\frac{\rho_u}{\rho_b}}$ was found to be nearly constant and approximately equal to 1.4, from the time when more or less complete combustion has taken place (about 390° CA) to the exhaust valve opening. An account of gas velocity increase improved prediction of instantaneous heat flux in the expansion stroke, but was still less than measured, perhaps because of two-dimensional heat transfer influence on increasing the measured value.

It has been shown that the prediction of instantaneous surface mean heat flux (for the whole cylinder area) on the basis of bulk mean temperature and measured velocity of charge is possible if one

included the effect of low heat fluxes expected on the cylinder liner. This is the reason for low heat fluxes predicted by previous correlations when compared with measured fluxes obtained on cylinder head or piston.

Analysis of the measured radiant flux in the present test engine and comparison with the findings of other investigators (Flynn and Sitkei) reported results, indicate that absorption coefficients of the flame are lower in the high swirl engine (present study) than observed in moderate swirl engines (Flynn 34) or prechamber engines (Sitkei 23). This observation was associated with less soot formation in high swirl engines where fuel-rich zones are less likely. The latter argument is supported by the findings of Macfarlane and Holderness (45) and Khan et al (64). The results suggested that the quality of mixture formation and combustion affects the concentration of carbon particles and, as a result, the radiation capacity of the flame. The quality of combustion affects the radiation period as well. The better the combustion, the shorter the flame radiation period. Therefore it is concluded that engine speed affects flame radiation as much as it modifies the quality of combustion and fuel distribution.

A survey of relevant literature showed that flame temperature measured in different types of diesel engines is approximately the same (Fig.6.49 and vary little with engine load. Accepting this fact and using the knowledge gained from measurements of instantaneous radiant flux in ordinary and prechamber diesel engines (Flynn, Oguri and Sitkei) and from present investigation in a high swirl diesel engine which covers a reasonable range. The estimated flame absorption coefficients K and its variation in these engines could be used in conjunction with estimated flame temperatures to predict fairly

accurately the radiant flux in similar engines. The flame emissivity (assuming an equivalent grey body) can be calculated accounting for combustion chamber shape, by the relationship:

$$\epsilon = 1 - e^{-KL} \tag{2.30}$$

in which $L = 3.6\ V/A$ in the equivalent beam length of the radiating gas mass, and the radiant flux by:

$$q_R = \epsilon\ \sigma\ T_F^4 \tag{2.29}$$

7.2 Suggestions for Further Work

The present investigation of instantaneous heat transfer and the use of instantaneous gas velocity has thrown some light on the possibility of predicting local heat fluxes inside the engine cylinder. Therefore in order to enable heat transfer calculations, methods of relating gas motion to engine geometry and running conditions must be developed for different types of engines, such as demonstrated by Dent and Derham (62) for the present high swirl diesel engine.

A further improvement as regards heat flux calculations could be reached by the study of flame development in the cylinder and direct measurements of instantaneous local soot concentration. The flame development could be investigated either by high speed photography, or by using ionization probes. The application of the latter method is in progress at Loughborough University (Mechanical Engineering Department). The measurement of soot concentration can be achieved by using ultra-violet light absorption method together with high speed photography to record a film calibration image as applied by Greeves and Meehan (95). Once this information is available, a direct correlation between radiant flux (measured simultaneously) and soot concentration can be obtained. The flame development would also allow for more accurate prediction of local convective heat flux.

Some aspects of the work reported here could be investigated further:

1) The low fluxes observed in the thin annular space under motored and fired conditions were related to low gas temperature in this space compared to the central zone.

This can be verified readily for motored operation by using resistance thermometers located at different regions.

2) The ionization probes (ion generator pick up) used by Ohigashi et al (50) for swirl measurement in motored engines, may be developed for application to fired engines. The success of detection of the probe under fired condition would provide valuable results on the magnitude of combustion induced gas motion. The development of this device is also in progress in the Mechanical Engineering Department, Loughborough University of Technology.

3) The effect of swirl (other parameters being the same) on flame radiation in diesel engines is necessary to distinguish its effect from any possible effect of engine speed observed in the present investigation. The results could then be related to fuel-air entrainment.

Now that a sensitive thermocouple can be manufactured, a better understanding of the convective heat transfer under controlled dynamic conditions may be obtained. The simultaneous measurements of the instantaneous surface heat flux together with instantaneous gas velocity (using hot wire anemometer) and gas temperature (using a resistance thermometer) in close proximity of the thermocouple junction, would provide a more accurate correlation between heat flux and gas conditions near the surface. Such a combined probe could be fixed in a reciprocating engine where, induction induced gas swirl could be varied or avoided. The effect of individual parameters, such as rate of compression, gas motion and their effect upon the phase lag between heat flux and driving parameters can be studied.

REFERENCES

1. Nusselt, J.F. "Die Warmeubergang in den Verbrennungs-kraftmaschinen', Z. Ver.dtsch.Ing.1923, Vol. 67, 692 and 708.

2. Woschni, G. "A Universally Applicable Equation for the Instantaneous Heat Transfer Coefficient in the Internal Combustion Engine" S.A.E. Paper 670931, 1967.

3. Chirkov, A.E. Stefanovski,B.S. "O dominiruyuschem sposbye pyeryedachi tepla v tsilindrach dvigatyelyei vnutryennyevo sgoraniya" Trudy Rostovsjova Instituta Injyenyerov Jyelyeznodorovonova Transporta 1958, 21.

4. Eichelberg,G. "Temperaturerlauf und Warmespannung in Verbrennungsmotoren" Forsch.Ing.Wes. 1923, No. 263.

5. Eichelberg, G. "Some New Investigations on Old Combustion Engine Problems" Engineering, Lon. 1939, Vol. 148, 463 and 547.

6. Annand,W.J.D. "Heat Transfer in the Cylinder of Reciprocating Internal Combustion Engines" Proc.Inst.Mech.Engrs. 1963, Vol.177, 973

7. Eichelberg,G. Pflaum, W. "Untersuchung eines hochaufgeladenen Dieselmotors" Z.Ver.dtsch.Ing. 1951, Vol. 93, 1113, English Translation in Mot. Ship 1952, Vol. 33, 18 and 58.

8. Pflaum, W. "New Investigations and Experience Relating to the Turbocharging of Large Two Stroke Engines" Cimac-A.11, 1962

9. Taylor, C.F. "Heat Transmission in Internal Combustion Engines" Proc. General Discussion on Heat Transfer. Inst. Mech.Engrs, London 1951, 397.

10. Pfriem, H. "Der Periodische Warmeubergang Beiklenen Druckschwonkungen" Forchg. Geb. Ing. Vol. 11 (1940) 67-75 (Translated in N.A.C.A. Technical Memorandum 1048)

11. Taylor, C.F. Toong, T.Y. "Heat Transfer in Internal Combustion Engines" Amer. Soc. Mech. Engrs. 1957, Paper No. 57-HT-17

12. Elser, K. "Der Instationare Warmeubergang in Diesel motoren" Mitt Inst. Thermodyn. Zurich, 1954, No. 15.

13. Oguri, T. "On the Coefficient of Heat Transfer Between Gases and Cylinder Walls of the Spark-Ignition Engines" Bull.Jap.Soc. Mech. Engrs. 1960, Vol. 3, 363

14. Overbye, V.D. Bennethum,J.E. Uyehara, O.A. Myers, P.S. "Unsteady Heat Transfer in Engines". Trans. Soc. Automot. Engrs. N.Y. 1961, Vol.69, 461.

15. Annand, W.J.D. Ma, T.H. "Heat Transfer in Compression Ignition Engines" Proc. Inst.Mech.Engrs. Vol. 185, 72/71, 1970-71

16. Knight, B.E. "The Problem of Predicting Heat Transfer in Diesel Engines", Proc. Inst. Mech.Engrs. 1964-65, Vol.179 (Pt. 3C)

17. Ma, T.H. "Instantaneous Heat Transfer in an Internal Combustion Engine". PhD Thesis, University of Manchester Institute of Science and Technology, (UMIST) 1969.

18. Henein, N.A. "Instantaneous Heat Transfer Rates and Coefficients between the Gas and Combustion Chamber of a Diesel Engine". S.A.E. Int. Auto. Eng. Congress, 1965, Paper 969B.

19. Alcock, J.F. "Air Swirl in Oil Engines" Proc. I.Mech.E. London, 1934, Vol. 128

20. Le Feuvre, T. Myers, P.S. Uyehara, O.A. "Experimental Instantaneous Heat Fluxes in a Diesel Engine and Their Correlation" S.A.E. Trans. Vol. 78, 1969, Paper 690464.

21. Alcock, J.F. Robson, J.V.B. Mash, C. "Distribution of Heat Flux in High Duty Internal Combustion Engines" Proc. Congres International des Machines a'Combustion, Zurich, 1957

22. Wendland,D.W. "The Effect of Periodic Pressure and Temperature Fluctuations on Unsteady Heat Transfer in a Closed System". N.A.S.A.-CR-72323, 1968.

23. Sitkei, G. Ramanaiah, G.W. "A Rational Approach for Calculation of Heat Transfer in Diesel Engines. S.A.E. Trans. 1972, Paper 720027.

24. Sitkei, G. "Contribution to the Theory of Heat Transfer in the Internal Combustion Engine" Konstruction. Vol. 14, No. 2(Feb. 1962) pp67-71

25. Belinskiy,L.M. "Thermal Radiation in the Chamber of a High Speed C.I. Engine" Trudy NILD, No. 1, 1955, Moscow.

26. Alcock, J.F. "Heat Transfer in Diesel Engines" Proc. Int. Heat Transfer Conference, Boulder, Instn. Mech.Engrs. London, 1961, 174.

27. French, C.C. "Design Problem of Heat Transfer" Auto Design. Ebg. Feb. 1963, 42-46

28. Brock, E.K. Glasspoole,A.J. "The Thermal Loading of Cylinder Head and Piston in a Medium Speed Oil Engine" I.Mech.E. Lond.Proc.Syp.Birmingham October 1964.

29. French, C.C. Hartles, E.R. "Engine Temperature and Heat Flow Under High Load Conditions" Proc.Inst.Mech.Engrs. Vol. 179, 1964-65 (Pt. 3C)

30. Steel, S. Wharton, A. Roeder,G.H. "Infrared Radiation from Otto Cycle Engine Explosion's Engineering" January 1936.

31. Lyn, W.T. "Diesel Combustion Study by Infrared Emission Spectroscopy" Journal of the Inst. of Petroleum, Vol. 43, No.398 Feb. 1957.

32. Ebersole, G.D. Myers, P.S. Uyehara, O.A. "The Radiant and Convective Components of Diesel Engine Heat Transfer" S.A.E. NY Paper, No. 701C 10-14 June 1963

33. Oguri, T. Inaba, S. "Radiant Heat Transfer in Diesel Engines" S.A.E. 1972, Paper 720023

34. Flynn, P. Mizusawa, M. Uyehara, O.A. Myers, P.S. "An Experimental Determination of the Instantaneous Potential Radiant Heat Transfer Within an Operating Diesel Engine" S.A.E. Trans. 1972, Paper 720022

35. Wendland, D.W. "The Effect of Periodic Pressure and Temperature Fluctuation on Unsteady Heat Transfer in a Closed System" NASA-CR-72323, 1968.

36. Walker, G. "Heat Transfer in a Gasoline Engine" The Engineer, Nov.24 1967, p690.

37. Hassan, H. "Unsteady Heat Transfer in a Motored Internal Combustion Engine" PhD Thesis, Loughborough University of Technology, 19

38. Bourne, E. "An Investigation of the Thermodynamic Performance of I.C. Engines with Particular Reference to Overall and Localised Heat Transfer" PhD Thesis, Leeds University, 1967.

39. Law, A.G. "Instantaneous Heat Transfer in an Opposed-Piston Two-Stroke Diesel Engine" PhD Thesis, UMIST, 1968.

40. Kim Dao Uyehara, O.A. Myers, P.S. "Heat Transfer Rates at Gas-Wall Interface in a Motored Piston Engine" S.A.E. Trans. Vol. 82, Sec.3(1973) Paper 730632

41. Willis, D.A. "Mapping of Air Flow Patterns in Engines with Induction Swirl" S.A.E. Trans. Vol. 75 (1967) Paper 660093.

42. Myers, P.S. Uyehara, O.A. Wilson, L.A. Watson, K.M. "Flame Temperature Measurements in Internal Combustion Engines" ASME Trans. Vol. 68 (1946) pp17-30

43. Hottel, H.C. Broughton,F.P. "Determination of True Flame Temperature and Total Radiation from Luminous Gas Flames" Industrial and Engineering Chemistry. Analytical Edition, Vol.4 1932, pp166-175.

44. Derham, J.A. "Air Motion in a Four Stroke Direct Injection Diesel Engine" PhD Thesis, Loughborough University of Technology, 1972.

45. Macfarlane,J.J. Holderness,F.H. "Laboratory Studies of Carbon Formation in Fuel-Rich Flames at High Pressures" Proc.Inst.Mech.Eng.Vol. 184, No.31 (1969-70)

46. Kunitomo,J. Kodama, K. "Radiation from Luminous Flames at High Pressures (Spray Combustion of Liquid Fuels). Bulletin of the JSME, Vol. 17, No. 113, Nov. 1974, p1486.

47. Maesawa, M. Tonaka, Y.O. Tsukamoto, Y. "Radiation from Luminous Flames of Liquid Fuel Jets in a Combustion Chamber" 12th International Symposium on Combustion, 1968, pp1229-1237

48. Thring, M.W. Beer, J.M. Foster, P.J. "The Radiative Properties of Luminous Flames" Inst.Mech.Engrs. Proc. 3rd Int. Heat Transfer Conf. Chicago, Aug. 1966, Vol. 5, A.I.Cho.E., N.Y. 1966, pp101-111.

49. Kamimoto, T. Matsuoka, S. Matsui, Y. Aoyagi, Y. "The Measurement of Flame Temperature and the Thermodynamic Analysis of Combustion Process in a Direct Injection Diesel Engine" Inst. Mech.Engrs. Paper C96/75. 1975.

50. Ohigashi, S. Hamamoto, Y. Tanabe, S. "Swirl - Its Measurement and Effect on Combustion in a Diesel Engine" Instn. Mech. Engrs. Paper C134/71.

51. Hottel, H.C. "Radiant Heat Transmission" Chapter III in Ref. (55)

52. Hottel, H.C. Sarofim, "Radiative Transfer," McGraw Hill, 1967.

53. Jakob, M. "Heat Transfer" John Wiley and Sons Inc. Vols. I and II 1957.

54. Gaydon, A.G. Wolfhard, H.G. "Flames, Their Structure, Radiation and Temperature" Chapman and Hall Ltd. Third Edition, 1970.

55. McAdams, W.H. "Heat Transmission" Third Edition, McGraw Hill Book Co. New York and London (1954).

56. Planck, M. "The Theory of Heat Radiation" New York, Dover Publications, 1959.

57. Hottel, H.C. Edgberg, R.B. "The Radiation of Furnace Gases" Trans. ASME, Vol. 63, 297 (1941), pp297-307.

58. Hudson, R.D. "Infrared System Engineering" John Wiley and Sons. Inc. 1969.

59. Willardson,R.K. Beer, A.C. "Semiconductors and Semimetals" Vol. 5, Infrared Detectors, Academic Press, 1970.

60. Huber, P. Brown, J.R. "Computation of Instantaneous Air Flow and Volumetric Efficiency" S.A.E. Auto. Engng. Congress, Paper 812B, 1964.

61. Lyn, W.T. "Calculation of the Effect of Rate of Heat Release on the Shape of Cylinder Pressure Diagram and Cycle Efficiency". IMechE. 'Automotive Div' Proc. 1960-61, pp34-45.

62. Dent, J.C. Derham, J.A. "Air Motion in a Four Stroke Direct Injection Engine" IMechE Proc. 1974, Vol. 188, 21/74.

63. Whitehouse,N.D. "Heat Transfer in a Quiescent Chamber Diesel Engine" Proc. IMechE. 1970-71. Vol. 185, 72/71

64. Khan, I.M. Greeves, G. Wang, C.H.J. "Factors Affecting Smoke and Gaseous Emission from Direct Injection Engines and a Method of Calculation" International Automotive Engng. Congress, Detroit, Mich Jan. 8-12, 1973. S.A.E. Paper 730169.

65. Morris, C.J. "The Modelling of Fuel Dispersion and Concentration in Direct Injection Diesel Engines" PhD Thesis, Loughborough University of Technology, 1975

66. Furaham, S. Enomoto, Y. "Piston Temperature of Automobile Gasoline Engine in Driving on the Road" Bulletin of the JSME, Vol. 16, No. 99, Sept. 1973, p385

67. Hovarton, M. "Beitrag Zur Awendung Des Hitzdraht-Anemometers for Stromungs Und Turbulenzmessungen in Ver Brennungs Motoren" Dr. Ing. Thesis, Technical University, Munich, 1971.

68. Schmidt, F. "The Internal Combustion Engine" Chapman and Hall 1965.

69. Annand, W.J.D. "Heat Transfer from Flames in Internal Combustion Engines" Chapter 24 in "Heat Transfer in Flames" edited by Afgan, N.H. and Beer, J.M., Halsted 1974.

70. Sulaiman, S.J. "Design and Development of a Special Surface Thermocouple" Report. Dept. Mech. Engng. Loughborough University of Technology, 1976.

71. Hackemann, P. "A Method for Measuring Rapidly Changing Surface Temperatures and its Application to Gun Barrels" Theoretical Research Translation, 1/46 Armament Research Department.

72. Bendersky, D. "A Special Thermocouple for Measuring Transient Temperature" 1953 Mech. Engng. Vol. 75, p117.

73. Burger, Van Cittert (Quoted in reference 76), 1930, Z.Phys. Vol. 66, 210.

74. Morrison, R.D. Lachenmager, R.R. "Thin Film Thermocouples for Substrate Temperature Measurement" 1963, Rev. Sci.Instrum, Vol.34, 106.

75. Hall, J.G. Hertzberg, A. "Recent Advances in Transient Surface Temperature Thermometry" Jet Porpulsion, 719-723 (Nov. 1958).

76. Marshall, R. Atlas, L. Putner, T. "The Preparation and Performance of Thin Film Thermocouples" J.Sci. Instrum, 1966, Vol. 43, 144.

77. Winding, C.C. Topper, L. Baus, B.V. "Metal-Film Resistance Thermometer for Measuring Surface Temperature" Industrial and Engng. Chemistry, Vol. 47, No. 3, 1955.

78. Laderman, A.J. Hecht, G.J. Oppenheim, A.K. "Thin Film Thermometry in Detonation Research" Temperature, Its Measurement and Control in Science And Industry. Vol. 3, Part 2, 1962.

79. Willeke, K. Bershader, D. "An Improved Thin Film Gauge for Shock-Tube Thermal Studies" The Review of Scientific Instruments, Vol. 44, No. 1 January 1973.

80. Holland, L. "Vacuum Deposition of Thin Films" Chapman and Hall, London 1956.

81. Siddall, G. "Vacuum deposition of dielectric films for Capacitors"

82. Ritter, E. Hoffmann, R. "Influence of Substrate Temperature on the Condensation of Vacuum Evaporated Films of MgF_2 and ZnS" J.Vac.Sci.Technol. Vol. 6 (1969) 773.

83. Carslaw, H.S. Jaeger, J.C. "Conduction of Heat in Solids" Oxford University Press, 1947.

84. Moeller, F.E. "Thermocouples for the Measurement of Transient Surface Temperature" Temperature, Its Measurement and Control in Science and Industry, Vol. 3, Part 2, 1962.

85. Vidal, R.J. "Transient Surface Temperature Measurements" Cornell Aeronaut. Lab. No. IM-1062-A-1.

86. Johns, G. "The Production of a Transient Surface Temperature Thermocouple" Final Year Project Report, Loughborough University of Technology, May 1971.

87. Wing, R.D. Saunders, O. "Oil Film Temperature and Thickness Measurements on the Piston Rings of a Diesel Engine" Inst. Mech. Engs. Proc. 1972, Vol. 186, 1/72.

88. Bendict, R.P. Russo, R.J. "A Note on Grounded Thermocouple Circuits" ASME Trans. Vol. 94, No. 2, June 1972.

89. Powell, R.W. "Correlation of Metallic Thermal and Electrical Conductivities for both Solid and Liquid Phases" Int. J. Heat Mass Transfer, Vol. 8, pp1033-1045.

90. Jamieson, J.A. "Infrared Physics and Engineering" McGraw Hill, 1963.

91. Kimmitt, M.F. Ludlow, J.H. Putley, E.H. "The Use of a Pyroelectric Detector to Measure Q-Switch CO2 Laser Pulse" Proc. IEEE, Vol. 56, 1250, 1968.

92. Cooper, J. "A Fast Response Pyroelectric Thermal Detector" J. Sci. Instrum. 1962, Vol. 39, p467.

93. Glass, A.M. "Ferroelectric Sr_{1-x} Ba_x Nb_xO as a Fast and Sensitive Detector of Infrared Radiation" Applied Physics Letters, Vol. 13, No. 4, 15 Aug. 1968.

94. Sulaiman, S.J. "Infrared Radiation Detector and the Pyroelectric Device in Particular" Departmental Report, 1976.

95. Greeves, G. Meehan, J.O. "Measurement of Instantaneous Soot Concentration in a Diesel Engine" Inst. Mech. Engrs. Paper C88/75, 1975, pp73-81

96. Wiebelt, J.A. "Engineering Radiation Heat Transfer" Holt Rinehart, and Winston, Inc. 1966.

97. Kays, W.M. "Convective Heat and Mass Transfer" McGraw Hill, 1966.

98. Eckert, E.R.G. Drake, R.M. Jr. "Analysis of Heat and Mass Transfer" McGraw Hill, 1972.

99. Schlichting,H. "Boundary Layer Theory" 6th Ed. McGraw Hill, New York, 1968.

APPENDIX (A)

EVALUATION OF INSTANTANEOUS HEAT FLUX FROM WALL TEMPERATURE MEASUREMENTS

The temperature variation in the working fluid causes cyclic variation of the heat flux into the exposed wall surface, and this is reflected in cyclic variation of the surface temperature which is recorded. It is supposed that heat flow through the cylinder wall is effectively one-dimensional (normal to the surface) at the location chosen. Thus the heat flow within the wall is represented by the Fourier equation:

$$\frac{\delta T}{\delta t} = \frac{k'}{\rho' C'} \frac{\delta^2 T}{\delta x^2} = \alpha \frac{\delta^2 T}{\delta x^2} \qquad (A.1)$$

where k' = thermal conductivity of wall material

ρ' = density of wall material

C' = specific heat of wall material

x = distance perpendicular to exposed surface.

If the temperature of the surface of the wall exposed to the working fluid is T_1 and that of the surface exposed to the coolant is T_2, we may write:

$$T_1 = B_1 + \sum_{n=1}^{\infty} (k_n \cos n\omega t + G_n \sin n\omega t) \qquad (A.2)$$

where the Fourier series represents the time-variation of the surface temperature, B_1, k_n and G_n are numerical coefficients determinate by analysis of the recorded temperature variation, and ω is the basic angular frequency of the cycle, equal to 2π times

the cycle repetition rate. We may suppose that the wall is thick enough for T_2 to be constant, $T_2 = B_2$.

The solution of equation A.1 with these boundary conditions is:

$$T = B_1 - \frac{(B_1 - B_2).x}{X} + \sum_{n=1}^{\infty} e^{-F.x} \left[k_n \cos(n\omega t - F.x) + G_n \sin(n\omega t - F.x) \right] \qquad (A.3)$$

where X = wall thickness, $F = \sqrt{(n\omega/2\alpha)}$.

Differentiation of this equation gives the temperature gradient, which multiplied by $(-k')$ gives the heat flux, the value at $x = 0$ must equal the heat flux from the gas (q/A):

$$\frac{q}{A} = k' \frac{(B_1 - B_2)}{X} + k' \sum_{n=1}^{\infty} F (G_n - k_n) \cos n\omega t + (G_n + k_n) \sin n\omega t \qquad (A.4)$$

Thus q/A can be calculated from the Fourier coefficients obtained by analysis of the wall surface temperature variation with time, using the computer program listed below. The computer program also calculated the bulk mean gas temperature from measured pressure and produced other useful data.

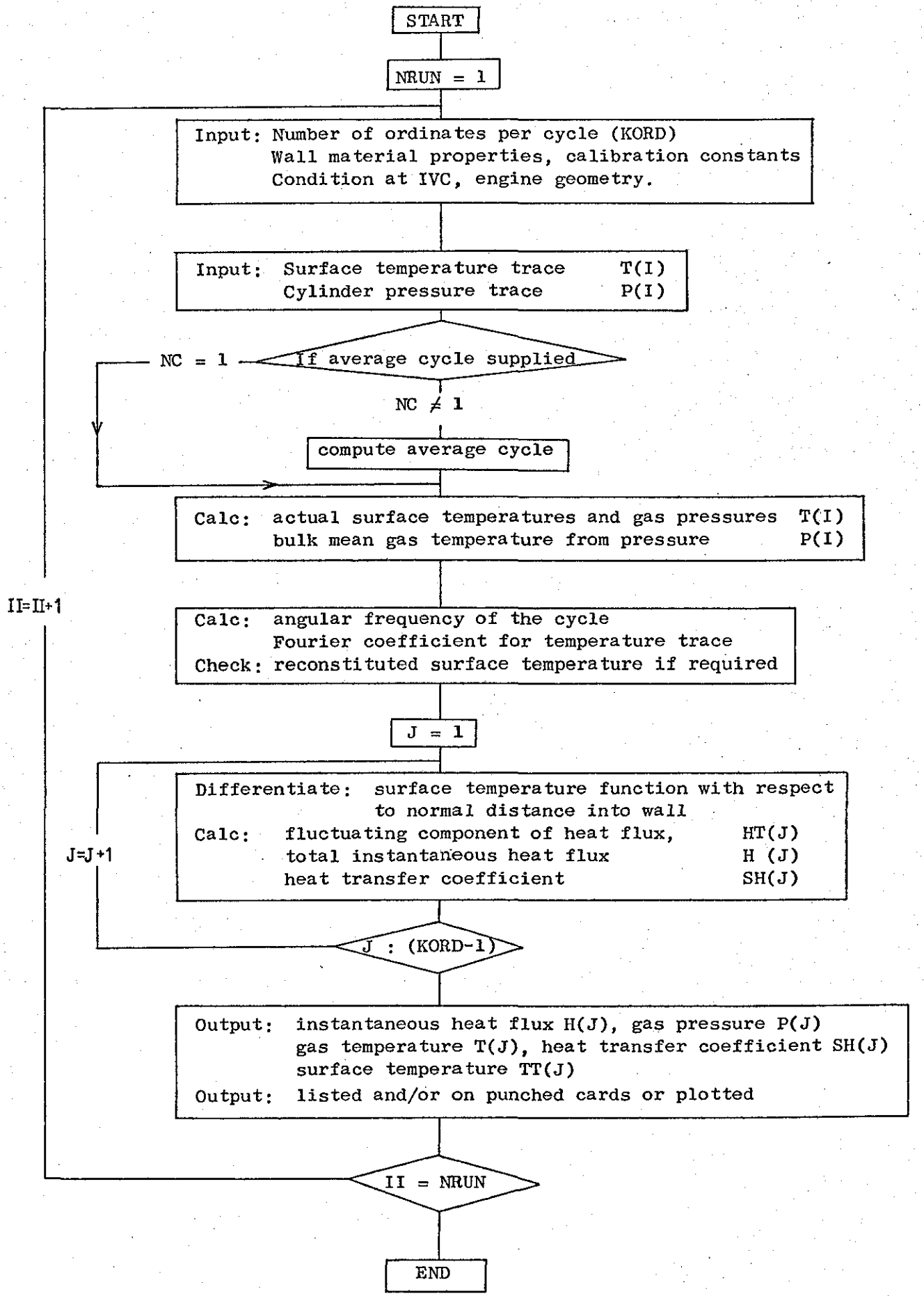

Fig. A.1 Schematic flow chart for the computation of instantaneous heat flux from surface temperature record

```
      MASTER HFO1
C        HEAT  FLUX  CALCULATIONS

C  PROGRAM CALCULATES INSTANTANEOUS HEAT FLUX FROM TRANSIENT SURFACE TEMP.
C  RECORDS FLUCTUATING TEMP. IS EXPRESSED BY FOURIER SERIES AS A FUNCTION OF
C  TIME AND DISTANCE INTO WALL X. THEN SERIES IS DIFFERENTIATED W.R.T.X. AND
C  MULTIPLIED BY CONDUCTIVITY OF WALL FOR X=0. THIS ADDED TO STEADY HEAT FLUX
C  TO GIVE TOTAL PERIODICAL HEAT FLUX AT GAS-WALL INTERFACE IN KW/MSQR.
      DIMENSION T(1000),ALP(160),BET(160),H(360),DEG(360),P(1000)
      DIMENSION RT(350),BE(160),AP(160)
      DIMENSION TG(300),SH(300),HT(300),ST(300)
      DIMENSION TT(350)
      DIMENSION TA(1000)
      DIMENSION V(300)
      INTEGER KORD,MRT,MLIN,NADJ,NRDNG
      READ(1,400)NRUN,NGO
  400 FORMAT(2I3)
      IF(NGO.EQ.1) CALL UTPOP
      DO 37 II = 1,NRUN
      READ(1,400)NC,MOT
      READ (1,40)KORD,MRT,MLIN,NADJ,NRDNG
      WRITE(2,40)KORD,MRT,MLIN,NADJ,NRDNG
   40 FORMAT(5I5)
      READ(1,41)SF,CONST,CALBF,VEFF,VIVC
   41 FORMAT(5F0.0)
      READ (1,11)E,X,CON,D,OD,R,TXC,TMIN,SCI,SCO,PGI,COMP,TGI
   11 FORMAT(13F0.0)
      WRITE(2,12)E,X,CON,D,OD,R,TXC,TMIN,SCI,SCO,PGI,COMP,TGI
   12 FORMAT(F4.1,F5.2,F5.3,F6.3,F5.1,F7.1,2F7.1,2F8.3,3F6.1)

C  IDENTIFIERS OR NAMES: T=SURFACE TEMP., ALP AND BET= FOURIER COEFFICIENTS,
C  H= HEAT FLUX, TX= OUTER WALL TEMP., DEG= C.A.DEGREE, RT= RECONSTITUTED TEMP.,
C KORD=NUMBER OF ORDINATES/CYCLE
C  F= CONSTANT= 2.X= WALL THICKNESS, CON= TH. CONDUCTIVITY OF WALL,D= TH. DIFFU-
C  SIVITY, OD= OUTPUT INTERVALS IN DEGREE, R= ENGINE R.P.M. TXC= CONST. PART OF
C  OUTSIDE WALL TEMP., TMIN= CONST. PART OF INSIDE SURFACE TEMP.(OR TEMP. CORRES
C  PONDING TO BIASED THERMOCOUPLE OUTPUT), SCI= SURFACE TEMP. SCALE DEGREES/MV,
C  SCO= OUTER TEMP. SCALE, DMIN,DMAX,HMIN,HMAX,DINS,HINS, ARE MIN. AND MAX. VALU
C  ES OF C.A.DEGREE AND HEAT FLUX AND CORRESPONDING AXES IN INCHES.
      M=NADJ
```

```
      READ (1,600)(T(I),I=1,NRDNG)
      WRITE(2,50)
   50 FORMAT(2X,10HINP SURFC TEMP DATA)
      WRITE(2,600)(T(I),I=1,NRDNG)
      READ(1,600)(P(I),I=1,NRDNG)
  600 FORMAT(2X,10F7.3)

C   CONTROL PARAMETERS"
C   NRUN= NO. OF DATA SETS
C   NGO= 1 OPEN AND CLOSE GRAPH PLOTTER AT CORRECT POINTS
C   MOT=1 MOTORED CONDITION, MOT#1 FIRED CONDITION (GAS TEMP. CALCULATION
C   NC= NO. OF CYCLES PER SET OF DATA
C   MRT= 1 IF RECONSTITUTED TEMP. DESIRED IN OUTPUT. MRT= 2 IF RT NOT DESIRED.
C   MLIN= 1 FOR GRAPH PLOT OF CURRENT DATA RESULTS.
C   MADJ= NUMBER OF UNWANTED TEMP. RECORDS ON FIRST TEMP. DATA CARDS

C   TO OBTAIN AVERAGE SURFACE TEMP. CYCLE FROM SEVERAL CYCLES.;
C   (OBJECT) : TO REMOVE OR REDUCE EFFECT OF ELECTRIC NOISE INTERFERANCE.
      IF(NC.EQ.1)GOTO 3
      DO 5 J=1,KORD
      K=J+M
      P(K)=P(K)
      T(K)=T(K)
      NC1=(NC-1)*KORD+K
      DO 303 I=K+KORD,NC1,KORD
      T(K)=T(K)+T(I)
  303 P(K)=P(K)+P(I)
      T(K)=T(K)/NC
      P(K)=P(K)/NC
    5 CONTINUE
    3 CONTINUE

      OD=720./(KORD-1)
      INT=F*360./OD

C   CALCULATES ACTUAL WALL SURFACE TEMP. FROM DATA
      SUM=0.0
      TMEP=0.0
      WORK=0.0
      DO 700 J=1,KORD
```

```
      I=J+M
      T(I)=SCI*T(I)
      SUM=SUM+T(I)
C  CALCULATE IMEP FOR WORKING CYCLE.
      PI=3.141593
      VCL=20.17E-4
      PA=0.0871
C  O=CON. ROD  LENGTH FT. : Q= STROKE  FT.
      O=0.408
      Q=0.3438
      V(1)=VCL
      TH=J*OD
      V(J+1)=VCL+PA*(O+Q*(1-COS(TH*PI/180.))/2-SQRT(O**2+Q**2*((COS(TH*P
     1I/180.))**2-1)/4))
      DV=V(J+1)-V(J)
C  CALCULATE GAS PRESSURE AND TEMP. FROM MEASURED PRESSURE DATA
      P(J)=(P(I)+CONST)*SF*CALBF+14.7
      IF(IOT.EQ.1)TG(J)=TGI*(P(J)/PGI)**(0.35/1.35)
      IF(IOT.NE.1)TG(J)=TGI*V(J)*P(J)/(VIVC*PGI)
      WORK=WORK+P(J)*DV
C  TO CONVERT PRESSURE TO UNITS OF (BAR)   BAR=14.5 PSI =10E5 N/MSQR.
      P(J)=P(J)/14.5
  700 CONTINUE
C  TSHN  IS MEAN VALUE OF TRANSIENT PART OF  SURFACE TEMPERATURE
      TSHN=SUM/KORD
      PIME=WORK/(PA*Q)
      E=KORD
      DO 2 J=1,KORD
      I=J+M
      TT(I)=TMIN+T(I)-TSHN
    2 N=I
      TXMEAN=TXC+SCO
      SMEAN=TMIN
      WRITE(2,402)R,COMP,PIME
  402 FORMAT(5X,F7.1,2X,10HR.P.M CASE,5X,F4.1,2X,17HCOMPRESSION RATIO,5X
     1,F7.2,2X,5HIMEP,///)
      WRITE(2,15)SMEAN,TXMEAN
   15 FORMAT(2X,15HINP MEAN TEMP= ,E14.7,5X,15HOUT MEAN TEMP= ,E14.7)
C  OBTAIN FOURIER COEFFICIENTS ALP AND BET
      AK=2./E
```

```
      OMEGA=AK*3.14159?27
      S1=SIN(OMEGA)
      C1=COS(OMEGA)
      C=C1
      S=S1
      LHR=(KORD-1)/2
      WRITE(2,1100)
 1100 FORMAT(48X,16HFOURIER  COEFFS.//21X,8HHARMONIC,12X,4HALPA,22X,4HBE
     1TA)
      DO 6 I=1,LHR
      U2=0.
      U1=0.
      T=KORD+U
      DO 4 K=2,KORD
      U0=(T(I)+2.*U1*C-U2)
      U2=U1
      U1=U0
    4 I=I-1
      ALP(I)=(T(1+M)+U1*C-U2)*AK
      BET(I)=U1*AK*S
      C2=C1*C-S1*S
      S=C1*S+S1*C
      C=C2
    6 WRITE(2,13)I,ALP(L),BET(L)
   13 FORMAT(21X,I3,2(10X,E14.7))
      ENDFILE 2
C  CALCULATE RECONSTITUTED TEMP IF DESIRED.
      GO TO (27,28),MRT
   27 THET=0.
      WRITE(2,32)
   32 FORMAT(79X,1H-)
      WRITE(2,30)
   30 FORMAT(29X,13HSURFACE TEMP.,8X,19HRECONSTITUTED TEMP.)
   25 DO 21 L=1,KORD
      RT(L)=0.
   22 DO 23 K=1,LHR
      W=K
   23 RT(L)=RT(L)+ALP(K)*COS(THET*W)+BET(K)*SIN(THET*W)
      THET=THET+OMEGA
      RT(L)=RT(L)+SMEAN
```

```
   21 CONTINUE
      DO 29 L=1,KORD
      J=L+M
   29 WRITE(2,26)TT(J),RT(L)
   26 FORMAT(17X,2(10X,E14.7))
   28 CONTINUE
C  CALCULATES HEAT FLUX AT DESIRED INTERVALS OF C.A.DEGREES
      INT=INT+1
      WRITE(2,1201)
 1201 FORMAT(79X,1H=)
      WRITE(2,1200)
 1200 FORMAT(2X,10HCRANK DEG.,1X,34HHEAT FLUX KW PER SQRM TOT AND TRNS,2
     1X,9HABS.P PST,3X,7HGAS T K,2X,8HSURF.T.C,6X,32HH T COEF.KWPMSQR K
     2TOT AND TRANS)
      W=(6.2831853*R)/(F*60.)
      THF=0.0
      DO 1 J=1,INT
      I=J+M
  300 A=J-1
      B=OD*3.1415927*A/(180.*F)
      H(J)=0.0
      DO 10 K=1,LHR
      AP(K)=ALP(K)+BET(K)
      BE(K)=BET(K)-ALP(K)
      G=K
      U=SQRT((G*W)/(2*D))
   10 H(J)=H(J)+CON*U*(AP(K)*COS(G*B)+BE(K)*SIN(G*B))
      HT(J)=H(J)*41.87
      H(J)=H(J)+CON*(SMEAN-TXMEAN)/X
      H(J)=H(J)*41.87
      THF=THF+H(J)
      Y=A*OD
      DEG(J)=Y
C  CALCULATE HEAT TRANSFER COEFFICIENT FROM CALCULATED TG,H AND SURF. T
      TT(J)=TT(I)
      TDIF=(TG(J)-(TT(J)+273))
      IF(TDIF.EQ.0.0) GOTO 54
      SH(J)=H(J)/TDIF
      ST(J)=HT(J)/TDIF
      GOTO 55
```

```
   54 SH(J)=50
      ST(J)=50
   55 CONTINUE
    9 WRITE(2,14)Y,H(J),HT(J),P(J),TG(J),TT(J),SH(J),ST(J)
   14 FORMAT(2X,F6.1,4X,E14.7,4X,F14.7,5X,F7.2,5X,F7.2,4X,F6.2,5X,E14.7,
     14X,F14.7)
      IF(IGO.NE.1) GOTO 19
      NIC=NINT(220/OD)
      NEO=NINT(500/OD)
      WRITE(4,200)(DEG(J),J=NIC,NEO),(P(J),J=NIC,NEO),(TG(J),J=NIC,NEO),
     1(H(J),J=NIC,NEO),(HT(J),J=NIC,NEO),(SH(J),J=NIC,NEO),(ST(J),J=NIC,
     2NEO)
  200 FORMAT(7E10.2)
   19 IF(IPLIN.NE.1) GOTO 20
C     GRAPH OUTPUT
C     DRAW AXES FOR GRAPH
      READ(1,1050) DMIN,DMAX,HMIN,HMAX,DINS,HINS,TMIN,TMAX,PMIN,PMAX,GMI
     1N,GMAX,SMIN,SMAX
      CALL UTP4A(DMIN,DMAX,HMIN,HMAX,DINS,HINS,19H CRANK ANGLE DEGREE,3,
     118H HEAT FLUX KW/M2  ,3)
      CALL UTP4B(DEG,H,INT,2)
      CALL UTP4A(DMIN,DMAX,GMIN,GMAX,DINS,HINS,19H CRANK ANGLE DEGREE,3,
     110HGAS TEMP K,2)
      CALL UTP4B(DEG,TG,INT,2)
   20 CONTINUE
 1050 FORMAT(7F0.0)
      AVHF=THF/INT
      AVTRF=AVHF-CON*41.87*(SMEAN-TXMEAN)/X
      WRITE(2,333) AVHF,AVTRF
  333 FORMAT(1H ,17H MEAN HEAT FLUX =,E14.7,10X,22HMEAN TRANS.HEAT FLUX
     1=,E14.7)
      M=N
   37 CONTINUE
      IF(IGO.EQ.1) CALL UTPCL
      STOP
      END
      FINISH
****
DOCUMENT DATA
```

APPENDIX (B)

EVALUATION OF CYLINDER CHARGE PROPERTIES AND PREDICTION OF HEAT FLUX

The programme originally developed by Annand (6) for performance calculations of four-stroke diesel engines, was modified for the present investigation. Essentially, the programme performs a stepwise integration of the differential form of the first law of thermodynamics as it applies to events between inlet valve closure and exhaust valve opening. Annand's equation (6) for heat transfer is used to describe heat transfer through the walls. The rate of fuel injection and of fuel evaporation are described by simple linear functions. The rate of heat release is described by triangular distribution over a period of 35-40^{o} CA (depending on fuel quantity and engine speed), with peak at midway Lyn (61). The start and duration of fuel injection is determined by needle lift and fuel line pressure measurements, and the evaporation is assumed to take place 3-4^{o} CA after the beginning of injection and for the same period of injection. Instantaneous constituents during combustion are evaluated assuming complete combustion of the reacted fuel. The charge is assumed to be homogeneous at all times and the charge properties at each instant are calculated by the methods of section (5.6).

In the present investigation, the induction and exhaust processes are not included in the calculation, and complete scavenge is assumed because of valve overlap. To start the calculation, the temperature of the entering fresh charge is estimated from its dependence on volumetric efficiency and on operating conditions as described in section (5.5). However, accepting the computed gas composition, the gas properties are evaluated at the bulk mean gas

temperature which is evaluated from the measured pressure and cylinder volume. The calculated gas temperature on the basis of the assumed heat release was low near TDC and high later, compared to the gas temperature evaluated from measured pressure. This suggested higher initial heat release in actual cases than the assumed triangular trend.

Once the charge properties are evaluated, the program calculates the heat flux using the different correlations considered (e.g. Annand's, Woschni's and flat plate equation).

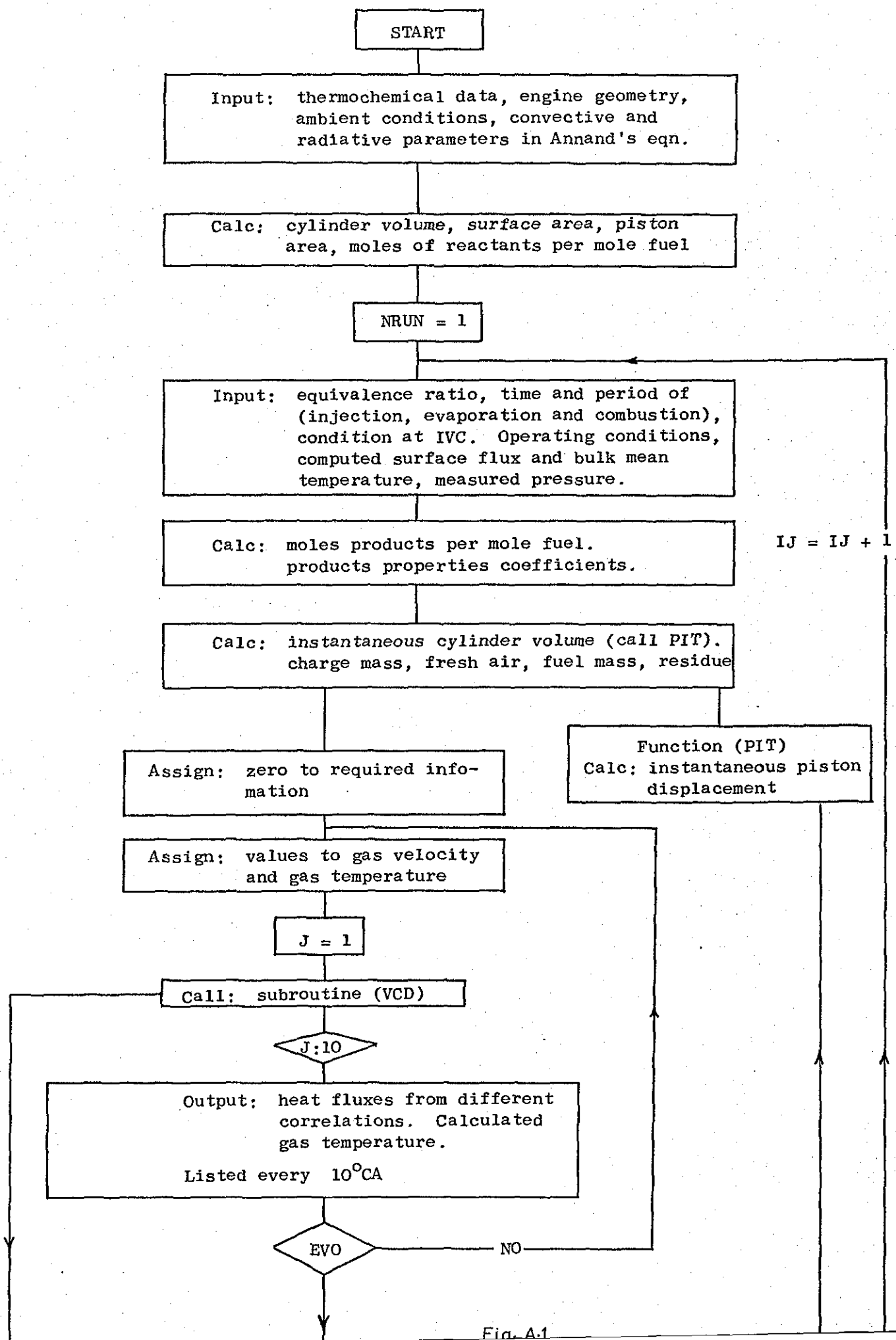
START
Input: thermochemical data, engine geometry, ambient conditions, convective and radiative parameters in Annand's eqn.
Calc: cylinder volume, surface area, piston area, moles of reactants per mole fuel
NRUN = 1
Input: equivalence ratio, time and period of (injection, evaporation and combustion), condition at IVC. Operating conditions, computed surface flux and bulk mean temperature, measured pressure.
Calc: moles products per mole fuel. products properties coefficients.
IJ = IJ + 1
Calc: instantaneous cylinder volume (call PIT). charge mass, fresh air, fuel mass, residue
Function (PIT) Calc: instantaneous piston displacement
Assign: zero to required infomation
Assign: values to gas velocity and gas temperature
J = 1
Call: subroutine (VCD)
J:10
Output: heat fluxes from different correlations. Calculated gas temperature.
Listed every 10°CA
EVO
NO

Fig. A.1

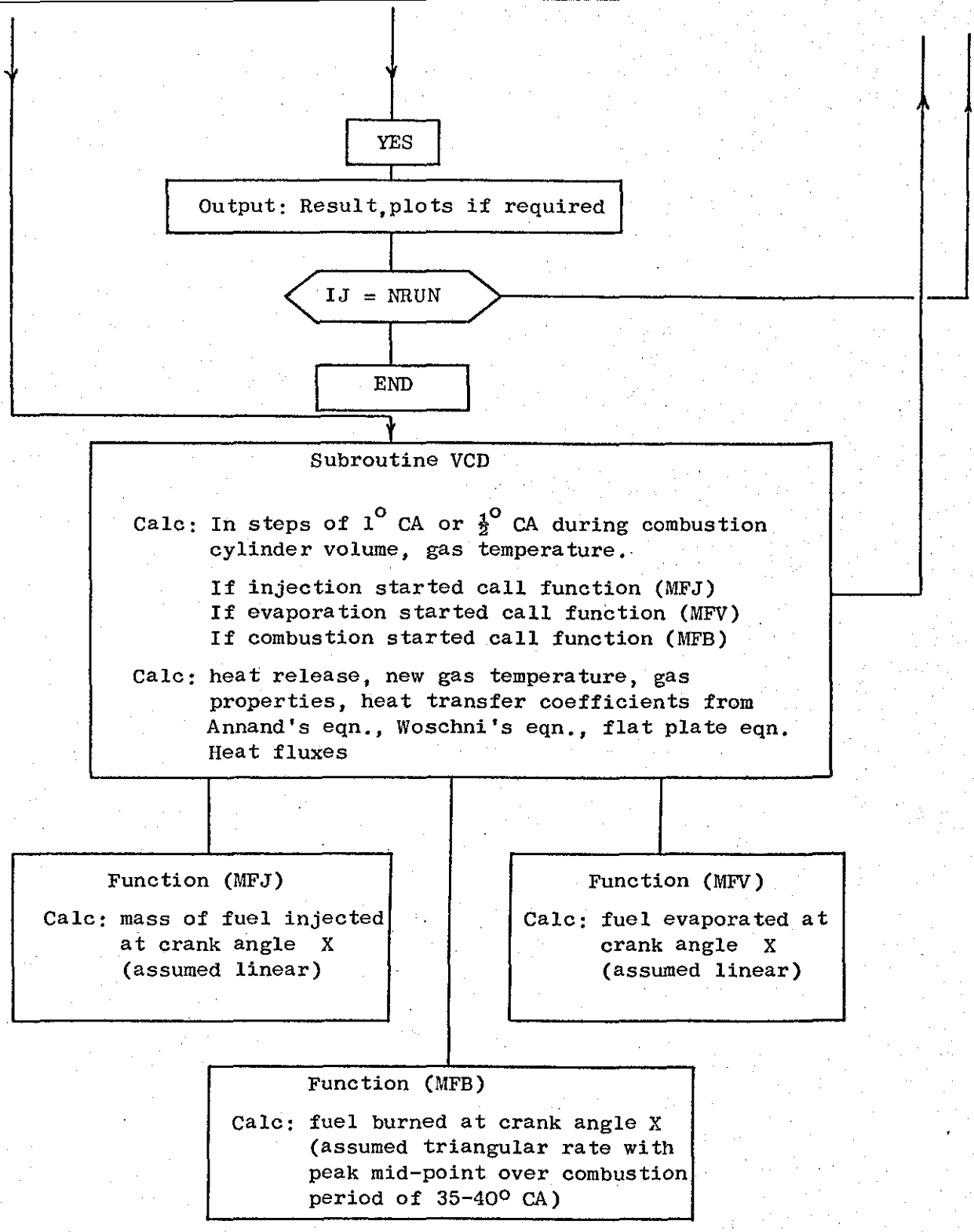

Fig. A.2 Schematic flow chart for the computation of cylinder change properties and prediction of instantaneous heat fluxes

```
      MASTER CIE2
C     PROGRAM USED TO CALCULATE HEAT FLUXES BY DIFFERENT CORRELATIONS
C     AFTER ESTIMATING CHARGE PROPERTIES AND CONDITION AND CALCULATE
C     CYCLE HEAT LOSS AND WORK
C   QA,QW,QF = ANNANS,WOSHNIS,FLAT PLATE HEAT FLUXES RESPECTIVELY
C     US=SWIRL,CAX=CA DEGREE OF MEASURED VALUES, HFX=HEAT FLUX,CFX=HEAT
C     TRANSFER COEFF.,PGX=PRESSUR,TGX=GAS TEMP.,CAD=CA DEGREE,HTX=TRANSINT
C     COMPONENT HEAT FLUX,CTX=H.T.COEFF. CORRESPNG TO HTX,PG&TG CALCTD
C     TEMPERATUR CALCULATED MEASURED PRESSURE AT 10 DEGREE INTERVALS
C     GAS PRESS. & TEMP.YNF &XRF=NUSSELT & RENOLDS NUMBER FACTORS, TGM=GAS
      DIMENSION HF(6),XK(14)
C**********
      DIMENSION QA(40),QW(40),QF(40),US(40),CAX(110),HFX(110),CFX(110),P
     1GX(110),TGX(110),CAD(40),HTX(110),CTX(110),PG(40),TG(40),YNF(40),X
     2RF(40),TGM(40)
      REAL JJ,L,N,HY,MA,MF,ML,MP,MR,MT,IC,IO,JB,JE,LC,LO,MPS,NO,MFS,M
      COMMON/DVC/N,VO,SS,LC,D,LO,H(6,14),HP(6),DU(6),RR,MA,MF,MFS,MPS,MP
     1,M,FX,A,B,PS,FF,SO,ZF,AL,CL,ZP,WP,AP,WL,CR,TL,P,MR,CONVF,UM(6),MT,
     2UH,UT,PIVC,TTVC,NTT
      COMMON/GEN/JB,JE,VB,VE,CR,CF,CC,CM,E,L,PI
      INTEGER CY,CZ
      DO 2 I=1,13,1
      READ(1,3)(H(J,I),J=1,6)
    2 CONTINUE
    3 FORMAT(6F0.0)
C     RR=UNIV.GAS CONST.  CHU/LB MOLE.C
      RR=1.9859
      NV=10
      CZ=101
    4 IF(CZ.EQ.18) GOTO 118
      IF(CZ.NE.0) GOTO 101
      GOTO 100
C**********
  101 READ(1,59) NRUN
      READ(1,59) NTT
      READ(1,33) NO,NGO
      IF(NGO.EQ.1) CALL UTPOP
   30 FORMAT(F0.0)
      WRITE(2,31)NO
   31 FORMAT(/1HO,6HDATA SET ,F3.0)
```

```
      CZ=50
  102 READ(1,32)D,L
   32 FORMAT(2F0.0)
      PI=3.141593
      SS=0.25*PI*D**2
      SWPT=SS*L
      IF(CZ.EQ.2)GOTO 5
  104 READ(1,30)LC
      IF(CZ.EQ.4)GOTO 5
  105 READ(1,30)R
    5 WRITE(2,34)
   34 FORMAT(1H ,4HBORE,3X,6HSTROKE,3X,6HCONROD,5X,2HCR/3H FT,6X,2HFT,5X
     1,5HRATIO,/)
      WRITE(2,35)D,L,LC,R
   35 FORMAT(1X,F5.3,3X,F5.3,6X,F6.4,5X,F5.1/)
      WRITE(2,36)SWPT
   36 FORMAT(1H ,18HSWEPT VOLUME CU FT/5X,F14.7)
      LO=R*L/(R-1)
      AP=SS
C    VO=TOTAL CYL. VOL.  CU.FT.
      VO=SS*LO
      IF(CZ.EQ.5.OR.CZ.EQ.4)GOTO 50
      IF(CZ.EQ.13) GOTO 50
  115 READ(1,30)A
      WRITE(2,43)A
   43 FORMAT(1H ,21HCONVECTIVE PARAMETER=,F4.2/)
      IF(CZ.EQ.15) GOTO 50
  121 READ(1,30) B
      WRITE(2,44) B
   44 FORMAT(15X,6HINDEX=,F5.3/)
      IF(CZ.EQ.21) GOTO 50
  114 READ(1,30) CR
      WRITE(2,45) CR
   45 FORMAT(3X,18HRADIANT PARAMETER=,E10.7)
      IF(CZ.EQ.14) GOTO 50
  116 READ(1,46) CA,HY,OX
C   SO MOL. O2 REQD. FOR COMPLETE COMBN. OF ONE MOL. FUEL
C    MF =MOLECULAR WEIGHT OF FUEL
      SO=CA+(HY/4)-(OX/2)
      MF=12*CA+HY+16*OX
```

```
      READ(1,46) AI,CL,ZF
   46 FORMAT(3F0.0)
C    CALCULATE ENERGY OF FUEL
      DO 6 I=1,6,1
      READ(1,30)H(I,14)
      DU(I)=-(HY*H(I,1)/2)-(CA*H(I,8))+(SO*H(I,10)*H(I,14))
      IF(I.NE.1) DU(I)=RR*DU(I)
    6 CONTINUE
      DU(2)=DU(2)-RR*(1-(HY/4)-(OX/2))
  123 READ(1,30)TI
      WRITE(2,47)TI
   47 FORMAT(1H ,16HFUEL TEMP.DEG.K=,F4.1)
      IF(CZ.EQ.23) GOTO 50
C*************
      DO 14 IJ=1,NRUN
  117 READ(1,30)FF
      WRITE(2,48)FF
   48 FORMAT(1H ,41HTRAPPED FUEL.AIR RATIO RELATIVE STOICHIO=,F6.4/)
C    CALCULATE NO. OF MOLES OF PRODUCT CONSTITUENTS /(FF)MOL OF FUEL
C    (X1) H2O,(X5) N2,X8 CO2,X10 O2
C    EX=TOTAL MOLES OF PRODCTS/(FF) MOLES FUEL
      X1=(HY*FF)/2
      X5=3.762*SO
      X8=CA*FF
      X10=(1-FF)*SO
      EX=X1+X5+X8+X10
C    HP(I)  AND ZP = PROPERTY PARAMETERS OF PRODUCTSOF COMBUSTION
C    MP= MOLECULAR WEIGHT OF PRODUCTS
      DO 7 I=1,6,1
      HP(I)=(X1*H(I,1)+X5*H(I,5)+X8*H(I,8)+X10*H(I,10))/EX
    7 CONTINUE
      ZP=(0.93*X1+1.62*X5+1.65*X8+1.45*X10)/(4.24*X1+5.29*X5+6.63*X8+4*X
     110)
      MP=(18*X1+28*X5+44*X8+16*X10)/EX
C    EX=TOTAL MOLES OF PRODUCTS/ONE MOLE FUEL
      IF(FF.GT.1E-6) EX=EX/FF
      IF(CZ.LT.18) GOTO 50
  122 READ(1,41) JR,JE,VB,VE
      IF(CZ.EQ.22) GOTO 8
  126 READ(1,46) CB,CE,CC
```

```
    8 WRITE(2,49)JB,VB,CB,JE,VE,CE
   49 FORMAT(1H ,22H  INJECT   EVAP   BURN/1H ,5HBEGIN,3F6.1/1H ,4HEND ,
     13F6.1/1H ,26HHEAT RELEASE PARAMETER=   ,F6.1)
      I=AINT(CC)
      X=CC-I
      XX=0.1*I
      XXX=(1-XX)*X
      WRITE(2,51)XXX,XX
   51 FORMAT(1H ,26HFRACTION BEFORE RATE PEAK=,F6.3,9H IN TAIL=,F5.2/)
      CM=CE
      IF(CZ.LT.30) GOTO 50
  108 READ(1,32) IC,EO
      WRITE(2,52)IC,EO
   52 FORMAT(1H ,16HIC ABDC  EO BBDC/1H ,2F6.1/)
      EO=360.-EO
      IF(CC.GT.1) CE=EO
      IF(CZ.EQ.8) GOTO 50
  116 READ(1,46) P1,T1,E
      WRITE(2,53)P1,T1,E
   53 FORMAT(1H ,26HCONDITIONS AT IC PRESSURE=,F5.2,3HATM,7HTEMP.K=,F6.1
     1,7HPURITY=,F6.3/)
      IF(CZ.LT.30) GOTO 30
  106 READ(1,30) N
      WRITE(2,38)N
   38 FORMAT(1H ,20HCRANKSHAFT SPEED RPM,F6.1)
C    PS=MEAN PISTON SPEED   FT/S
      PS=N*L/30.
   39 WRITE(2,40)PS
   40 FORMAT(19HPISTON SPEED FTPSEC,F6.1/)
      IF(CZ.LT.30) GOTO 50
  113 READ(1,41)WH,WI,WL,WP
   41 FORMAT(4F0.0)
      WRITE(2,42)WH,WI,WL,WP
   42 FORMAT(1H ,23HWALL TEMP  DEG K LINER=,F5.1/11X,11HINLT VALVE=,F5.1
     1/17X,5HHEAD=,F5.1/15X,7HPISTON=,F5.1/)
  120 READ(1,33)S,NS
   33 FORMAT(F0.0,I0)
      PI=3.141593
      CONVE=0.662
  109 READ(1,30) FD
```

```
      WRITE(2,54) ED
   54 FORMAT(1H ,12HACCURACY  T ,F5.2/)
   50 READ(1,59) CY
      WRITE(2,110)
  110 FORMAT(3X,7HCA-ADC,2X,8HTG.DEG.K,4X,6HPG.PSI,4X,10HMA.LB.MOL.,2X,
     114HMF.CHRGE.LBMOL.,1X,13HQLOSS CHU/MIN,1X,9HQAN.KW/M2,4X,9HQWO.KW/M
     22,5X,9HQEP.KW/M2)
C**********
      READ(1,61) NP,NPX,RJ
      READ(1,62)(US(I),I=1,NP),(CAX(I),I=1,NPX),(PGX(I),I=1,NPX),(TGX(I)
     1,I=1,NPX),(HFX(I),I=1,NPX),(HTX(I),I=1,NPX),(CFX(I),I=1,NPX),(CTX(
     2I),I=1,NPX),(TGH(I),I=1,NP)
   61 FORMAT(2I0,F0.0)
   62 FORMAT(7F0.0)
      READ(1,64)DMIN,DMAX,HMIN,HMAX,DINS,HINS,TMIN,TMAX,PMIN,PMAX,CMIN,C
     1MAX
   64 FORMAT(6F0.0)
      P=P1
      T=T1
      PIVC=P1
      TIVC=T1
      X=NS*S
      X=X-AINT(IC/X)
C     V=INST. CYL. VOL.  CU.FT
C     M=CHARGE MASS  LB MOLE
C     MA=FRESH AIR CHARGE  LB.MOLE
C     MPS=MASS OF PRODUCTS LEFT=RESIDUE MR
C     MFS=MASS OF FUEL INTRODUCED,ML=FUEL IN LIQUID FORM
      V=VO-SS*PIT(IC,X)
      M=P*V/(CONVE*RR*T)
      MA=E*M
      MT=MA
      MPS=M-MA
      MR=MPS
      MFS=0.0
      ML=0.0
      E=0.21*EE*MA/SO
      U=0.0
C     CALCULATE INTERNAL ENERGY OF CHARGE
      DO 1 J=2,6
```

```
      T=8-J
      UM(I)=H(I,13)*HA+HP(I)*HPS
      U=(U+UM(I))*T
    9 CONTINUE
      UM(1)=H(1,13)*HA+HP(1)*HPS
      UM(2)=UM(2)-H
      U=(U-T*HS)*RR+UM(1)
      W=0.0
      Q=0.0
      QP=0.0
      PX=0.0
C**********
      QAN=0.0
      QWO=0.0
      QFP=0.0
      VG=PS
   10 NSS=NS
      SE=S
C**********
      ATST=X/10.-ANINT(X/10)
      IF(ATST.GT.0.0) GOTO 63
      NK=NINT(IC)
      NK=NINT((X-NK)/10)+2
      VG=(2*PI*RJ*WS(NK))/60.
      TP=TGH(NK)
   63 CONTINUE
C     ::::::::::::::
      CRNS=CB-NS*S
      IF(X.LT.CRNS.OR.X.GT.CM) GOTO 11
      NSS=NINT(2*NS*S)
      SE=0.5
C    CALL SUBROUTINE (VCD) TO CALCULATE STEP BY STEP W,Q,T,P,...
   11 DO 12 J=1,NSS,1
C**********
      CALL VCD(X,T,U,V,DQ,DQP,DW,SE,ED,RJ,VG,QAN,QWO,QFP,YNU,XRE,TP)
      W=W+DW
      Q=Q+DQ
      QP=QP+DQP
      IF(P.GT.PX) PX=P
   12 CONTINUE
```

```
      IF(CV.EQ.0) GOTO 13
      PPSI=14.69*P
C**********
      WRITE(2,55) X,T,PPSI,HA,H,Q,QAN,QWO,QFP
   55 FORMAT(1H ,3F10.2,6F14.7/)
      IN=NINT((X-IC)/10)
      QA(IN)=QAN
      QW(IN)=QWO
      QF(IN)=QFP
      CAD(IN)=X+180
      TG(IN)=T
CC  PRESSURE CONVERTED TO UNITS OF  (BAR)
      PG(IN)=P*0.987
      YNF(IN)=YNU
      XRF(IN)=XRE
      HTX(IN)=YNU*2*PI*RJ/D
      CTX(IN)=XRE*VG*PI*2*RJ/(PS*D)
   13 IF(X.LT.EO) GOTO 10
      PINEP=(38.5*W)/(PI*L*D*D)
      PEAKP=14.69*PX
      HCOLT=0.5*G*N
      HPIST=0.5*QP*N/(15*D**2*PI)
      WRITE(2,57)PINEP,PEAKP,HCOLT,HPIST
   57 FORMAT(1H /,11H INEP.PSI= ,F6.1/,18H PEAK PRESSURE PSI,F6.1/,23H H
     1EATTO COOLNT CHUPMIN=,E14.7/,28H FLUX TO PISTON CHUPSQFT.SEC,E14.7
     2/)
C**********
C  CALL GRAPH PLOTTER  AND ADJUST AXIS SCALES
      IF(NGO.NE.1)GOTO 157
      CALL UTP4A(DMIN,DMAX,HMIN,HMAX,DINS,HINS,19H CRANK ANGLE DEGREE,3,
     118H HEAT FLUX KW/M2  ,3)
C  DRAW  GRID ON GRAPH.
      CALL GRID(DMIN,DMAX,HMIN,HMAX,DINS,HINS)
      CALL UTP4B(CAX,HEX,NPX,2)
      CALL UTP4B(CAD,QF,NP,2)
      CALL UTP4A(DMIN,DMAX,HMIN,HMAX,DINS,HINS,19H CRANK ANGLE DEGREE,3,
     118H HEAT FLUX KW/M2  ,3)
      CALL UTP4B(CAD,QW,NP,2)
      CALL UTP4B(CAD,QA,NP,2)
      CALL UTP4A(DMIN,DMAX,TMIN,TMAX,DINS,HINS,19H CRANK ANGLE DEGREE,3,
```

```
     110HGAS TEMP,K,2)
      CALL UTP4B(CAX,TGX,NPX,2)
      CALL UTP4B(CAD,TG,NP,2)
  157 CONTINUE
      WRITE(2,112)
  112 FORMAT(1H /,3HCAD,13H   D/K M2.C/KW,15H RF (RO.PS.D/Z),15H2#.RJ/K M
     12.C/KW,18HRF (RO.VG.2#.RJ/Z)/)
      DO 14 I=1,NP
      WRITE(2,58) CAD(I),YNF(I),XRF(I),HTX(I),CTX(I)
   14 CONTINUE
   58 FORMAT(1H ,F4.0,4E14.7)

      READ(1,59) C7
   59 FORMAT(I0)
      IF(C7.EQ.0) GOTO 60
      ENDFILE 2
   60 GOTO 4
  100 CONTINUE
      IF(NGO.EQ.1) CALL UTPCL
      STOP
      END



C***********
C    SUBROUTINE CALCULATE STEP-BY-STEP CHARGE PROPERTIES AND HEAT FLUXES
      SUBROUTINE VCD(X1,T1,U1,V1,DQ,DQP,DU,DX,FT,RJ,VG,QAN,QWO,QFP,YNU,X
     1RF,TP)
      REAL MFB,MBJ,MFV
      REAL K,MB,MJ,MC,N,LC,LO,MA,MF,MFS,MPS,MP,MR,JR,JE,L,M,MT
      COMMON/DVC/N,VO,SS,LC,D,LO,H(6,14),MP(6),DU(6),RR,MA,MF,MFS,MPS,MP
     1,M,EX,A,B,PS,FF,SO,ZF,AL,CL,ZP,UP,AP,WL,CR,TL,P,MR,CONVF,UM(6),MT,
     2WH,U1,PIVC,TTVC,NTT
      DIMENSION TC(3),TX(3)
      COMMON/GEN/JR,JE,VB,VE,CB,CF,CC,CM,F,L,PI
      X2=X1+DX
      DT=DX/(6*N)
      V2=VO-SS*PIT(LC,X2)
C    ALSUB=EXPOSED LINER AREA SQR.FT
      ALSUB=PI*D*(LO-PIT(LC,(X1+X2)/2))
```

```
      T2=T1*(V1/V2)**0.35
      PHOT=PIVC*(0.030353/V2)**1.35
      DTDX=(T2-T1)/DT
C     CALCULATE CHARGE CP
C     CP=SPECIFIC HEAT  CHU/C
      CP=0.0
      DO 15 J=2,6
      IF(NTT.EQ.2) T1=TP
      I=8-J
      CP= CP*T1*(H(I,13)*MA+H(I,14)*MFS*HP(I)*MPS)*I
   15 CONTINUE
      IF(X2.LT.C1.OR.X2.GT.CE) GOTO 65
      IF(FF.LT.0.00001)GOTO 65
      UB=DU(6)
      DO 16 J=1,5
      I=6-J
      UB=UB*T2+DU(I)
   16 CONTINUE
      T2=T2+(HFB(X2)-HFB(X1))*UB/(CP-RR*M)
   65 TC(1)=T2
      NSUB=2
C     MC=MOLECULAR WEIGHT OF CHARGE MIXTURE
C     CALCULATE VISCOSITY&CONDUCTIVITY OF CHARGE
C     Z=GAS VISCOSITY   LB/FT,SEC
C     K=GAS CONDUCTIVITY  CHU/FT.SEC.C
      MC=(28.97*MA+MF*MFS*MPS*MP)/M
      Z=(1.71*MA+7F*MFS*SQRT(MF)+7P*MPS*SQRT(MP))/(5.385*MA+MFS*SQRT(MF)
     1+MPS*SQRT(MP))
      Z=0.000001*Z*T1**0.645
      K=CP*Z/(0.7*MC*M)
      QD=A*K*((M*PS*D*MC/(V1*Z))**R)*DT/D
C**********
      HAN=(K/D)*((M*PS*D*MC/(V1*Z))**0.7)
      VW=((2.28*PS/3.28)+0.00324*1.057*TIVC*(P-PHOT)/PIVC)
      TWO=1./((T1)**0.53)
      DWO=1./((0.102)**0.2)
      HWO=110*DWO*((P*1.0333)**0.8)*TWO*((VW)**0.8)
      DIML=2*PI*RJ
      HFP=((0.037*K)/(DIML))*((M*VG*DIML*MC/(V1*Z))**0.8)*((0.7)**0.333)
      VNU=D/(K*20.44)
```

```
      XRE=M*NC*PS*D/(V1*Z)
   70 TSUB=TC(NSUB-1)
      IF(X2.LT.JB.OR.X2.GT.(CF+DX)) GOTO 75
      IF(FF.LT.0.00001)GOTO 75
C     ML=MASS OF BURNED FUEL, MJ= MASS INJECTED   NMOLES
C     MPS=MOLES OF PRODUCTS DUE TO COMBN. OF MB MOLES FUEL
C     MA=MASS OF FRESH AIR CORRESPONDING TO YET UNBURNED FUEL
C      M=TOTAL MASS(MOLES) IN CYL.
      MB=MEB(X2)
      MJ=MEJ(X2)
      MPS=MB*EX*HB
      ML=MJ-MEV(X2)
      MFS=MJ-MB-ML
      MA=MT-SO*MC/(0.21*FF)
      M=MA+MFS+MPS
C     CALCULATE INTERNAL ENERGY OF CHARGE
      DO 17 J=1,6
      I=7-J
      UM(I)=H(I,14)*MFS+H(I,13)*MA+HP(I)*MPS
   17 CONTINUE
      UM(2)=UM(2)-M*ML*CL/RR
      UM(1)=UM(1)+ML*AL
   75 TS=0.5*(T1+TSUB)
CC    CALCULATE HEAT TRANSFER BY CONVN.&RADIATION
      DQP=QD*(TS-UP)*AP
      DQ=DQP*QD*((TS-UH)*SS+(TS-WL)*ALSUB)
      IF(XI.LT.CB) GOTO 80
      TR=TS**4
      QR=CR*(TR-WP**4)*DT*AP
      DQP=DQP+QR
      DQ=DQ+QR+CR*DT*((TR-WH**4)*SS+(TR-WL**4)*ALSUB)
   80 QI=0.0
      IF(FF.LT.0.0001) GOTO 81
      IF(JF.LT.X2.AND.X2.LT.(JF+DX)) QI=(MJ-MEJ(XI))*(AL+CL*TL)
   81 TS=T1*ALOG(TSUB/T1)
C     CALCULATE WORK TRANSFER
      DW=RR*M*T1*ALOG(V2/V1)
      IF(TS.NE.0.0) DW=DW*(TSUB-T1)/TS
      TS=TSUB*UM(6)
      DO 18 J=3,5
```

```
      T=8-J
      TS=(TS*UM(I))*TSUB
   18 CONTINUE
      TX(NSUB)=((U1+QI-DQ-DW-UM(1))/RR-TSUB*TS)/UM(2)
      IF(NSUB.EQ.3) GOTO 85
      TC(2)=TX(2)
      NSUB=3
      GOTO 70
   85 TC(3)=TX(3)-(TX(3)-TX(2))*(TX(3)-TC(2))/(TX(3)-TX(2)-TC(2)+TC(1))
      IF(ABS(TC(3)-TC(2)).LT.ET) GOTO 90
      TC(1)=TC(2)
      TX(2)=TX(3)
      TC(2)=TC(3)
      GOTO 70
   90 U1=U1+QI-DQ-DW
      V1=V2
      T1=TC(3)
      XI=X2
      P=U*RR*CONVE*T1/V1
C**********
      QAN=20.44*WAN*(0.80*(T1-WH)-6*DTDX/(PI*P))
      QWO=(WWO*4.2/3600.)*(T1-WH)
      QFP=WFP*20.44*(T1-WH)
      RETURN
      END


C     ::::::::::::::
C    FUNCTION CALCULATE PISTON DISPLACEMENT FROM TDC POSITION
      FUNCTION PIT(LC,X)
      REAL K,MB,MI,MC,N,LC,LO,MA,WF,MFS,MPS,MP,MR,JB,JE,L
      COMMON/GEN/JB,JE,VB,VE,CB,CE,CC,CM,E,L,PI
      RA=PI*X/180
      PIT=0.5*L*(1-LC-COS(RA)+SQRT(LC**2-(SIN(RA))**2))
      RETURN
      END
```

```
C     FUNCTION CALCULATE FUEL INJECTED AT (X) CA LINEAR OVER INJTN PERIOD
      REAL FUNCTION MFJ(X)
      REAL K,MB,MJ,MC,N,LC,LO,MA,MF,MFS,MPS,MP,MR,JB,JE,L
      COMMON/GEN/JB,JE,VB,VE,CB,CE,CC,CM,F,L,PI
      IF(X.LT.JB.OR.X.EQ.JB) MFJ=0.0
      IF(X.GT.JE.OR.X.EQ.JE) GOTO 200
      MFJ=(X-JB)*F/(JE-JB)
      GOTO 201
  200 MFJ=F
  201 RETURN
      END

C     FUNCTION CALCULATE FUEL EVAPORATED (LINEAR)
      REAL FUNCTION MFV(X)
      REAL K,MB,MJ,MC,N,LC,LO,MA,MF,MFS,MPS,MP,MR,JB,JE,L
      COMMON/GEN/JB,JE,VB,VE,CB,CE,CC,CM,F,L,PI
      IF(X.LT.VB.OR.X.EQ.VB) GOTO 203
      IF(X.GT.VE.OR.X.EQ.VE) GOTO 202
      MFV=(X-VB)*F/(VE-VB)
      GOTO 204
  202 MFV=F
      GOTO 204
  203 MFV=0.0
  204 RETURN
      END

C     FUNCTION CALCULATE MASS OF FUEL BURNED AT (X) CA DEGREE (ASSUMED
C     TRIANGULAR HEAT RELEASE WITH PEAK MIDDPOINT DURING COMBUSTION PERIOD
C     WHICH IS ESTIMATED TO BE 35~40 DEGREE CA DEPENDING ON LOAD
      REAL FUNCTION MFB(X)
      REAL K,MB,MJ,MC,N,LC,LO,MA,MF,MFS,MPS,MP,MR,JB,JE,L
      COMMON/GEN/JB,JE,VB,VE,CB,CE,CC,CM,F,L,PI
      IF(X.LT.CB.OR.X.EQ.CB) GOTO 208
      IF(X.GT.CE.OR.X.EQ.CE) GOTO 207
      C=CC-AINT(CC)
      D=1-0.1*(CC-C)
      E=CE-CB
      A=D*E
      IF(X.LT.(CB+C*E).OR.X.EQ.(CB+C*E)) GOTO 206
      B=A*(1-((CB-X)/E)**2/(1-C))
```

```
      A=CR
      IF(CC .GT. 1) A=CR-(1.-C)*(1.-D)*E**2/((CE-CM)*D)
      IF(X .LT. A .OR. X .EQ. A) GOTO 205
      MFB=F*(1.-(1.-D)*(CE-X)**2/((CE-CM)*(CE-A)))
      GOTO 206
  205 MFB=D
      GOTO 206
  206 MFB=A*(((X-CR)/E)**2)/C
      GOTO 209
  207 MFB=F
      GOTO 209
  208 MFB=0.0
  209 RETURN
      END

      SUBROUTINE GRID(XMIN,XMAX,YMIN,YMAX,XINS,YINS)
C     DRAWS A GRID ON A SET OF AXES PROVIDED BY UTP4A IN THE MASTER .   C
      DIMENSION X(2),Y(2)
      NX= IFIX(XINS)
      NY= IFIX(YINS)
      X(1)= XMIN
      Y(1)= YMIN
      Y(2)= YMAX
      DX= (XMAX-XMIN)/XINS
      DO 1 I=1,NX
      X(1)= X(1)+DX
      X(2)= X(1)
    1 CALL UTP4B(X,Y,2,3)
      X(1)= XMIN
      DY=(YMAX-YMIN)/YINS
      DO 2 I=1,NY
      Y(1)= Y(1)+DY
      Y(2)= Y(1)
    2 CALL UTP4B(X,Y,2,3)
      RETURN
      END
      FINISH
****
DOCUMENT DATA
```